Title
Advancing Nanomaterial Usage in Agriculture: Engineering Nanomaterials Towards Nanomaterial-Mediated Plant Genetic Engineering

Permalink
https://escholarship.org/uc/item/7mg0g7ph

Author
Goh, Natalie Shang-Yi

Publication Date
2022

Peer reviewed|Thesis/dissertation

Advancing Nanomaterial Usage in Agriculture: Engineering Nanomaterials Towards
Nanomaterial-Mediated Plant Genetic Engineering

By

Natalie Shang-Yi Goh

A dissertation submitted in partial satisfaction of the

requirements for the degree of

Doctor of Philosophy

in

Chemical Engineering

in the

Graduate Division

of the

University of California, Berkeley

Committee in charge:

Professor Markita P. Landry, Chair
Professor Matthew Francis
Professor David Schaffer

Spring 2022

Advancing Nanomaterial Usage in Agriculture: Engineering Nanomaterials Towards
Nanomaterial-Mediated Plant Genetic Engineering

Abstract

Advancing Nanomaterial Usage in Agriculture: Engineering Nanomaterials Towards
Nanomaterial-Mediated Plant Genetic Engineering

by

Natalie Shang-Yi Goh

Doctor of Philosophy in Chemical Engineering

University of California, Berkeley

Professor Markita P. Landry, Chair

Losses in crop yield from climate variations and proliferation of insects and pathogens threaten to leave a large proportion of the world's population vulnerable, predominantly those from low-income regions whose livelihoods are dependent on agribusiness. Moreover, rising populations and increasing reliance on plants for energy, food, medicine, and chemicals provide additional stress on our conventional agricultural system. To ensure agricultural sustainability and food security, there is a cogent need to engineer crop varieties with traits such as abiotic and biotic stress resistance and increased production of useful plant products. Traditional plant breeding to produce cultivars with desired phenotypes is too time and resource consuming to support future sustainability, and breeding lacks controls over acquired traits other than the traits of interest. Plant genetic engineering is a promising alternative to traditional plant breeding, though is primarily limited by the efficient delivery of genetic engineering biomolecules such as RNA, DNA, and proteins across plant biological barriers. This includes the cellulosic and multi-layered plant cell wall and double-layered membrane of the cell, nucleus, chloroplast, and mitochondrion. Nanoparticles have emerged as promising materials for use as biomolecule carriers into plant systems. Owing to their highly tunable chemical and physical properties, nanoparticles can be synthesized and functionalized to achieve targeted localization and cargo release. The full potential of nanoparticles in agriculture remains underexplored; nanomaterials and conjugation approaches have yet to be tested, and there remains a lack of design heuristics towards engineering nanoparticles in agriculture. Functional nanoparticle design is a complex, multivariable optimization process that necessitates a fundamental understanding of nanoparticle interactions with plants across various length scales, as well as probing structure-function relationships.

This dissertation presents a holistic overview of RNA, DNA, and protein delivery to plants. I develop a microscopy and molecular biology-based workflow for probing nanoparticle-plant interactions, specifically, assessing how nanoparticle morphology impacts transport within a plant leaf and their cargo delivery capabilities. This study focused on using gold nanoparticles for foliar delivery of small-interfering RNA, and revealed that contrary to expectations, nanoparticle entry into cells is not necessary for efficient siRNA cargo delivery. Subsequently, I contribute a novel system to the nanoparticle delivery toolbox by designing and validating a single-walled carbon nanotube (SWNT)-based system for plasmid DNA delivery to plants. Notably, while traditional DNA delivery methods result in undesired transgene integration into plants, this SWNT-based

platform achieves DNA delivery and gene expression without transgene integration. In addition to gold nanoparticles and SWNTs, in recent years, multiple nanoparticle-mediated systems have been shown to deliver RNA and DNA. However, there remains a dearth of literature demonstrating protein delivery into walled plant cells. I outline the unique challenges and potential strategies that can be used to advance nanoparticle-mediated protein delivery. All the studies outlined in this dissertation have been conducted on the bench-scale, though an eventual goal will involve translating this platform to widescale field utilization. I summarize the potential obstacles to field translation and detail approaches to probing nanoparticle behavior and function in a complex biological environment.

The findings presented in this dissertation lay the foundation for uncovering structure-function relationships for nanoparticles as biomolecule delivery vehicles. Furthermore, they represent unique formulations to add to the toolbox of RNA and DNA delivery. In sum, this work strives to advance RNA, DNA, and protein delivery to plants and provides a roadmap towards achieving translation of these technologies from the lab to the field.

To my mother, for her steadfast love and unwavering support over the years, and my father, who passed on too soon. I hope I make you both proud.

Contents

List of Figures

List of Tables

Acknowledgments

First, I would like to thank my advisor, Professor Markita Landry, for her support and mentorship. It is difficult to express how valuable of a role model Markita has been over the years – she has been approachable, communicative, supportive, and encouraging. Her keen eye and optimism have provided a natural counter to my innate pessimism in data interpretation. I am grateful for Markita granting me the independence to explore research questions that satiate my curiosity and for affording the understanding when many of the fledgling ideas did not pan out. It has been my absolute pleasure and privilege to grow as a scientist under her tutelage. As I move onto the next chapter of my career, I hope to create as nurturing an environment as Markita has done for me.

Thank you to the Landry Lab, both past and present, for being an incredibly vibrant environment to work in. Thank you to Gözde Demirer, Rebecca Pinals, and Jeff Wang for being incredible mentors who I've had the pleasure of learning from. Your passion, dedication to science, and patience continue to inspire me. To the Landry Lab of the past: Abraham Beyene, Linda Chio, Gözde Demirer, Darwin Yang, Rebecca Pinals, Gabriel Dorlhiac, Huan Zhang, Travis Del Bonnis O' Donnell, Younghun Sung, Sanghwa Jeong, and Ian McFarlane, thank you for playing an active role in building the Landry Lab to what it is today. I'll miss our happy hours, bike rides, and board game nights. To Sarah Yang and Frankie Cunningham, I appreciate that I had you two to push through prelims and quals together. I'll miss Chris Jackson, my ever smiling and supportive partner in industry collaborations. Thanks also to Alison Lui, Nicole Navarro, and Jeff Wang for being my rock-solid sounding boards for both life and scientific advice. To the current Landry Lab, I'm looking forward to the lab culture you'll cultivate and all the amazing work you'll be doing! Thank you also to my undergraduate mentees, Kenny Celis and Kaushik Seshadri, who have spent countless hours at the bench working on various projects that stretched your patience and knowledge.

Thank you to Carlet Altamirano, Sigrid Allen, and Ruby Nelson for the administrative (and emotional) support over the years. I've always looked forward to catching up with Carlet in Gilman and absconding with some chocolate to get me through the day. Thank you to the Foundation for Food and Agriculture Research (FFAR) for funding my research. In particular, a big thank you to Rebecca Dunning, the 2019-2022 FFAR Fellows, and my writing group (Maria Gannett, Gwen Donley, and Lovepreet Singh) who have made this program so special. I have been blown away by the diversity of research we do and the immense passion with which you pursue scientific questions. More than that, I have received so much comfort and support within this cohort that I could not imagine doing without. You all continue to inspire me to be a passionate scientist who create a nurturing and brave environment. I look forward to continued reunions over the years.

Graduate school has had its ups and downs, and I've had the support of many friends along the way. Kara Fong and Lori Kaufman led me through my first semester of graduate school classes; I've missed our homework groups and boba breaks. Thank you to the San Pablo house in all of its iterations: Kara Fong (current and future research rock star), Sarah Yang, David Brown, Julie Fornaciari, Wyatt Ochs, Mike Gerhardt, and Isaac Zakaria. There's no one else I'd rather be spending lockdown with watching Avatar: The Last Airbender and having house dinners with amidst a pandemic. To the Rose St house – thanks for welcoming me with open arms to watch women's soccer or going on walks, bike rides, and finding sweet treats. Friends near and far who

I've kept up with over the years – Team WACK (Will, Alex, Caroline, and Kate), Da Gangzz (Elaine, Jinni, JoYip, Yifeng, Linn, and Viv), Shenanigans (Ali, Colleen, Katherine, Kate, Anna, and Susan), and Amy Penick – thank you for your companionship despite my consistent absence in virtual or in-person meetups. Thank you also to friends from Cornell who have trooped through graduate school with me: Robert Lee, Linnette Teo, Brielle Hohne, Aditya Misra, and Justine Lee.

To my family – Pua Siew Cheng, Amanda Goh, and Vanessa Goh, thank you for supporting me in pursuing my interests. To my mother in particular – we may not always see eye-to-eye but thank you for always being there when I need you. I appreciate you giving me the freedom and the means to explore my own path, even though it's taken me away from home for the past 9 years. I feel incredibly lucky to have had a mother who has worked so hard to make sure we are not in want of anything, and who has planned far ahead to make sure we are in good stead even when you are not around. Thanks to Isaac Berkowitz for being a pillar of support in times of stress (rarely am I ever not stressed) and for the delicious home-cooked meals you've made that are garlic- and onion-free. I cherish the Yosemite adventures we've had and look forward to planning more. Thank you to Alan Berkowitz and Miriam Straus for your friendship and I cherish our shared love for word games; I look to both of you as prime examples of having built careers where you truly love what you do. I hope to do the same.

I grew up not knowing what a Ph.D. was, being told that there were three paths to a good life: become a doctor, lawyer, or accountant. I believed there *had* to be more than those paths to happiness and, with naïve determination, flew halfway around the world to study Chemical Engineering at Cornell University. I learnt about doctorate degrees in college, and only considered pursuing a Ph.D. in my Junior year. I decided to pursue a Ph.D. because I wanted a 'safe space' to learn, grow, make mistakes, and grow into an independent thinker. I feel incredibly lucky to have landed in the Landry Lab, where I have learnt so much and met amazing colleagues and mentors who continue to challenge and inspire me. Though cliché, the adage 'it takes a village' rings true. I have only gotten to where I am because of support and assistance from countless people. As I continue my scientific journey, I hope to maintain a passion for learning and take an active part in cultivating a constructive environment for others to grow as well.

1 Introduction

1.1 Challenges in Food and Agriculture

The global food system is stark in its scale and complexity – valued at $10 trillion a year, it has grown into a highly interdependent network of producers, distributors, consumers, and other stakeholders and drives a large proportion of economic trade and resource use[1]. Despite its contribution to the global economy, the development and rapid growth of this food system has perpetuated a host of undesirable humanitarian and environmental impacts. This, along with increasing pressures on food production stemming from population growth and climate change, necessitates urgent changes in the food system to ensure needs are met.

Global population growth is putting pressure on existing food systems boost yields or increase production scales. The global population is expected to grow from 7.9 billion in 2022 to 10.8 billion in 2100, representing almost a 37% increase. Furthermore, as incomes in developing countries grow, demands for more resource-intensive products such as meat, dairy, and seafood are projected to grow as well. The food system needs to expand to increase production as well as grow to meet consumer demand.

Climate change and pest and pathogen proliferation pose a challenge to driving up supply to match demand. Largely attributed to human activity, climate variations comprise of but are not limited to heat waves, droughts, rising sea levels, and marked changes in precipitation levels and patterns. These climate changes have direct and drastic impacts on agriculture, resulting in heat and water stresses that are detrimental to yield. Additionally, specialization has led to the proliferation of monocultures which are far more susceptible to pest and pathogen spread[2]. Altogether, agricultural intensification and environmental changes from human activity have shaped a food system that may lack the robustness needed to meet growing demand.

Furthermore, global food systems are operating at a magnitude where continuous expansion of land and increases in resource use are neither possible nor sustainable. Approximately half of the habitable land around the world is used for agriculture, in addition to agriculture accounting for almost 70% of freshwater usage[3,4]. We can no longer proportionally increase land and water usage to increase production quantities. Additionally, agricultural processes contribute to a fourth of global greenhouse gas emissions, which in turn impacts climate variations[5]. Notably, we are increasingly facing resource limitations; repeated intensive land usage without adequate regeneration practices also depletes crop yield and harms soil health over time, limiting production capabilities. Freshwater availability is also increasingly limited[3].

The excessive use of chemicals such as pesticides, herbicides, fertilizer, and antibiotics in agriculture is detrimental to the environment and to human health. Pest and weeds contribute to high levels of yield loss, with pesticides, herbicides, and fertilizers added to combat these problems and increase yield. Despite their key role in ensuring a stable food supply, the widespread and repeated application of these chemicals has serious implications. They leach into their surroundings, resulting in pollution of groundwater and harmful effects on beneficial biota such as honey bees and birds[6,7].

Food and agricultural systems have led to the establishment of large-scale animal production facilities to increase production efficiencies. However, these production processes often involve placing animals in confined spaces, which is both unethical and detrimental to animal health. These living conditions and poor animal health are optimal breeding grounds for the spread of disease throughout the livestock population. A common approach to combating this is the use of antibiotics, whereby inappropriate use can result in the spread of pathogenic-resistant organisms that exacerbate antibiotic resistance issues in human health.

Our food system needs to expand to feed a growing population in a manner that is sustainable. However, unsustainable agricultural practices and resource limitations mean that it is unlikely for us to be able to achieve these goals. Drastic changes to the food system need to be made in order to prevent further environmental pollution, biodiversity loss, and inefficient resource usage.

1.2 Approaches to Addressing Agricultural Challenges

The environmental and resource issues present with the current food system have been studied extensively. In recent decades, there have been palpable shifts towards addressing these agricultural challenges in a multi-pronged manner. These approaches span behavioral changes and technological advancements, broadly including strategies to increase resource use efficiency, shifting human dietary patterns, and producing new crop varieties and alternatives to chemical use.

1.2.1 Increasing Resource Use Efficiency

Farming management strategies that aim to make the best use of limited resources such as land and nutrients are gaining traction. Healthy soils are essential to ensuring consistent crop yields and longevity of the land use. Soils are composed of minerals, organic matter, water, and air, and play host to a complex array of microorganisms known as the soil microbiome, which is heavily implicated with high crop productivity. Conventional tillage methods break up the soil and allow for the inclusion of fertilizers throughout the soil but can destroy the soil structure needed for microbiome growth and increase the likelihood of soil erosion. Studies have shown that minimum and reduced tillage practices can reduce soil erosion, thus prolonging the longevity of arable and productive land.

Fertilizer nutrient use efficiencies have been declining in recent decades, potentially due to overuse and high nutrient loss resulting from inappropriate timing and methods of fertilizer application[8]. Nanofertilizers, which can be formulated to induce gradual release of fertilizers over time, have been touted as a potential solution to increasing fertilizer use efficiencies without needing to perfectly time treatments. Other exciting developments in this space include novel products from companies such as Pivot Bio and Sound Agriculture which leverage microbial engineering and small molecule treatments to increase nutrient availability to crops, thereby reducing the need for fertilizer overuse.

The building of sustainable food systems in urban areas plays a key role in growing foods that are environmentally sustainable and healthy. Specifically, the use of urban spaces to grow food decreases the length of food supply chains, thereby minimizing resources dedicated to food transportation across long distances. Furthermore, urban food systems are shown to increase urban resident engagement with local food systems and have the potential to improve food access within urban areas[9].

1.2.2   Shifting Dietary Patterns

Diets that are highly plant-based and low in meat and dairy consumption are associated with lower greenhouse gas emissions and resource use. Livestock and animal products inherently require more resources to produce – land is needed to grow food to feed the livestock as well as for them to graze and water is needed over their lifetime. While producing 1 kcal of plant protein requires an input of approximately 2.2 kcal, energy inputs to obtain an equivalent 1 kcal of meat or dairy products are three to twenty times higher[10]. Transitioning dietary patterns towards increasing the proportion of plants in an average diet have a high potential to reduce the demand-side pressure on current food systems.

Certainly, preferences for meat and dairy are rising with increasing incomes in developing countries. Aside from social policies or educational initiatives aiming to shift dietary patterns to decrease meat and dairy consumption, there is a growing 'alternative protein' industry that aims to create novel substitutes to animal-based products with lower nutrient, water, and land footprints. In producing substitutes that closely replicate the behavior, taste, appearance, and texture of animal-based products, their goal is to shift consumers' dietary patterns towards more sustainable products without depriving their desire for meat and dairy products. In the last decade, investments in the alternative protein space have skyrocketed. Broadly split into three categories: plant-based, fermentation, and cultivated alternative proteins, this industry garnered $5 billion of invested capital in 2021[11]. Fueled by investments and consumer demand, alternatives to beef, eggs, milk, and countless other animal-based products have been entering the market in recent years by companies like Impossible Foods, Eat Just, and Nature's Fynd. The market for alternative protein products is expected to reach at least $290 billion by 2035 and compose 11% of the overall protein market[12]. This trend marks a promising movement towards creating alternatives to animal-based products that reduce resource usage and greenhouse gas emissions.

1.2.3   Engineering Novel Crops and Sustainable Alternatives

Advances in biotechnology have revealed new strategies to generating crops with desired traits – increased yields, increasing nutrient use efficiencies, and resistance to drought, heat, or disease. These strategies involve tuning gene expression to obtain desired phenotypes, which can be achieved in a transient or permanent manner. In ensuring heritable changes with successive generations of a crop, permanent changes in gene expression tend to be preferred. We further discuss trait engineering in **Chapter 1.3**.

Additionally, there are a growing number of companies seeking to create sustainable alternatives to products used in agriculture. GreenLight Biosciences, for instance, seeks to use double-stranded RNA formulations as a replacement for pesticides and fungicides in pest and fungal management. Central to the appeal of this technology is that (i) RNA formulations are designed to be specific to their target and will not cause harmful effects to humans upon exposure and (ii) RNA does not accumulate in the environment and instead degrades over time.

Despite all the technological-driven innovations and advancements we have discussed thus far, we also need to recognize that political will is a major player in ensuring food security and food system sustainability. Nutritional deficiencies and hunger are prevalent throughout the world despite levels of food production being sufficient to feed everyone on the planet. Technological changes can only go so far; issues with the food system ultimately need to be resolved by partnering

technology with infrastructural improvements in food distribution and social policies to ensure equitable food access.

1.3   Modulating Plant Gene Expression to Obtain Desired Traits[*]

Genetic engineering of crops has evolved to overcome limitations in traditional breeding, as breeding is slow, laborious and lacks precise control over plant genotype and phenotype generation. Modern biotechnology enables rapid development of crop variants with disease and pest resistance, stress tolerance, higher yield, and enhanced nutritional value. In this section, we discuss the fundamental principles of plant genetic engineering and genome editing and summarize the uncertain global regulatory landscape for genetically engineered crops.

1.3.1   Plant Genetic Engineering

Genetic engineering refers broadly to manipulating a cell's genome and gene expression profile. Techniques for genetic engineering may cause recombinant protein expression, up/down regulation of a gene, permanent gene knockout, targeted mutations in the host gene, or insertion of large foreign DNA segments into the host genome. Genome modifications may be transient, permanent, or heritable and involve many types of biomolecules - most commonly RNA, DNA, and proteins which are sometimes taken up passively by cells, but often require enhanced delivery techniques such as gene guns, microinjection, electroporation, sonoporation, nanoparticle-assisted delivery, and engineered bacteria or viruses. In plants, genetic engineering is hindered by the cell wall, requiring delivery methods that are highly host-specific or limited by challenges in plant regeneration. While protoplasts (unwalled plant cells) are also commonly used in genetic engineering, regeneration of treated protoplasts into a mature plant is highly time consuming and involves a series of complex steps.

1.3.2   Plant Genome Engineering

Nuclease-enabled genome editing refers to techniques where genes are removed or changed with engineered nucleases, a class of enzymes that perform targeted double-stranded breaks (DSBs) at specific locations in the host genome. When nucleases perform DSBs, the cell undergoes homology-directed repair (HDR) or non-homologous end-joining (NHEJ) to repair the cut. NHEJ is a random, error-prone repair process that involves realignment of a few bases such that the high error frequency provides a simplistic pathway for gene knockout. HDR is a non-random repair process requiring large stretches of sequence homology, allowing for precise edits by introducing customized homologous recombination sequences for gene knockout, knock-in, and targeted mutations. Prominent tools in genome editing are zinc finger nucleases (ZFNs), transcription activator-like effector nucleases (TALENs), and CRISPR (clustered regularly interspaced short palindromic repeat)-Cas (CRISPR associated) systems. In the 1990s, ZFNs became the first nuclease system engineered for selectable genome editing in bacteria[13]. TALEN and CRISPR-Cas genome editing systems were developed for bacteria and eukaryotes more recently, around 2009 and 2012, respectively[14–17]. Composed of protein complexes containing a DNA-binding domain and a DNA-cleaving domain, ZFNs and TALENs rely on protein/DNA recognition to induce endogenous DNA repair. CRISPR-Cas systems are composed of a nuclease protein (Cas) and a

---

[*] Portions of **Chapter 1.3 – 1.6** published as Cunningham, F.J.*, Goh, N.S.*, Demirer, G.S., Matos, J.L. and Landry, M.P., 2018. Nanoparticle-mediated delivery towards advancing plant genetic engineering. *Trends in biotechnology*, *36*(9), pp.882-897.

guide RNA (gRNA) with sequence homology to the genomic target, and therefore rely on the formation of a ribonucleoprotein (RNP) complex to induce HDR or NHEJ. While all three systems have their drawbacks, CRISPR-Cas has revolutionized the field of genome editing owing to its relatively superior simplicity, efficiency, and multiplexing ability (i.e. simultaneous editing of different genes) over ZFNs and TALENs.

1.3.3   Global Landscape of Regulatory Uncertainty Towards Genetically Engineered Crops

Since 1996, global Genetically Modified Organism (GMO) cultivation has increased 110-fold to 185 megahectares in 2016[18] (**Figure 1-1**). The U.S. is a leader in GMO production but highly regulates production of modified crops which poses, among other challenges, significant financial barriers to commercialization of new crop variants[19]. The U.S. GMO pipeline is product-based but sensitive to plant pests, such that *Agrobacterium* automatically triggers regulation while other methods of gene delivery are often deregulated if the product is non-transgenic[19,20]. European Union GMO regulation is process-based and affects any organism whose genome has been modified other than by mating or natural recombination[21], but includes exceptions for certain types of mutagenesis that will likely exempt modern gene editing[22].

The advent of nuclease-based gene editing has set forth a global reevaluation of the legislation surrounding genetically engineered crops, wherein several leading GMO cultivators have exempted non-transgenic genome-edited plants from regulation (**Figure 1-1**). However, due to differences in regulatory philosophy and public opinion, several countries oppose deregulation of non-transgenic genome edited plants and it remains unclear how enforcement of GMO status will proceed in the future[23]. Despite the heterogenous and dynamic global regulatory landscape, nuclease-based genome editing currently plays a critical role in overcoming regulatory restrictions and ensuring scientific progress as well as commercial implementation of engineered crop variants.
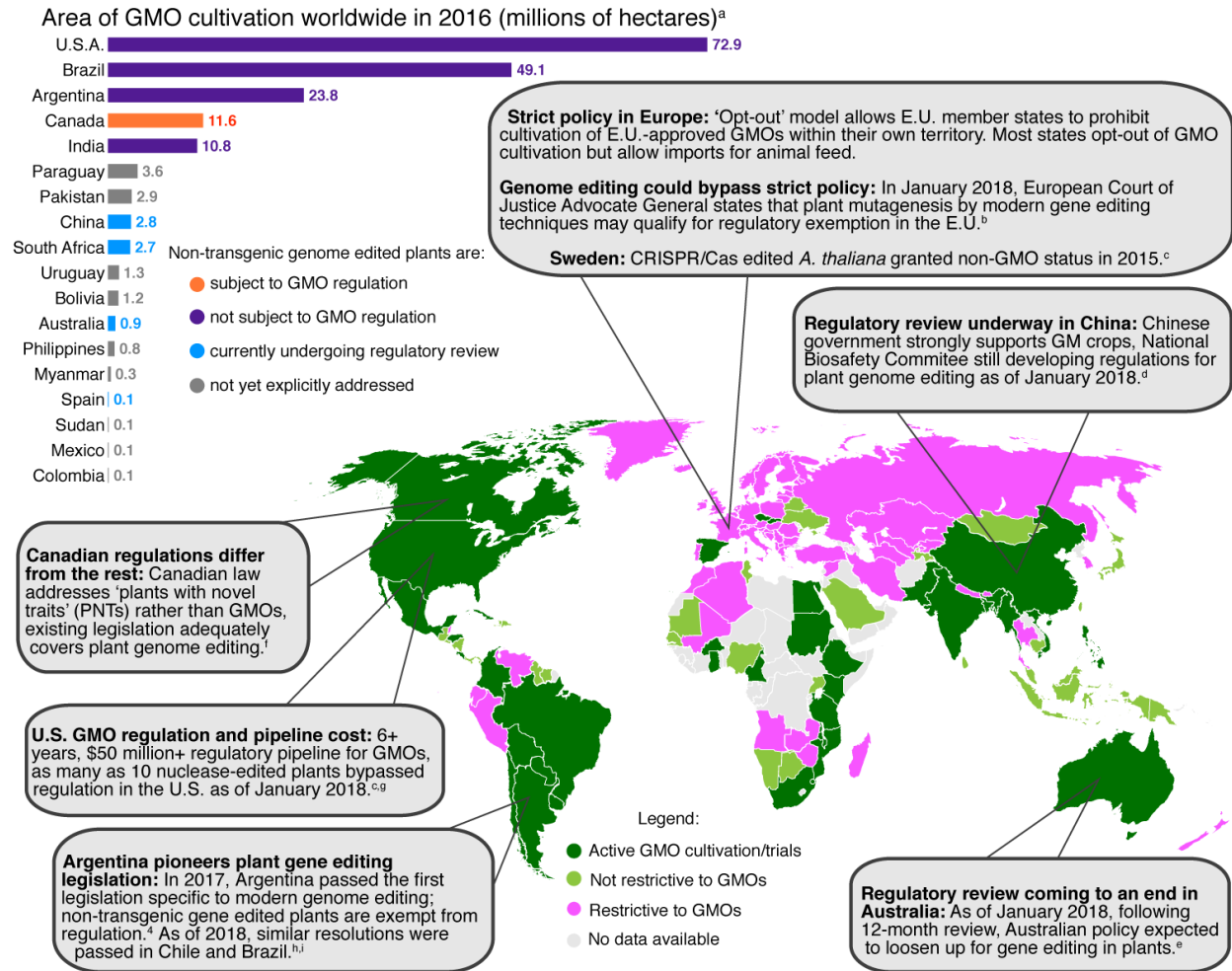
Figure 1-1. GMO cultivation and regulatory attitudes worldwide.
Despite a long, expensive regulatory pipeline, the U.S. is a leader for GMO cultivation worldwide, followed by Brazil and Argentina, with Argentina being the first to directly address modern genome editing techniques in GMO legislation. European and Australian regulatory attitudes are strict but have recently evolved as of January 2018, suggesting that regulations for genome edited plants will soon be relaxed in these regions. Nuclease-based edits without transgene integration escape regulation even in countries with large agricultural GMO industries and complex regulatory systems. [a18], [b22], [c23], [d24], [e25], [f26], [g27].

1.4 Traditional Delivery Methods for Plant Genetic Engineering

1.4.1 Agrobacterium-Mediated Delivery

Agrobacterium tumefaciens is a soil bacterium that infects a wide range of dicots**,** causing crown gall disease. The formation of a gall on the host plant is achieved via the stable transfer, integration, and expression of bacterial DNA in infected plants. Engineering of the *Agrobacterium* plasmid by substitution of the gall-inducing virulence genes with genes of interest confers the ability of *Agrobacterium* to transform the host plant. For this reason, *Agrobacterium* has been harnessed as a tool for plant genetic transformation since the early 1980s[28].

Genetic transformation occurs through a process involving T-DNA (transfer DNA) export, targeting, and insertion into the plant nuclear genome. The export of T-DNA from the bacterium to the plant cell is facilitated by the activity of virulence genes present in the tumor inducing-plasmid of *Agrobacterium* but are not themselves transferred. These virulence genes are expressed in the presence of phenolic inducers such as acetosyringone produced by wounded plant cells. *Agrobacterium* attaches to plant cells, where border sequences on either side of the T-strand (a single-stranded copy of the T-DNA sequence) are cleaved. The T-strand is then carried by a transporter with a nuclear localization sequence and integrated into the plant nuclear genome. Integration occurs at random positions in the genome via non-homologous recombination (NHR), a repair pathway for double-stranded breaks in DNA.

1.4.2   *Biolistic Delivery*

A form of biolistic particle delivery (also called particle bombardment), the gene gun is a physical method that is commonly applied for plant genetic transformations. Developed in 1982 by Sanford et. al[29], the process involves gold or tungsten microparticles (or microcarriers) coated with genetic cargo that are accelerated by pressurized helium (He) gas into plant cells, rupturing cell walls and membranes. The gene gun consists of three main parts: a rupture disk, macrocarrier (holding microcarrier particles), and stopping screen. The rupture disk is a membrane designed to burst at a critical pressure of He gas. When He gas is accelerated to the desired pressure, the rupture disk bursts, creating a shock wave that propels the macrocarrier towards the plant cells. The macrocarrier's momentum is stopped by the stopping screen, which allows genetic cargo-loaded microcarriers to pass and enter the plant cells.

Unlike *Agrobacterium*-mediated transformation, biolistic delivery can result in transformation of the nuclear, plastidal, or mitochondrial genomes due to the nonspecific localization of genetic cargo. Consequently, more DNA needs to be delivered with biolistic delivery than agrobacterium-mediated delivery when targeting the nuclear genome.

1.4.3   *Limitations of Current Methods for Plant Biomolecule Delivery*

Current biomolecule delivery methods to plants experience challenges that hinder their scope of use (

Table 1-1). Methods such as electroporation, biolistics, *Agrobacterium*-mediated delivery, or cationic delivery typically target immature plant tissue (protoplasts, calli, meristems, or embryos) and require the regeneration of genetically modified progeny plants, which can be time-consuming, challenging, and efficient protocols have only been developed for a narrow range of plant species. Biolistic particle delivery circumvents the cell wall via mechanical force, but often damages portions of target tissue in the process and causes low levels of gene expression modulation that is sparse and sporadic. *Agrobacterium*-mediated delivery is subject to orthogonal challenges, the largest of which being that *Agrobacterium* displays narrow host and tissue specificity, even between specific cultivars of the same species[30]. *Agrobacterium* generally experiences lower transformation efficiency for both delivery and regeneration in monocotyledonous plants (monocots) over dicotyledonous plants (dicots). Additionally, *Agrobacterium* yields random DNA integration, which can cause disruption of important genes, or insertion into sections of the genome with poor or unstable expression[31]. Random DNA integration, however, can be prevented by utilizing magnifection with non-integrating viruses[32], or by using a plasmid deficient in T-DNA insertion[33].

Plant genetic engineering has lagged behind progress in animal systems; conventional methods of biomolecule delivery to plants remain challenged by intracellular transport through cell walls, and in turn limit plant genetic transformation efficacy. To date, plant biotechnology lacks a method that allows passive delivery of diverse biomolecules into a broad range of plant phenotypes and species without the aid of external force and without causing tissue damage. We posit nanotechnology as a key driver in the creation of a transformational tool to address delivery challenges and enhance the utility of plant genetic engineering.

Table 1-1. Scope of use summary for plant biomolecule delivery methods.

Delivery Method	Adverse Effects of Delivery	Target Species/ Tissue	Cargo Type and Size	Limitations
Physical				
Biolistic Particle (Gene Gun) Mediated Delivery	Damage to target tissue & cargo, low penetration depth, random integration	Depends on tissue type[+]/ Calli, embryos, leaves	DNA, siRNA, miRNA, ribonucleoproteins (RNPs), large cargo size	Targeting leaves requires detachment from plant which limits time to observe delivery effects; targeting embryos requires laborious regeneration protocols whose effectiveness is highly species/cultivar-dependent
Electroporation	Damage to target tissue, nonspecific transport of material through pores may lead to improper cell function	Unlimited/ Protoplasts[^], meristems, pollen grains	Nucleic acids (DNA, siRNA, miRNA)	Limited cargo carrying capacity
Chemical				
Polymer-Mediated Delivery	High charge densities induce cytotoxicity	Species amenable to protoplast regeneration/ Protoplasts[^]	Nucleic acids (DNA, siRNA, miRNA)	Regeneration is highly inefficient for most species in transient studies and requires tissue culture
Biological				
Agrobacterium	Can lead to apoptosis and necrosis, random	Narrow range of plant species, esp.	Limited to DNA, large	Leaf-targeted delivery is transient and gene edits are not transmitted to progeny,

Mediated Delivery	integration	restricted from monocots[#]/ mature plants, immature tissue, protoplasts	cargo size	but allow diverse biological studies; requires tissue culture (except Arabidopsis) to generate progeny; exhibits high host-specificity
Viral Delivery	Virus integration (can be mitigated by using non-integrating viruses)	Host plant species restrictions/ Mature plants, meristems	Nucleic acids (DNA, siRNA, miRNA), very limited cargo size	Highly limited cargo carrying capacity

While most biomolecule delivery methods to plants can deliver a variety of gene editing reagents, DNA plasmids are arguably the most common cargo of interest; DNA loading capacities are a useful metric for the upper limit for cargo sizes each method can sustain.

+While biolistic particle mediated delivery can theoretically be utilized in unlimited target species, the ability to target species depends on the target tissue (by extension, cell wall structural strength) and capability of available equipment

^ The use of protoplasts as target tissue necessitates regeneration protocols and progeny segregation that are time-consuming and in addition challenged by the limited plant species amenable to protoplast regeneration.

#Progress has been made on increasing transformation efficiency in recalcitrant monocots[34].

1.5 Nanoparticle Usage in Plant Systems

1.5.1 Nanoparticles[†]

Nanomaterials are traditionally defined as materials with at least one dimension measuring under 100 nm, whereby the reduced size can confer unique physical, chemical, and biological properties to the material compared to its bulk counterpart [35]. Because of their unique and tunable properties, nanomaterials have enabled numerous novel applications in the fields of energy and electronics[36,37], medicine and healthcare[38,39], biotechnology[40] and agriculture[41]. Specifically, nanomaterials have engendered the field of bionanotechnology – the intersection of biology and nanotechnology in which nanotechnology is applied to fields such as medicine, molecular biology, synthetic biology, biochemistry, and agriculture. Several sub-fields of bionanotechnology, such as nanomedicine, have leveraged nanomaterials for the development of drug delivery systems that can deliver drugs to specific cells using nanoparticles, thus lowering overall drug consumption and side-effects. Similarly, but more recently, nanomaterials have begun to advance plant science and agriculture through the usage of engineered nanoparticles that serve as nano-carriers, containing herbicides, fertilizers, chemicals, or genes, which target particular plant parts to release their content[42]. Additionally, many studies report that certain nanoparticles also facilitate plant growth and overall plant health[43–45].

In addition to their high degree of tunability, NPs possess several advantages that validate their widespread use, with particular emphasis in the biomedical industry. Most NPs can be prepared with consistent properties for low batch-to-batch variability, and can be designed to target biological systems, tissues, cells, or sub-cellular structures with high specificity[46]. Moreover, NP-mediated gene and drug delivery can overcome common issues faced with viral vectors; NPs are less immunogenic and oncogenic, and can carry diverse and much larger cargo, although the increased NP sizes raise the challenge of bypassing biological barriers[47]. Furthermore, the effects of NP use have yet to be thoroughly studied, though existing research points to size and dose-dependent cytotoxicity as a potential source of toxicity[48,49].

NPs are typically classified based on morphology and chemical properties. The most common categories include polymeric[50], lipid[51], magnetic[52], metallic[53], and carbon-based NPs[54] (**Figure 1-2**). NPs can be synthesized with either a top-down or bottom-up approach using techniques such as lithography[55], deposition[56], and self-assembly[57].

PARTICLE SIZE SCALES

BIOLOGICAL SIZE SCALES
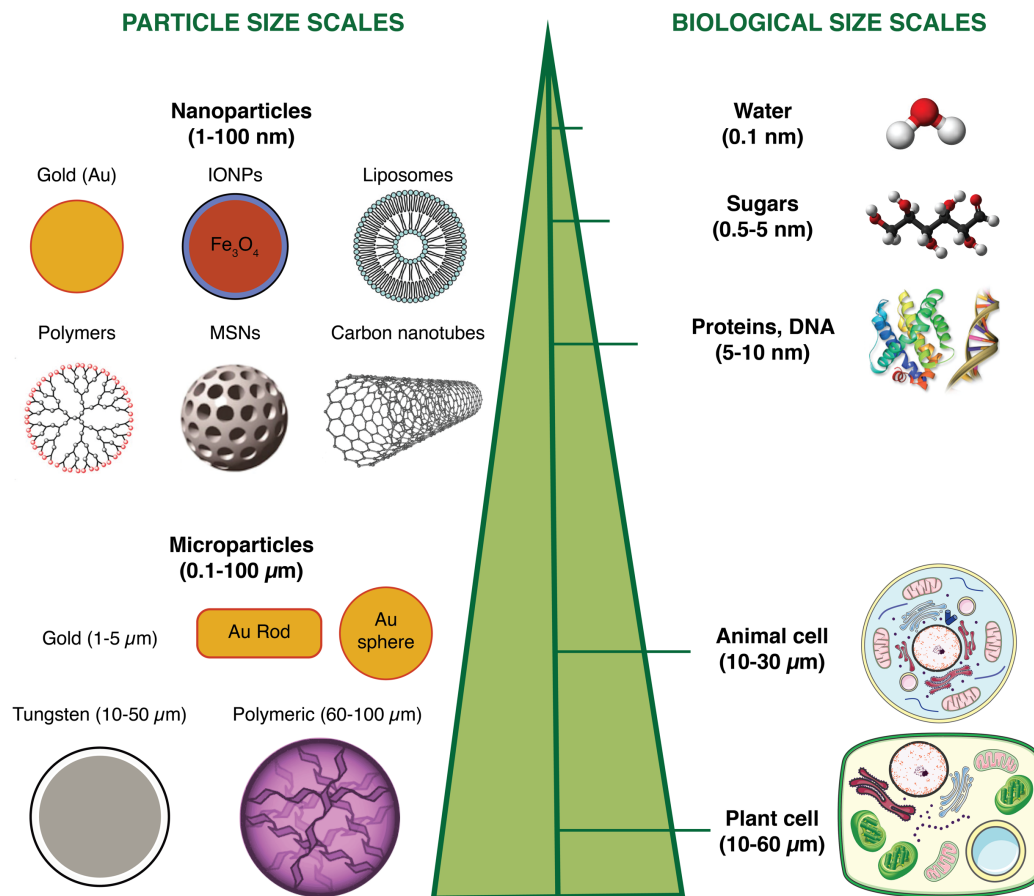
Figure 1-2. Scale comparison of engineered materials with biological components.

1.5.2 Nanoparticles as Delivery Vehicles

Nanotechnology has advanced a variety of fields including manufacturing, energy, and medicine. Of particular interest is the use of nanoparticles as molecular transporters in cells, an area that has largely focused on molecular delivery in animal systems. Nanoparticles allow manipulation on a subcellular level, giving rise to a previously unattainable degree of control over exogenous interactions with biological systems. Increasingly, nanoparticles have been seen as promising vehicles in plant systems as well for the delivery of biomolecules (further discussed in **Chapter 1.6**), pesticides, and fertilizers.

Nanopesticides and nanofertilizers leverage the tunability of nanoparticle properties to help increase the use efficiency of pesticides and fertilizers, thereby reducing the total quantities of chemical pesticides and fertilizers applied. This not only decreases farming costs but also serves to limit excessive chemical application and unintended runoff. Generally, pesticides and fertilizers are encapsulated within or mixed with the core structure of the nanoparticle, enabling a slow and controlled release of active ingredients over time. The use of various materials in nanopesticides and nanofertilizers has been well-studied and covered more extensively in review articles[58].

1.5.3   Nanoparticles as Sensors

Agricultural practices are innately demanding of resources such as land, water, and fertilizer. However, variability across field conditions means that resources are often under- or over-applied, leading to either decreased yield or excessive agrochemical usage. One approach to account for this variability is precision agriculture, which involves gathering site-specific data on crop and soil conditions that can be used to improve resource allocation. In particular, nanoparticle-based sensors can be used to gather agroecological data including pesticide accumulation and heavy metal and plant pathogen detection. Leveraging the innate physicochemical properties of nanomaterials, these sensors can be designed for highly sensitive, specific, and reproducible measurements of a target analyte. The scope and practicality of nanosensor use will be further covered in **Chapter 5**.

1.5.4   Nanoparticles as Growth Stimulants

Nanomaterial interactions with plants have been studied in the context of generating inexpensive materials for growth stimulation. Though the mechanism through which this happen is not well understood, nanoparticles such as multi-walled carbon nanotubes, silicon dioxide, and titanium dioxide have stimulated seed germination upon application[59–61]. Additionally, amongst others, carbon-based nanomaterials and silver nanoparticles have been shown to induce beneficial effects on shoot growth as measured by length and weight[62,63]. Certainly, these effects are highly dependent on concentration, site of introduction, surface charge, and plant species[64]. An excessive introduction of nanomaterials can also result in detrimental effects on the plant, which motivates prudent use of nanoparticles in this manner. Notably, we have yet to achieve a strong understanding of nanomaterial-plant interactions and the accumulation and fate of nanoparticles in plants, which continues to limit practical usage in field applications.

1.6   Nanoparticle-Mediated Delivery

1.6.1   Nanoparticle-Mediated Biomolecule Delivery in Animal Systems

The small size of nanoparticles and their highly-tunable chemical and physical properties have enabled nanoparticle engineering to bypass biological barriers and even localize in sub-cellular domains of CHO and HeLa cells, among others[65–68]. Nanoparticles serve as non-viral, biocompatible, and non-cytotoxic vectors that can transport a range of biomolecules (small molecules, DNA, siRNA, miRNA, proteins, and RNPs)[69–74] to biological cells. To this end, various features of nanoparticles including size, shape, functionalization, tensile strength, aspect ratio, and charge have been tuned for efficient intracellular biomolecule delivery to animal systems. Furthermore, "smart" nanoparticles have been developed to achieve responsive release of cargo for increased control of site-specificity[75]. Various NPs have been manufactured and are responsive to a range of stimuli, including temperature[76], pH[77], redox[78], and the presence of enzymes[79].

1.6.2   Bridging Nanoparticle Usage from Animal Systems to Plants

In contrast to the proliferate studies demonstrating nanoparticle-mediated delivery in animals, analogous research in plants is relatively sparse (**Figure 1-3**), owing to the transport challenge imposed by the plant cell wall which renders biomolecule delivery more challenging than for most mammalian systems. Nevertheless, knowledge gained from biomolecule delivery to animals provides a blueprint for translation to plant systems and could accelerate advancements in NP-mediated plants biomolecule delivery. Nanoparticle-mediated delivery may overcome the three foremost limitations of current delivery techniques in plant systems by controlling NP size to

traverse the cell wall, tuning charge and surface properties to carry diverse cargo, and greater breadth in utility across plant species.

Nanoparticle-mediated delivery in animals have successfully carried many types of cargo indiscriminately, unlike methods for plants such as *Agrobacterium*, which can only deliver DNA. For instance, Wang and colleagues report nanoparticle-mediated RNP delivery via lipid encapsulation[80]. Additionally, plastid engineering is not achievable with *Agrobacterium*, which only targets the plant nuclear genome and cannot target the chloroplast or mitochondrial genomes. Conversely, targeting moieties can be attached to NPs to obtain subcellular localization and modification of the desired genome. Hoshino and coworkers demonstrate the delivery of quantum dots to the nucleus and mitochondria of Vero cells using respective localizing signal peptides[81]. Active targeting and controlled release is not achievable with conventional plant biomolecule delivery methods, but has been demonstrated in animal systems with NP-based delivery: Davis and colleagues designed a polymeric NP with a human transferrin protein targeting ligand and polyethylene-glycol (PEG) on the NP exterior to deliver siRNA to human melanoma tumor cells specifically[70], while Lai and coworkers studied stimuli-responsive controlled release of drug molecules and neurotransmitters encapsulated within mesoporous silica NPs (MSNs) to neuroglia cells[82]. Drawing inspiration from progress in NP-mediated delivery for animal systems, NP-mediated controlled delivery and release of biomolecules without species limitations in plants is a forthcoming goal.

(a) NPs classes commonly employed in genetic cargo delivery

Bio-Inspired NPs
· Calcium phosphate
· Chitosan
· Liposomes

Genetic Cargo Delivered (a)-(d)
DNA   RNA   Protein   RNP

Genetic cargo has been delivered in:
- Both animal and plant systems
- Animal systems only
- Plant systems only
- Neither system

Metallic / Magnetic NPs
· Gold
· Silver
· Iron Oxide

Genetic Cargo Delivered (t)-(x)
DNA   RNA   Protein   RNP

Carbon-Based NPs
· Single-walled carbon nanotubes
· Multi-walled carbon nanotubes
· Fullerenes

Genetic Cargo Delivered (e)-(g)
DNA   RNA   Protein   RNP

Silicon-based NPs
· Silica spheres
· Mesoporous silica NPs (MSNs)
· Silicon carbide

Genetic Cargo Delivered (h)-(k)
DNA   RNA   Protein   RNP

Polymeric NPs
· Polyethylene-glycol (PEG)
· Poly(lactic-co-glycolic acid) (PLGA)
· Polyethylenimine (PEI)

Genetic Cargo Delivered (l)-(s)
DNA   RNA   Protein   RNP

(b) Modes of NP-mediated cargo delivery

Biolistic
Electroporation / Sonoporation / Optoporation
Magnetofection
Microinjection
Cationic Transfection
Incubation
Infiltration
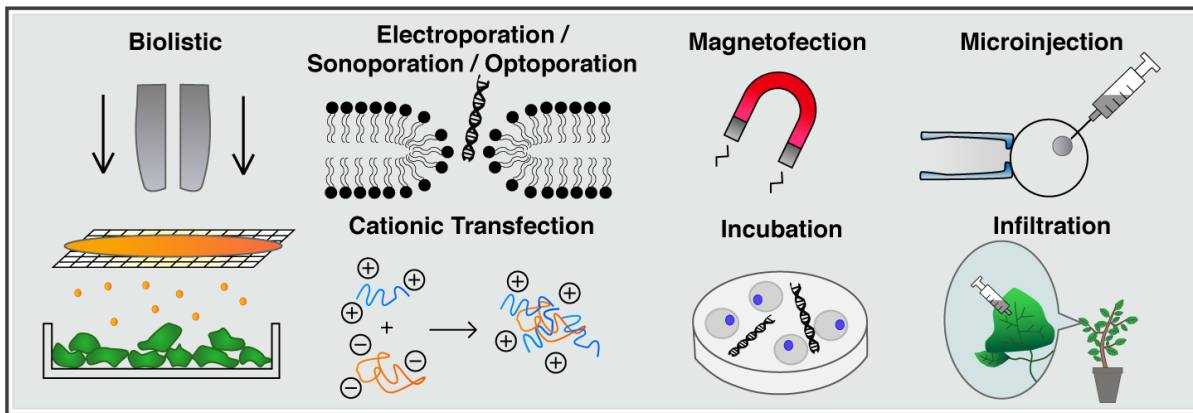
Figure 1-3. NP-mediated genetic cargo delivery to animals and plants.
a Nanoparticles that are commonly used in both animal and plant systems cover five major categories: bio-inspired, carbon-based, silicon-based, polymeric, and metallic / magnetic. We provide a visual comparison of delivery of various genetic cargo (deoxyribonucleic acid (DNA), ribonucleic acid (RNA), proteins (site-specific recombinases or nucleases), and ribonucleoprotein (RNP)) with each of the five NP types across animal and plant systems. It is evident that NP-mediated delivery has been utilized with a greater variety of genetic cargo in animals than in plants. **b** NP-mediated cargo delivery is conducted via various means. Physical methods include biolistic particle delivery, creating transient pores in the cell membrane with electric fields, soundwaves, or light, magnetofection, and microinjection. Non-physical methods include cationic carriers, incubation, and infiltration. [a83], [b84], [c85], [d86], [e87], [f88], [g89], [h90], [i91], [j92], [k93], [l94], [m95], [n96], [o97], [p98], [q99], [r100], [s101], [t102], [u103], [v104], [w105], [x106]

1.6.3 Barriers to Biomolecule Delivery in Plant Cells[‡]

1.6.3.1 The Plant Cell Wall

While a complete structure-function landscape of physical and chemical NP properties that drive cargo loading and cellular internalization remains elusive, a heuristic approach to nanocarrier design is a useful starting point. NP uptake and transport throughout plant tissue is limited by pore diameters, setting size exclusion limits (SELs) for various tissues and organs that are discussed extensively in the literature. The cell wall is commonly thought to exclude particles >5-20 nm, although recently NPs up to 50 nm in diameter have been reported as cell wall-permeable through unclear mechanisms[107,108]. For genetic engineering applications, where cytosolic or nuclear localization is necessary to affect gene function, the plasma and nuclear membranes are additional barriers to delivery. In practice, the cell wall (SEL <50 nm) plays a dominant role in NP size limitations, as the cell membrane SEL is much larger (>500 nm)[108].

To effectively deliver biomacromolecules into a walled plant cell, the cargo and carrier must bypass two main key barriers: the plant cell wall, and the plasma membrane. Plant cells are surrounded by an extensive network of biopolymers knitted together to form a multilamellar matrix hydrogel cell wall that restricts access to the plasma membrane[109]. Generally, NP uptake and transport through plant tissue is limited by pore diameters, setting size exclusion limits (SELs) for various tissues and organs that are discussed extensively in the literature[107,108,110–114]. The size exclusion limit (SEL) of the cell wall has been probed using a number of methods including gas adsorption[115], topographical EM studies[116,117], and uptake of dye-labeled nanoscale materials of defined sizes[118,119]. Although uptake of some large 100-nm NPs in walled plant cells has been reported[120,121], evidence suggests a sub-10 nm or 100-kDa protein SEL. Diffusion remains the widely-accepted mechanism through which NPs are purported to bypass the cell wall to access the plasma membrane, though it remains unclear how NPs near or above the SEL of the cell wall access the symplast. However, without greater evidence, we cannot discount biotransformation and subsequent *in situ* particle genesis or injurious application methods such as tissue infiltration[122,123] as being the source of detected NPs above the SEL.

A major impediment to overcoming the cell wall challenge is the over-reliance on diffraction-limited fluorescence microscopy in assessing exogenous particle internalization. The presence of the thin symplast pressed against the perimeter of the plant cell, coupled with the diffraction limit of visible light (~200-nm), makes it difficult to distinguish whether fluorescent signals originate from the symplastic or apoplastic region of the plant cell. Additionally, fluorescent labels often overlap with emission wavelengths of endogenous plant autofluorescence. It is possible to address this via plasmolysis induction[124–126] to increase cytosolic visualization or by using super-resolution microscopy, though both approaches have their drawbacks–plasmolysis induces drastic morphological changes in cells, and super-resolution microscopy requires specialized equipment and expertise.

1.6.3.2 Membrane Penetration and Endosomal Escape

Upon passing the cell wall, nanomaterials have been suggested to enter the symplast via a variety of mechanisms including endocytosis[127], plasmodesmata[128], or physical disruption[129] (**Figure 1-4**). However, the majority of these studies have been performed in suspension cells, which do not recapitulate tissue structure and have been reported to possess half-plasmodesmata that exposes the cell membrane to the extracellular environment[130]. The most investigated mechanism for cellular uptake of NPs is endocytosis. Clathrin-mediated endocytosis has been identified as the dominant endocytic process in plant cells and appears to operate analogously to animal cells[131]. Most examples of NP uptake in walled plant cells do not leverage specific pro-endocytic motifs. Instead, studies take advantage of the natural tendency of NPs to trigger endocytosis; thus, it remains unclear whether NP functionalization with a cell-penetrating domain would enhance their cellular entry in plants.
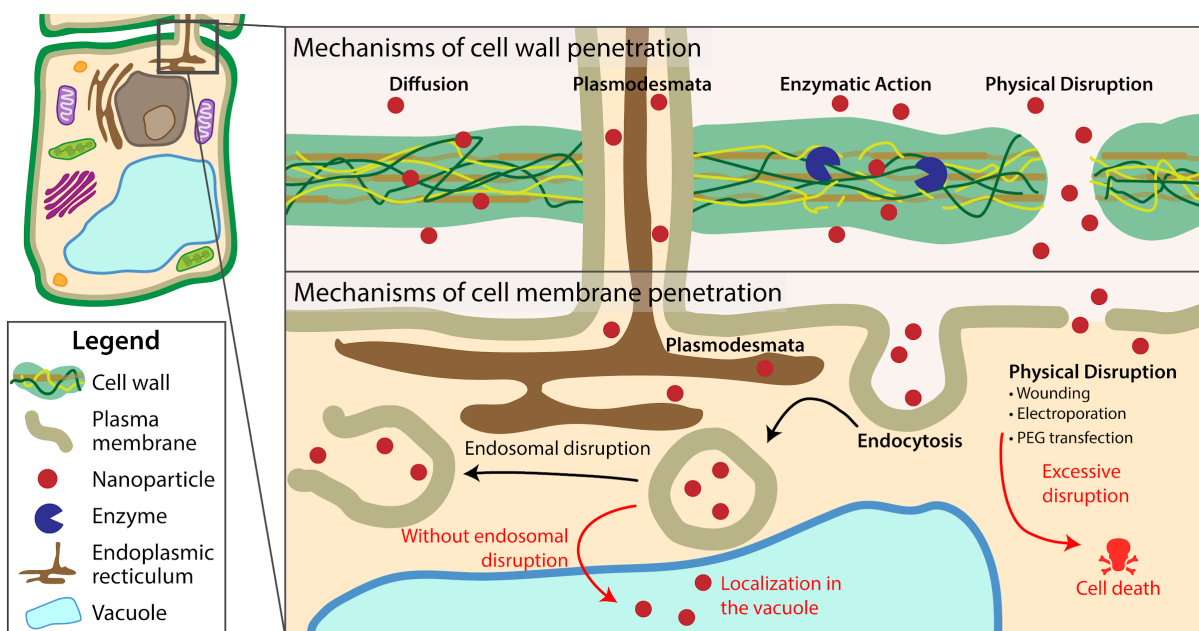
Figure 1-4. Overview of mechanisms of nanoparticle penetration through cell walls and cell membranes.
Nanomaterials (red circles) might bypass the cell wall by diffusion, by entering through existing plasmodesmata transport channels, or by harnessing chemical or physical disruption strategies to increase the wall size exclusion limit[128,129,132,133]. Penetrating cell membranes may similarly occur by utilizing the plasmodesmata, inducing endocytosis, or transient or permanent physical disruption of the membrane[127–129]. Endosomal escape must occur after endocytosis to evade sequestration into lytic organelles.

Upon endocytosis, delivered materials must escape the endosome. Without a method to escape the endosome, endocytosed materials are sequestered into lytic organelles such as the central vacuole or lysosomes and are consequently destroyed[134]. In mammalian systems, polycationic polymers, cell-penetrating peptides (CPPs), or other chemical agents delivered in concert with the cargo have proven successful for cytosolic delivery[135–137]. Despite practical successes, the mechanism through

28

which polycation-mediated endosomal disruption occurs is still under debate[138,139], and it remains unclear if endosome-disrupting tools can be translated for use in plant systems. However, some reports of cytosolic delivery of nucleic acids and proteins using polycation-rich polymers exist in plants[140,141]. For example, recent work by Liu and coworkers used a commercially available cationic lipid formulation to deliver Cas9 RNP to *Nicotiana* protoplasts[142].

1.6.4 Nanomaterials for Plant Genetic Engineering

To date, most literature on NP-plant systems focuses on plant-based metallic nanomaterial synthesis[143], agrochemical delivery[144], and NP uptake showing both valuable and deleterious effects on plant growth[114,145]. Dicot and monocot plants exhibit variable degrees of direct uptake of many NP types, including mesoporous silica NPs (MSNs)[146], carbon nanotubes (CNTs)[147], quantum dots[148], and metal/metal oxide NPs[149–151]. Once taken up, certain types of NPs exhibit phytotoxicity via vascular blockage, oxidative stress, or DNA structural damage[114]. Conversely, NPs have been shown to improve root/leaf growth and chloroplast production[145]. Tradeoffs between phytotoxicity and growth enhancement as a function of species, growth conditions, NP properties, and dosage are not well-understood and call for more studies with a focus on nanoparticle physical and chemical properties. Closing the knowledge gap in plant physiological response to NP uptake is important and should be pursued in parallel with the enhancement of plant science using engineered nanomaterials, as the 'nanorevolution' in targeted delivery to animals suggests tremendous potential for analogous progress in plants.

NPs are valuable materials for intracellular biomolecule delivery owing to their ability to cross biological membranes, protection and release of diverse cargoes, and multifaceted targeting via chemical and physical tunability. Such properties have enabled NPs to revolutionize targeted delivery and controlled release in mammalian systems. However, nanocarrier delivery in plants remains largely underexplored due to the cell wall, which is typically overcome by chemical or mechanical aid. Passive biomolecule delivery to plants is promising for minimally invasive, species-independent *in vivo* genetic engineering of plants, especially for transient expression in somatic tissue (**Table 1-2**). The potential of NP-based plant delivery methods is underscored by the limitations of *in vitro* plant studies in general, wherein regeneration capacity varies widely across species, genotype, and even within a single plant depending on developmental age of source tissue[152]. Currently, stable transformation requires progeny regeneration from embryogenic calli regardless of the delivery method (**Table 1-2**). Thus, parallel optimization of delivery and regeneration is necessary to improve efficiency and expand stable transformation capabilities to all plant species.

Table 1-2. Challenges in plant genetic engineering and proposed advantages of NP delivery.

Desired outcome	Non-heritable* (somatic/transient expression)			Heritable (germline/stable transformation)	
Targeted tissue	Leaves	Roots	Protoplasts	Zygotic embryo	Somatic embryogenic calli
Tissue-specific biological and experimental challenges	• Cell wall • Inefficient cellular uptake • Epidermal barrier	• Cell wall • Inefficient cellular uptake	• Cell wall degradation protocol • Inefficient cellular uptake	• Cell wall • Inefficient subcellular localization • Embryo collection/ calli induction • Calli regeneration	• Cell wall • Inefficient subcellular localization • Totipotency/ calli induction • Calli regeneration
Proposed advantages of NP-delivery	• NP-cell wall permeability • NP-stomata permeability [120] • Anionic NPs root-to-shoot vascular translocation [153] • Passive uptake or direct mesophyll injection without gene gun or protoplasts • Tunable NP properties and ligands for subcellular targeting	• NP-cell wall permeability • Cationic NP root accumulation [153] • Passive uptake without gene gun or protoplasts • Tunable NP properties and ligands for subcellular targeting	• Tunable NP properties and ligands for subcellular targeting	• NP-cell wall permeability • Tunable NP properties and ligands for subcellular targeting	• NP-cell wall permeability • Tunable NP properties and ligands for subcellular targeting

While these somatic tissues (leaves, roots, protoplasts) are most commonly targeted for transient expression experiments, heritable outcomes may be derived from them through somatic embryogenesis (dedifferentiation of somatic tissue).

In 2007, Torney and colleagues were the first to demonstrate NP delivery of DNA and chemicals to *Nicotiana tabacum* plants via biolistic-delivery of 100 – 200 nm gold-capped MSNs[91]. In this study, a chemical expression inducer was loaded into MSN pores (~3nm) that were subsequently covalently capped with gold nanoparticles. The capped MSNs were then coated with GFP plasmids and delivered by gene gun to *Nicotiana tabacum* cotyledons, wherein GFP expression was triggered upon uncapping and release of the expression inducer[91]. This seminal paper demonstrated proof of concept that strategies common for NP delivery of DNA to mammalian systems can be adapted to plants. Notably, gold-MSNs were also used for biolistic codelivery of DNA and proteins, namely GFP and Cre-recombinase, demonstrating the ability of MSNs to deliver proteins for gene editing[93]. Many delivery strategies still require a gene gun, electromagnetic field, or protoplast PEG-transfection[93,103,154–157] as NP structure-function parameters have not yet been fully optimized to bypass the cell wall (**Table 1-3**). However, for these systems where mechanical or chemical aid is necessary for internalization, the small size and high surface area of nanocarriers still offers superior performance over conventional methods. For instance, Torney and colleagues' pioneering MSN study achieved transgene expression with 1,000x less DNA than required by conventional PEG-transfection in protoplasts[91].

A few examples show promise for NP-mediated passive delivery to plants *in vitro*[83,158,159] and *in vivo*[160,161] in, for example, *N. tabacum* protoplasts[159] and *Arabidopsis thaliana* roots[160,161], respectively (**Table 1-3**). While many more studies are needed to optimize NP properties and functionalization, these early results are promising for further exploration of NPs as a plant biomolecule delivery platform that addresses shortcomings of conventional methods. Furthermore, with the advent of nuclease-based gene editing technologies, it is of great interest to optimize the delivery of these revolutionary genetic engineering tools by exploring NP-based delivery strategies for these diverse biomolecular cargoes.

Table 1-3. Select summary of NP-mediated genetic engineering in plants.

	NP type	Cargo	Plant Species; Cell/Tissue type	Delivery Method	Comments	Ref., Year
With external aid	Gold capped MSNs	GFP plasmid; chemical expression inducer	*N. tabacum* cotyledons; *Z. mays* embryos	Biolistic	Codelivery and controlled release of DNA and chemicals	[91], 2007
	Poly-L-lysine coated starch NPs	GFP plasmid	*Dioscorea zingiberensis C.H.Wright* calli suspension	Sonoporation	5% transient expression efficiency; some integration occurs	[155], 2008
	Gold-plated MSNs	GFP and mCherry plasmids; GFP protein	*Allium cepa* epidermis tissue	Biolistic	DNA and protein codelivery	[154], 2012
	Magnetic gold NPs	β-glucuronidase (GUS) plasmid	*Brassica napus* protoplasts and walled cell suspension	Magnetic field	Transient GUS expression	[156], 2013
	Gold-plated MSNs	AmCyan1 and DsRed2 plasmids; Cre protein	*Z. mays* embryos	Biolistic	DNA and protein codelivery; both transient and stable expression	[93], 2014
	Dimethylaminoethyl methacrylate (DMAEM) polymer NPs	Yellow fluorescent protein (YFP) and GFP plasmids	*N. tabacum* and *Ceratodon purpureus* protoplasts	PEG transfection	Both transient and stable expression	[157], 2017

21

	Magnetic Fe$_3$O$_4$ NPs	Selectable marker gene plasmids	*Gossypium hirsutum* pollen	Magnetic field	~1% efficiency for generating stable transgenic seeds	[103], 2017
***In vitro* without external aid**	Polyamidoamine (PAMAM) dendrimer NPs	GFP plasmid	*Agrostis stolonifera L.* calli	Passive	48.5% cells showed transient expression	[158], 2008
	Calcium phosphate NPs (CaPNPs)	GUS plasmid	*Brassica juncea* hypocotyl explants	Passive	80.7% stable transformation efficiency	[83], 2012
	Organically functionalized CNTs	YFP plasmid	*N. tabacum* protoplasts and leaf explants	Passive	Both transient and stable expression	[159], 2015
***In vivo* without external aid**	Organically functionalized MSNs	mCherry plasmid	*A. thaliana* roots	Passive	46.5% transient expression efficiency	[161], 2013
	PAMAM dendrimer NPs	Double-stranded DNA for RNA interference	*A. thaliana* roots	Passive	Developmental gene silencing led to systemic phenotypes	[160], 2014
	Polymer functionalized CNTs	GFP plasmid; siRNA for transgenic GFP silencing	*E. sativa*, *N. benthamiana* and *T. aestivum* leaves	Passive	95% transient silencing efficiency; transient expression in mature leaves	[88]

1.6.5   Outlook for Nanomaterials for Plant Genetic Engineering

Genetic engineering of plants has greatly accelerated scientific progress and paved the way for crop variants with improved growth characteristics, disease and pest resistance, environmental stress tolerance, and enhanced nutritional value. In parallel, advances in site-specific genome editing technologies have optimized the precision with which genetic engineering of organisms can be accomplished. However, conventional methods of plant genetic engineering and genome editing are limited in scope primarily due to the cell wall, which imposes a barrier to efficient delivery of biomolecules that could potentially be overcome by nanoparticles.

NPs have recently emerged as a novel method of targeted biomolecule delivery in mammalian cells especially for clinical applications. However, exploration of nanocarriers for biomolecule delivery in plants remains a nascent field with much potential for the future of plant biotechnology and genome editing. Preliminary studies show that NPs with proper surface chemistry and physical properties analogous to those developed for animal systems can deliver biomolecules to plants *in vivo* and *in vitro* with improvements over conventional methods. However, as of yet, most nanocarriers in plants still require assistance from conventional methods (i.e. gene gun) or are limited to *in vitro* studies. To realize the full scientific and humanitarian potential in genetic engineering of both model and crop species, especially with the advent of nuclease-based genome editing, a promising focus will be to optimize NPs as efficient and ubiquitous delivery vessels of diverse biomolecules, tunable across cargo types, species, and tissues, for both transient and stable genetic engineering. However, because germline transformation is currently limited to only one model plant species (*Arabidopsis*), even a ubiquitous delivery strategy for precise genome editing would be limited by the success of regenerating progeny from somatic tissue. A remarkable, yet quite conceivable, future accomplishment of nanoparticle delivery in plants could be enablement of unprecedented, highly parallel genetic studies that elucidate the precedents for success in tissue regeneration, and the direct manipulation of germline plant cells.

1.7   Scope of Dissertation

This dissertation contains four chapters, in addition to an introductory and concluding chapter. Each chapter relates to how nanoparticles might be engineered for usage in plants, broadly spanning nanoparticles as vehicles for biomolecule delivery as well as nanosensor applications. Here, I provide an overview of each chapter to provide transitions between chapters.

Chapter 2 presents a microscopy and molecular biology-based workflow characterizing plant nanoparticle transport and siRNA delivery in plant leaves. This study strives to answer the following: (i) how nanoparticle characteristics (i.e. morphology, surface chemistry) influence nanoparticle transport within a plant leaf, and (ii) how these differences in transport impact delivery efficiency. While studies have been performed on how nanoparticle characteristics influence translocation and fate of nanoparticles in a plant, an end-to-end study of how NP characteristics influence delivery outcomes had yet to be conducted. The work laid out in this chapter is the first systematic assessment of how nanoparticle shape and aspect ratio affect nanoparticle transport at the cellular level. The results of this study are particularly useful to the plant-nano community, as they suggest that nanoparticle entry into cells is not strictly necessary for efficient siRNA delivery.

Chapter 3 covers the development of a single-walled carbon nanotube platform capable of efficient plasmid DNA delivery. In this chapter, we seek to create a nanoparticle-based platform for biomolecule delivery that can be used in both model plants and agriculturally relevant crops without mechanical aid. Accordingly, we describe the design of a carbon nanotube-based system, validation of successful expression of a reporter protein in both monocot and dicots, and further confirmation that this platform is non-integrating and enables transient gene expression. This platform demonstrates promising use in CRISPR-based editing and could have the potential to generate novel plants in a rapid and high-throughput manner.

Chapter 4 focuses on the practicality of protein delivery into walled plant cells. Despite advances in nanoparticle-based platforms for RNA and DNA, there remain few solutions for protein delivery. This is particularly due to unique challenges that exist with proteins, which span the variability in protein sizes as well as vulnerabilities to structural perturbations which lead to loss of function. This chapter outlines current and potential strategies towards achieving protein delivery with a specific focus on conjugation and loading chemistries.

Chapter 5 represents a transition away from nanoparticle-mediated biomolecule delivery strategies and towards pondering the application of nanoparticle-based systems in more complex biological and ecological environments. Fundamentally, the introduction of nanoparticles to a biological milieu results in interactions between biomolecules such as proteins and the nanoparticles. The formation of a biocorona results in an increase in nanoparticle size and surface chemistry, which can impact nanoparticle transport within the plant and most importantly, function. We believe that biocorona formation is one of the chief impediments to translating nanoparticle-based systems from the benchtop into fields. This chapter discusses the importance of studying biocorona formation in the context of nanosensors and argues that an improved understanding of biocorona formation can inform functional nanoparticle design. Though nanosensor-specific examples have been provided in this chapter, the considerations laid out are broadly applicable to nanoparticles used in agriculture.

2 Nanoparticle Cellular Internalization is Not Needed for siRNA Delivery into Plants

2.1 Chapter Abstract

Rapidly growing interest in nanoparticle-mediated delivery of DNA and RNA to plants requires a better understanding of how nanoparticles and their cargoes translocate in plant tissues and into plant cells. However, little is known about how the size and shape of nanoparticles influences transport in plants and delivery efficiency of their cargoes, limiting development of nanotechnology in plant systems. Here, we employ non-biolistically delivered DNA-modified gold nanoparticles (AuNP) spanning various sizes (5-20 nm) and shapes (spheres and rods) to systematically investigate their transport following infiltration into *Nicotiana benthamiana (Nb)* leaves. Generally, smaller AuNP demonstrate more rapid, higher, and longer-lasting levels of association with plant cell walls compared to larger AuNP. We observe internalization of rod-shaped but not spherical AuNP into plant cells, yet surprisingly, 10 nm spherical AuNP functionalized with small-interfering RNA (siRNA) are most efficient at siRNA delivery and inducing gene silencing in mature plant leaves. These results indicate the importance of nanoparticle size in efficient biomolecule delivery, and, counterintuitively, demonstrate that efficient cargo delivery is possible and potentially optimal in the absence of nanoparticle cellular internalization. Results highlight nanoparticle features of importance for transport within plant tissues, providing a mechanistic overview of how nanoparticles can be designed to achieve efficacious bio-cargo delivery for future developments in plant nanobiotechnology.[§]

2.2 Introduction

The growth of nanobiotechnology, whereby nanomaterials are designed for use in biological systems, has added new dimensionality to pharmaceutical and drug delivery development and married the fields of chemistry, biomedical engineering, and material science. Their small size, tunable physicochemical and optical properties, and high surface-to-volume ratio render nanoparticles (NPs) versatile scaffolds to be functionalized as carriers or probes for therapeutic and diagnostic purposes. In recent years, the use of nanomaterials in plant science has greatly enabled advances in agriculture. These developments include crop management improvement, plant-pathogen protection, nutrient and pesticide delivery, monitoring of plant and soil health, and creation of crop varieties with desirable traits such as high yield and stress resistance[121,162,163]. In plant genetic engineering, nanomaterials have also been used as vehicles for the delivery of plasmid DNA[88,91,164], siRNA[165–169], and proteins[93] to whole plants.

Nanoparticle (NP)-mediated biomolecule delivery technologies for plants have leveraged the material properties of nanoparticles to overcome the unique barriers of plant cells. Examples of

---

these materials include mesoporous silica nanoparticle (MSNs)[91,93], single walled carbon nanotubes (SWNTs)[88,147,164,168], DNA nanostructures[166], layered double hydroxide nanosheets[165,170], and more recently, gold nanoparticles[167,169]. These works exploit the small size and high tensile strength of NPs to bypass biological barriers. Moreover, the diverse conjugation chemistries available for cargo conjugation to NPs and the high degree of control over NP morphology and surface functionalization enable certain NPs to penetrate through plant tissues[171,172]. While NP-mediated biomolecule delivery in plants has been demonstrated with nanoparticles of various sizes and surface modifications, little is known about how these design variables affect translocation, cellular uptake, and ultimately bio-cargo utilization in plants. Comprehensive studies in mammalian systems[173–176] and simulations of NP-cell membrane interactions[177–180] have underscored the importance of NP size and shape for bio-delivery – yet, these studies are usually not applicable to walled plant cells. In particular, studies in mammalian systems have revealed how size and shape can affect NP interaction with cells and thus influence the uptake pathway and internalization efficiency, guiding design strategies for nanoparticle-based biomedical applications[181]. However, analogous studies in plant systems have not been performed yet, limiting the development of plant nanobiotechnologies and the assessment of their intended and unintended impacts on plants, agricultural systems, and the environment.

The plant cell wall is composed of a complex network of biopolymers that gives rise to a semipermeable matrix[182] and is a unique barrier to consider for the uptake of NPs into plant cells[183]. While the permeability of the plant cell wall is dynamic, studies commonly suggest that the upper limit of the pore diameters range from 5 to 20 nm[107,108]. An abundance of studies in mammalian systems have demonstrated that NP interactions with cells are morphology-dependent, and similar dependencies may also dictate NP interactions with plants. There is therefore a cogent need to understand NP-plant interactions to inform how NPs can be designed for use with minimal environmental disruption and maximal efficacy. The process of NP uptake, translocation, and accumulation in plants can be broadly split into three tiers[184]: (i) macroscale – quantifying translocation and accumulation in plant organs, (ii) microscale – studying NP transport through and interactions with plant tissues and vasculature, and (iii) molecular – revealing the manner of NP association on a cellular or sub-cellular level. Of note, most studies have been performed on the macroscale[185,186], though some studies have begun to explore the effect of NP properties on uptake at the microscale[171,187] and the molecular scale[188,189]. These studies are valuable to understand how NPs and their surface chemistries might impact translocation and long-term accumulation throughout a plant. However, NP features enabling molecular-scale translocation of NPs within plant tissues and into plant cells, and subsequent bio-cargo delivery, remain to be determined.

Although gold microparticles and certain larger AuNP are broadly used for biolistic delivery of biological cargoes in plants, their non-biolistic delivery remains largely unexplored. In this study, we designed a library of DNA-functionalized gold nanoparticles (DNA-AuNPs) of varying sizes and shapes and evaluated their leaf tissue transport to plant cells over time. We used confocal microscopy, transmission electron microscopy (TEM), and synchrotron X-ray fluorescence (µXRF) imaging to track AuNP fate v following abaxial (from the bottom) infiltration into leaves, and directly visualize NP interactions with plant cells. Based on these results, we established a

size- and shape-dependent mechanism of DNA-AuNP transport to and passage across plant cell walls and demonstrate here that biocargo delivery into plant cells can be independent of nanoparticle cellular internalization. Our results highlight the importance of nanoparticle morphology in transport within plant tissues and suggest that efficient cellular siRNA delivery can be achieved even without NP carrier internalization into cells.

2.3 Results and Discussion

2.3.1 Preparation and Characterization of DNA-AuNP

Five gold nanoparticles of various morphologies were used in this study: 5 nm, 10 nm, 15 nm and 20 nm gold nanospheres (AuNS), and a 13-by-68 nm gold nanorod (AuNR) of aspect ratio ~5.2 (**Error! Reference source not found.a**). To obtain colloidally-stable particles, AuNP were functionalized using a pH-assisted method[190] with single-stranded DNA sequences with a 3' thiol modifier followed by a 10-nucleotide poly-adenosine sequence (**Table 2-1** and **Table 2-2**). Citrate-stabilized AuNP and functionalized DNA-AuNP were characterized with UV-Vis-NIR spectroscopy, dynamic light scattering (DLS), and TEM imaging. AuNS have a size-dependent surface plasmon resonance (SPR) peak at approximately 520 nm and AuNR have characteristic transverse and longitudinal peaks at 520 nm and 960 nm (**Error! Reference source not found.b**), and the SPR peaks showed small redshifts post-functionalization (**Table 2-1**). DLS characterization (**Table 2-3, Figure 2-7**, and **Figure 2-8**) and TEM (Error! Reference source not found.**c** and **Figure 2-9**) demonstrate successful functionalization and the high homogeneity of AuNP and DNA-AuNP, and the number of DNA molecules per AuNP are quantified (**Table 2-4**) with AuNP possessing higher surface areas loading more DNA, as expected. DNA-AuNP were next tagged with a Cy3 fluorophore via complementary strand hybridization and abaxially-infiltrated into mature leaves of *Nicotiana benthamiana* (*Nb*) plants using a needleless syringe (**Error! Reference source not found.d**).
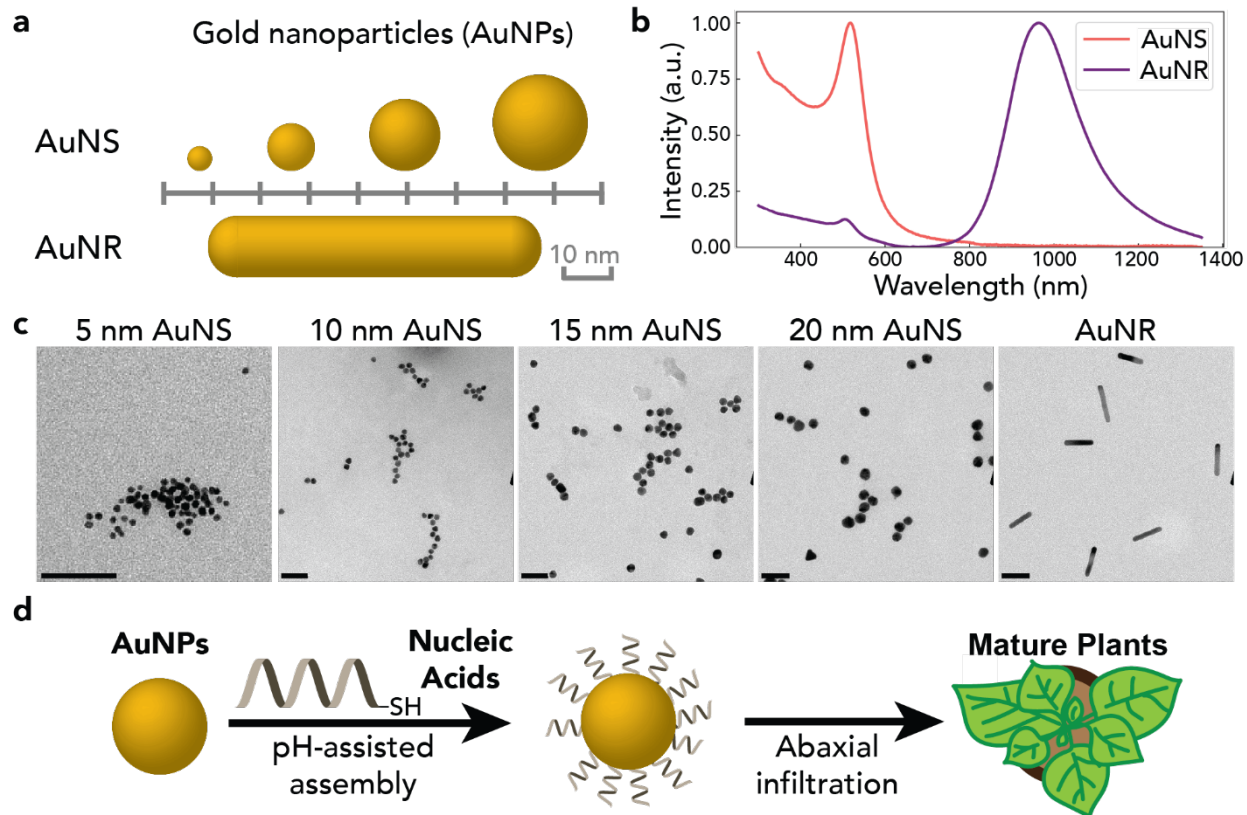
Figure 2-1. DNA-AuNP preparation and characterization.
a AuNP samples used in this study: 5, 10, 15, and 20 nm gold nanospheres (AuNS), and 13 by 68 nm gold nanorods (AuNR). **b** Representative UV-Vis-NIR spectra of 10 nm AuNS and AuNR demonstrate characteristic AuNS and AuNR absorbance peaks. **c** TEM characterization of AuNP indicates high degrees of monodispersity. Scale bar: 50 nm. **d** AuNP are functionalized with thiol-modified nucleic acids via a low-pH assisted method, followed by abaxial infiltration into mature plant leaves. Throughout this study, infiltration was performed in lieu of spray-based nanoparticle application to ensure even wetting of the plant leaf tissue.

2.3.2 *AuNP Transport through Leaf Tissue and Association with Plant Cells*

Following nanoparticle characterization, we tested the morphology- and size-dependent ability of AuNP to transit within the leaf interstitial space and associate with plant cell walls. To track DNA-AuNP in plant tissue, we hybridized a Cy3-modified complementary DNA strand to the thiol-modified DNA on AuNP (**Table 2-1**). Cy3-labeled DNA-AuNP (Cy3-DNA-AuNP) with a normalized Cy3 concentration of 400 nM and thus differing concentrations of AuNP (**Table 2-4**) were abaxially-infiltrated into the leaves of a transgenic mGFP5 *Nb* plant. Leaves were adaxially (top) imaged with confocal microscopy to capture Cy3 signal from Cy3-DNA-AuNP and GFP signal from the transgenic *Nb* cytosol. The colocalization fraction between Cy3 and GFP channels represented the relative ability of Cy3-DNA-AuNP to diffuse within the leaf interstitial space and associate with (and/or enter, see **Section 2.6.2.1 below**) plant cells (**Error! Reference source not found.a**).

Colocalization analyses of Cy3-DNA-AuNP with cytosolic mGFP5 ranging from 30 min to 24 h post-infiltration reveals maximum colocalization fractions at varied timepoints that depend on AuNP core shape and size (**Error! Reference source not found.b**, maxima: black bars), with the exception of 20 nm AuNS, for which no maximum was observed. Confocal images in **Error! Reference source not found.c** show the Cy3-DNA-AuNP signal as the red channel, intracellular GFP as the green channel, and colocalization signal from the two channels in white. With the exception of the 20 nm AuNS, all DNA-AuNP experienced an increase in colocalization fractions as a function of time post-infiltration before reaching a maximum, followed by a decrease in colocalization values over longer incubation times (**Figure 2-10**, **Figure 2-11**, **Figure 2-12**, **Figure 2-13**, and **Figure 2-14**). For DNA-AuNS, the time required to reach maximum AuNP colocalization with plant cells was faster for smaller nanoparticles – for 5, 10, and 15 nm, the time corresponding to the colocalization maxima were 1, 2, and 12 h post-infiltration. For 20 nm DNA-AuNS, no statistically significant change in the colocalization fractions occurred within 24 h, and longer post-infiltration times of 48 and 72 h did not yield a maximum value. For DNA-AuNR, the maximum colocalization fraction occurred sharply at 6 h post-infiltration.

We attribute the time-dependent increase in colocalization fraction to the time required for DNA-AuNP to travel through plant tissue and intercalate between cells. Interestingly, the different time-dependent accumulation of DNA-AuNS versus DNA-AuNR suggest a shape-dependent effect on NP transport in plant tissues. Additional confocal experiments with a lower aspect ratio AuNR support this hypothesis (see **Section 2.6.3.1 below**, **Figure 2-15**, and **Figure 2-16**). The decrease in Cy3 signal at longer incubation points is potentially due to the loss of Cy3 fluorescence with photobleaching or quenching by molecular interactions[191], or apoplastic[192] (space beyond the cell plasma membrane) transport decreasing Cy3 presence within the imaged area (See **Section 2.6.3.2 below, Figure 2-17**, and **Figure 2-18**). Altogether, our data suggest that AuNS core size plays an essential role for DNA-AuNP transport in plant tissues. 5, 10, and 15 nm DNA-AuNS and DNA-AuNR with diameters less than 15 nm can diffuse within the leaf interstitial space and associate with plant cell walls and membranes in a size and shape-dependent manner, with times for maximal cellular association ranging drastically from 1 to 12 h. These findings support prior hypothetical observations that larger nanoparticles take longer to diffuse through plant tissue and associate with plant cells, with an upper 20 nm NP core size limit[93].
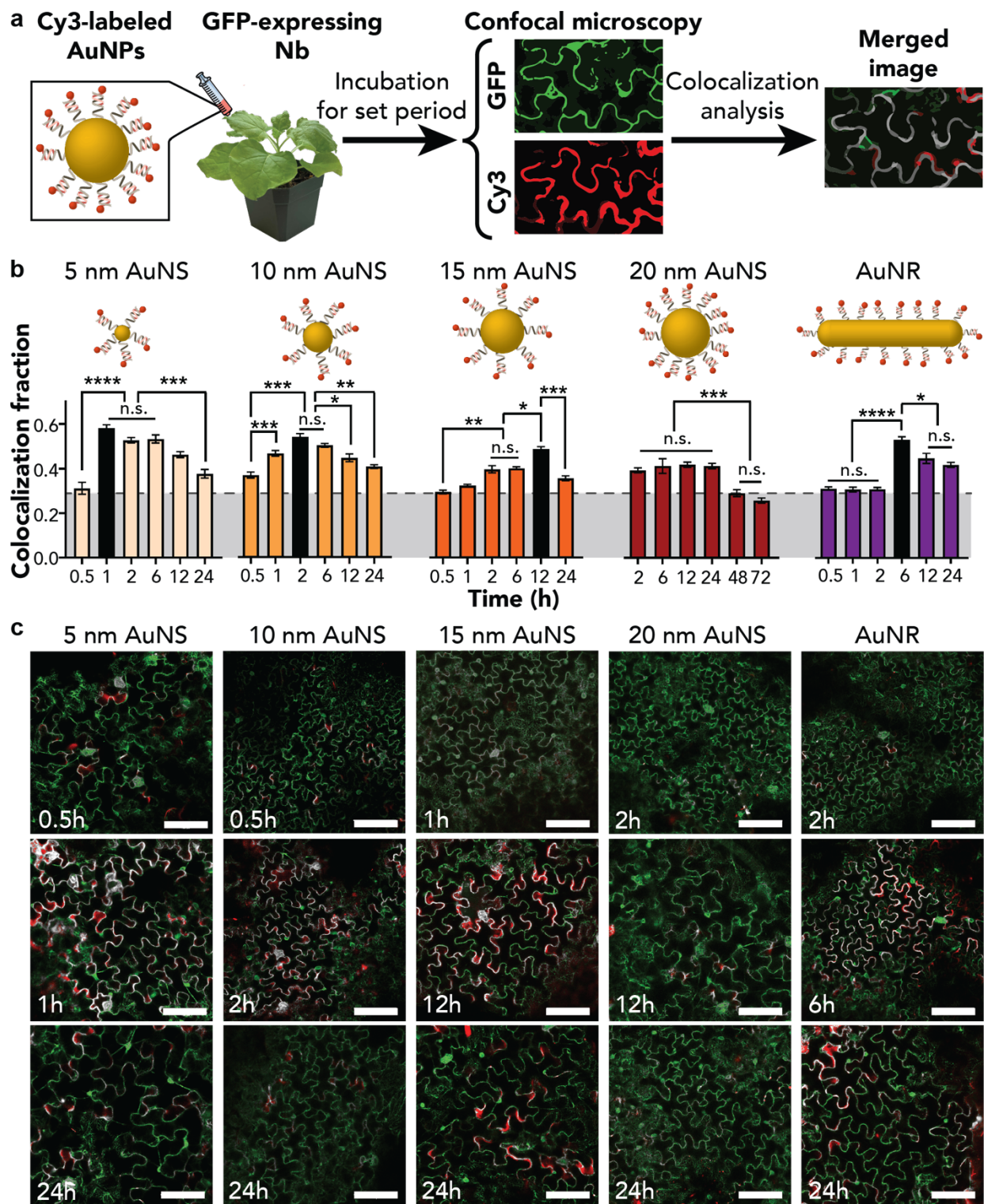
Figure 2-2. Cy3-tagged DNA-AuNP association with plant cells following infiltration into transgenic mGFP5 *Nicotiana benthamiana* (*Nb*) leaves.

a Workflow for fluorescent AuNP tracking in leaves via confocal microscopy. AuNP labeled with 400 nM Cy3-DNA abaxially infiltrated into mGFP5 *Nb* leaves (with GFP fluorescence as a

cytosolic marker) and colocalization fractions analyzed under confocal microscopy as a relative measure of AuNP cell wall association. **b** Time-series of colocalization fractions for Cy3-DNA-AuNP demonstrate size and shape dependent AuNP transport in plant tissues. Grey denotes maximum colocalization fractions obtained with a free Cy3-DNA control (**Figure 2-19** and **Figure 2-20**). 5nm AuNS, ****$p<0.0001$, ***$p=0.0008$; 10nm AuNS: ***$p=0.0003$, **$p=0.0030$, *$p=0.0357$; 15nm AuNS: **$p=0.0056$, *$p=0.0276$, ***$p=0.0009$; 20nm AuNS: ***$p=0.0004$; AuNR: ****$p<0.0001$, *$p=0.0115$ in one-way ANOVA, n.s.: not significant; error bars indicate s.e.m. n=3). **c** Cy3-DNA-AuNP infiltrated *Nb* leaves with regions of colocalization (white) between intracellular GFP (green) and Cy3 (red) channels. Images corresponding to incubation times included for each of the five AuNP samples include before, during, and after the time for co-localization values to reach the maximum level. Scale bar: 100 μm.

2.3.3   *AuNS Association with Plant Cells*

To confirm NP fate on a sub-cellular scale, we next implemented TEM of NP-treated leaves to directly visualize AuNP in plants (Error! Reference source not found.). DNA-AuNP infiltrated *Nb* leaves were fixed and sectioned 24 h post-infiltration, with progressively increased magnifications provided for 5, 10, 15, and 20 nm AuNS including arrows marking AuNS associated with a single cell wall, and unfilled arrows marking AuNS sandwiched between two neighboring cell walls (Error! Reference source not found. and **Table 2-4**). Characteristic cellular structures like chloroplasts and cell walls are used as indicators to determine whether AuNS are localized within the extracellular or intracellular spaces.

Across all samples, a high density of AuNS associated with plant cell walls, with smaller AuNS associating more than larger AuNS. Our colocalization analysis demonstrated that the size of the AuNS affects their translocation efficiency within plant tissues, whereby larger AuNS experience greater difficulty bypassing biological barriers. Notably, 5, 10, and 15 nm DNA-AuNS TEM images showed AuNS intercalating into a single cell wall, whereas the 20 nm AuNS images depicted AuNS sandwiched between two cell walls and thus unassociated with a single cell (Error! Reference source not found.**d** and **Figure 2-21)**. Across all samples, we saw no instances of AuNS within or proximal to the intracellular space of plant cells, suggesting that AuNS internalization into plant cells is minimal, if it occurs at all (additional confirmation in **Figure 2-22**). The higher degree of plant leaf cell association of smaller AuNP based on TEM agree with their respective higher colocalization values obtained with our confocal microscopy results.
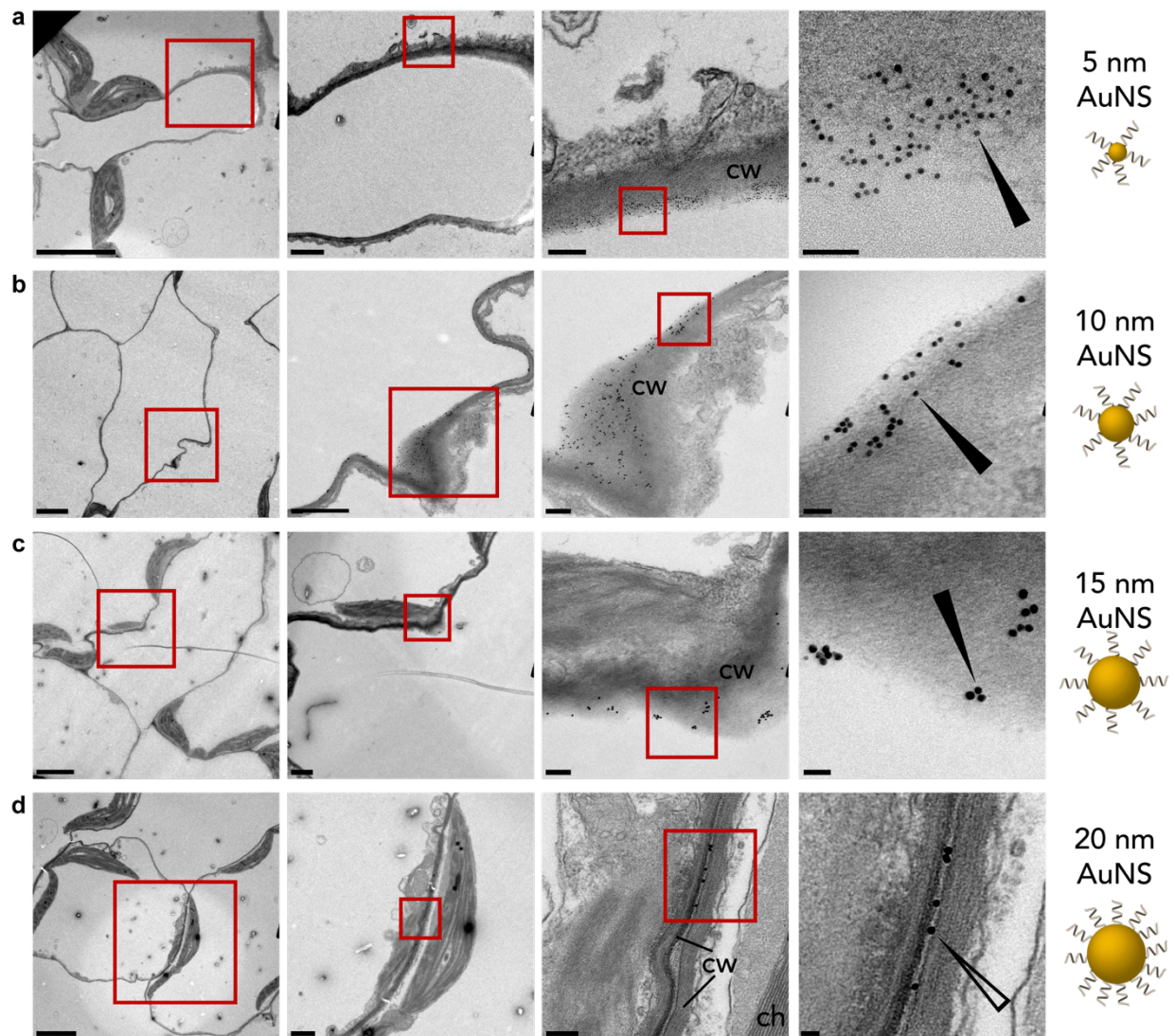
Figure 2-3. TEM of DNA-functionalized AuNS treated *Nicotiana benthamiana* (*Nb*) leaves. Representative TEM images of *Nb* plants 24h post-infiltration with DNA-functionalized AuNS of **a** 5 nm, **b** 10 nm, **c** 15 nm, and **d** 20 nm diameters. Images are progressively magnified from left to right, with red boxes indicating magnifications. Annotations represent cell wall (cw) and chloroplast (ch). Solid and unfilled arrows indicate nanoparticles associated with a single cell wall or found between cell walls, respectively. Scale bars (from left to right) are 5 μm, 1 μm, 0.2 μm and 50 nm.

2.3.4   *AuNR Association with and Internalization into Plant Cells*

Analogous to the AuNS TEM experiments, *Nb* leaves exposed to DNA-AuNR were prepared for TEM analysis 24 h post-infiltration. In contrast to AuNS, we identified several AuNR inside plant cells (Error! Reference source not found.**a**). The striped arrow pinpoints AuNR found within plant cells, supported by the presence of chloroplasts next to the identified AuNR. In addition, several instances of AuNR piercing into the cell walls were observed, orienting along a tangent or perpendicular to the cell wall (Error! Reference source not found.**b** and **Figure 2-23**).

Previous theoretical and experimental studies of NP internalization in mammalian cells indicate that NP shape greatly influences the contact curvature with the lipid membrane and dictates the endocytic pathway and angle of entry[179]. In particular, high-aspect ratio NPs tend to rotate to orient themselves perpendicular to the cell membrane during internalization into mammalian cells[180], whereby the rotation facilitates the penetration and transport of NPs[193]. From our TEM data, we therefore analyzed AuNR in the extracellular space of plant cells with respect to their orientation relative to the cell wall tangent (Error! Reference source not found.**c** and **Figure 2-24**). In total, 41.7 %, 21.9 %, and 36.4 % of AuNR oriented between 0-30 °, 30-60 °, and 60-90 ° with the cell wall respectively (**Figure 2-24** and **Table 2-5**). We posit that the AuNR demonstrate a stronger preference for initially orienting parallel to the cell wall, where 22.5 % of AuNR formed an acute angle between 0-10 ° with the cell wall. In addition, compared to the 11.1 % proportion expected randomly (see **Section 2.5.9.2 below** and **Table 2-5**), 14.2 % of AuNR were oriented between 80-90 ° relative to the plane of the cell wall. Considering the rigid and porous structure of the cell wall, we posit that AuNR experience re-orientations to bypass the cell wall and membrane for plant cell internalization, similar to the phenomenon previously identified in mammalian systems suggesting that asymmetric nanoparticles are entropically favored for membrane interactions[179,180,193].

To further verify the importance of AuNP morphology in transport through plant leaf tissues, we performed µXRF mapping on cross-sections of DNA-AuNP (10 and 20 nm DNA-AuNS, and DNA-AuNR) infiltrated WT *Nb* leaves prepared 24 h post-infiltration. Compared with a water-infiltrated control (**Figure 2-25**), all AuNP samples show Au signal throughout the leaf cross-section (Error! Reference source not found.**d**). µXRF mapping confirmed that transport of 20 nm DNA-AuNP through leaf tissue is size-limited, limiting their transport past the leaf cuticle or initial layer of epidermal cells (**Figure 2-26** and **Figure 2-27**). In comparison, smaller 10 nm DNA-AuNS and DNA-AuNR demonstrate highly homogeneous transport within the leaf cross-section, as seen from consistent Au counts throughout the leaf's full thickness (**Figure 2-28**, **Figure 2-29**, **Figure 2-30**, and **Figure 2-31**).

Hypothesized mechanisms for NP internalization into plant cells include endocytosis, entry through the plasmodesmata, and NP acting as 'nanospears' to 'pierce' membranes[193]. To better understand AuNR plant cell internalization, we assessed the impact of endocytosis inhibition on Cy3-DNA-AuNP association with plant cells using confocal microscopy. We infiltrated the leaves of mGFP5 *Nb* with endocytosis inhibitors (either wortmannin[194] or ikarugamycin[195]), then infiltrated the same area with Cy3-DNA-AuNP (10 nm AuNS or AuNR) 30 min later. Colocalization analysis was performed 6 h post-AuNP infiltration by normalizing values for samples treated with endocytosis inhibitors to controls without inhibitors.

As shown in Error! Reference source not found.**e**, samples pre-treated with either wortmannin or ikarugamycin endocytosis inhibitor induced a marked decrease in colocalization fraction for AuNR but no significant change for 10 nm AuNS (**Figure 2-32**). Wortmannin is an inhibitor of phosphoinositol-3 kinase activity and disrupts protein transport to vacuoles[194,196]. While the mechanism of action of ikarugamycin is undetermined, it is often used as an inhibitor of clathrin-mediated endocytosis[195,197]. Despite their different modes of action on plant cell trafficking, both wortmannin and ikarugamycin inhibit entry of Cy3-DNA-AuNR, whereas neither affects the colocalization values of 10 nm Cy3-DNA-AuNS with the plant cell cytosol. These experiments,

which are based on a disruption of the plant cell's native endocytic pathways, together with our TEM results, suggest that AuNR do internalize into plant cells through energy-dependent mechanisms while AuNS do not internalize into plant cells.

Based on these findings, we propose a mechanism of AuNP transport within plant leaf tissues (Error! Reference source not found.**f**). Briefly, upon introduction to mature plant leaves, both DNA-AuNS and DNA-AuNR transport to the periphery of plant cells in a size-dependent manner and experience a high degree of association with the cell wall. AuNR may orient in parallel to the cell wall during initial contact and reorient perpendicularly when bypassing the cell wall, which supports proposed mechanisms of rotation-based cell wall entry of rod-shaped nanomaterials[180,193]. After passage through the cell wall, endocytosis is a likely mechanism of AuNR entry across the cell membrane.
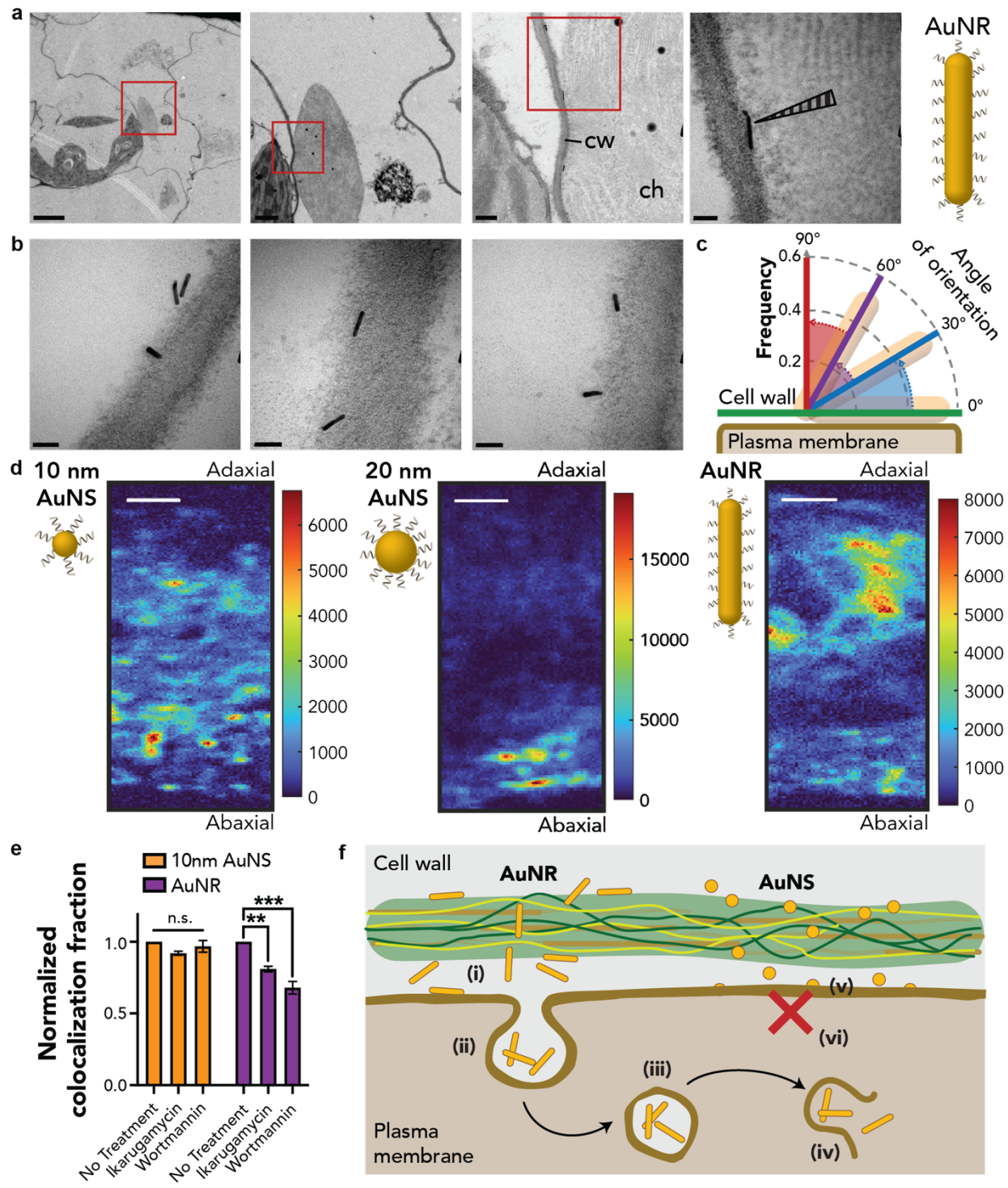
Figure 2-4. TEM and μXRF imaging of DNA-AuNP treated *Nb* leaves and mechanism of morphology-dependent AuNP transport.
a TEM images of *Nb* plants 24h post-infiltration with DNA-functionalized AuNR. Annotations represent cell wall (cw) and chloroplast (ch). Scale bars (from left to right) are 5 μm, 1 μm, 0.2 μm, and 50 nm. **b** AuNR exhibited a variety of orientations upon contact with the cell wall, including AuNR 'piercing' the cell wall, a potential mode of NP internalization. Scale bar: 50 nm.

c Proportion of AuNR observed within an angle range depicted by radial magnitude shaded slices. Statistical analysis shows AuNR orientation maximizes contact area with the cell wall (0-30 °) and minimizes orientations perpendicular to the cell wall (60-90 °) for N = 324 AuNR (**Table 2-5**). **d** μXRF Au distribution map of *Nb* leaf cross section exposed to 5 μg of 10 nm and 20 nm DNA-AuNS and DNA-AuNR. Intensity values correspond to Au Lα_1 fluorescence emission counts. All maps are positioned with the abaxial side facing down (side of infiltration). Scale bar: 50 μm. **e** Colocalization fractions between Cy3 and GFP channels for Cy3-tagged DNA-functionalized 10nm AuNS and AuNR infiltrated into mGFP5 *Nb* leaves treated with endocytosis inhibitors ikarugamycin or wortmannin. No change in colocalization fraction values was observed with AuNS, though AuNR samples in leaves treated with ikarugamycin or wortmannin demonstrated a significant decrease in colocalization fractions normalized to untreated samples. (AuNR, **p=0.007; ***p=0.0005 in two-way ANOVA, n.s.: not significant; error bars indicate s.e.m. n=3). **f** Mechanistic schematic for AuNS and AuNR association or internalization into plant cells. (i) AuNR may orient on their long ends to 'pierce' cell walls. (ii)-(iv) AuNR found in intact plant cells likely enter through endocytosis. (v) AuNS show high association with the cell wall, but (vi) no instances of any sized AuNS were identified inside plant cells within 24h.

2.3.5   Sub-20 nm AuNP Enable Delivery of siRNA for Gene Silencing in Nb Plants

Targeted downregulation of certain plant proteins is known to confer disease resistance in crops. Therefore, an attractive 'greener' alternative to the use of herbicides in agriculture is RNA interference, which involves the delivery of small-interfering RNA molecules (siRNA) that interfere with the production of a specific plant protein. However, siRNA is a molecule that is difficult to deliver across the cell wall due to its high susceptibility to degradation[198,199]. We therefore evaluated the use of AuNP as delivery vehicles to enable transient gene silencing through siRNA delivery into *Nb* leaves. AuNP samples of varying morphologies and sizes were functionalized with pre-hybridized siRNA targeting the GFP gene to obtain siRNA-functionalized AuNP (**Table 2-1**, **Table 2-2**, and **Table 2-4**). In addition to UV-Vis-NIR (**Figure 2-6**) and DLS characterization (**Figure 2-33**), uranium-based staining of siRNA-AuNP under TEM showed a visible halo surrounding AuNPs, suggesting successful siRNA-functionalization (Error! Reference source not found.**a**).

Prior to siRNA delivery in plants, we conducted *in vitro* experiments to probe the ability of AuNP to protect siRNA. Following incubation with a high concentration of RNase A (1.2 μg/mL), nuclease inactivation, and siRNA liberation from the AuNP surface, we quantified the concentration of remaining siRNA. While free siRNA demonstrated extreme susceptibility to endonuclease degradation, a strong protective effect was afforded by the 10 nm AuNS and AuNR (Error! Reference source not found.**b** and **Table 2-6**). Free siRNA is degraded within 10 min of endonuclease exposure (7 ± 4 % remaining), while 10 nm AuNS and AuNR exhibit 54 ± 5 % and 64 ± 6 % intact siRNA by 240 min. We further confirmed that AuNS of all sizes – 5, 10, 15, and 20 nm AuNS – provide significant protection against siRNA endonuclease degradation (**Figure 2-34**).

Next, we investigated the possibility of siRNA delivery using AuNP carriers, even without nanoparticle internalization into plant cells. We tested siRNA bioavailability by measuring RNA released from siRNA-AuNP infiltrated leaves with anion exchange fast protein liquid

chromatography (FPLC)[200] and agarose gel electrophoresis, which both confirmed that siRNA becomes bioavailable following infiltration into plant leaves (**Figure 2-35** and **Figure 2-36**). We further verified that siRNA becomes liberated from siRNA-AuNP in plant biofluids (both apoplastic fluid and plant lysate), and that this result is consistent across all AuNP, with a gel-based assay (**Figure 2-37** and **Figure 2-38**). These results confirm that siRNA can be liberated from the AuNP surface in the plant extracellular or intracellular environment. These results are significant because they confirm that siRNA-AuNP in the apoplast are protected against nuclease degradation and that siRNA can become bioavailable proximal to the cell wall. To test the mechanism of nucleic acid release from AuNP, we used a fluorescence-based dynamic exchange assay[201] (**Figure 2-39**) to track cargo release from AuNP. We incubated 15 nm AuNS conjugated with Texas Red fluorophore-labeled DNA (TR-DNA-AuNS) with plant apoplastic fluid, which resulted in TR-DNA cargo release from the AuNS surface over time (Error! Reference source not found.**c**). Additionally, pH and the presence of the reactive oxidative species (ROS) H_2O_2 did not result in significant TR-DNA desorption (**Figure 2-40**), suggesting that neither the dynamic pH within the apoplast[202] (~pH 6) nor an increase in ROS commonly implicated with plant mechanical and environmental stress[203,204] are major contributing factors to cargo availability from AuNS. These experiments demonstrate that cargo loaded onto AuNS located in the apoplast can desorb from the AuNP carrier, making the siRNA bioavailable, through a surface exchange mechanism involving cargo displacement due to biomolecule adsorption onto the AuNS surface (See **Section 2.6.2.2 below**).

GFP-targeting siRNA-AuNP were next infiltrated into GFP-expressing *Nb* leaves at a normalized siRNA concentration of 100 nM as previously used[168]. We extracted mRNA and protein from treated leaf tissue and quantified the efficiency of GFP silencing at the mRNA level 1-day post-infiltration (dpi) via RT-qPCR, and protein-level GFP silencing 3-dpi via Western blot (Error! Reference source not found.**d**). We initially hypothesized that only AuNR would enable efficient siRNA delivery and GFP silencing, since only AuNR were found to enter plant cells within the timescale of our experiments. Surprisingly, we observed GFP silencing with both AuNS and AuNR, where smaller AuNS were generally more effective at silencing than larger AuNS: 10 nm AuNS showed the greatest amount of silencing across all AuNP on both the mRNA (99 %) and protein (48 %) levels. Reduction in GFP mRNA transcripts 1-dpi were 8 % (free siRNA), 8 % (20 nm AuNS), 29 % (15 nm AuNS), 39 % (AuNR), 42% (5 nm AuNS), and 99 % (10 nm AuNS) (Error! Reference source not found.**c** and **Figure 2-41**). Similarly, we measure a concomitant reduction in protein levels on 3-dpi (Error! Reference source not found.**d** and **Section 2.6.3.3 below**). We also confirmed that gene silencing was transient via RT-qPCR and Western blot analyses of 10 nm siRNA-AuNS infiltrated leaves 7-dpi (Error! Reference source not found.**e**), in which mRNA and protein levels returned to baseline several days after treatment. We next confirmed that GFP gene silencing was specific to the GFP-targeting siRNA sequence: 1-dpi RT-qPCR analysis of nonsense siRNA-functionalized 10 nm AuNS showed no silencing of the GFP gene, as expected (**Figure 2-42**). Taken together with our findings that apoplastic fluid constituents can induce siRNA desorption from AuNP, these results stand in contrast with the assumption that NP cellular internalization is required for biomolecular cargo delivery, whereby our results suggest that the internalization of NPs is not necessary for efficient siRNA delivery and gene silencing in plants.

Lastly, we confirmed the biocompatibility of nucleic acid (NA) -functionalized AuNP constructs. To our knowledge, the biocompatibility of NA-functionalized AuNP in plants has not been studied. To gauge the response of *Nb* to NA-functionalized AuNP, we infiltrated *Nb* leaves with either buffer or AuNP and performed a RT-qPCR analysis of mRNA transcript levels for 13 genes associated with various stress responses (**Table 2-1**, **Table 2-4**,

Table 2-7, and **Section 2.6.2.3 below**). We sampled leaves at various timepoints to study the effect of the infiltration itself versus the effect of the AuNP (10 nm AuNS). Results in **Figure 2-43** show upregulation of several stress-related genes for both citrate-stabilized and siRNA-AuNS immediately post-infiltration, which return to basal expression levels 1-dpi. We further confirmed the recovery to baseline levels of gene expression by probing the respiratory burst oxidase homolog B (*NbrbohB*) stress gene 1-dpi of 10 nm siRNA-AuNS and siRNA-AuNR (**Figure 2-44**). Results show that neither caused any significant change in *NbrbohB* gene expression. Additionally, a visual observation of infiltrated leaves immediately and 3-dpi of AuNP reveals no visible morphological changes (**Figure 2-45**). Taken together, these results suggest any stress response to AuNP is transient and is unlikely to result in physiological changes, suggesting that AuNP can serve as a biocompatible siRNA-delivery vehicle to plants.
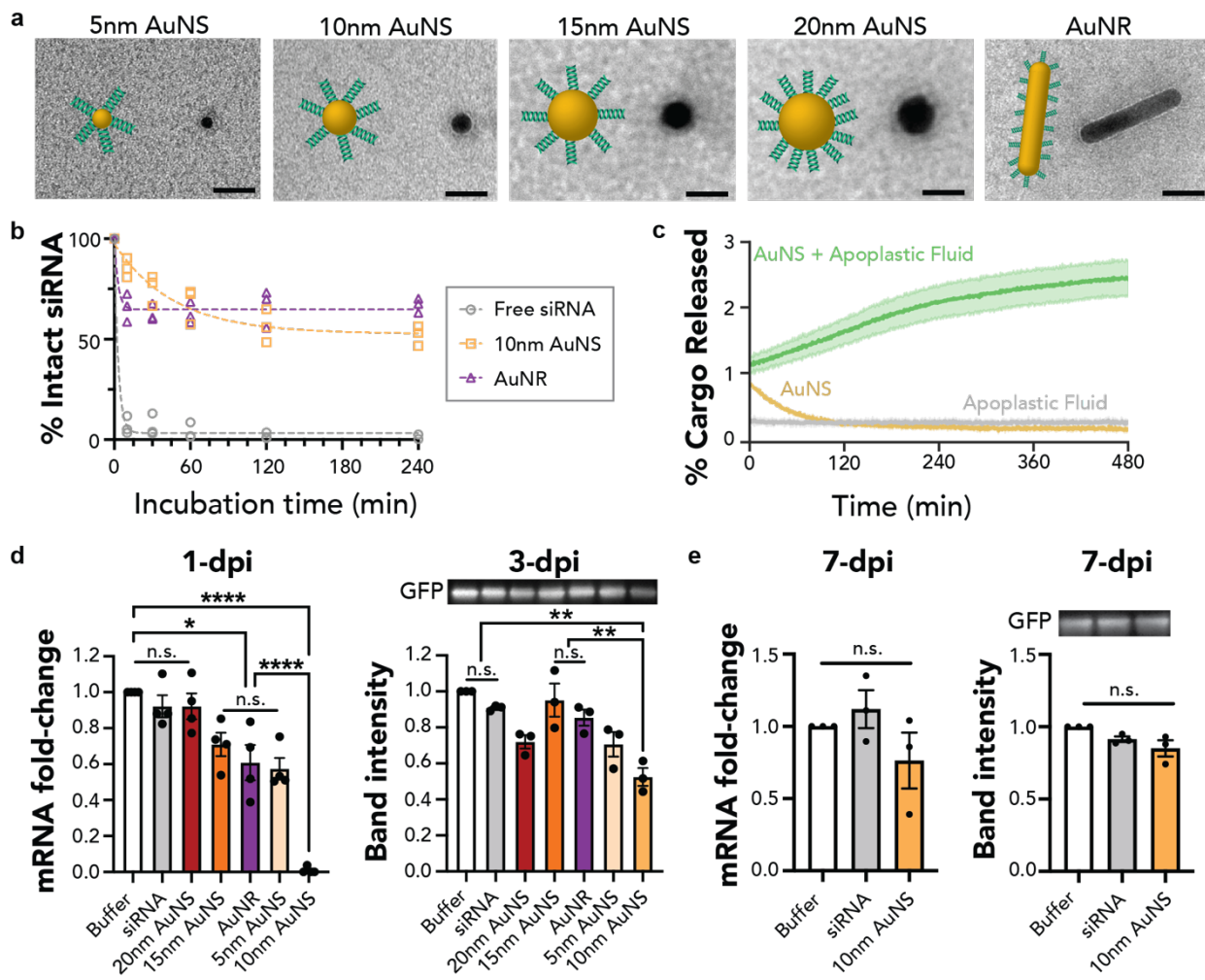
Figure 2-5. Size and morphology-dependent AuNP-siRNA delivery in mGFP5 *Nb* leaves.

49

a TEM of stained siRNA-functionalized AuNP. Scale bar: 20nm. **b** AuNP protect siRNA from endoribonuclease RNase A degradation. siRNA-loaded 10nm AuNS and AuNR were incubated with RNase A for 10, 30, 60, 120, and 240 min prior to quantification of intact siRNA. **c** Fluorophore-tagged cargo desorbs from the AuNP surface in the presence of apoplastic fluid (green) with negative controls 0.3x PBS added to TR-DNA-AuNP (yellow) and apoplastic fluid alone (gray). Shaded error bars indicate s.e.m. (n=2). **d** RT-qPCR and Western blot quantification of GFP mRNA fold-change and protein expression, 1- and 3-days post-infiltration (dpi) respectively of mGFP5 *Nb* plant leaves treated with siRNA-AuNP loaded with 100 nM siRNA. (RT-qPCR: *p=0.0411, and ****p< 0.0001 in one-way ANOVA on day 1; n.s.: not significant; error bars indicate s.e.m. (n=4).) (Western: **p=0.0020, 0.0074 in one-way ANOVA on day 3; error bars indicate s.e.m. (n=3).) **e** RT-qPCR and Western blot analyses showing GFP mRNA and protein expression levels, respectively, return to baseline 7 dpi with siRNA-AuNP in *Nb* leaves. Controls represent 0.3x PBS buffer-infiltrated leaves. (RT-qPCR: One-way ANOVA on day 7; n.s.: not significant; error bars indicate s.e.m. (n=3).) (Western: One-way ANOVA on day 7; n.s.: not significant; error bars indicate s.e.m. (n=3).)

2.4   Conclusions

We systematically employed a series of DNA-AuNP with various sizes (5-20 nm) and shapes (sphere and rod) to investigate how morphology impacts nanoparticle interaction with and uptake into plant cells following infiltration into mature *Nb* leaves. We find that smaller AuNS associate with plant cell walls faster than their larger counterparts, with a plant cell wall size exclusion limit of ~20 nm[107,108]. Our assays further reveal that while sub-20 nm AuNP associate with plant cell walls, AuNS of all sizes do not enter plant cells. Interestingly, we find that AuNR do enter plant cells, despite having a similar smallest dimension to the 10 nm AuNS studied. Lastly, mechanistic studies allude to endocytosis as a major contributor to AuNR internalization into plant cells.

Our findings suggest that smaller nanoparticles such as our 5, 10, and 15 nm AuNS experience greater freedom of movement to convective flows within leaf tissues and are thus more easily transported to individual cell walls. Separately, analysis of hundreds of AuNR suggest that rods may translocate across the plant cell wall through a rotation-mediated process that positions rods favorably at acute angles with respect to the plane of the cell wall.

We lastly demonstrate that siRNA loaded AuNP below 20 nm enable silencing of a GFP transgene. Interestingly, gene silencing is accomplished by all sub-20 nm AuNS despite their lack of cell internalization. We achieve the highest efficiency of gene silencing – 99% - with non-cell internalizing 10 nm siRNA-loaded AuNS. We hypothesize that the interaction of the AuNP with individual plant cell walls increases their residence time proximal to cells, providing more opportunity for siRNA permeation into and utilization by plant cells. Cell wall-associated AuNP act as a reservoir for siRNA, releasing siRNA from the gold surface upon exchange with biomolecules in the surrounding biofluids whilst simultaneously protecting the siRNA cargo from nuclease degradation (**Figure 2-46**). These findings underscore our conclusion that while AuNP do not need to enter cells to deliver their cargoes, yet AuNP must intercalate into the plant cell wall for their cargoes to be efficiently utilized: it is insufficient for AuNP to reside between cells for cargo delivery. These unintuitive shape- and size-dependent transport, internalization, and silencing efficiencies of NA-functionalized AuNP motivate a non-canonical approach to

development of future plant nanobiotechnologies, including rational design of AuNP for delivery of various payloads such as mRNA and protein to advance plant biotechnology and agriculture.

2.5 Materials and Methods

2.5.1 Plant Growth, Maintenance, and Leaf Infiltration

Transgenic mGFP5 *Nicotiana benthamiana* seeds (obtained from the Staskawicz Lab, UC Berkeley) and transgenic 16C *Nicotiana benthamiana* seeds (obtained from the Falk Lab, UC Davis and the Scholthof Lab, Texas A&M University) were germinated and grown in SunGro Sunshine LC1 Grower soil mixture within the growth chamber (740 FHLED, HiPoint). mGFP5 *Nb* plants encode for GFP with an ER-localization signal, yet confocal imaging (unpublished) demonstrates a qualitatively distinct profile from the commonly used 16C *Nb* variant which is also GFP-expressing. When imaged, mGFP5 plants exhibit more homogeneous cytosolic GFP expression compared to 16C plants that occasionally demonstrate distinct puncta of GFP expression within the cytosol. Nevertheless, GFP signal from mGFP5 *Nb* originates from the cytosol, and this phenomenon is used for downstream analyses. Partway into this work, we experienced reliability issues with GFP expression levels in mGFP5 plants and obtained 16C seeds which demonstrated more reliable GFP expression. Experiments utilizing 16C seeds (all of which are contained in the supplement) have been specifically noted. The plants were grown in 4-inch pots under LED light (100-150 µmol/m^2-s) and a 14/10 light/dark photoperiod at 23 °C and 60 % humidity. All experiments were done with intact leaves in plants 4 weeks of age, where plants were incubated in the growth chamber until the time of data collection. Young leaves (approximately 2x3 cm in size) were infiltrated with a 1 mL needleless syringe on the abaxial side of the leaves after a tiny puncture had been made with a 10 µL pipette tip.

2.5.2 AuNP Functionalization

AuNP were functionalized with thiol-functionalized DNA or RNA (SH-DNA/SH-RNA, see detailed sequences in **Table 2-1**) by using a facile pH-assisted method reported previously by Zhang et al[190]. The nanoparticles were resuspended in 0.3x PBS to obtain DNA- or RNA-functionalized AuNP at desired concentrations. Fluorophore-tagged AuNP (Cy3-DNA-AuNP) were obtained by adding a Cy3-DNA sequence complementary to DNA on the AuNP. The Cy3-DNA-AuNP solution was then incubated at 40 °C for 30 min, then cooled to room temperature for at least an hour prior to use.

2.5.3 Nanoparticle Characterization

2.5.3.1 UV-Vis-IR Spectroscopy Measurements

Spectrophotometric measurements of AuNP were carried out in Sub-Micro Quartz Cuvettes (Cole-Parmer) with a UV-3600 Plus UV-Vis-NIR Spectrophotometer (Shimadzu North America).

2.5.3.2 Dynamic Light Scattering (DLS) Measurements

DLS measurements were taken with the Zetasizer Nano ZS (Malvern Analytical). Citrate-stabilized AuNP and NA-AuNP in 2 mM citrate and 0.3x PBS buffer respectively were diluted to OD1, placed in disposable cuvettes (Malvern), and set up for DLS measurement.

2.5.3.3 Transmission Electron Microscopy (TEM)

The structure of the AuNP or oligonucleotide functionalized AuNP was examined using a JEOL 1200EX instrument, and the interactions of AuNP with plant cells was studied with a Tecnai 12 TEM (Berkeley Electron Microscope Lab). AuNP were drop casted on plasma-treated Formvar carbon-coated TEM grids (Ted-Pella), then imaged at an acceleration voltage of 120 kV. To visualize siRNA on NA-AuNP, TEM grids with drop casted NA-AuNP were placed face-down on a 2 % methanolic uranyl acetate droplet for 30 s, removed, and blotted with filter paper and air-dried prior to imaging.

2.5.3.4 Quantification of Nucleic Acids on AuNP

The number of DNA and siRNA strands on each functionalized gold nanoparticle was quantified via a KCN desorption assay previously reported by Baldock et al[205]. 100 mM KCN solution (pH=12) was added to a known concentration (calculated from the UV-Vis-NIR spectra) of DNA-AuNP or siRNA-AuNP. After being left overnight, the absorbance spectrum was collected, and Beer's Law used to calculate DNA concentration at 260 nm. A calibration curve was used to obtain an extinction coefficient for siRNA. The number of DNA and siRNA molecules per AuNP was calculated by dividing the DNA concentration by the AuNP concentration.

2.5.4 Tracking of AuNP in Nb Leaves

2.5.4.1 Co-Localization Analysis of Cy3-Labeled AuNP with GFP

100 µL Cy3-DNA-AuNP at a Cy3-DNA concentration of 400 nM were infiltrated into plant leaves and left on the benchtop at 20 °C for the desired incubation time. For samples used to investigate nanoparticle internalization pathway, 40 µM wortmannin or 10 µM ikarugamycin solutions were infiltrated into target leaves 30 min prior to Cy3-DNA-AuNP introduction. To prepare infiltrated leaves for confocal imaging, a small leaf section was cut and mounted between a glass slide and #1 thickness cover slip, focusing on areas 1-3 mm radially outward from the infiltration site. Imaging was performed on the adaxial side in an effort to reduce extraneous signal from any Cy3-DNA remaining on the cuticle of the abaxial (infiltration) side. A Zeiss LSM 710 confocal microscope was used to image the plant tissue with 488 nm and 543 nm laser excitation for GFP and Cy3 signal collection respectively. The collection window for Cy3 was adjusted to 550-604 nm to avoid crosstalk between Cy3 and leaf chlorophyll autofluorescence. Images were obtained at 20x magnification. The same imaging parameters and quantification analyses were applied to samples imaged on different days. Separately, a Zeiss LSM 880 confocal microscope was used to obtain GFP and Cy3 confocal images for the 24 h samples of the AuNR3 colocalization analyses at identical excitation and collection ranges to the LSM 710 – controls were run across both scopes to ensure similar consistency in images (**Figure 2-19**). Due to equipment availability and logistical limitations, a Zeiss LSM 780 confocal microscope was used to collect z-stacks to track AuNS movement in leaves over time and distance (**Figure 2-17**). In this experiment, an 8-mm punch was used to obtain leaf discs that were then adaxially imaged. A laser excitation of 488 nm, 514 nm, and 633 nm for GFP, Cy3, and chloroplast autofluorescence signal was used, with collecting windows set between 492-551 nm, 551-631 nm, and 637-759 nm respectively.

2.5.4.2 Transmission Electron Microscopy (TEM)

To study AuNP internalization, leaves infiltrated with AuNP were cut into small pieces approximately 1 mm by 3 mm in size. Leaf samples were fixed using 2 % glutaraldehyde and 2 % Tween 20 in 0.1 M sodium cacodylate buffer (pH 7.2), then subject to microwave-assisted vacuum to remove air in the vacuoles. Samples were post-fixed with 1 % osmium tetroxide in 0.1 M sodium cacodylate buffer (pH 7.2), dehydrated with acetone, and transferred into epoxy resin for embedding. Finally, epoxy resin-embedded samples were cut into 100-nm-thin cross-sectioned films using a Reichert-Jung Ultracut E microtome, then transferred onto bare Cu TEM grids for imaging at an acceleration voltage of 120 kV.

2.5.4.3 Synchrotron X-ray Fluorescence (µXRF) Imaging

WT *Nb* leaves were infiltrated with an equivalent quantity of DNA-AuNP (0.05 mg/mL in 100 µL). 24 h post-infiltration, infiltrated leaves were harvested, cut, and placed in a disposable mold (Tissue-Tek Biopsy Cryomold) in OCT (Tissue-Tek O.C.T. Compound). Molds were placed in a vacuum chamber and subject to house vacuum for 3 cycles of 20-min treatment to enable OCT permeation into the leaves. Following vacuum treatment, slices were frozen at -20 °C for 1 h. Using a CryoStar NX50 (Epredia) at -7 °C (optimized for lowest temperature to preserve sample structural integrity with consistent results), the slices were then cut into 100 µm-thick slices, mounted onto ultra-thin quartz cover slips (19 mm x 19 mm, Chemglass), and stored at -20 °C prior to beamline exposure.

X-ray fluorescence (XRF) images were acquired at the X-ray fluorescence Microprobe beamline 10.3.2 of the Advanced Light Source at Lawrence Berkeley National Laboratory[206]. Frozen samples were transported on dry ice and transferred onto a Peltier stage kept at -22 °C. All XRF maps were recorded at an incident photon energy of 13834.2 eV (100 eV above the Au L_2-edge) with a beam spot size of 7 x 7 µm using a Canberra 7-Element Silicon Drift Detector (Mirion Technologies). For Au maps, Lα1 fluorescence emission (9713 eV) counts were recorded. Coarse maps were first acquired with 30 x 30 µm pixels using 80 ms dwell time/pixel, followed by finer maps using 7 x 7 µm and 2 x 2 µm pixels, using 100 ms dwell time/pixel.

2.5.5 Nuclease Protection

siRNA functionalized AuNP (concentrations corresponding to 0.2 µM siRNA) were incubated with 1.2 µg/mL RNase A at room temperature. Post-incubation, the endonuclease was inactivated with DEPC, and KCN added to a final concentration of 18 mM to facilitate NP decomposition. Post-overnight incubation at 4 °C, 20 µL of the samples were added to 180 uL of Quant-iT microRNA Assay Kit (Life Technologies, Thermo Fisher Scientific) reagents and fluorescence was read with an Infinite M1000 PRO microplate reader (Tecan). Free siRNA controls were included for each timepoint. Duplicate measurements were made for each of the three experimental replicates.

In a separate experiment, DNA-AuNP loaded with siRNA containing a 15-nt complementary overhang were incubated with RNase A at room temperature. Post-incubation, the nuclease was inactivated with DEPC addition, then the AuNP solution treated with 8 M urea at 37 °C for 30 min to disrupt interactions between DNA-AuNP and siRNA. Free siRNA controls were included for

each timepoint. Samples were loaded and run on a 3 % agarose gel pre-stained with SYBR Gold at 70 V for 25 min. The resulting gels were imaged using a Typhoon FLA 9500 (General Electric), and gel band intensities analyzed using FIJI and GelBandFitter[207].

2.5.6 Tracking Cargo Desorption and Availability on AuNP

2.5.6.1 Anion Exchange Fast Protein Liquid Chromatography (FPLC)

Leaves of WT *Nb* were infiltrated with 100 µL containing 100 nM of siRNA or 10 nm siRNA-AuNS in 0.3x PBS. The infiltrated areas were harvested immediately and 10-min post-infiltration and frozen in liquid nitrogen. RNA was extracted following the protocol described in Toni et al.[208] with certain modifications. We used TRIzol (Thermofisher Scientific) instead of phenol, and Phasemaker tubes (Thermofisher Scientific) were used to separate the aqueous phase.

30-40 µg of each sample was diluted with nuclease-free water to a concentration of 100-200 ng/µL. The diluted samples were subsequently filtered with a 0.22-µm filter before FPLC purification at 4 °C (AKTA FPLC system, HiTrap Q HP (1 mL, GE Healthcare) anion exchange column, flow rate: 0.5 mL/min). Buffer A (20 mM Tris-HCl, pH 8.0) and Buffer B (1.25 M NaCl + A) were used for the mobile phase with a linear gradient of 0-100% Buffer B over 25 column volumes (CV). The absorbance was monitored at 280 nm and fractions were collected in 0.5 mL aliquots. For an RNA sample, the 280 nm absorbance is approximately 25 % of the 260 nm peak (data not included in manuscript). Fractions corresponding to peaks identified close to the anticipated siRNA elution point were run on a 3.5 % agarose gel (pre-stained with SYBR Gold) at 100 V for 50 min, then imaged to verify the presence of a siRNA fragment.

2.5.6.2 siRNA Desorption in Plant Biofluid

Apoplastic fluid from mature leaves was extracted from month-old WT *Nb* plants following the protocol outlined by O'Leary et al[209]. Plant lysate was obtained in an identical fashion to protein extraction for Western blot analysis as described previously. The protein content of the apoplastic fluid and lysate was quantified using the Pierce 660 nm Protein Assay.

To test the effect of biofluid incubation across apoplastic fluid and plant lysate, 2 µg of protein was incubated with 10 nm siRNA-AuNS (final concentration of 300 nM siRNA) on the benchtop for 24 h, upon which the AuNS was centrifuged and the supernatant collected. The supernatant was run on a 3 % agarose gel to visualize any intact siRNA that had desorbed from the siRNA-AuNP.

To probe the effect of apoplastic fluid incubation across various siRNA-AuNP, 4 µg of protein was incubated with siRNA-AuNP (final concentration of 300 nM siRNA, note this corresponds to different molar concentrations of gold) on the benchtop for 24 h, upon which the AuNP were centrifuged and the supernatant collected. The supernatant was run on a 3.5 % agarose gel.

2.5.6.3 Fluorescence-Based Dynamic Exchange Assay

DNA-AuNP dynamic exchange studies were completed as described previously[201]. Briefly, the same DNA-AuNP conjugation protocol was employed using 15 nm diameter AuNP with

fluorophore-labeled, thiolated DNA (5' Texas Red-labeled and 3' thiol-modified A_{10} single-stranded DNA oligos; abbreviated TR-DNA). Fluorescent TR-DNA was tracked in the presence of various solution conditions and the displacement of DNA from the AuNP surface was monitored as an increase in TR fluorescence. For the apoplastic fluid condition, 40 µL of undiluted WT *Nb* apoplastic fluid was added to 10 µL of 25 nM TR-DNA-AuNP in 0.3x PBS solution (final concentration of 5 nM TR-DNA-AuNP). For all other experimental conditions, 25 µL of 2x-concentrated solution was added to 25 µL of 2x-concentrated TR-DNA-AuNP. All experiments were run in duplicate. Solutions were added via microchannel pipette into a 96-well PCR plate (Hard Shell PCR Plates, Bio-Rad) and mixed by pipetting. The plate was sealed with an optically transparent adhesive seal (Microseal 'B' Plate Sealing Film, Bio-Rad) and briefly spun down on a benchtop centrifuge. Fluorescence time series readings were measured in a Bio-Rad CFX96 Real Time qPCR System by scanning the Texas Red channel every 30 s for 8 h at 22.5 °C (lid heating off).

2.5.7   Analyzing GFP Silencing in Nb Leaves using siRNA-AuNP

2.5.7.1   Reverse Transcriptase-Quantitative PCR (RT-qPCR)

siRNA-AuNP loaded with 100 nM siRNA were infiltrated into plant leaves and left on the benchtop at 20 °C for 24 h or 7 days upon which total RNA was extracted. Two-step RT-qPCR was performed to quantify GFP gene silencing with the following commercially available kits: RNeasy plant mini kit (QIAGEN) for total RNA extraction from leaves, iScript cDNA synthesis kit (Bio-Rad) to reverse transcribe total RNA into cDNA, and PowerUp SYBR green master mix (Applied Biosystems) for RT-qPCR. The target gene in our qPCR was mGFP5 (GFP transgene inserted into *Nicotiana benthamiana*), and EF-1 (elongation factor 1) was chosen as the housekeeping (reference) gene[210,211]. Primers (see detailed sequences in **Table 2-1**) for these genes (fGFP, rGFP, fEF1 and rEF1) were ordered from IDT and used without further purification. An annealing temperature of 60 °C was used for RT-qPCR, which was run for 40 cycles. RT-qPCR data was analyzed by the ddCt method[212] to obtain the normalized GFP gene expression-fold change with respect to the EF-1 housekeeping gene and control sample. For each sample, RT-qPCR was performed as 3 technical replicates (3 reactions from the same isolated RNA batch), and the entire experiment consisting of independent infiltrations and RNA extractions from different plants was repeated 3 times (3 biological replicates).

2.5.7.2   Western Blot

siRNA-AuNP loaded with 100 nM siRNA were infiltrated into plant leaves and left on the benchtop at 20 °C for 3 or 7 days upon which proteins were extracted. Briefly, infiltrated leaves were cut, frozen in liquid nitrogen, and ground with a mortar and pestle. 350 µL lysis buffer (10 mM Tris/HCl (pH 7.5), 150 mM NaCl, 1 mM EDTA, 0.1 % NP-40, 5 % glycerol, and 1 % protease inhibitor cocktail) was added to the resulting powder, vortexed, spun down, and kept on ice. All samples were incubated at 50 °C for 3 min, centrifuged at 16,000 g for 30 min, and the supernatant transferred to a new tube to obtain extracted proteins. Protein concentration of samples were quantified using a Pierce 660 nm Protein Assay (Thermo Fisher), and concentrations of proteins standardized with the addition of lysis buffer. Loading dye was added to protein solutions, incubated at 95 °C for 10 min, and centrifuged at 16,000 g for 15 min. All sample wells were normalized to the same amount of total protein. A 4-20 % Mini-PROTEAN Precast Protein Gel (BIORAD) was loaded with samples and run at 120 V for 60 min with a Mini-PROTEAN Tetra

Cell (BIORAD). The gel was included in a sandwich with a methanol activated PVDF membrane, placed in cold 1x Tris/Glycine buffer, and run at 400 mA for 60 min. To verify equal protein loading, RuBisCO band intensities were qualitatively verified with Ponceau Red staining (**Supplementary Note 6**). Post-transfer, the membrane was rinsed with 1x TBST buffer three times, with 5 min in between each rinse, followed by a 60-min incubation with 5 % BSA in TBST, and three rinses with 1x TBST including incubations. The membrane was incubated at 4 °C on a shaker with rabbit antibody anti-GFP (1:3000 dilution) overnight, rinsed with TBST, incubated for 60 min with goat anti-rabbit antibody (1:5000 dilution), rinsed with TBST. The membrane was washed briefly in MilliQ water, exposed to Pierce ECL Western Blotting Substrate (Thermo Scientific), and immediately imaged. 3 biological replicates were collected, and band intensity analyses done on each.

2.5.8   *Probing the Response of AuNP Infiltration into Nb with RT-qPCR*

13 total genes associated with various types of stress responses were selected to understand the impact of AuNP infiltration into *Nb*. 16C *Nb* leaves were infiltrated with buffer, citrate-stabilized 10 nm AuNS (same AuNS concentration as siRNA-AuNS), and 10 nm siRNA-AuNS (siRNA concentration of 100 nM). Leaves were harvested immediately post-infiltration and 24 h post-infiltration, frozen in liquid nitrogen, and lysed with a bead beater. Subsequent RNA extraction, cDNA synthesis, and RT-qPCR was performed as previously described. For the *NbrbohB* analysis performed using 10 nm siRNA-AuNS and siRNA-AuNR, we used mGFP5 *Nb* leaves infiltrated with buffer, free siRNA, and siRNA-AuNP (corresponding to 100 nM siRNA) and harvested tissue 1-day post-infiltration for downstream RT-qPCR analysis.

2.5.9   *Statistics and Data Analysis*

2.5.9.1   *Confocal Cy3-GFP Co-Localization Data*

Data collection for each sample was done in triplicate, with 10-15 technical replicates (non-overlapping confocal field of views from each leaf) collected for each biological replicate (an infiltration into a unique plant). Each field of view was analyzed with ImageJ analysis software to obtain a co-localization proportion as given by the Mander's Overlap Coefficient, and all fields of view were averaged to obtain a single value for that biological replicate. Data are expressed as each mean from the 3 biological replicates, with error bars denoting standard error of the mean (s.e.m.). Significance is measured with one-way ANOVA with Tukey's multiple comparisons test. For the incubation time-varied experiments, in order of the 5 nm AuNS, 10 nm AuNS, 15 nm AuNS, 20 nm AuNS, and AuNR confocal experiments, F=36.07, 21.95, 18.65, 35.29, and 75.64, where the corresponding p-value for all the aforementioned experiments was **** $p<0.0001$. For the AuNR3 confocal experiments, F=18.50 and p=0.0003. For the endocytosis inhibitor assay, the significance of the 10 nm AuNS and AuNR results was similarly measured with one-way ANOVA with Tukey's multiple comparisons test; F=2.621 and p=0.1520, F=33.46 and p=0.0006 (***) respectively. For confocal z-stacks, ZEISS ZEN software was used to create orthographic projections and FIJI was used to calculate total Cy3 intensity. The uniformity of Cy3 signal was estimated using a sum projection of the z-stacks in imaged leaves. An autocorrelation function was calculated from the radial integrated intensity profile on each sum projection (FIJI).

2.5.9.2 TEM Data

To quantify angle of NR orientation with respect to the cell wall, ImageJ's Measure function was used to draw tangents to local cell wall contacting NR and direction of NR long axis. The resulting difference in angle (acute) was used. The likelihood estimation for finding randomly oriented AuNR at a given angle included simplifying assumptions that the tissue sectioning process did not impact AuNR orientation and that the 2-dimensional image would accurately represent its 3-dimensional configuration. Accordingly, an equal likelihood spread over 9 buckets (0-10 °, 10-20 °, …, 80-90 °) would result in a percentage of 11.1 %.

2.5.9.3 μXRF Imaging Data

Maps were normalized to the incident beam intensity and dwell time, then deadtime corrected and decontaminated. μXRF data processing was performed with a suite of LabVIEW custom software programs (National Instruments) available at Beamline 10.3.2 (http://xraysweb.lbl.gov/uxas/Beamline/Software/Software.htm) and further processed with a custom Matlab program available at the beamline.

2.5.9.4 Nuclease Protection Data

For Quant-iT based quantification, data collection for each sample was done in triplicate, with fluorescence measurements performed in duplicate and the numerical average used for further analysis. Background fluorescence from remnant DNA and background noise was subtracted from all samples. The proportion of intact siRNA at time T was obtained using the following equation,

$$\% \ Intact \ siRNA_{t=T} = \frac{Counts_{t=0} - Counts_{t=T}}{Counts_{t=0}} * 100\% \qquad 2\text{-}1$$

Data are expressed as each mean from the 3 replicates, with error bars denoting standard error of the mean. For the experiment in Error! Reference source not found.**b**, significance is measured with two-way ANOVA with Tukey's multiple comparisons test; for time (n=6), column factor (n=3), and subject (n=9), F=267.6 and p<0.0001, F=186.7 and p<0.0001, and F=4.953 and p=0.0013 respectively. For the experiment in **Figure 2-34**, significance is measured with two-way ANOVA with Tukey's multiple comparisons test; for time (n=6), column factor (n=5), and subject (n=15), F=239.2 and p<0.0001, F=248.1 and p<0.0001, and F=1.041 and p=0.4242 respectively.

For the gel-based quantification probing nanoparticle protection against endonucleases, data collection for each sample was done in triplicate. Following band intensity quantification and deconvolution, the proportion of intact siRNA at time T was obtained using an analogous equation to Equation 2-1. Data are expressed as each mean from the 3 replicates, with error bars denoting standard deviation. Significance is measured with two-way ANOVA with Tukey's multiple comparisons test; for time (n=5), column factor (n=3), and subject (n=9), F=21.07 and p=0.0010, F=45.85 and p=0.0002, and F=26.11 and p<0.0001 respectively.

2.5.9.5 Fluorescence-Based Dynamic Exchange Assay Data

Data collection for each sample was done in duplicate. Fluorescence values were converted to molar concentrations with standard curves for TR-DNA in each solution condition tested, using

the value at time 100 min to ensure solution equilibration. Standard curves for TR-DNA in 0.3x PBS were used for the apoplastic fluid case, based on limited biofluid availability and the minimal contribution to apoplastic fluid to the baseline fluorescence (Error! Reference source not found.**c**, gray line). All TR-DNA standard curves were measured for the same time duration as the experiments to ensure the fluorescence readings were time stable. To calculate the percentage of DNA released, raw fluorescence readings were converted to a molar amount of DNA using the relevant standard curve and divided by the expected molar amount of DNA present, calculated using the experimentally determined DNA loading value per AuNP (**Table 2-4**).

2.5.9.6   RT-qPCR Data

GFP silencing experiments comprised of 3 biological replicates, whereby 3 separate leaves are infiltrated per sample and analyzed with RT-qPCR. Each biological replicate consisted of 3 technical replicates for the RT-qPCR reaction. No template controls and no reverse transcriptase controls were also performed. Data are expressed as each mean from the 3 biological replicates, with error bars denoting standard error of the mean. Significance is measured with one-way ANOVA with Tukey's multiple comparisons test. For 1-day and 7-day experiments, F=30.26 and $p<0.0001$, F=1.803 and p=0.2436 respectively. For the 1-day AuNR3 experiment, F=0.87 and p=0.0040. For the *NbrbohB* stress gene experiment, F=0.4437 and p=0.7283.

2.5.9.7   Western Blot Data

Western blot experiments to quantify GFP comprised of 3 biological replicates, whereby 3 separate leaves are infiltrated per sample and proteins extracted for further analysis. Data are expressed as the mean from the 3 biological replicates, with error bars denoting standard error of the mean. Significance is measured with one-way ANOVA with Tukey's multiple comparisons test. For 3-day and 7-day experiments, F=10.26 and p=0.0002, F=2.122 and p=0.2010 respectively.

2.6 Chapter Supporting Information

2.6.1 *Supplementary Figures and Tables*
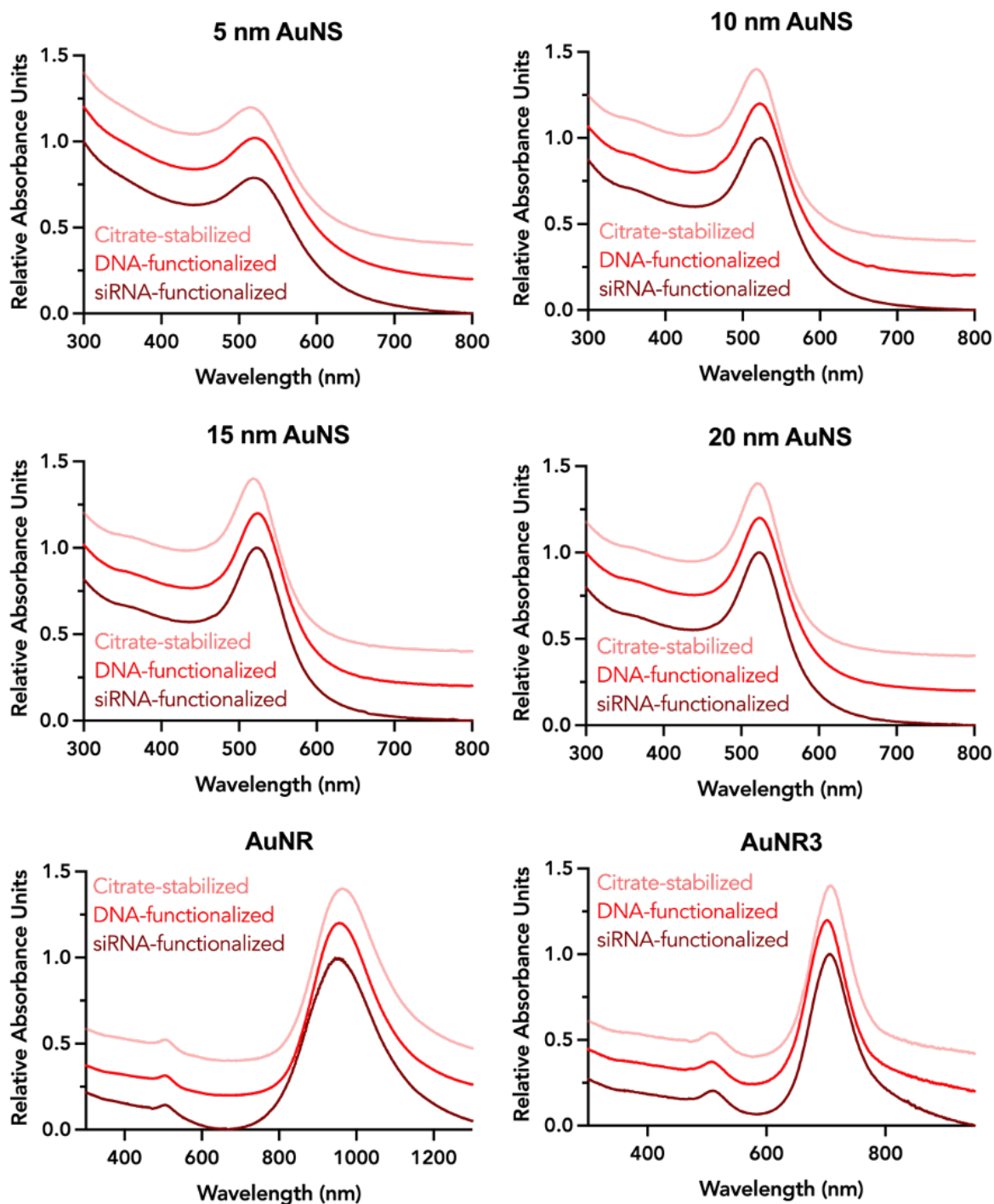
Figure 2-6. UV-Vis spectra of pristine citrate-stabilized AuNP, DNA-AuNP, and siRNA-AuNP confirm colloidal stability of nucleic acid-functionalized AuNP.
A small redshift in the functionalized AuNS SPR peaks suggest successful functionalization.
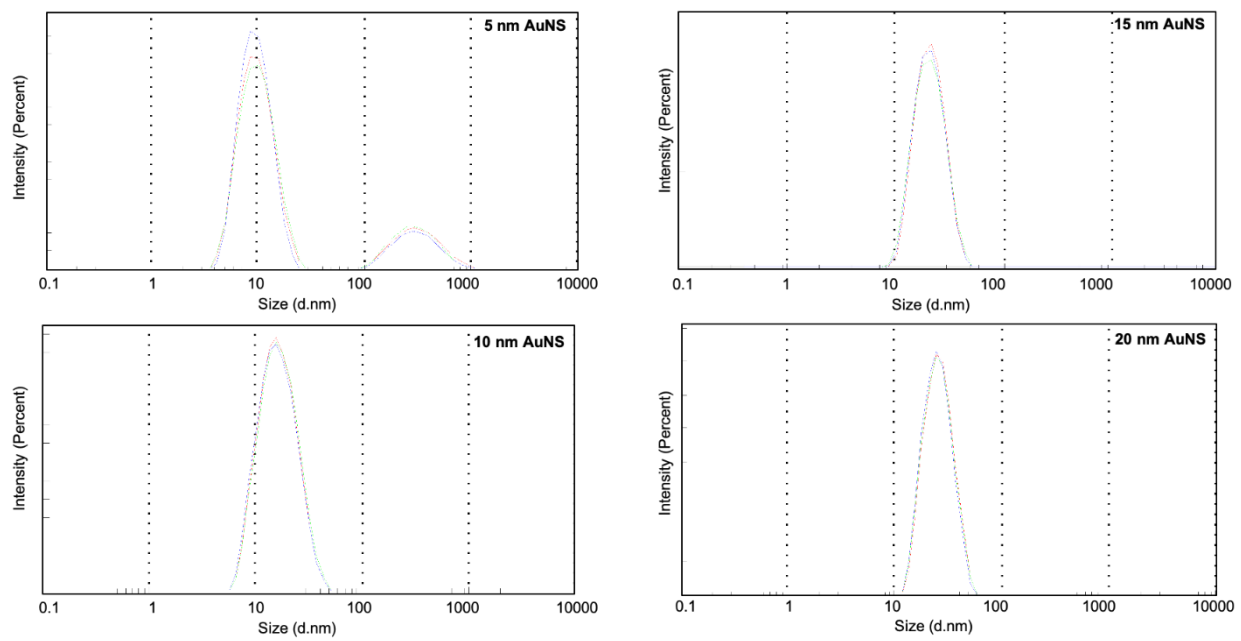
Figure 2-7. DLS spectra of citrate-stabilized AuNS.
Aggregates may present in 5 nm AuNS sample.
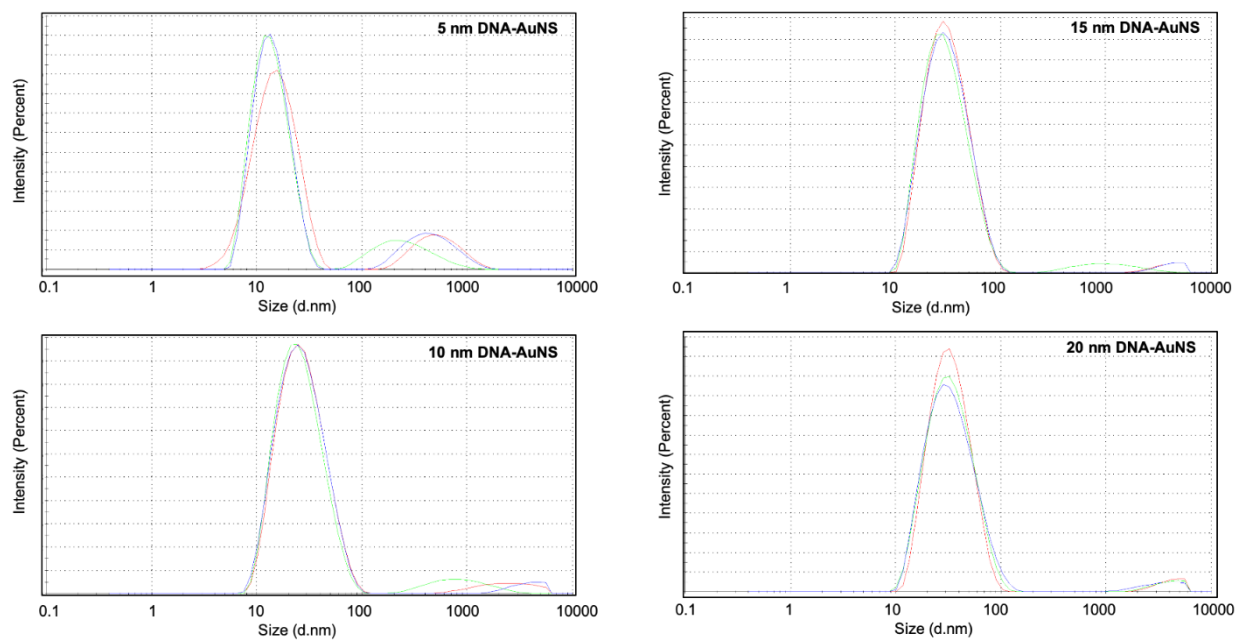
Figure 2-8. DLS spectra of DNA-AuNS.
Small amounts of aggregation might present across all DNA-AuNS.
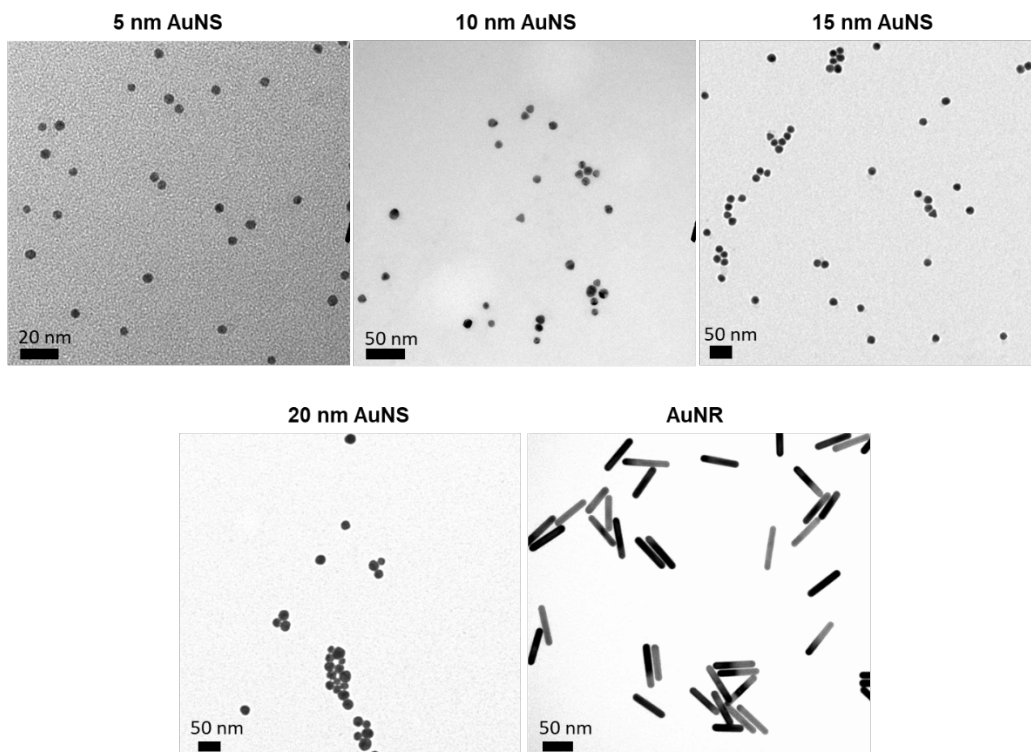
Figure 2-9. TEM images of DNA-AuNP.
Scale Bar: 20 nm for 5 nm AuNS, and 50 nm for other AuNP.
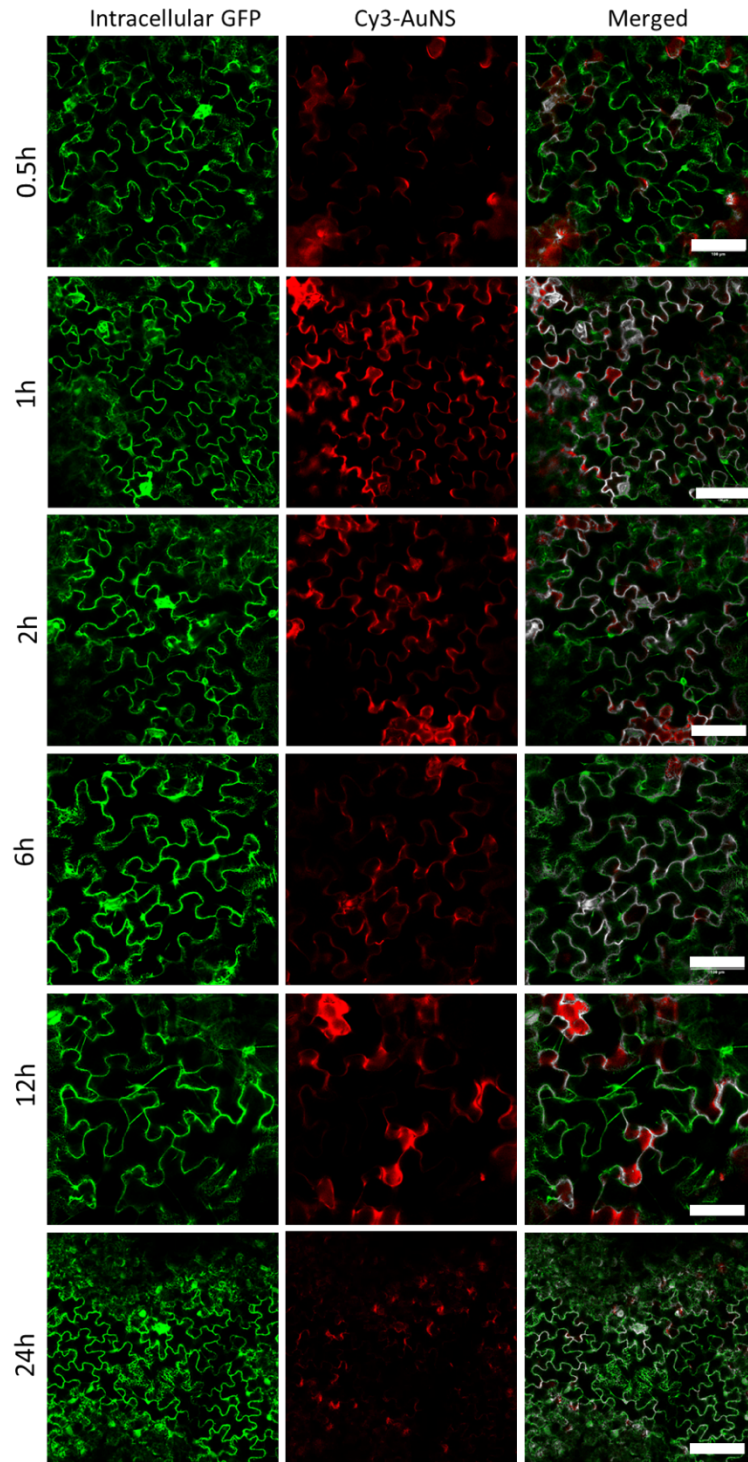
Figure 2-10. Representative confocal images of 5 nm Cy3-DNA-AuNS infiltrated into *Nicotiana benthamiana* **(***Nb***) leaves for various incubation times.**
Scale bar: 100 μm.
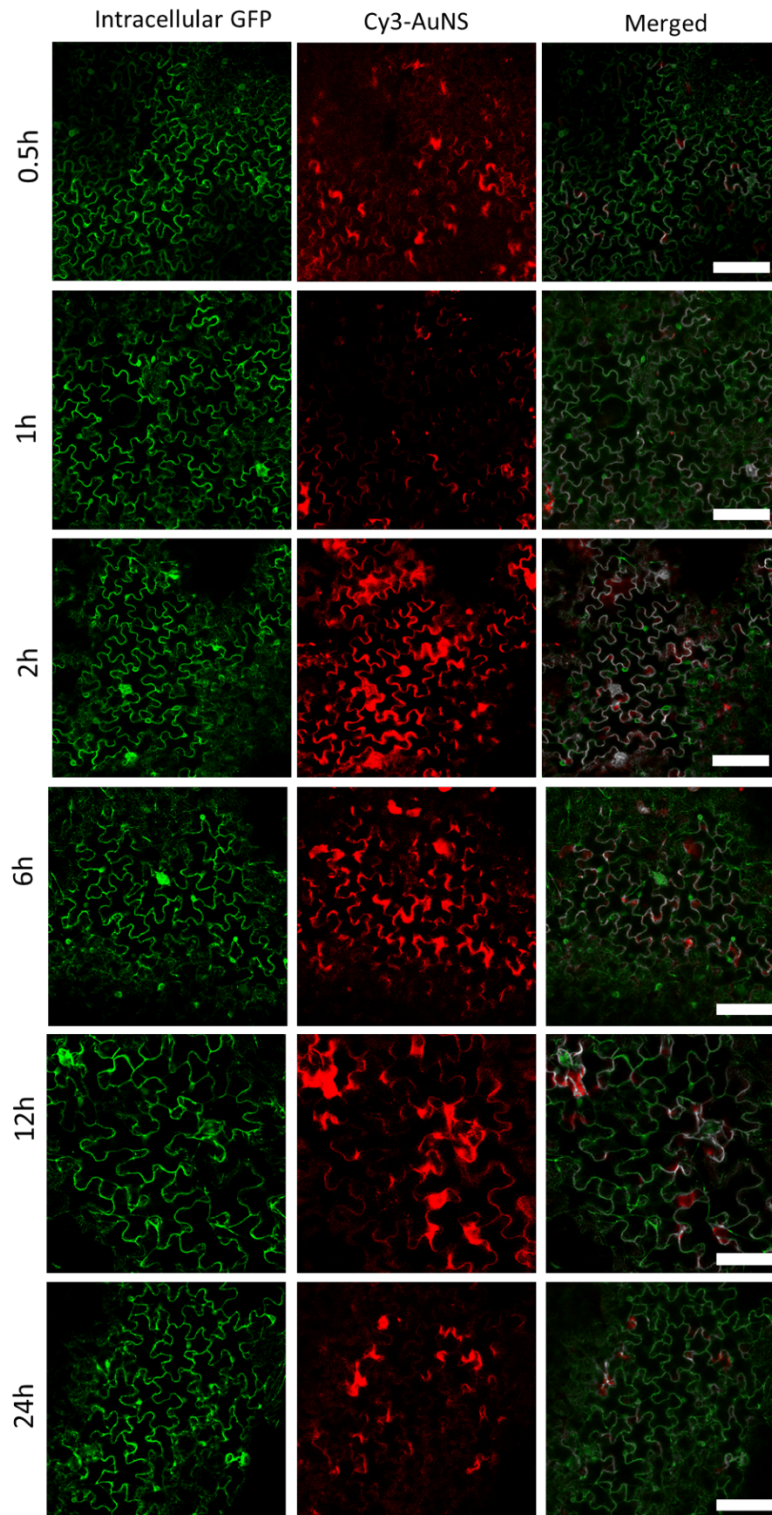
Figure 2-11. Representative confocal images of 10 nm Cy3-DNA-AuNS infiltrated into *Nb* leaves for various incubation times.
Scale bar: 100 μm.
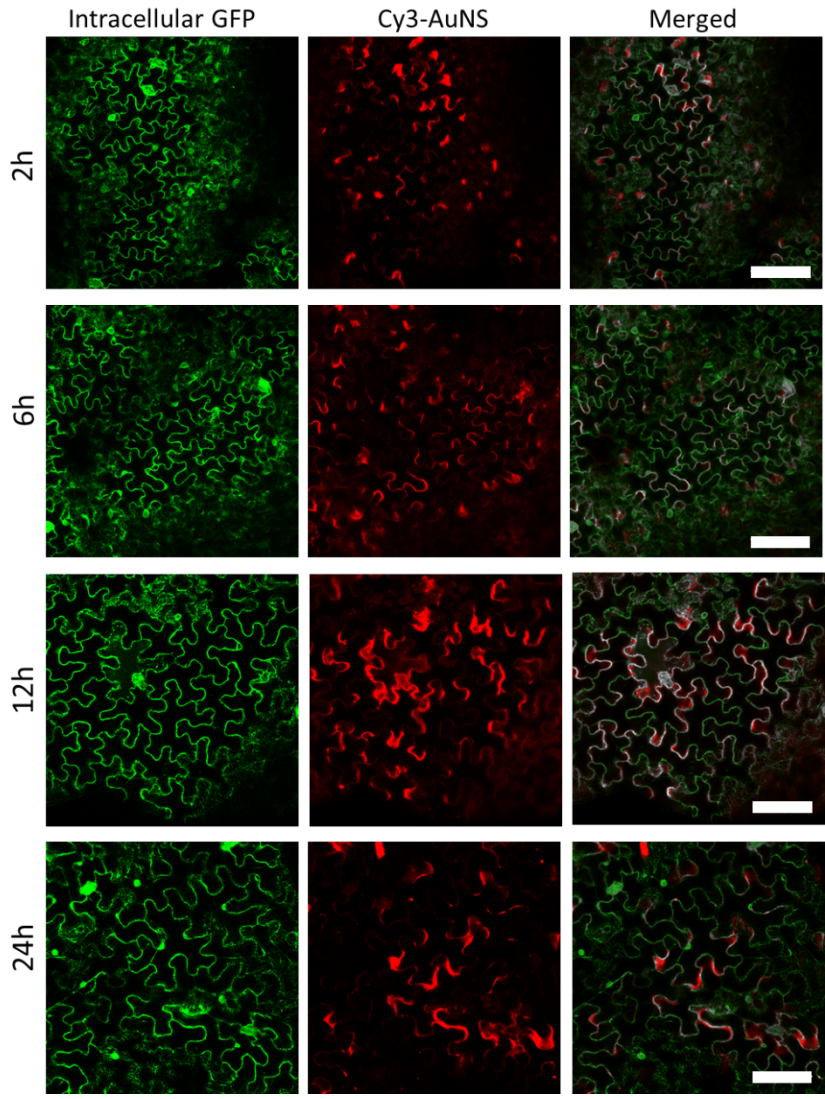
Figure 2-12. Representative confocal images of 15 nm Cy3-DNA-AuNS infiltrated into *Nb* leaves for various incubation times.
Scale bar: 100 μm.
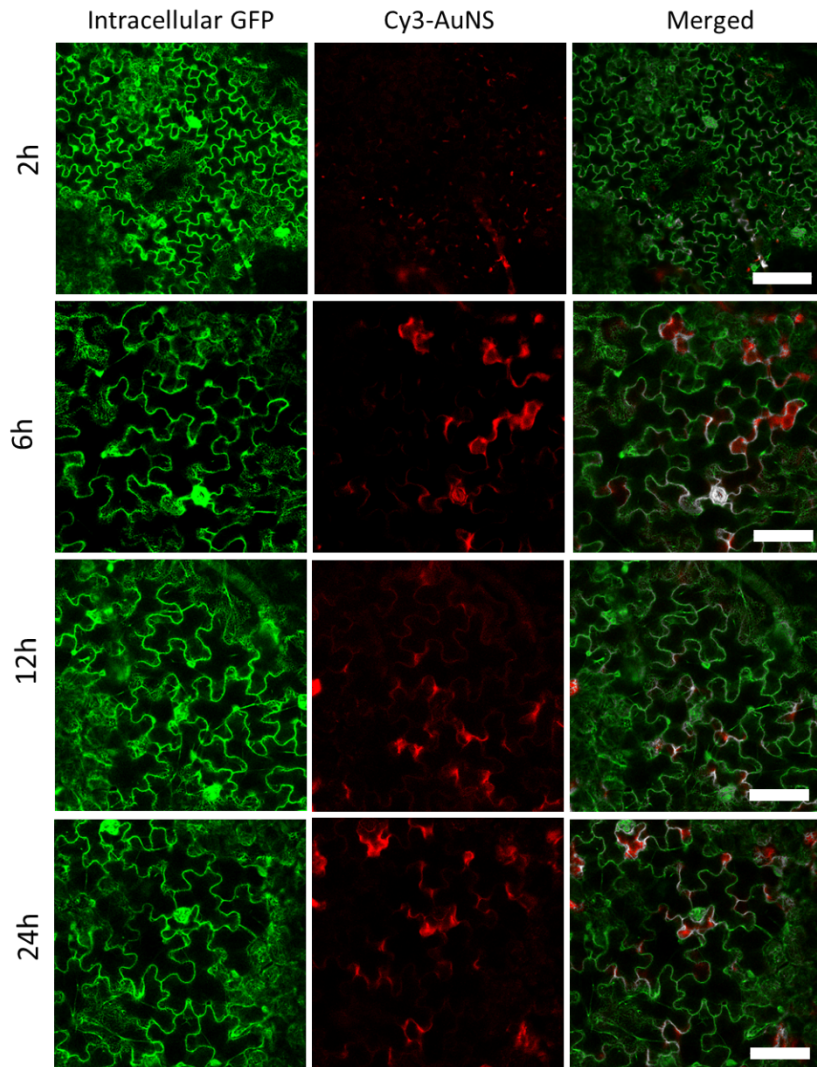
Figure 2-13. Representative confocal images of 20 nm Cy3-DNA-AuNS infiltrated into *Nb* leaves for various incubation times.
Scale bar: 100 μm.
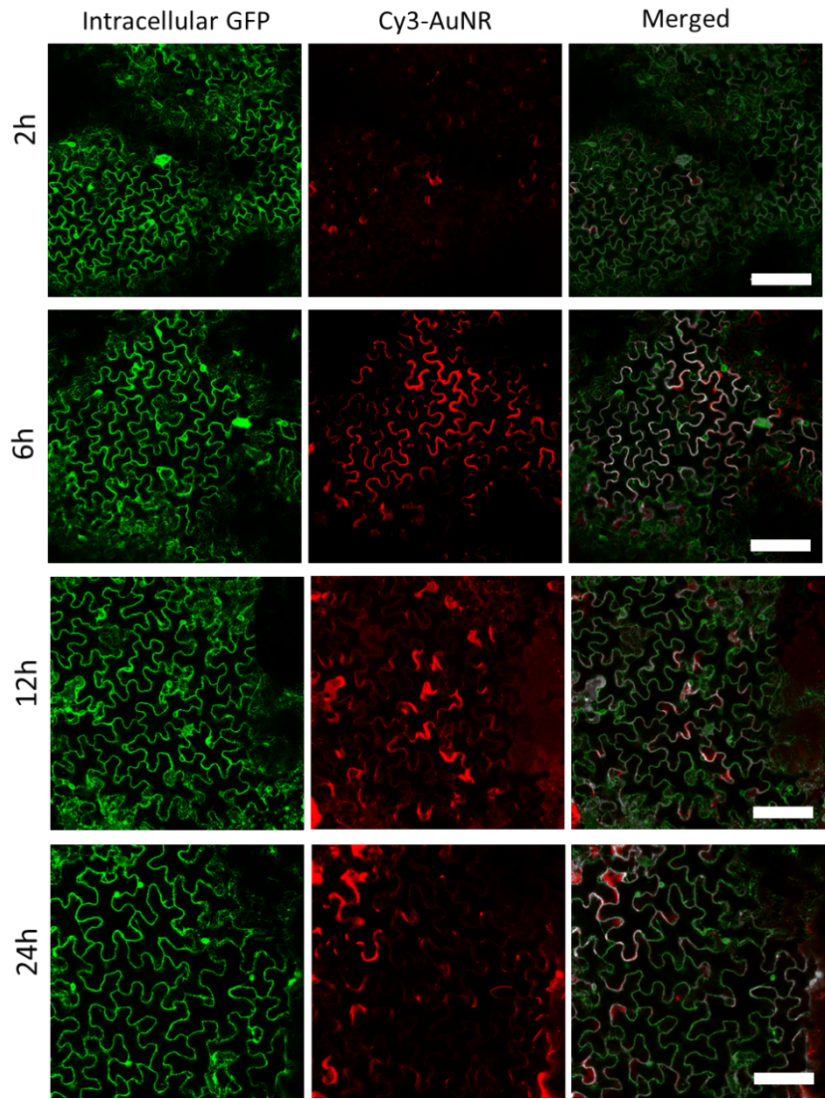
Figure 2-14. Representative confocal images of Cy3-DNA-AuNR infiltrated into *Nb* leaves for various incubation times.
Scale bar: 100 μm.
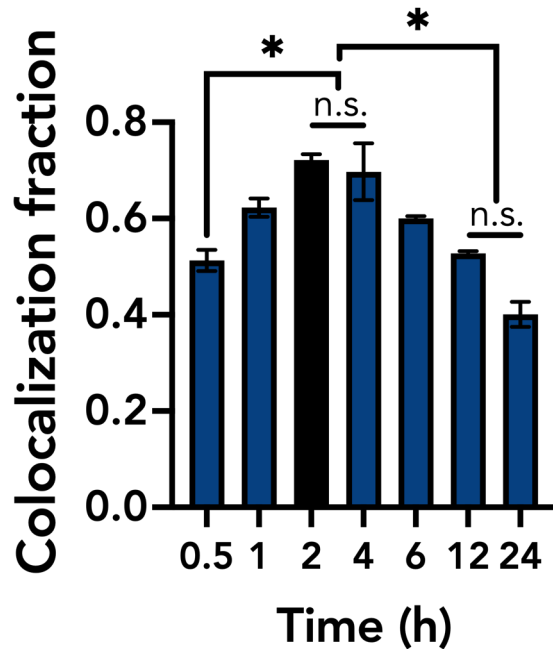
Figure 2-15. Cy3-DNA-AuNR3 association with plant cells following infiltration into 16C *Nb* leaves.

Cy3-DNA-AuNR3 (10 nm x 30 nm, aspect ratio 3) corresponding to 400 nM of Cy3 was infiltrated into 16C *Nb* leaves and imaged under confocal microscopy at defined timepoints. Similar to the 10 nm AuNS, we observe a maximum colocalization fraction at the 2 h timepoint (that is not statistically significantly different from the 6 h timepoint). We note a higher colocalization fraction in general compared to our other confocal-based studies and attribute this potentially to realignment of the microscopy setup as well as the different line of GFP-expressing transgenic *Nb* plants used. Nevertheless, the colocalization fractions shown are still comparable between timepoints for this AuNR. *p≤0.0197, ≤0.0308 in one-way ANOVA; n.s.: not significant; error bars indicate s.e.m. (n=2).
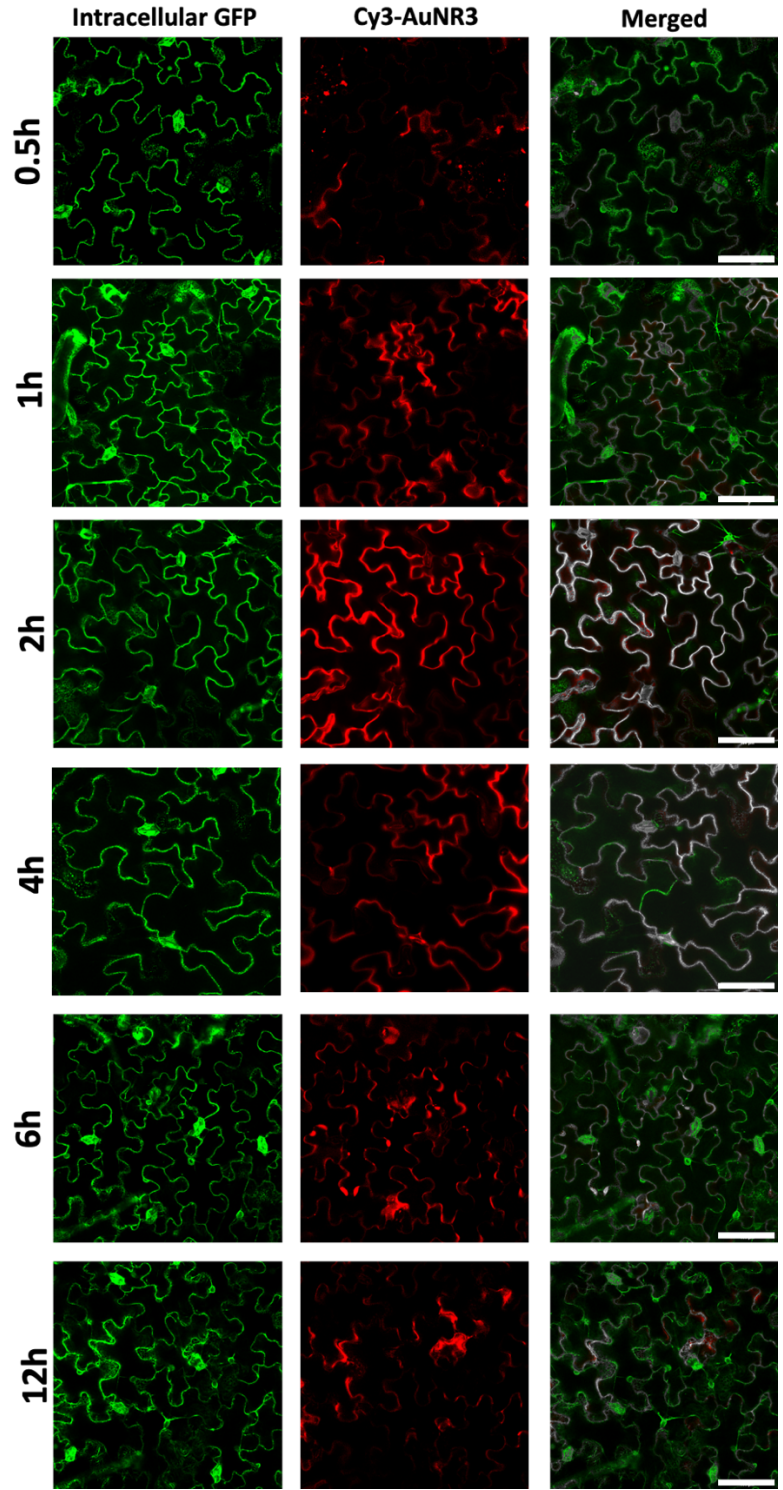
Figure 2-16. Representative confocal images of Cy3-DNA-AuNR3 infiltrated into 16C *Nb* leaves and imaged at various timepoints post-infiltration.
Scale bar: 100 μm.
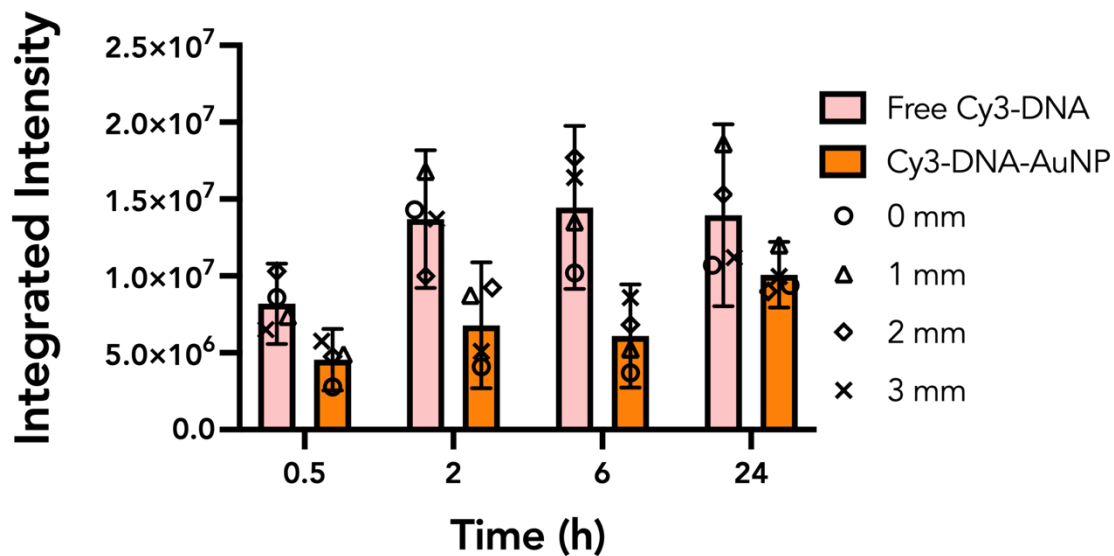
Figure 2-17. Integrated Cy3 intensity of free Cy3-DNA and Cy3-DNA-AuNP in 16C *Nb* leaf imaged various distances from the infiltration site over time.
16C *Nb* leaves were infiltrated with free Cy3-DNA (400 nM) and 10 nm Cy3-DNA-AuNP (concentrations corresponding to 400 nM Cy3-DNA), and z-stacks were collected from the abaxial side as a function of distance from infiltration site (0-3 mm) and time post-infiltration (0.5 h, 2 h, 6 h, 24 h). The graph plots integrated Cy3 intensity over each collected z-stack against time for each infiltrated sample. At longer times (2 h onwards), we observe a leveling-off of total signal from Cy3-DNA suggesting equilibration of Cy3-DNA within the area analyzed. Meanwhile, total signal from Cy3-DNA-AuNP broadly increases with time. We attribute this phenomenon to a longer time needed for AuNP diffusion through leaf tissue as well as a recovery in Cy3-fluorescence upon desorption from the AuNP surface over time. Error bars represent 95 % CI.
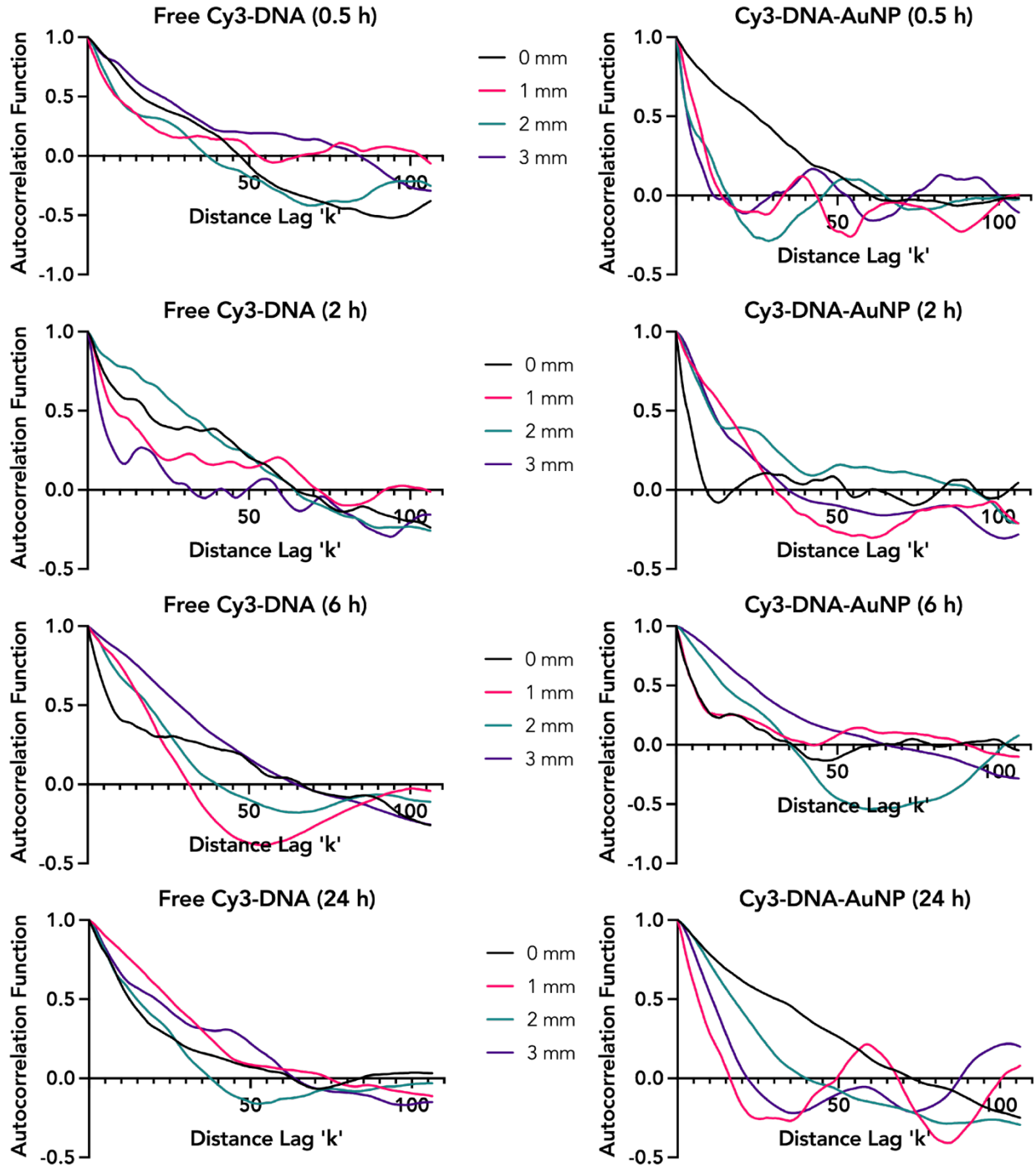
Figure 2-18. Uniformity of Cy3-DNA signal from free Cy3-DNA versus 10 nm Cy3-DNA-AuNP in 16C *Nb* leaf imaged various distances from the infiltration site over time.
A radial intensity profile was collected from the sum projection of each z-stack and used to generate an autocorrelation function (ACF). From the ACF, we can detect autocorrelation in the fluorescence intensity at varying radii and therefore length scales. Periodicity in the autocorrelation function indicates regularly spaced or regularly sized objects within the sum projection. Relatively uniform ACF or rapidly decaying ACF indicates uniform or highly random Cy3 fluorescence. While most ACFs are rapidly decaying, we note some interesting observations. Free Cy3-DNA

displays evident periodicity at 2 h, consistent with our confocal observations where majority of the Cy3 signal is found proximal to cytosolic GFP in the perimeter of the cell. This periodicity is lost in later timepoints, visually supported by a 'smearing' or more diffuse Cy3 signal under confocal microscopy. In contrast, Cy3-DNA-AuNP displays periodicity over multiple timepoints (0.5 h, 2 h, 24 h), suggesting strong and relatively consistent association with the cell wall or cytosolic GFP.
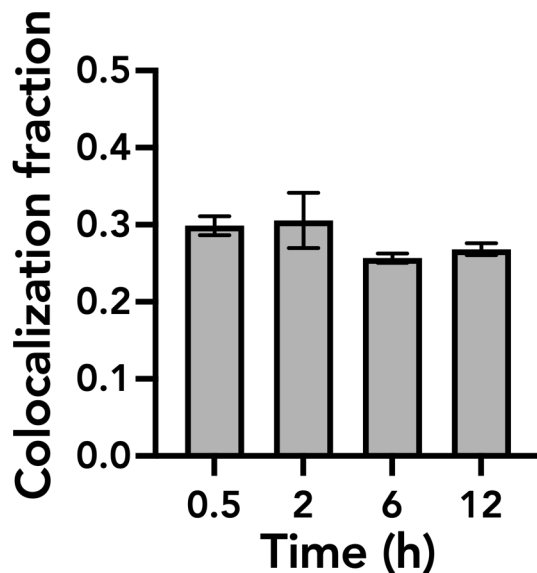
Figure 2-19. Free Cy3-DNA association with plant cells following infiltration into 16C *Nb* leaves.

Free Cy3-DNA (400 nM) was infiltrated into 16C *Nb* leaves and imaged under confocal microscopy (Zeiss LSM 710 and LSM 780) at defined timepoints. We observe consistent colocalization fractions across timepoints and utilize the highest average for the timepoints sampled (2 h) as the base level of background signal across other Cy3-DNA-AuNP association studies (grey dashed line in Error! Reference source not found.**b**). In one-way ANOVA, p=0.2953; error bars indicate s.e.m. n=3.
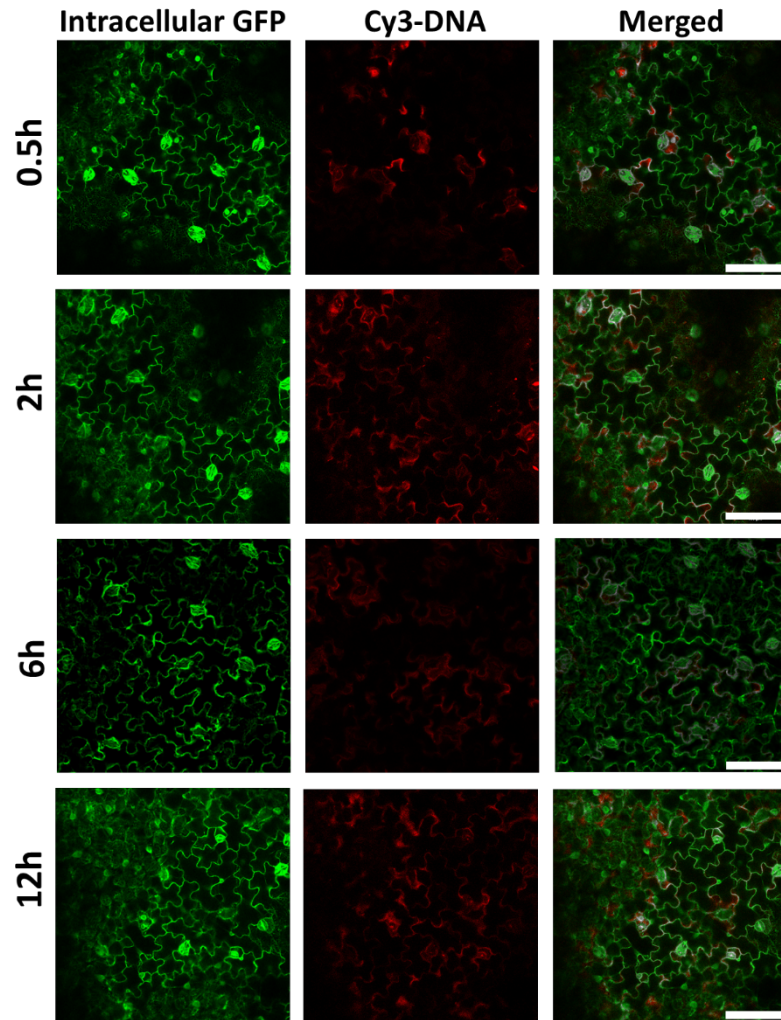
Figure 2-20. Representative confocal images of free Cy3-DNA infiltrated into *Nb* leaves at various incubation times (0.5, 2, 6 and 12 h).
Scale bar: 100 μm.
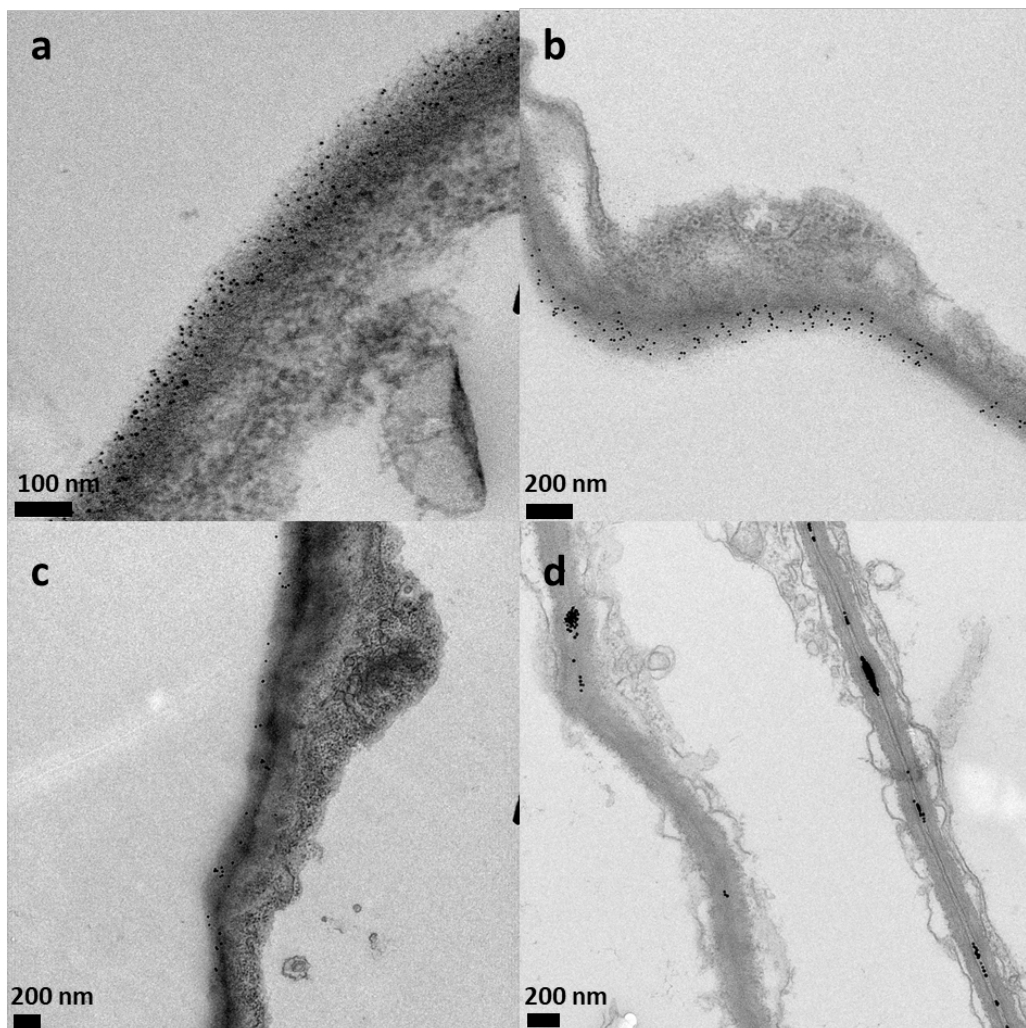
Figure 2-21. Additional TEM images of DNA-AuNS treated *Nb* leaves 24 h post-infiltration.
a 5 nm DNA-AuNS, **b** 10 nm DNA-AuNS, **c** 15 nm DNA-AuNS, and **d** 20 nm DNA-AuNS.
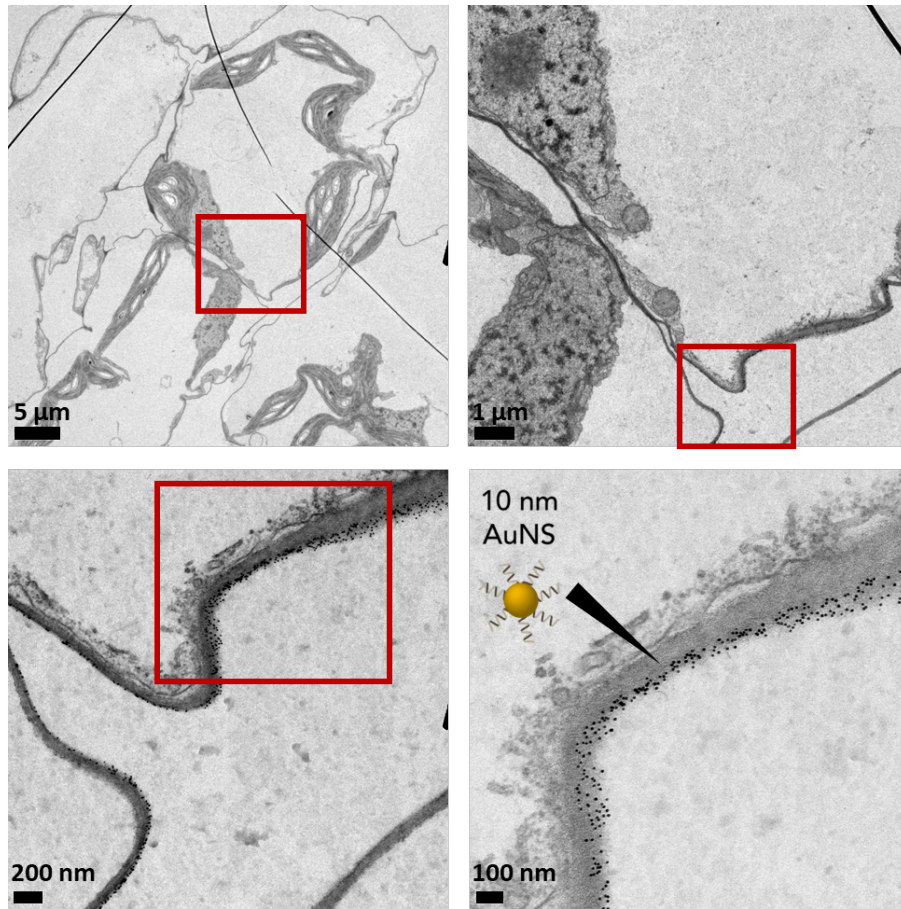
Figure 2-22. Additional TEM images of 10 nm DNA-AuNS treated *Nb* leaves 6 h post-infiltration showing AuNS association with cell walls (black arrow).
6 h post-infiltration is past the timepoint of maximum association (2 h) observed under confocal analysis. Similar to the 24 h sample, a high density of AuNS was intercalated with cell walls facing the extracellular space, with no observed instances of AuNS inside cells.
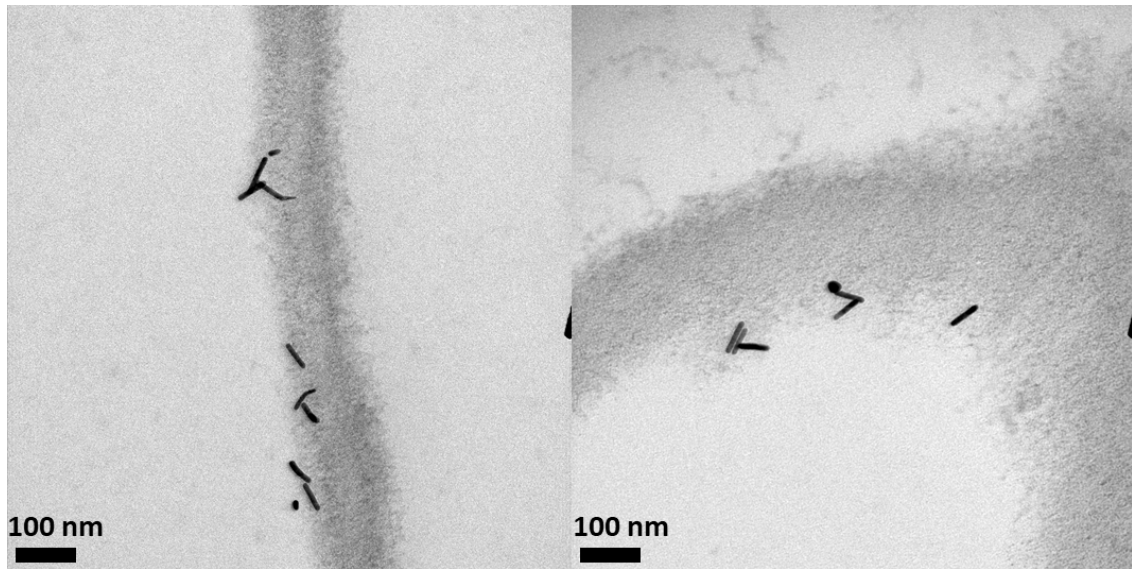
Figure 2-23. Additional TEM images of DNA-AuNR treated *Nb* leaves showing AuNR piercing into the cell walls.
Several AuNR demonstrate travel past the cell wall-apoplast interface and partially penetrated the cell wall.
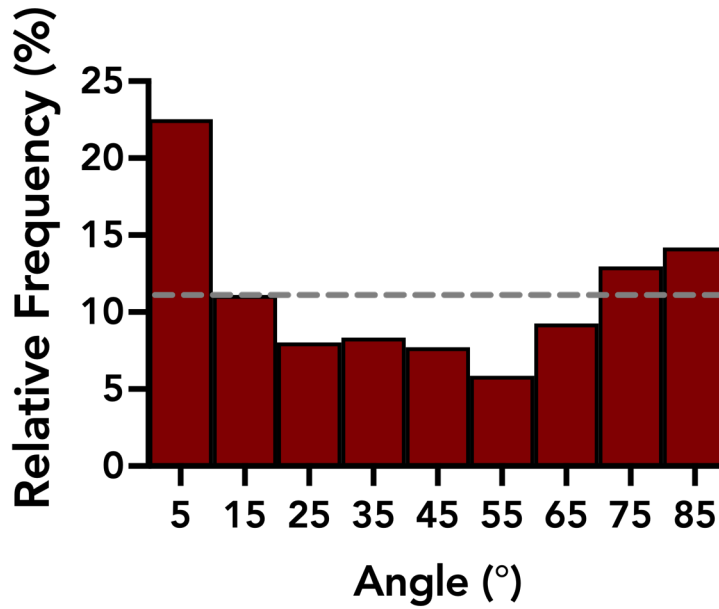
Figure 2-24. Histogram of AuNR orientations quantified with respect to cell wall tangent. AuNR at 90 ° are perpendicular to the local region of the cell wall, and AuNR at 0 ° are parallel to the cell wall (n=324). X-axis labels mark the center of each of the 9 bins. Dashed line represents predicted percentage orientation of 11.1% assuming AuNR orientations were random. Histogram values can be found in **Table 2-5**.
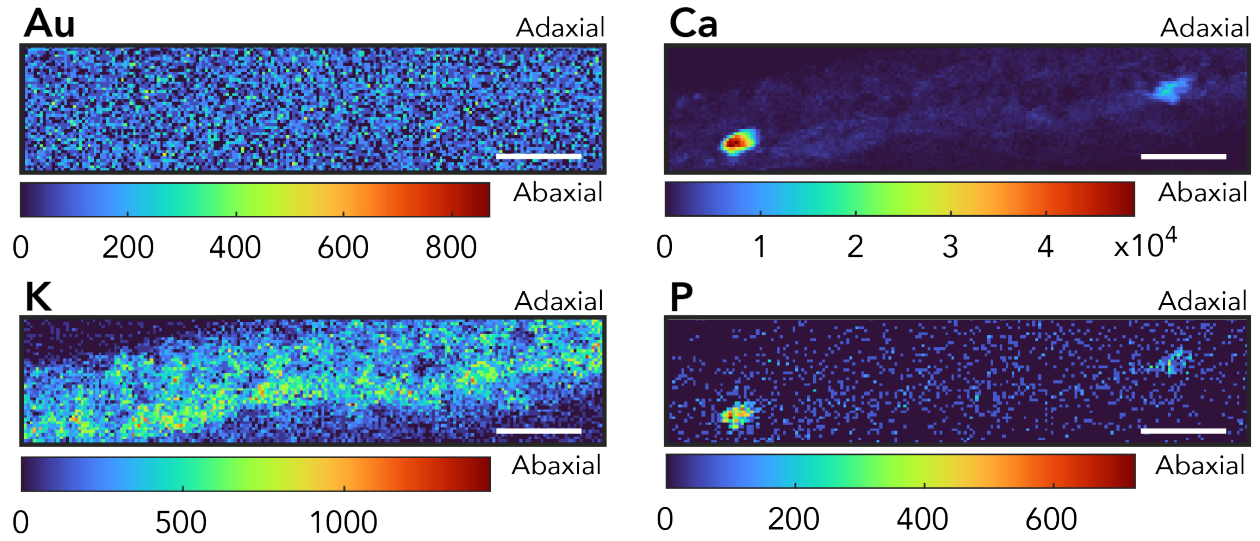
Figure 2-25. μXRF distribution maps of gold, calcium, potassium, and phosphorous of the cross-section of a WT *Nb* leaf infiltrated with water (7 x 7 μm pixels).
Scale bars: 200 μm.
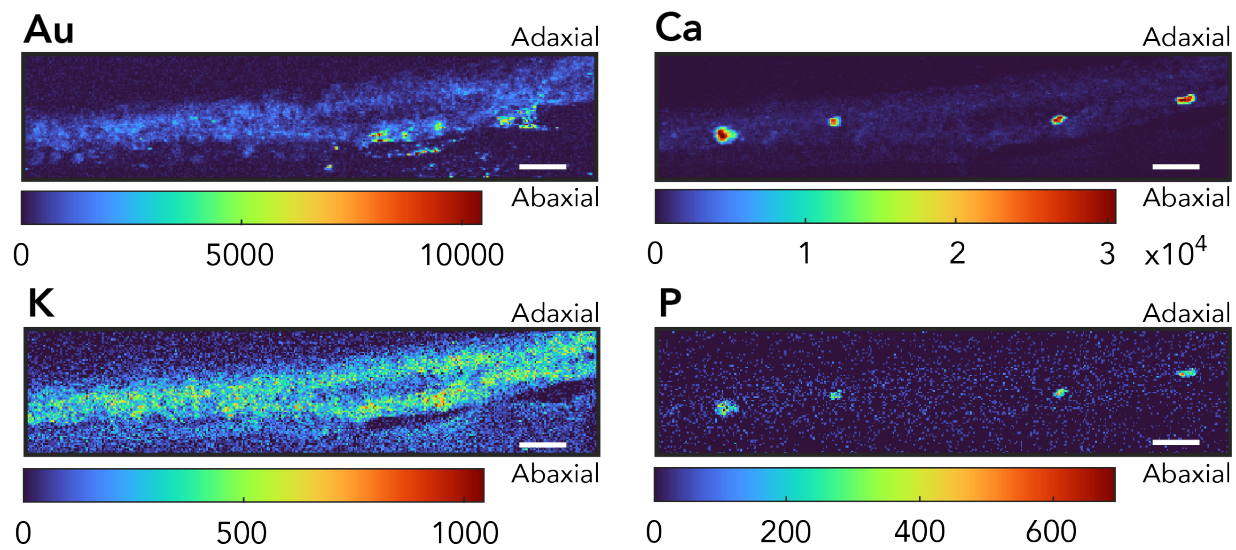
Figure 2-26. µXRF distribution maps of gold, calcium, potassium, and phosphorous of the cross-section of a WT *Nb* leaf infiltrated with 20 nm DNA-AuNS (7 x 7 µm pixels). Scale bars: 200 µm.
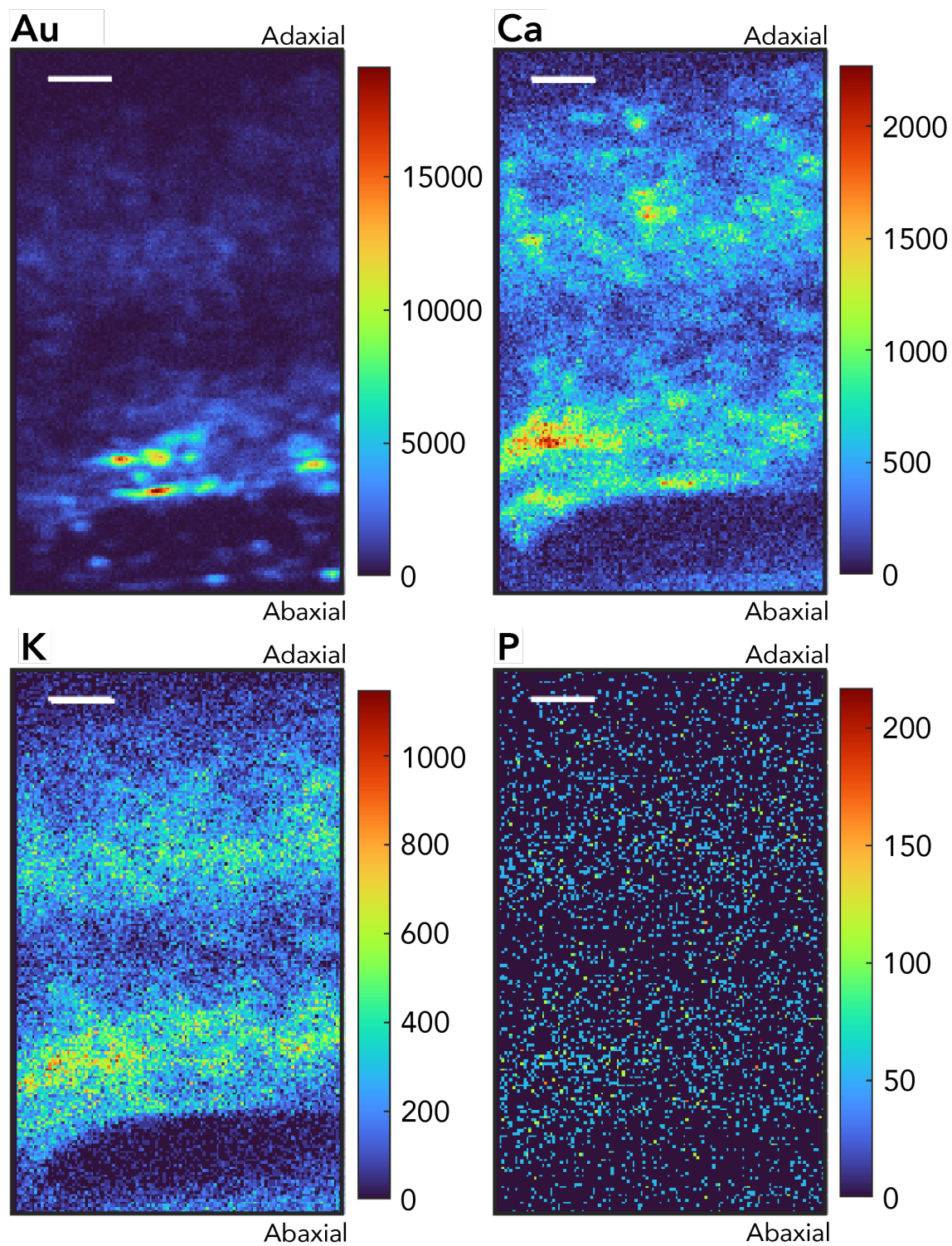
Figure 2-27. µXRF distribution maps of gold, calcium, potassium, and phosphorous of the cross-section of a WT *Nb* leaf infiltrated with 20 nm DNA-AuNS (2 x 2 µm pixels). Scale bars: 50 µm.
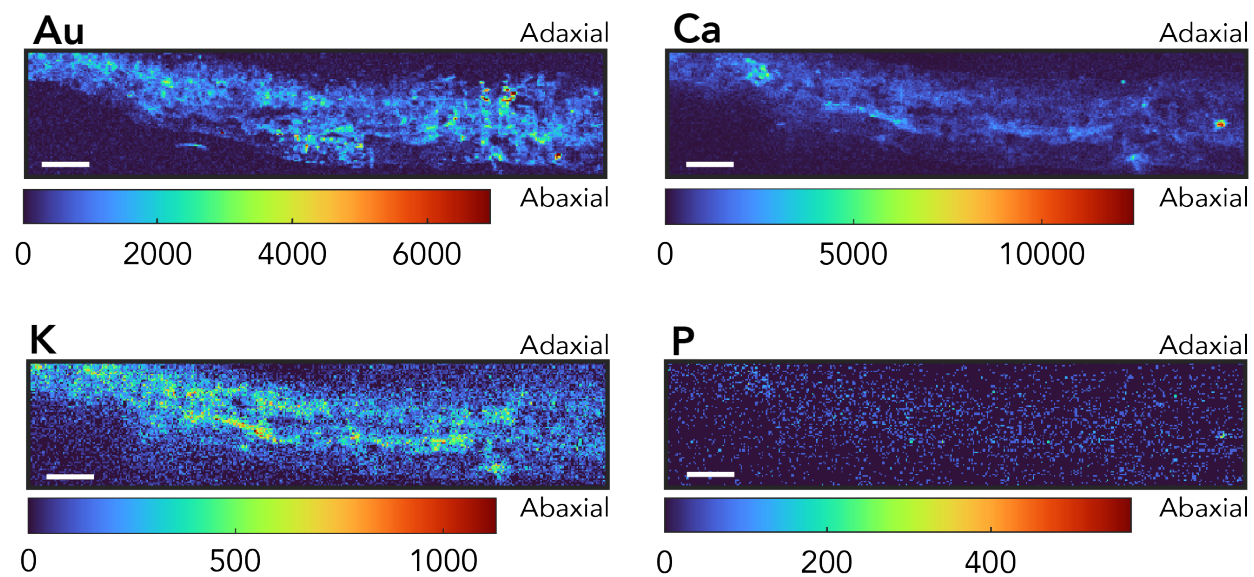
Figure 2-28. μXRF distribution maps of gold, calcium, potassium, and phosphorous of the cross-section of a WT *Nb* leaf infiltrated with 10 nm DNA-AuNS (7 x 7 μm pixels). Scale bars: 200 μm.
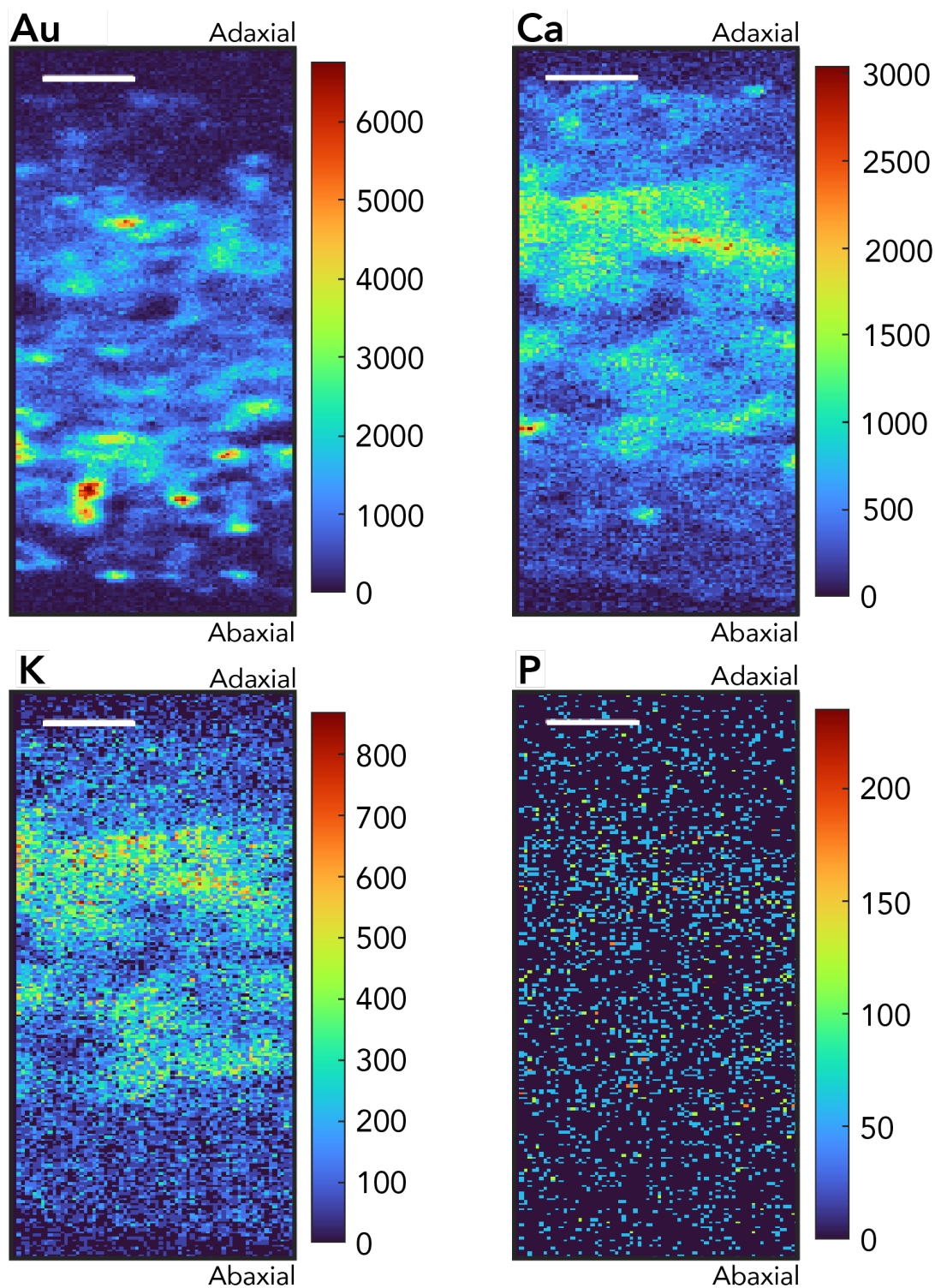
Figure 2-29. µXRF distribution maps of gold, calcium, potassium, and phosphorous of the cross-section of a WT *Nb* leaf infiltrated with 10 nm DNA-AuNS (2 x 2 µm pixels). Scale bars: 50 µm.
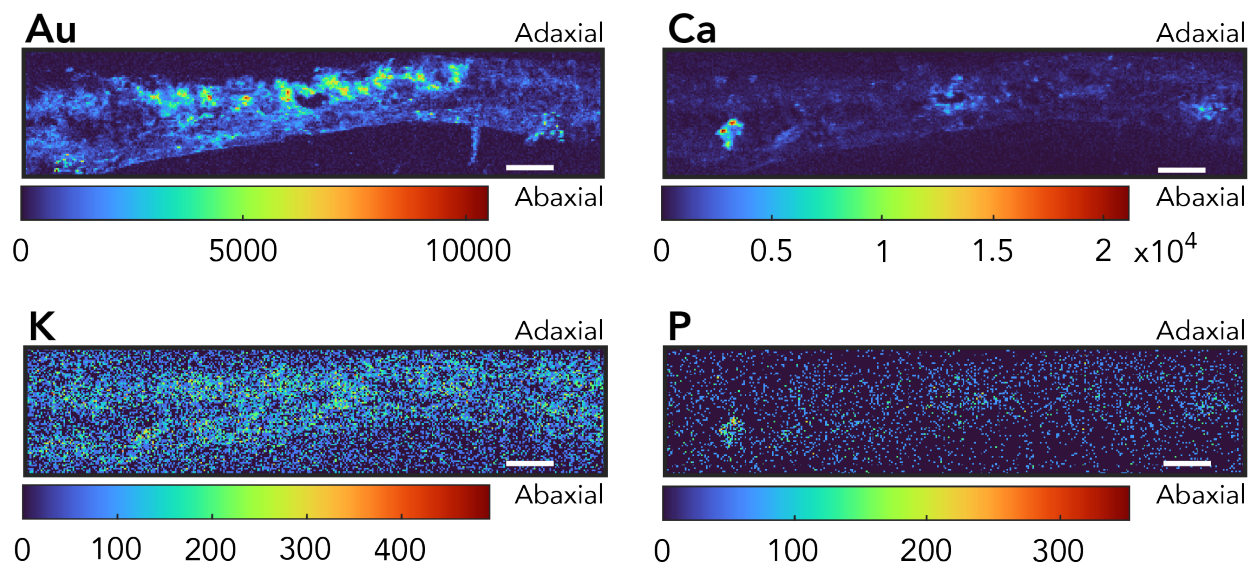
Figure 2-30. µXRF distribution maps of gold, calcium, potassium, and phosphorous of the cross-section of a WT *Nb* leaf infiltrated with DNA-AuNR (7 x 7 µm pixels). Scale bars: 200 µm.
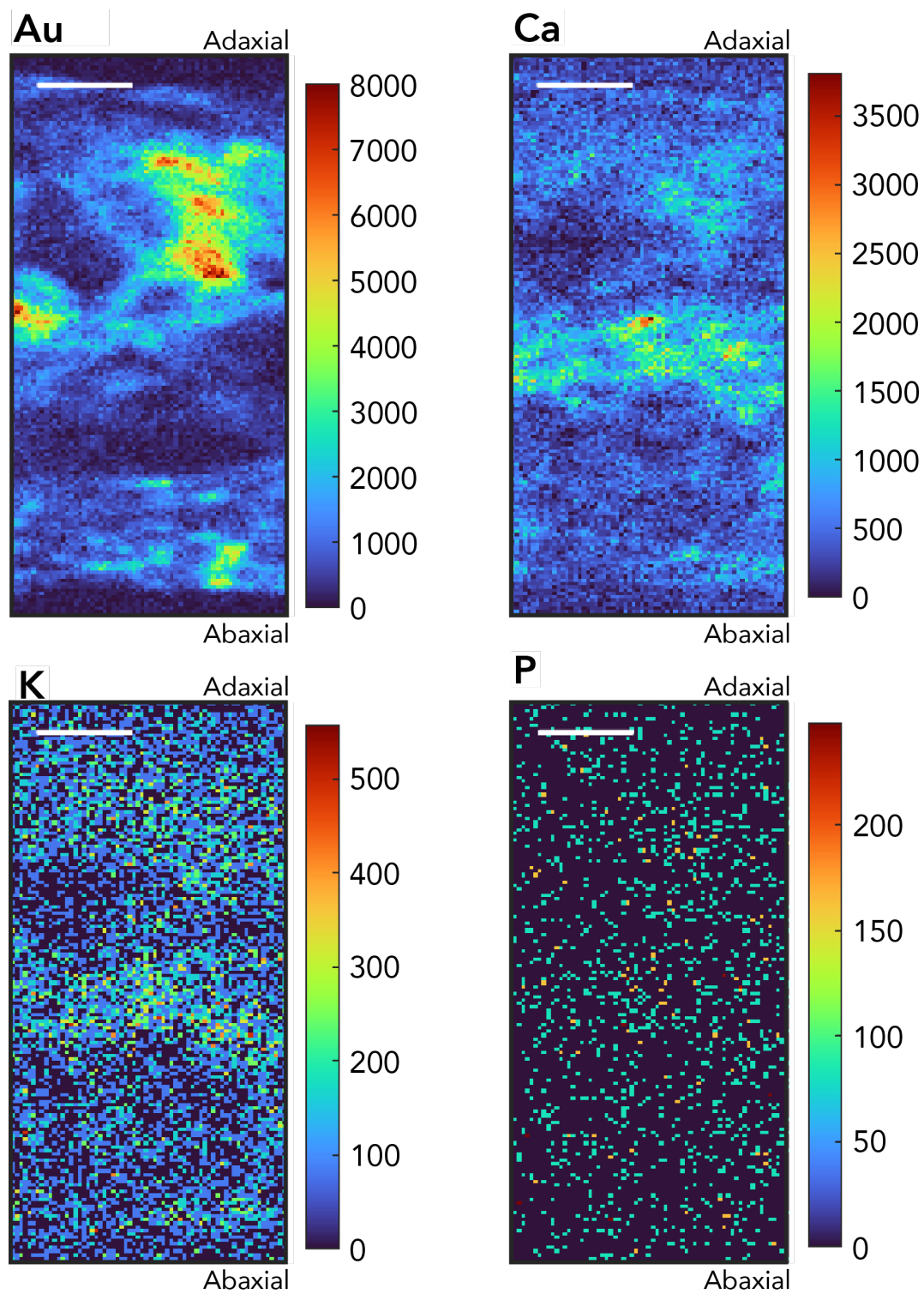
Figure 2-31. μXRF distribution maps of gold, calcium, potassium, and phosphorous of the cross-section of a WT *Nb* leaf infiltrated with DNA-AuNR (2 x 2 μm pixels).
Scale bar: 50 μm.
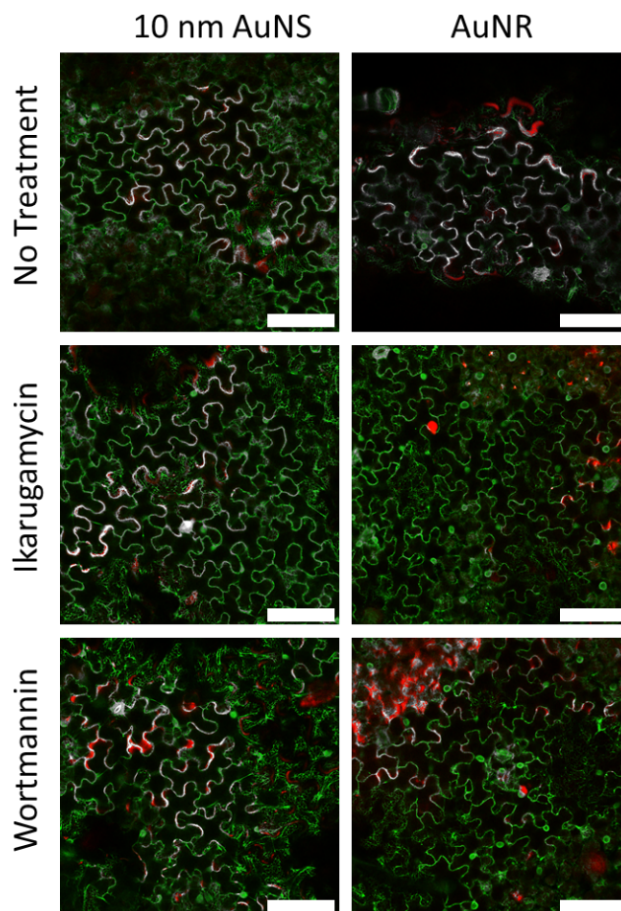
Figure 2-32. Representative confocal images of Cy3-DNA-AuNP in leaves treated with plant endocytosis inhibitors ikarugamycin or wortmannin.
Scale bar: 100 μm. Fluorescence signal from Cy3-DNA (red channel), along with results shown in **Figure 2-4e**, show decreased colocalization signal between Cy3-DNA and intracellular GFP in Cy3-DNA-AuNR leaves treated with endocytosis inhibitors. In addition to impacting NR internalization, these results also suggest that Cy3-DNA association with and internalization into plant cells are reduced in the presence of endocytosis inhibitors.
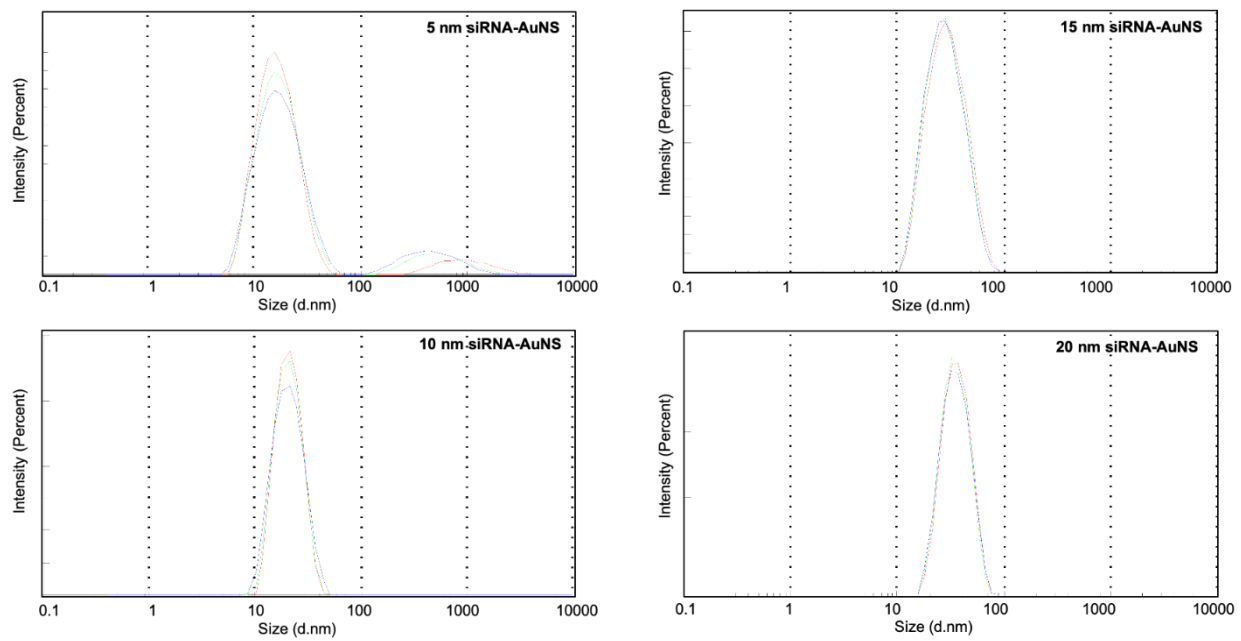
Figure 2-33. DLS spectra of siRNA-AuNS.
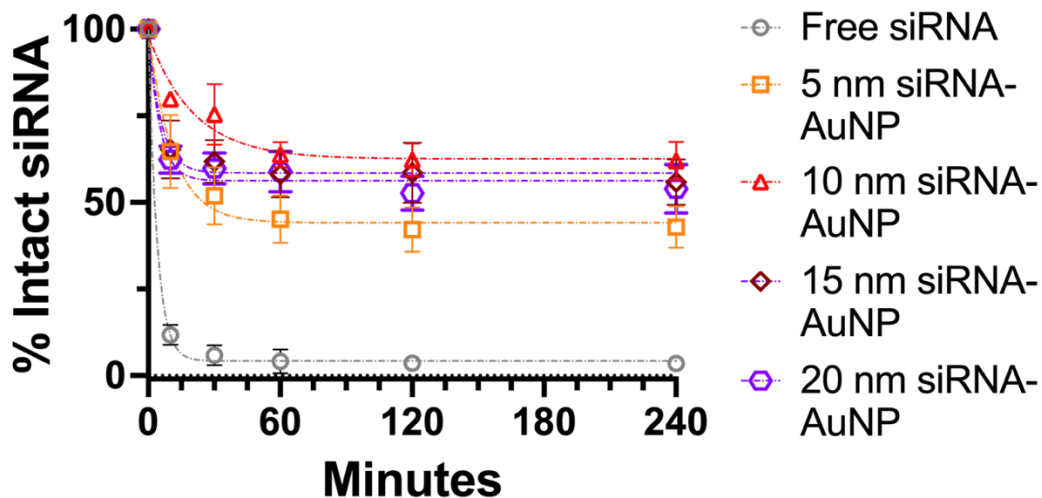
Figure 2-34. AuNS protect siRNA from endoribonuclease RNase A degradation.
Equivalent siRNA concentrations of 5 nm, 10 nm, 15 nm, and 20 nm AuNS (corresponding to approximately 0.2 µM siRNA) were incubated with RNase A for 10, 30, 60, 120, and 240 min. The resulting solutions were centrifuged, and supernatants quantified via the Quant-iT microRNA plate reader assay. At every timepoint past 0 min, the protective effect of all AuNS is statistically significant from free siRNA ($p < 0.05$).
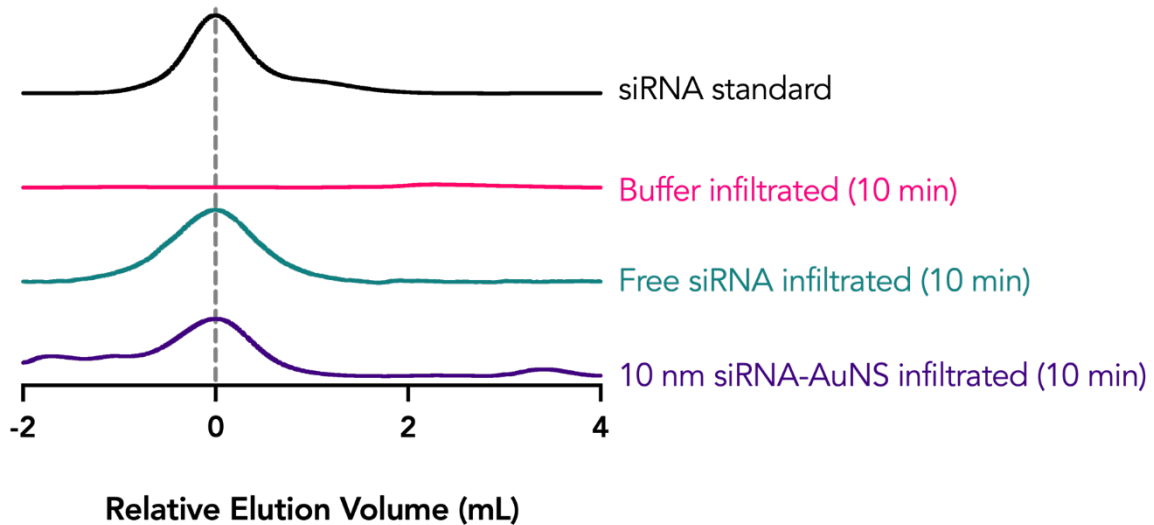
Figure 2-35. Anion exchange FPLC elution profile of RNA extracted from *Nb* leaves.
WT *Nb* leaves infiltrated with buffer, free siRNA, or 10 nm siRNA-AuNS and harvested 10 min post-infiltration. RNA was extracted from these samples and run on an anion exchange FPLC column. Absorbance spectra of each sample is plotted against relative elution volume, the volume corresponding to the % Buffer where siRNA elution was expected to occur. RNA from buffer infiltrated leaves does not give rise to noticeable absorbance peaks in close proximity to the expected elution volume. Peaks identified proximal to the expected elution volume were run on an agarose gel against an siRNA standard to confirm the size of the detected RNA (**Figure 2-36**). For each sample, volume fractions collected within absorbance peaks were confirmed via gel electrophoresis to contain siRNA where noted, and the associated absorbance peaks were centered to 0 relative elution volume on the x-axis. Both free siRNA and siRNA-AuNS RNA samples display absorbance peaks at expected elution points that match the siRNA standard, suggesting that siRNA becomes bioavailable following infiltration into plant leaves.
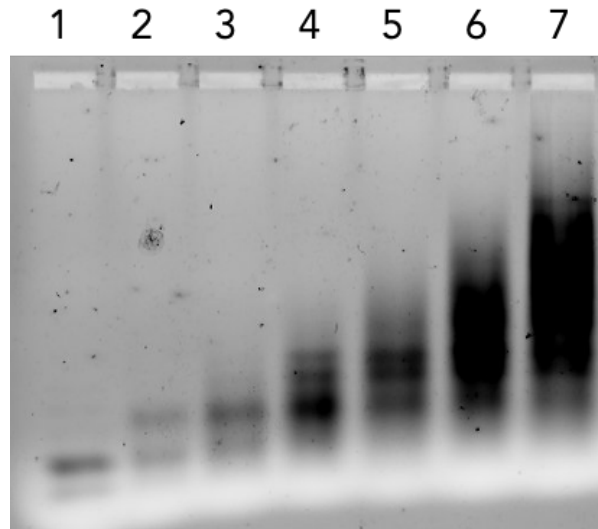
Figure 2-36. Gel confirmation of anion exchange FPLC volume fractions for 10 nm siRNA-AuNS infiltrated sample.

Volume fractions collected from the anion exchange FPLC experiment were run on a 3.5% agarose gel against a free siRNA standard to verify the size of the fragment identified under anion exchange FPLC. Lane 1: siRNA standard. Lane 2 – 7: volume fractions in 0.5 mL steps starting from approximately -0.5, 0.5, 1, 1.5, and 2 mL from the relative elution volume respectively. A band at the same size as the siRNA standard can be seen in Lane 2. Notably, even volume fractions that do not exhibit absorbance peaks contain RNA as visualized with a gel (data not included). This suggests the anion exchange FPLC assay may lack the sensitivity to detect low quantities of RNA. Nevertheless, the peaks corresponding to siRNA are evidently present as seen from the collected absorbance spectra.
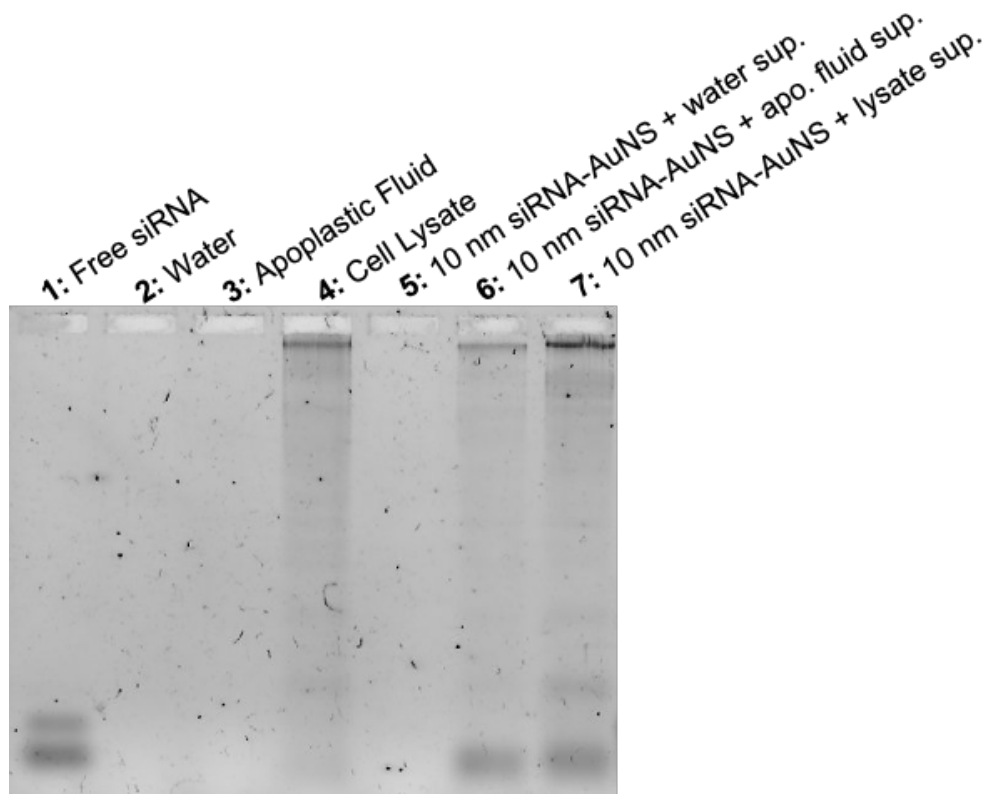
Figure 2-37. Incubation with plant biofluids induces siRNA desorption from the surface of siRNA-AuNS.

10 nm siRNA-AuNS were incubated with water, apoplastic fluid, or plant cell lysate on the benchtop. 24 h post-incubation, the solutions were centrifuged, and supernatants collected to run on a 3% agarose gel. We note the emergence of a band in both the 10 nm siRNA-AuNS samples incubated with apoplastic fluid and cell lysate that corresponds to the size of free siRNA. This suggests that there is desorption of intact siRNA from 10 nm siRNA-AuNS in plant biofluids.
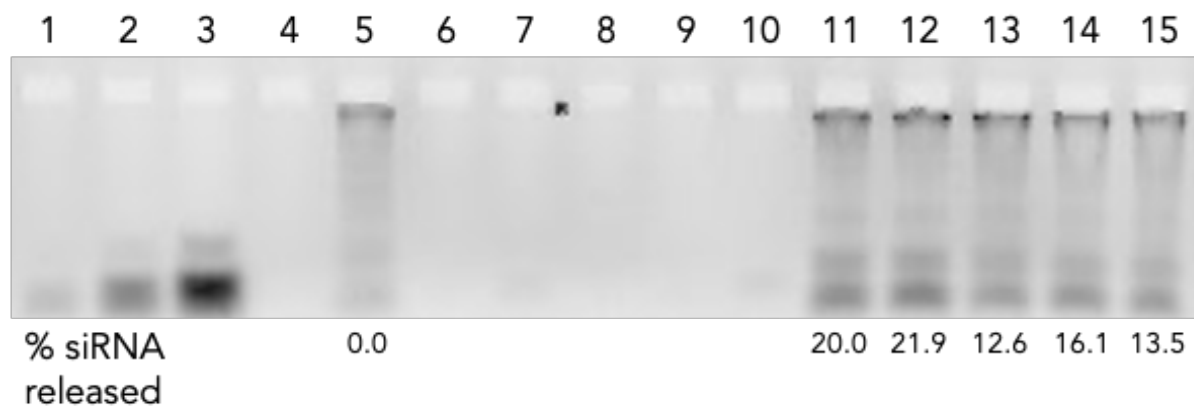
Figure 2-38. siRNA desorption from siRNA-AuNP incubated in apoplastic fluid.
siRNA-AuNP were separately incubated in buffer or apoplastic fluid on the benchtop for 24 h, before being centrifuged to pellet the AuNP, and the supernatant was removed and run on a 3.5% agarose gel. Lanes 1 – 3: varying concentrations of the free siRNA standard (corresponding to 3%, 13%, and 33% release of the functionalized siRNA respectively). Lanes 4 – 5: buffer and apoplastic fluid respectively. Lanes 6 – 10: Supernatant of the 5 nm, 10 nm, 15 nm, 20 nm siRNA-AuNS and siRNA-AuNR respectively incubated in buffer. Lanes 11 – 15: Supernatant of the 5 nm, 10 nm, 15 nm, 20 nm siRNA-AuNS and siRNA-AuNR respectively incubated in apoplastic fluid. The intensity of the siRNA bands was quantified via FIJI, and values included below the relevant wells.
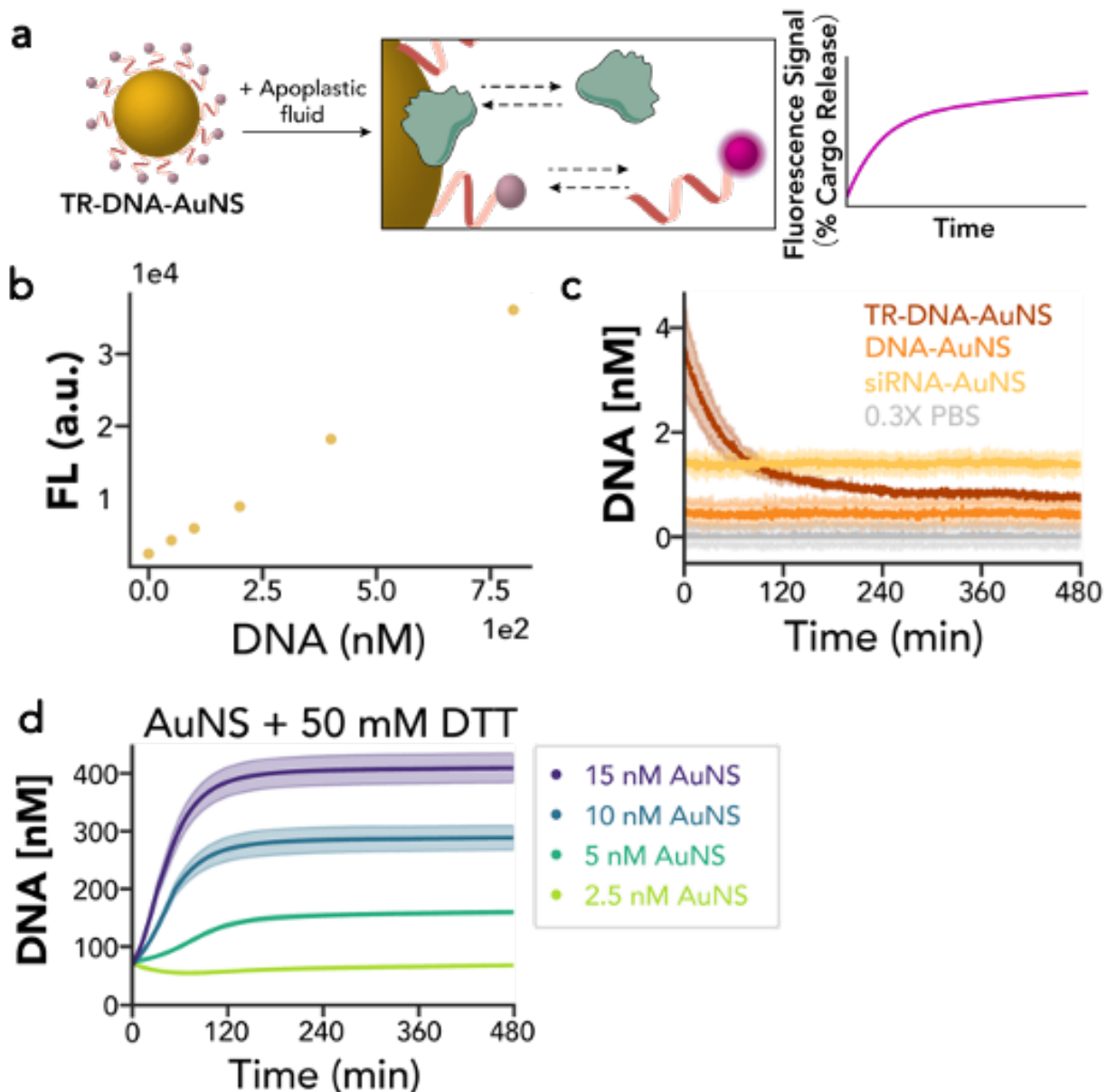
Figure 2-39. Quantification of DNA desorption from the AuNS surface with a fluorescence-based dynamic exchange assay.

a Schematic of fluorescence-based dynamic exchange assay. Apoplastic fluid extracted from *Nb* WT leaves was added to 15 nm Texas Red-labeled DNA-AuNS (TR-DNA-AuNS). Initially, the TR-DNA proximal to the AuNS surface exhibits quenched fluorescence. Proteins or other constituents of the apoplastic fluid can interact with the surface of the AuNS, causing a liberation of TR-DNA from the AuNS and resulting in an increase in the TR fluorescence signal. Apoplastic fluid was diluted by a factor of approximately 5 – 40x[213] needed to remain within the dynamic range of this *in vitro* assay, thus it is expected that *in planta* nucleotide release will be far greater than observed in this assay. **b** Representative TR-DNA calibration curve for the fluorescence-based dynamic exchange assay. Fluorophore concentrations were chosen within the range of linear fluorescence signal. An equal volume of 0.6x PBS is added to a free TR-DNA to final concentrations of 0, 50, 100, 200, 400, and 800 nM TR-DNA and 0.3x PBS (n=2). The

fluorescence signal over time is stable. A standard curve was run on each separate plate in the relevant solution conditions and used to convert fluorescence signal to free DNA concentrations. **c** Control experiments for the fluorescence-based dynamic exchange assay. 0.3x PBS was added to 15 nm TR-DNA-AuNS (red), 15 nm DNA-AuNS (orange), or 15 nm siRNA-AuNS (yellow), all to final concentrations of 5 nM AuNS. AuNP that have not been fluorophore-labeled contribute negligibly to baseline fluorescence. Shaded error bars represent standard error between experimental replicates (n=2). **d** DNA desorption from the AuNS surface in the presence of reducing agents measured by the fluorescence-based dynamic exchange assay. Dithiothreitol (DTT), a small molecule known to displace molecules on the surface of AuNP[214,215], was added to 15 nm TR-DNA-AuNS, to final concentrations of 50 mM DTT with 2.5, 5, 10, or 15 nM TR-DNA-AuNS. Increasing Texas Red fluorescence indicates TR-DNA desorption from the optically quenching AuNP surface in the presence of DTT. 0.3x PBS injected into TR-DNA-AuNS as a control displayed negligible free DNA (**c** in current figure). Shaded error bars represent standard error between experimental replicates (n=2). The amount of TR-DNA released from the AuNP scales with the AuNP concentration in solution, as expected.
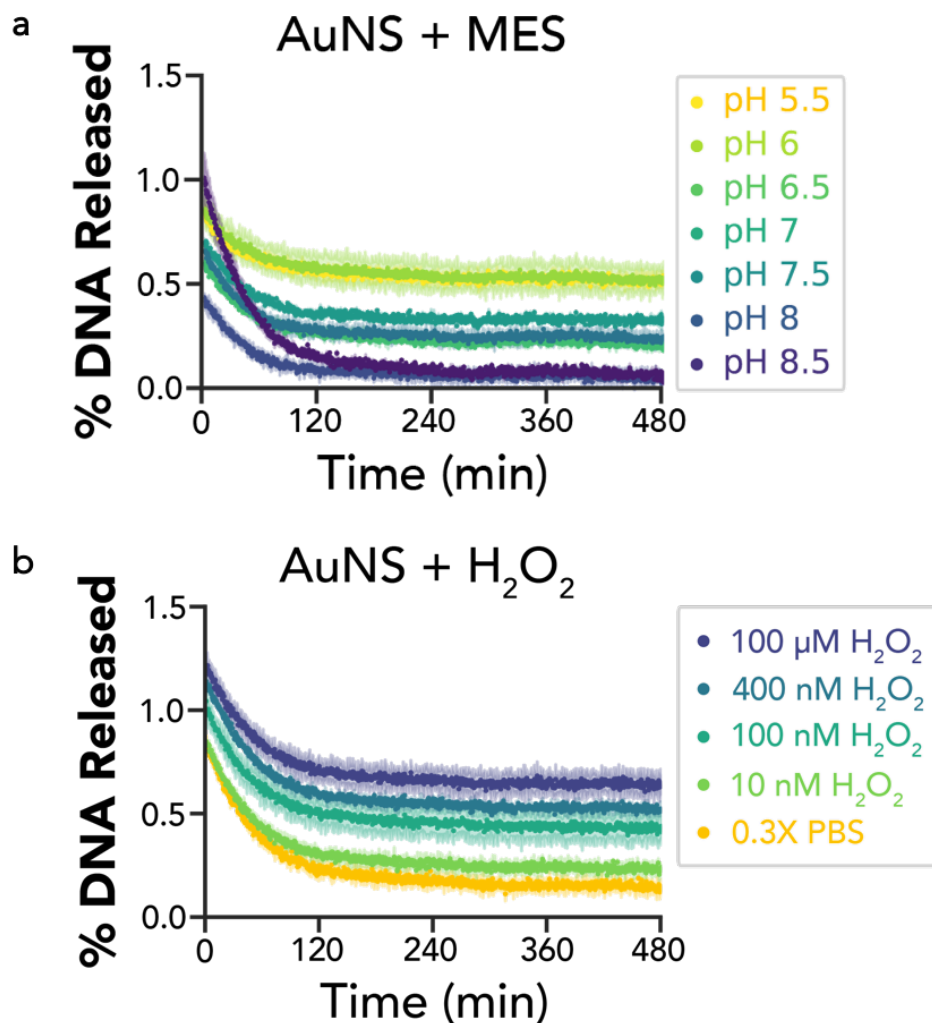
Figure 2-40. Negligible DNA desorption in the presence of varying pH environments or H₂O₂ concentrations measured by a fluorescence-based dynamic exchange assay.
a MES buffer of pH ranging from 5.5 to 8.5 (in 0.5 increments) was added to 15 nm Texas Red-labeled DNA-AuNS (TR-DNA-AuNS), to final concentrations of 50 mM MES buffer with 5 nM TR-DNA-AuNS. Shaded error bars represent standard error between experimental replicates (n=2). **b** H₂O₂ ranging from 20 nM to 200 μm was added to 15 nm TR-DNA-AuNS, to a final H₂O₂ concentration of 10 nM to 100 μm and 5 nM TR-DNA-AuNS. Shaded error bars represent standard error between experimental replicates (n=2).
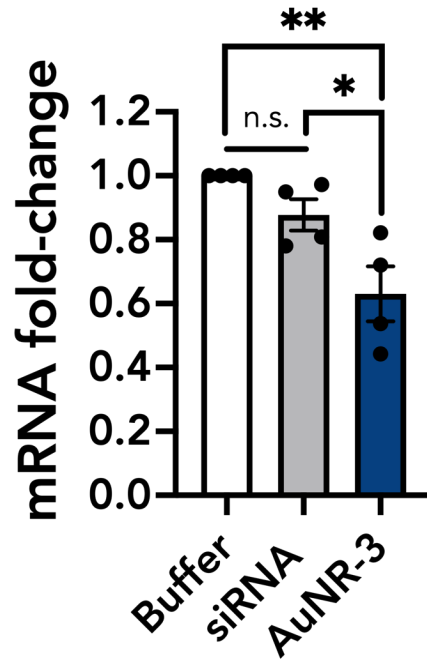
Figure 2-41. qPCR analysis of GFP gene 1-day post infiltration of siRNA-AuNR3.
Buffer, free siRNA, or siRNA-AuNR3 (equivalent to 100 μM siRNA) were infiltrated into 1-month-old 16C *Nb* leaves and qPCR analysis performed 1-day post-infiltration. Free siRNA results in a consistent decrease drop in GFP mRNA expression across all samples, though this change is not statistically significant. The siRNA-AuNR3 results in sample silencing. **p=0.0034, and *p=0.0329 in one-way ANOVA; n.s.: not significant; error bars indicate s.e.m. (n=4).
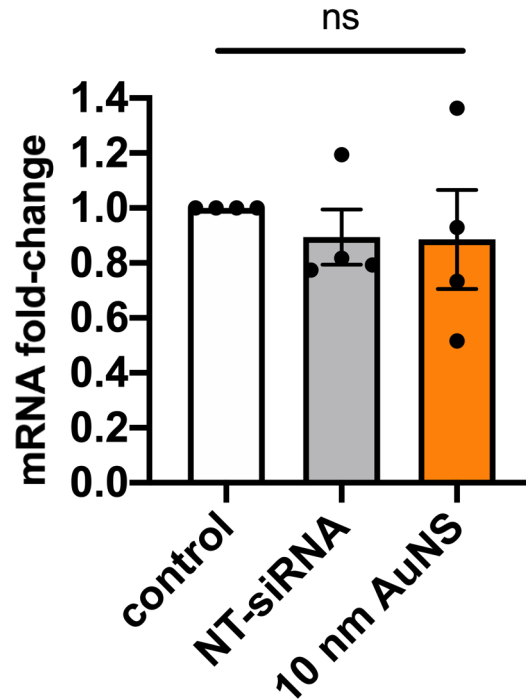
Figure 2-42. RT-qPCR analysis of GFP gene 1-day post infiltration of non-target siRNA-AuNP.

Buffer, free non-target siRNA (NT-siRNA), or 10 nm NT-siRNA-AuNS were infiltrated into 1-month-old *Nb* leaves and RT-qPCR analysis was performed 1-day post-infiltration. There is some variability in GFP mRNA expression levels in both free NT-siRNA and 10 nm NT-siRNA-AuNS samples, though there is no statistically significant difference between the three sample groups. The sequence of NT-siRNA[168] is included in **Table 2-1**.
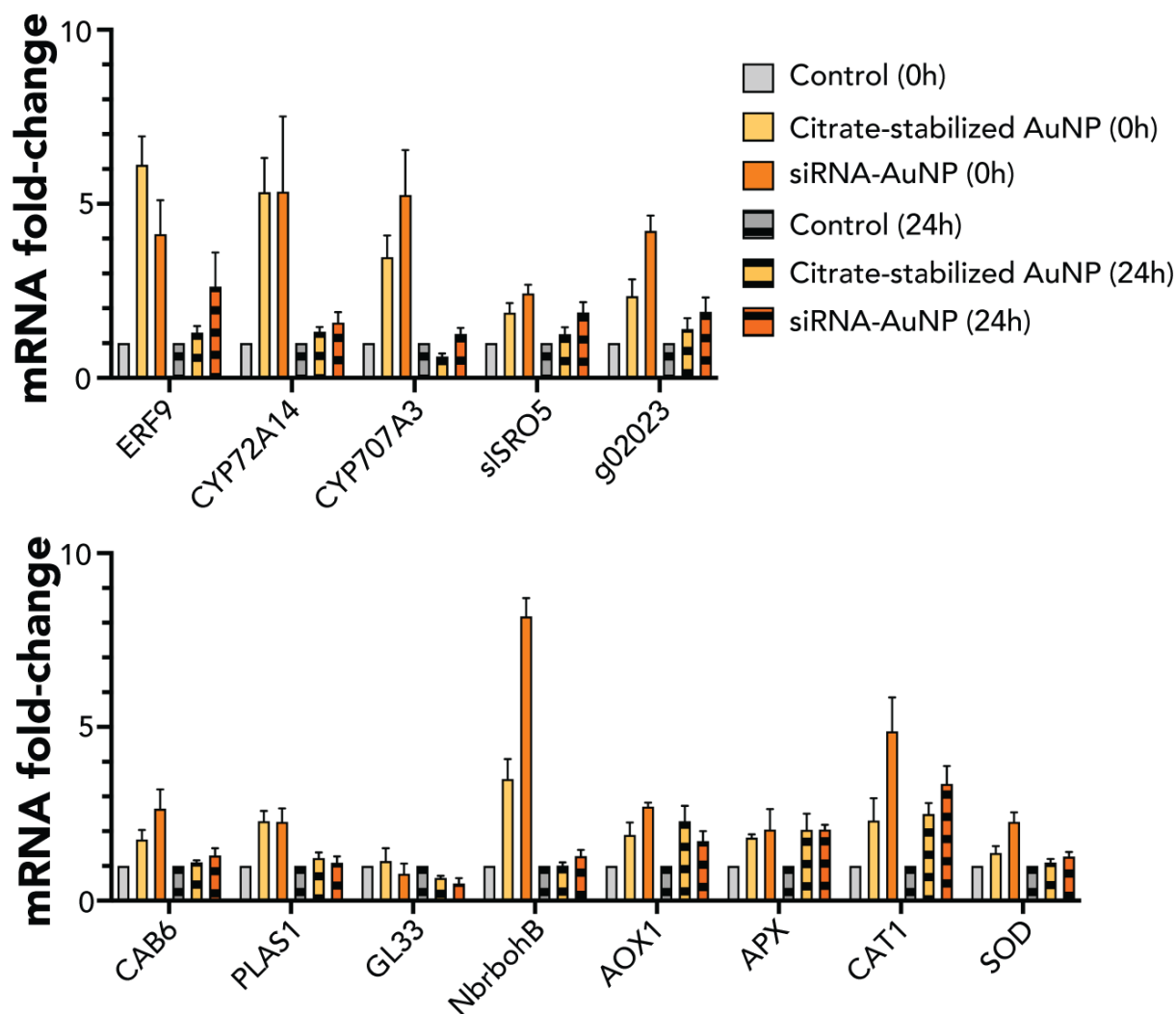
Figure 2-43. RT-qPCR analysis of 13 different stress-associated genes upon infiltration of 10 nm citrate-stabilized AuNP and siRNA-AuNP.

RNA was extracted from 16C *Nb* leaves infiltrated with buffer (control), 10 nm citrate-stabilized AuNS, or 10 nm siRNA-AuNS immediately (0 h) and 1-day (24 h) post-infiltration. A RT-qPCR analysis of 13 stress-associated genes reveals a strong upregulation of these genes for both the citrate-stabilized AuNS and siRNA-AuNS at early time points that decreases 1-day post-infiltration. Of note, GL33 expression levels fall 1-day post-infiltration. A two-way ANOVA with Tukey's multiple comparisons test was run; error bars indicate s.e.m. (n=4). Statistical analysis results can be found in **Table 2-8,** and primers used in **Table 2-1**.
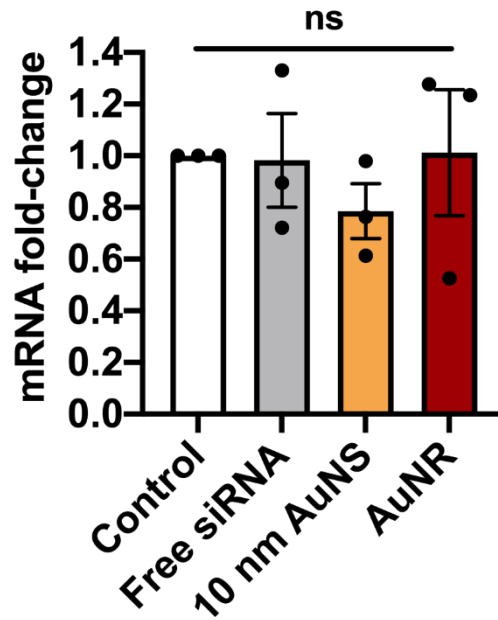
Figure 2-44. RT-qPCR analysis of *NbrbohB* gene 1-day post-infiltration of siRNA-AuNP. *NbrbohB* is a *Nb* stress gene that is upregulated in response to various types of stress, including biotic, heat, and mechanical stress[216], and has been used as a proxy for gauging toxicity responses in the presence of nanomaterials[88,168].

Figure 2-45. Photos of *Nb* leaves prior to and post-infiltration with AuNP.
Photos of 16C *Nb* leaves were taken directly prior to, directly after, 1 h, and 3-day post-infiltration with buffer, 10 nm siRNA-AuNS, and siRNA-AuNR (normalized to 100µL of 100 µM siRNA). Markers were used to demarcate the wetted area. Infiltrated 10 nm siRNA-AuNS can be observed by its characteristic red color centered around the infiltration spot. The intensity of this red decreases over time (1 h vs 3-days post-infiltration), potentially due to leaf growth, nanoparticle biotransformation, or apoplastic transport away from the infiltration site.
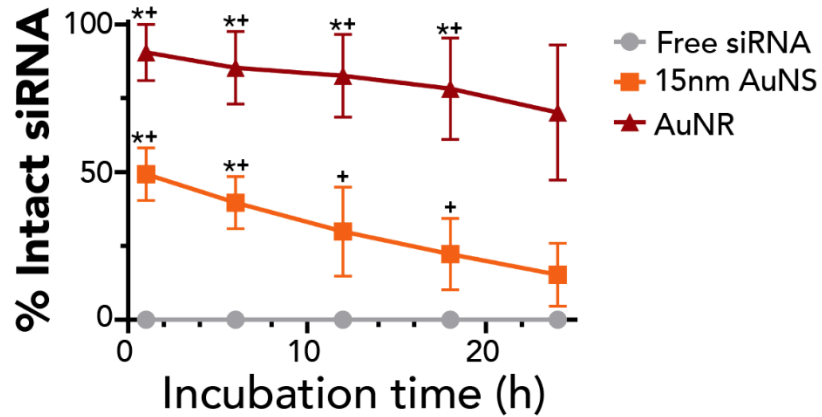
Figure 2-46. AuNP protect siRNA from endoribonuclease RNase A degradation over 24 hours.

3 % agarose gel of 15 nm siRNA-AuNS or siRNA-AuNR incubated with RNase A for 1, 6, 12, 18, and 24 h, with gel band intensities normalized to siRNA standards and used to calculate extent of siRNA degradation. A two-way ANOVA analysis and Tukey's multiple comparisons test was run. * demonstrates $p < 0.05$ when comparing AuNR and free siRNA at a certain timepoint, and + demonstrates $p < 0.05$ when comparing AuNR and 15 nm AuNP at a certain timepoint. Error bars represent standard error (n=3).

Table 2-1. Sequences of oligonucleotides used in Chapter 2.

Primers targeting the GFP, EF1, and NbrbohB genes used for RT-qPCR were designed using the PrimerQuest Tool. The remaining primers used were designed using Primer-BLAST based off sequences pulled from the Sol Genomics Network. Genes with an asterisk were used for only preliminary RT-qPCR studies and not pursued due to high cycle numbers (~35).

Name	Sequence (5'-3')	Amplicon Length
SH-DNA	TAC ACG CAT CCT TAG AAA AAA AAA A-SH	
Cy3-DNA	CTA AGG ATG CGT GTA-Cy3	
TR-DNA-SH	TR-AAA AAA AAA A-SH	
SH-sense siRNA	SH-AAA AAA AAA ArGrG rUrGrA rUrGrC rArArC rArUrA rCrGrG rArAT T	
Antisense siRNA	rUrUrC rCrGrU rArUrG rUrUrG rCrArU rCrAC C	
SH-sense NT-siRNA	SH-AAA AAA AAA ArUrA rArGrG rCrUrA rUrGrA rArGrA rGrArU rArCT T	
Antisense NT-siRNA	rGrUrA rUrCrU rCrUrU rCrArU rArGrC rCrUrU rATT	
GFP	F: AGT GGA GAG GGT GAA GGT GAT G R: GCA TTG AAC ACC ATA AGA GAA AGT AGT G	123
EF1	F: TGG TGT CCT CAA GCC TGG TAT GGT TG R: ACG CTT GAG ATC CTT AAC CGC AAC ATT CTT	160

101

NbrbohB	F: TTT CTC TGA GGT TTG CCA GCC ACC ACC TAA	228
	R: GCC TTC ATG TTG TTG ACA ATG TCT TTA ACA	
NAC042*	F: CAA ACA GGG TGA CAG GTT CT	111
	R: ATG ACT TCT TCA GCC CAA TAC A	
ERF9	F: GTC ATC CTC ATC GTC GTC GT	119
	R: CCG ACG AAG TAG CCC GAA AA	
CYP72A14	F: GCT ATG GGG TGA AGA TGC AGA	117
	R: GTC CTT GGT CCC CAT CCA AA	
CYP707A3	F: ACA TTC ACC ACA GCC CAG AC	116
	R: ACA TGA GTG GAC CCC ATT GC	
REIL1*	F: AGCCTACAAACGCCATTCCA	123
	R: TAGCGGTGCCATTCGGATTT	
slSRO5	F: TGG AAC AGG ACA GTG GCA TC	142
	R: GGC GAC TCT GAA ACT GAC CA	
AOX1	F: GCA GTG GTG ACG TGG GTT AG	174
	R: AGG CGG AAC ACC CCA ATA AC	
APX	F: TGC CAC CAA GGG TTC TGA C	196
	R: TTC CCC GCT CAA AAG TTC CT	
CAT1	F: TTC CCC GTC TTC TTC ATC CG	100
	R: GGA CCC TCC AAT TCT CCT GG	
SOD	F: AGC AGA CGG ACC TTA GCA AC	104
	R: GGC TCC AGT GCT CCA TAG TC	
g02023	F: TTA GCA ATT CCA GAT GCG GC	110
	R: TTC CCA TAC TTC ACC GGA ACG	
CAB6	F: GTT CCG GTA GAG TCC AAG CC	103
	R: GCT CCT GGG TAC CAT AAC GG	
PLAS1	F: GAA AGA CGT TGG TGC TGT CG	103
	R: TAG ACC GCC ATC ATC GCT AC	
GL33	F: TAT CAG TTC CCG ACG GAC CA	132
	R: CAG GAG TGA CCG CAG CTT TA	

Table 2-2. DNA and siRNA functionalization details of AuNP *via* the pH-assisted method.

AuNP type	Concentration for nucleic acid functionalization	Molar ratio for functionalization (AuNP:DNA or siRNA)	Centrifugation speed (x 1000g)
5nm AuNS	90 nM	1:167	23
10nm AuNS	20 nM	1:300	17
15nm AuNS	8 nM	1:500	14
20nm AuNS	2.4 nM	1:800	8
AuNR3	8 nM	1:1000	9.5
AuNR	2 nM	1:7500	8.5

Table 2-3. DLS data of AuNS, DNA-AuNS, and siRNA-AuNS.
Standard deviation of experimental replicates is included (n=3).

AuNP type	Citrate-AuNS	DNA-AuNS	siRNA-AuNS
5 nm AuNS	11.2±0.4 nm	15.4±0.7 nm	17.1±0.7 nm
10 nm AuNS	14.8±0.1 nm	20.2±0.6 nm	19.3±0.3 nm
15 nm AuNS	18.8±0.2 nm	27.8±0.5 nm	25.1±0.4 nm
20 nm AuNS	23.1±0.4 nm	30.3±0.3 nm	32.5±0.4 nm

Table 2-4. Quantity of DNA and siRNA functionalized on AuNP and detailed concentrations used for AuNP in experiments.
For TEM experiments, we retained the same ratio of AuNP concentrations used in confocal analysis to ensure a consistent comparison between confocal and TEM data.

AuNP type	# DNA/AuNP	# siRNA/AuNP	AuNP concentrations		
			Confocal	TEM	RT-qPCR and Western blot
5 nm AuNS	10±1	10±2	40 nM	20 nM	10 nM
10 nm AuNS	26±2	26±10	15 nM	7.5 nM	3.8 nM
15 nm AuNS	70±6	59±18	5.7 nM	2.9 nM	1.7 nM
20 nm AuNS	97±4	92±14	4.1 nM	2.1 nM	1.1 nM
AuNR-3	49±2	48±3	8.2 nM	N.A.	2.1 nM
AuNR	128±21	125±36	3.2 nM	1.6 nM	0.8 nM

Table 2-5. Summary of TEM-quantified AuNR orientation relative to the cell wall.
To estimate the percentage of randomly oriented AuNR being found at a particular angle of orientation to the plant cell wall, we assumed that the TEM slice imaged sections fixed leaf tissues in an unbiased manner. Accordingly, the AuNR displayed in the TEM images would be unbiased, allowing the 2-dimensional image to represent the 3-dimensional configuration. Considering randomly oriented AuNR being placed into 9 even bins (0° - 10°, 10° - 20°, …, 80° - 90°), the likelihood of AuNR found in a single bin would be $1/9^{th}$ of 100%, giving rise to 11.1%. A Chi-squared test between the number of observed AuNR as binned compared to randomly oriented AuNR demonstrated statistical significance (χ^2=24.92, **p=0.0016).

Angle of orientation (°)	Number of AuNR	Percentage of AuNR measured (%)	Percentage of randomly oriented AuNR (%)
0 – 10	73	22.5	11.1
10 – 20	36	11.1	11.1
20 – 30	26	8.0	11.1
30 – 40	27	8.3	11.1
40 – 50	25	7.7	11.1
50 – 60	19	5.9	11.1
60 – 70	30	9.3	11.1
70 – 80	42	13.0	11.1
80 – 90	46	14.2	11.1

Table 2-6. Statistical significance values for nuclease protection assay (Figure 2-5b).
Significance was measured with a two-way ANOVA with Tukey's multiple comparisons test; for time (n=6), column factor (n=3), and subject (n=9), F=267.6 and p<0.0001, F=186.7 and p<0.0001, and F=4.953 and p=0.0013 respectively. Means with the same letter have statistically significant differences. Upper-case letters indicate results with p < 0.05, and lower-case letters indicate results with p < 0.001.

Time Elapsed (min)		Free siRNA	10 nm AuNS	AuNR
	Column Names	A	B	C
0	% Intact	100	100	100
	Column comparisons			
10	% Intact	6.8	85.4	65.9
	Column comparisons	bC	C	
30	% Intact	6.7	75.2	62.8
	Column comparisons	bc		
60	% Intact	3.9	67.8	62.8
	Column comparisons	Bc		
120	% Intact	1.8	56.4	66.2
	Column comparisons	BC		
240	% Intact	1.0	52.1	66.9
	Column comparisons	Bc	C	

Table 2-7. Summary of genes utilized in RT-qPCR quantification of stress-related genes.

Gene	Locus/ Accession Number	Activity
NbNAC042[217]	Niben101Ctg15860g00004.1	Ortholog of a tomato gene (Solyc02g069960) that is induced by pattern-triggered immunity
ERF9[218]	Niben101Scf11706g00010.1	Ethylene responsive transcription factor, involved in both biotic and abiotic stress responses
CYP72A14[219]	Niben101Scf14022g00011.1	Cytochrome P450 encoding gene
CYP707A3[219]	Niben101Scf01873g01004.1	Cytochrome P450 encoding gene
slSRO5[219]	Niben101Scf01764g02004.1	Responsive to abiotic stress, drought, and salt stress
REIL1[219]	Niben101Scf02868g05009.1	Zinc finger protein
NbrbohB[216]	AB079499	Respiratory burse oxidative homolog
AOX1[220]	KF367455	Mitochondrial alternative oxidase 1a, an essential defense component in plant response to environmental stress
APX[221]	AB610799.1	Ascorbate peroxidase, a ROS scavenging gene
CAT1[221]	EU998969.1	Catalase, a ROS scavenging gene
SOD[221]	Niben101Scf09401g00007.1	Superoxide dismutase, a ROS scavenging gene
g02023[222]	Niben101Scf01075g02023	Uncharacterized, possible ortholog of *Brassica napus* (BnaA05g33450D)
GL33[222]	Niben101Ctg13946g00001	Germin-like protein subfamily 3 member 3
PLAS1[222]	Niben101Scf00539g07027	Plastocyanin A'/A''
CAB6[222]	Niben101Scf08975g01010	Chlorophyll A-B binding protein

Table 2-8. Statistical significances for RT-qPCR quantification of stress-related genes.
Significance was measured by a two-way ANOVA with Tukey's multiple comparisons test; for time (n=2), column factor (n=3), and subject (n=9) for each individual gene. Means with the same letter have statistically significant differences. Upper-case letters indicate results with $p<0.05$, and lower-case letters indicate results with $p<0.001$. Empty entries for the column comparisons row denotes that there was no statistically significant difference between any of the three samples within that timepoint.

Gene of interest	Collection time post-infiltration		Buffer	10 nm citrate-stabilized AuNS	10 nm siRNA-AuNS
		Column names	A	B	C
ERF9	10 min	Average mRNA fold-change	1.00	6.12	4.13
		Column comparisons	bC		
	24 h	Average mRNA fold-change	1.00	1.30	2.63
		Column comparisons			
CYP72A14	10 min	Average mRNA fold-change	1.00	5.33	5.35
		Column comparisons	BC		
	24 h	Average mRNA fold-change	1.00	1.33	1.59
		Column comparisons			
CYP707A3	10 min	Average mRNA fold-change	1.00	3.47	5.25
		Column comparisons	Bc		
	24 h	Average mRNA fold-change	1.00	0.62	1.26
		Column comparisons			
slSRO5	10 min	Average mRNA fold-change	1.00	1.88	2.43
		Column comparisons	Bc		
	24 h	Average mRNA fold-change	1.00	1.26	1.88
		Column comparisons	C		
NbrbohB	10 min	Average mRNA fold-change	1.00	3.50	8.18
		Column comparisons	bc	c	
	24 h	Average mRNA fold-change	1.00	1.01	1.28
		Column comparisons			
AOX1	10 min	Average mRNA fold-change	1.00	1.90	2.71
		Column comparisons	c		
	24 h	Average mRNA fold-change	1.00	2.29	1.72
		Column comparisons	B		
APX	10 min	Average mRNA fold-change	1.00	1.81	2.05
		Column comparisons			
	24 h	Average mRNA fold-change	1.00	2.04	2.05
		Column comparisons			
CAT1	10 min	Average mRNA fold-change	1.00	2.31	4.88
		Column comparisons	c	C	
	24 h	Average mRNA fold-change	1.00	2.49	3.36
		Column comparisons			
SOD	10 min	Average mRNA fold-change	1.00	1.38	2.27

		Column comparisons	Bc		
	24 h	Average mRNA fold-change	1.00	1.11	1.27
		Column comparisons			
g02023	10 min	Average mRNA fold-change	1.00	2.35	4.23
		Column comparisons	Bc	C	
	24 h	Average mRNA fold-change	1.00	1.40	1.90
		Column comparisons			
CAB6	10 min	Average mRNA fold-change	1.00	1.76	2.65
		Column comparisons	c		
	24 h	Average mRNA fold-change	1.00	1.11	1.30
		Column comparisons			
PLAS1	10 min	Average mRNA fold-change	1.00	2.29	2.27
		Column comparisons	BC		
	24 h	Average mRNA fold-change	1.00	1.23	1.10
		Column comparisons			
GL33	10 min	Average mRNA fold-change	1.00	1.14	0.78
		Column comparisons			
	24 h	Average mRNA fold-change	1.00	0.65	0.50
		Column comparisons			

2.6.2 Supplementary Notes

2.6.2.1 Resolution Limitations of Microscopy

We are working within the confines of a diffraction-limited system when analyzing Cy3 and GFP colocalization under confocal microscopy. Our TEM findings suggest that colocalization values measured in diffraction-limited confocal microscopy represent both cellular internalization and also NP-cell wall association and cannot distinguish between the two. While confocal microscopy can inform the accumulation and presence of AuNP in the proximity of plant cells, we are resolution-limited and cannot distinguish if the AuNP are associating with the outer cell wall, between the cell wall and cell membrane, or within the cell. Considering the Abbe diffraction limit constraining the observation of sub-wavelength features, traditional confocal microscopy alone cannot localize NP into plant cells[223]. As such, other techniques such as TEM were used to track the passage of AuNP into plant cells.

2.6.2.2 Addressing the Impact of Free Cy3-DNA on Interpretation of Confocal Data

As demonstrated in the dynamic ligand exchange experiments in **Error! Reference source not found.c**, DNA-functionalized AuNPs may experience DNA desorption upon exposure to the biomolecules in the apoplast. We recognize that free Cy3-DNA that has desorbed from Cy3-DNA-AuNPs will still fluoresce, perhaps to a greater extent than Cy3-DNA-AuNPs as they will not be subject to dye quenching that occurs proximal to the AuNP surface. Additionally, under confocal microscopy, we cannot distinguish between free Cy3-DNA signal from Cy3-DNA-AuNP signal. The possibility of free Cy3 signal increases with time and should be considered especially in the context of samples imaged at long timescales (eg. 2-3 days). To help address this, we have included a grey line in **Error! Reference source not found.b** representing the maximum colocalization fraction obtained with free Cy3-DNA infiltrated *Nb* samples. This line distinguishes between free

Cy3-DNA signal and Cy3-DNA-AuNP signal. At 24 h, none of our samples display colocalization fractions proximal to the grey free Cy3-DNA line. The sole exception is the 20 nm DNA-AuNS which was imaged at 48 h and 72 h to probe the possibility of a maximum fraction at long timescales. In this context, we are confident that our colocalization fraction analysis and subsequent conclusions from our confocal data follow as a result of visualizing Cy3-DNA-AuNP signal and not free Cy3-DNA signal.

2.6.2.3   RNA-seq Analyses

RNA-seq analyses of siRNA-functionalized nanoparticle exposure to *Arabidopsis thaliana* reveal that the dominant responses associated with nanoparticle exposure include response to biotic stimulus, hypoxia responses, and response to chemical stimulus[224]. Accordingly, we selected several genes associated with each of these response pathways, as well as genes associated with general oxidative stress. More information regarding each gene (accession numbers, if available) are provided in

Table 2-7 and primers are available in **Table 2-1**.

2.6.3   Supplementary Discussion

2.6.3.1   Shape-Dependent Effects on NP Transport in Plant Tissues

Previous studies in mammalian cells reported that cellular association and internalization of DNA-AuNP is greatly affected by their shape and aspect ratio[225]. Additionally, nanorods travel more rapidly than spherical counterparts in tissues[193]. Similar mechanisms may drive the observed rapid AuNR colocalization kinetics in plant tissues, and this effect might also be aspect ratio dependent: we conducted a time-course (ranging from 0.5 h to 24 h) colocalization study with a lower aspect ratio AuNR (AuNR3, 10 nm x 30 nm). Unlike the previous AuNR of aspect ratio ~5.2 (13 nm x 68 nm), DNA-AuNR3 did not display a sharp increase in colocalization fraction prior to reaching the maximum. However, the DNA-AuNR3 did experience a faster maximum level of colocalization at 2 h (**Figure 2-15** and representative confocal images in **Figure 2-16**), similar to the 10 nm DNA-AuNS. This result further supports that size (in the smallest NP dimension) is a key factor for DNA-AuNP travel in plant tissue.

2.6.3.2   Cy3 Transport in Leaves is Time-Limited for the Region of Study

To verify that the phenomena observed were not laterally distance-dependent within our region of study (1-3 mm from infiltration site), we collected z-stacks (images taken at different focal distances) of Cy3 signal generated from free Cy3-DNA or 10 nm Cy3-DNA-AuNS. An integrated intensity analysis of the z-stacks suggested a stronger dependence of signal on time post-infiltration rather than distance from infiltration point (**Figure 2-17**), affirming our focus on time-dependent transport. Further analysis via an autocorrelation function calculation suggests that the 10 nm Cy3-DNA-AuNS associate with regularly sized structures (such as plant cells) compared to more randomly dispersed free Cy3-DNA (**Figure 2-18**), supporting visual observations of the confocal images.

2.6.3.3   Transience of Gene Silencing on the Protein Level

We measure a 9 % (free siRNA), 28 % (20 nm AuNS), 5 % (15 nm AuNS), 15 % (AuNR), 29 % (5 nm AuNS), and 48 % (10 nm AuNS) reduction in GFP levels on Day 3 via Western blot analysis in leaves treated with AuNP. The transience of gene silencing likely contributes to variabilities in protein-level silencing kinetics, where less-effective AuNP samples such as 20 nm AuNS that take

a longer time to associate with cells may induce silencing more slowly than their smaller counterparts, leading to variabilities in protein-level silencing when assessed at the same 3-day timepoint.

Across all samples, we note that only the 10 nm AuNS showed statistically significant protein-level silencing over non-infiltrated or free siRNA infiltrated controls at the timepoints assayed. Indeed, the lower degree of silencing observed with AuNR (Error! Reference source not found.**c** and **Figure 2-41**) relative to most AuNS could be due to post-endocytosis endosomal entrapment of AuNR[226–228].

3 Carbon Nanotube-Enabled Delivery of DNA in Mature Plants

3.1 Chapter Abstract

Genetic engineering of plants is at the core of sustainability efforts, natural product synthesis, and crop engineering. The plant cell wall is a barrier that limits the ease and throughput of exogenous biomolecule delivery to plants. Current delivery methods either suffer from host-range limitations, low transformation efficiencies, tissue damage, or unavoidable DNA integration into the host genome. Here, we demonstrate efficient diffusion-based DNA delivery into intact plants of several species with pristine and chemically functionalized high aspect ratio nanomaterials. Efficient DNA delivery and strong protein expression without transgene integration is accomplished in *Nicotiana benthamiana* (*Nb*), *Eruca sativa* (arugula), *Triticum aestivum* (wheat) and *Gossypium hirsutum* (cotton) leaves and arugula protoplasts. We find that nanomaterials not only facilitate biomolecule transport into plant cells but also protect polynucleotides from nuclease degradation. Our work provides a tool for species-independent and passive delivery of genetic material, without transgene integration, into plant cells for diverse biotechnology applications.[**]

3.2 Introduction

Despite several decades of advancements in biotechnology, most plant species remain difficult to genetically transform[229]. A significant bottleneck facing efficient plant genetic transformation is biomolecule delivery into plant cells through the rigid and multi-layered cell wall. Currently, few well-established delivery tools exist that can transfer biomolecules into plant cells, each with considerable limitations. *Agrobacterium*-mediated delivery[230] is the most commonly used tool for gene delivery into plants with limitations of efficient delivery to a narrow range of plant species and tissue types, and inability to perform DNA- and transgene-free editing[231]. The one other commonly used tool for plant transformation is biolistic particle delivery (also called gene gun)[29], which can deliver biomolecules into a wider range of plant species but faces limitations of only bombarded-site expression, plant tissue damage when high bombardment pressures are used[229], possible limitation of the specimen size and positioning in the biolistic chamber, and the requirement of using a substantial amount of DNA to achieve the desired delivery efficiency. For transient expression of heterologous proteins in plants, the use of plant viral vectors such as Tobacco mosaic virus, Potato virus X, and Cowpea mosaic virus[232] is beneficial for large-scale production of industrially-relevant proteins. However, viral vectors are only compatible with select plant species and expression cassette sizes, which limits the plant host and hinders expression of large or multiple proteins simultaneously. Additionally, the use of viral vectors, even if used for transient expression of gene editing systems, are usually subject to regulatory purview owing to the pathogenic origin of viruses and that some viruses integrate portions of their genetic material into the plant host genome[233].

[**] Portions published as Demirer, G.S., Zhang, H., Matos, J.L., Goh, N.S., Cunningham, F.J., Sung, Y., Chang, R., Aditham, A.J., Chio, L., Cho, M.J. and Staskawicz, B., 2019. High aspect ratio nanomaterials enable delivery of functional genetic material without DNA integration in mature plants. *Nature nanotechnology*, *14*(5), pp.456-464.

While nanomaterials have been studied for gene delivery into animal cells[234,235], their potential for plant systems remains under-studied[236]. Several reports describe uptake of nanomaterials by plant cells; however, most of these foundational studies deliver only non-functional cargoes[146], are done in protoplast cell culture[97], or use mechanical aid (gene gun[237] or ultrasound[238]) to enable nanoparticle entry into walled plant cells. Mesoporous silica nanoparticles[239] (MSNs), DNA nanostructures and DNA origami[166], and layered double hydroxide (LDH) clay nanosheets[165,170,240] have demonstrated the possibility of nanoscale internalization into walled plant cells without strong mechanical aid to deliver functional biological cargoes. In the MSN study, researchers demonstrated passive delivery of plasmid DNA loaded MSNs into *Arabidopsis* roots by co-culture, an important initial development for passive nanoparticle transport in model plant species root cells[239]. Important developments with LDHs have shown effective delivery of RNAi molecules (double-stranded RNAs) for gene silencing in model species *Nicotiana tabacum*[165], paving the way towards future developments in plant bionanotechnology; however, to our knowledge, LDH has yet to be implemented for plasmid DNA delivery to enable gene expression studies.

To-date, there has yet to be a plant transformation method that enables high-efficiency plasmid DNA delivery, without transgene integration, in a plant species-independent manner. Herein, we address the long-standing challenge of DNA delivery to mature model and non-model plants with nanomaterials, filling a key void in the plant transformation toolkit. With certain surface chemistries, high aspect ratio nanomaterials such as carbon nanotubes (CNTs) have been observed to passively traverse extracted chloroplast[241] and plant membranes[188] owing to several figures of merit: high aspect ratio, exceptional tensile strength, high surface area-to-volume ratio, and biocompatibility. When bound to CNTs, biomolecules are protected from cellular metabolism and degradation[242], exhibiting superior biostability compared to free biomolecules. Moreover, single-walled carbon nanotubes (SWCNTs, or SWNTs) have strong intrinsic near-infrared (nIR) fluorescence[243,244] within the tissue-transparency window and thus benefit from reduced photon scattering, allowing for tracking of cargo-nanoparticle complexes deep in plant tissues. However, previous incorporation of CNTs in plant systems is limited to exploratory studies of CNT biocompatibility[147,241,245] and sensing of small molecules in plant tissues[188,246] by introducing CNTs complexed to synthetic fluorescent dyes or polymers.

Herein, we develop a SWNT-based platform, which further advances the field of nanoparticle directed plant transformation. We generate and validate a platform that can deliver plasmid DNA into both model and crop plants with high efficiency, no toxicity, without mechanical aid, and without transgene integration: a combination of features that is not attainable with existing plant transformation approaches. Covalently functionalized SWNTs were used to deliver DNA into mature *Nicotiana benthamiana*, arugula, wheat, and cotton leaves, generating strong protein expression. This study establishes that CNTs, which are below the size exclusion limit of the plant cell wall (at least one dimension at or below ~ 20 nm), could be a promising solution for overcoming plant biomolecule delivery limitations in a species-independent and non-integrating manner and could enable high-throughput plant genetic transformations for a variety of plant biotechnology applications.

3.3 Results and Discussion

3.3.1 Grafting DNA on Carbon Nanotube Scaffolds

For the transgene expression study, we developed an electrostatic grafting method to load green fluorescent protein (GFP)-encoding plasmids on SWNTs. Carboxylated SWNTs (COOH-SWNT) are first covalently modified with a cationic polymer (poly-ethylenimine, PEI) to carry a net positive charge. Next, positively charged CNTs (PEI-SWNT) are incubated with negatively charged DNA vectors (**Figure 3-1a**). The attachment of PEI and adsorption of DNA on SWNTs is verified by AFM via SWNT height increases after each step (**Figure 3-1b**). Nanoparticle heights before and after reaction with PEI are measured to be 1.3 nm and 8.1 nm for COOH- and PEI-SWNT, respectively, confirming PEI binding. AFM also reveals that SWNT height increases from 8.1 nm to 16.3 nm after incubation with DNA vectors, as expected, further confirming DNA grafting on SWNTs (**Figure 3-1c**).
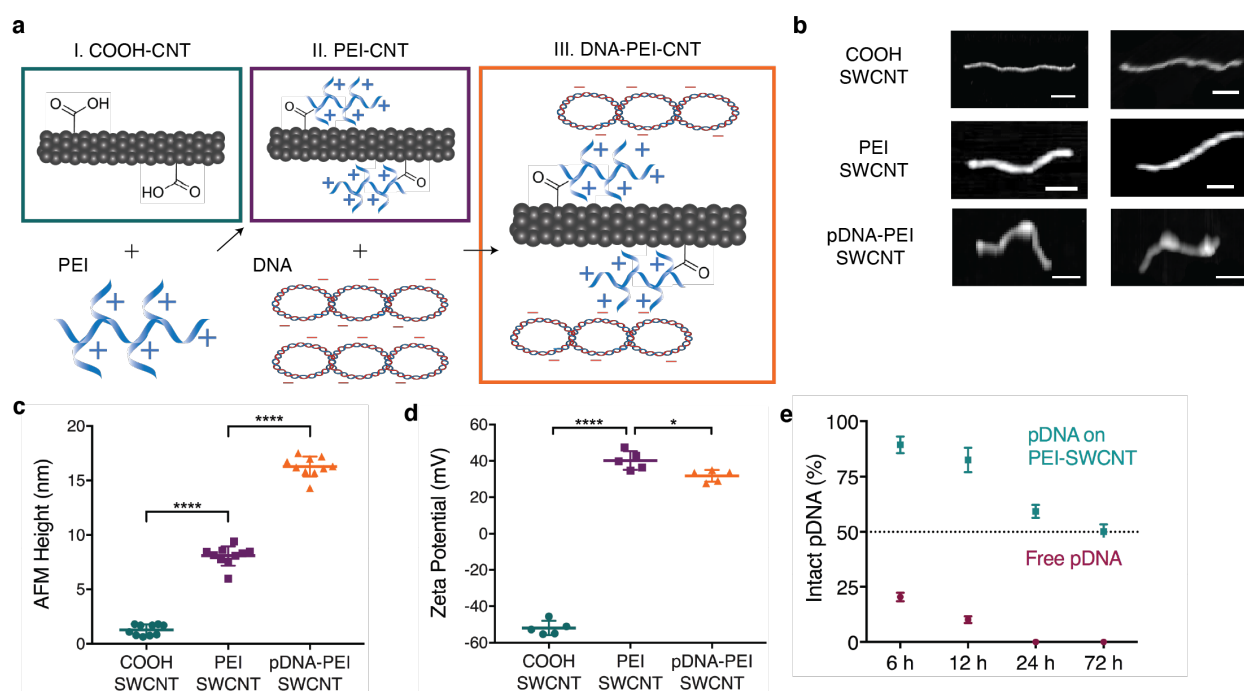
Figure 3-1. Scheme for grafting DNA on SWNT scaffold and characterization of DNA-SWNT conjugates.
a DNA grafting on PEI-modified carboxylated CNTs through electrostatic attachment. **b** Representative AFM images of carboxylated SWNTs, PEI modified SWNTs, and plasmid DNA loaded PEI modified SWNTs. Scale bars, 100 nm. **c** Average height profile of SWNTs before and after PEI reaction and pDNA loading measured via AFM. ****$P < 0.0001$ in one-way ANOVA. Error bars indicate s.d. (n = 10). **d** Zeta potential measurements of SWNTs before and after PEI reaction and pDNA loading measured via dynamic light scattering (DLS). *$P = 0.0191$ and ****$P < 0.0001$ in one-way ANOVA. Error bars indicate s.d. (n = 5). **e** Degradation of free pDNA vs. pDNA on PEI-SWNTs by plant nucleases obtained from a leaf lysate solution suggests pDNA protection on SWNT scaffolds. Error bars indicate s.d. (n = 3).

The covalent attachment of PEI and electrostatic adsorption of DNA on CNTs is also confirmed through zeta potential measurements (**Figure 3-1d**), after extensive washing of free unreacted PEI. The initial zeta potential of -51.9 mV for COOH-SWNT increases to +40.2 mV after reaction with positively-charged PEI, and subsequently decreases to +31.7 mV when incubated with negatively charged DNA, confirming PEI attachment and DNA adsorption. Further characterization (zeta potential, AFM height and length) of electrostatically prepared SWNT conjugates is summarized in **Figure 3-4**.

Intracellular stability of DNA loaded PEI-SWNT conjugates was assessed by incubating conjugates with proteins at total protein concentration similar to plant intracellular conditions. After 3 days of PEI-SWNT incubation with proteins, half of the DNA remains adsorbed on the nanoparticles (**Figure 3-4**), suggesting a similar stability in plant tissues. We also show that DNA adsorbed on PEI-SWNTs is partially protected from endonuclease degradation compared to free DNA, when incubated with total proteins extracted from plant leaves. Following a 3-day incubation with plant cell lysate, 100% of free DNA is degraded, whereas 50% of DNA on DNA-PEI-SWNTs remains intact (**Figure 3-1e** and **Figure 3-4**). DNA protection on SWNTs is further validated via single molecule total internal reflection fluorescence (smTIRF) microscopy: upon treatment with S1 nuclease, free DNA is degraded by 81.4%, whereas DNA on SWNTs is only degraded by 49.8%, commensurate with our bulk assays (**Figure 3-5**).

3.3.2   DNA Delivery into Mature Plants with Carbon Nanotubes

Functional gene expression studies were implemented with arugula and cotton plant leaves to demonstrate the applicability of our platform to transform crop plants in addition to traditional model laboratory species, such as *Nicotiana benthamiana*. Furthermore, gene delivery and protein expression studies are carried out with wheat plants demonstrating that our platform is also applicable to transform monocot plant species in addition to dicot plants.

After preparation of DNA-SWNT conjugates with GFP-encoding DNA plasmids or linear PCR amplicons with dialysis or electrostatic grafting, DNA-SWNTs were infiltrated into the true leaves of mature plants by introducing a small puncture on the abaxial surface of the leaf lamina with a pipette tip and infiltrating the solution with a needleless syringe. Post-infiltration, we hypothesize that DNA-SWNTs traverse the plant cell wall and membrane to enter the plant cell (**Figure 3-2a**). To confirm internalization of nanoparticles into mature leaf cells, Cy3 tagged DNA-SWNTs were delivered to plant leaves and the nanoparticle fate was assessed with confocal microscopy of the infiltrated leaf tissue (**Figure 3-2b**). For this experiment, a GFP mutant *Nb* plant was used, which constitutively expresses GFP so that we may co-localize the Cy3 fluorescence from the DNA-SWNTs with GFP fluorescence from inside the cells. When Cy3-DNA is delivered without SWNTs, we do not observe co-localization of Cy3 fluorescence with GFP (due to lack of Cy3 fluorescence), suggesting that Cy3-DNA alone does not internalize into cells. However, when Cy3-DNA-SWNTs are delivered into the leaves, we observe 62% co-localization between the Cy3 and intracellular GFP channels, which suggests efficient internalization of DNA-SWNTs into the plant cell cytoplasm (**Figure 3-2b**). Internalization of nanoparticles into mature leaf cells is also shown in wildtype *Nb* plants via high resolution confocal imaging, which demonstrates Cy3-DNA-SWNT localization both in the cell cytosol and nucleus (**Figure 3-6**).
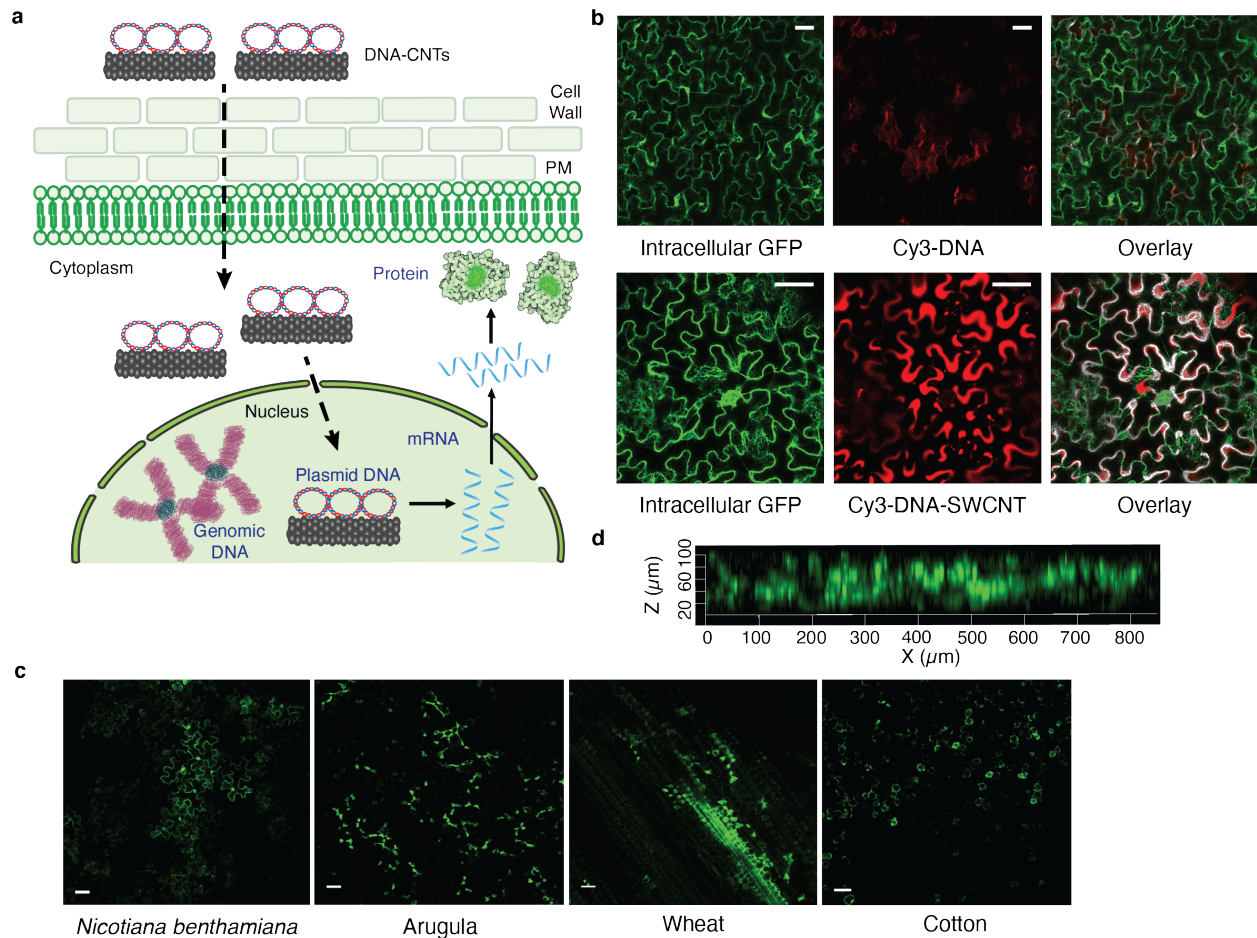
Figure 3-2. GFP-Encoding DNA delivery into mature plant leaves with SWNTs.
a Schematic depicting DNA-SWNT trafficking in plant cells and subsequent gene expression (dotted lines represent trafficking steps and the rigid lines represent gene expression steps). **b**, Nanoparticle internalization into mature plant cells is shown by imaging Cy3 tagged DNA-SWNTs with confocal microscopy, compared to a control sample of Cy3 tagged DNA without SWNTs, in a transgenic mGFP5 *Nb* plant. **c**, Wild type *Nb*, arugula, wheat, and cotton leaves infiltrated with DNA-SWNTs are imaged with confocal microscopy to determine GFP expression levels in the leaf lamina of each plant species. **d** Z-stack analysis of the fluorescence profile of the DNA-SWNT treated arugula leaf close to the infiltration area.

Leaves infiltrated with DNA-SWNTs for GFP expression are imaged with confocal microscopy, and expression of GFP is observed in the cells of the leaf lamina 72-hours post-infiltration in all plant species tested; *Nb*, arugula, wheat, and cotton (**Figure 3-2c**). Z-stack analysis of the fluorescence profile of the DNA-SWNT treated leaves shows that GFP fluorescence originates from the full thickness of the leaves, confirming that SWNT nanocarriers diffuse and penetrate through the full leaf profile (**Figure 3-2d**). No GFP expression is detected in the leaves when free DNA vectors, PEI-DNA complexes, or PEI-SWNTs are delivered in control studies (**Figure 3-7**).

3.3.3   Testing the Persistence of Carbon Nanotube-Mediated Gene Expression

We further demonstrate that SWNT-mediated gene expression is transient in mature plant leaves, independent of the plant species. Representative confocal images of pDNA-PEI-SWNT infiltrated *Nb* (**Figure 3-3a**) and corresponding quantitative fluorescence intensity analysis of these images demonstrate that the highest GFP fluorescence intensity at Day 3 disappears by Day 10 (**Figure 3-3b**). Similar GFP expression profiles at Day 3 and 10 are also verified with arugula, wheat, and cotton mature leaves (**Figure 3-3c-e**). Compared to SWNT-mediated expression, however, *Agrobacterium*-mediated GFP expression in mature arugula leaves did not cease at Day 10, as shown by confocal imaging (**Figure 3-3f**) and GFP fluorescence intensity quantification (**Figure 3-3g**), supporting the established concept of DNA integration with *Agrobacterium*-mediated delivery[247].
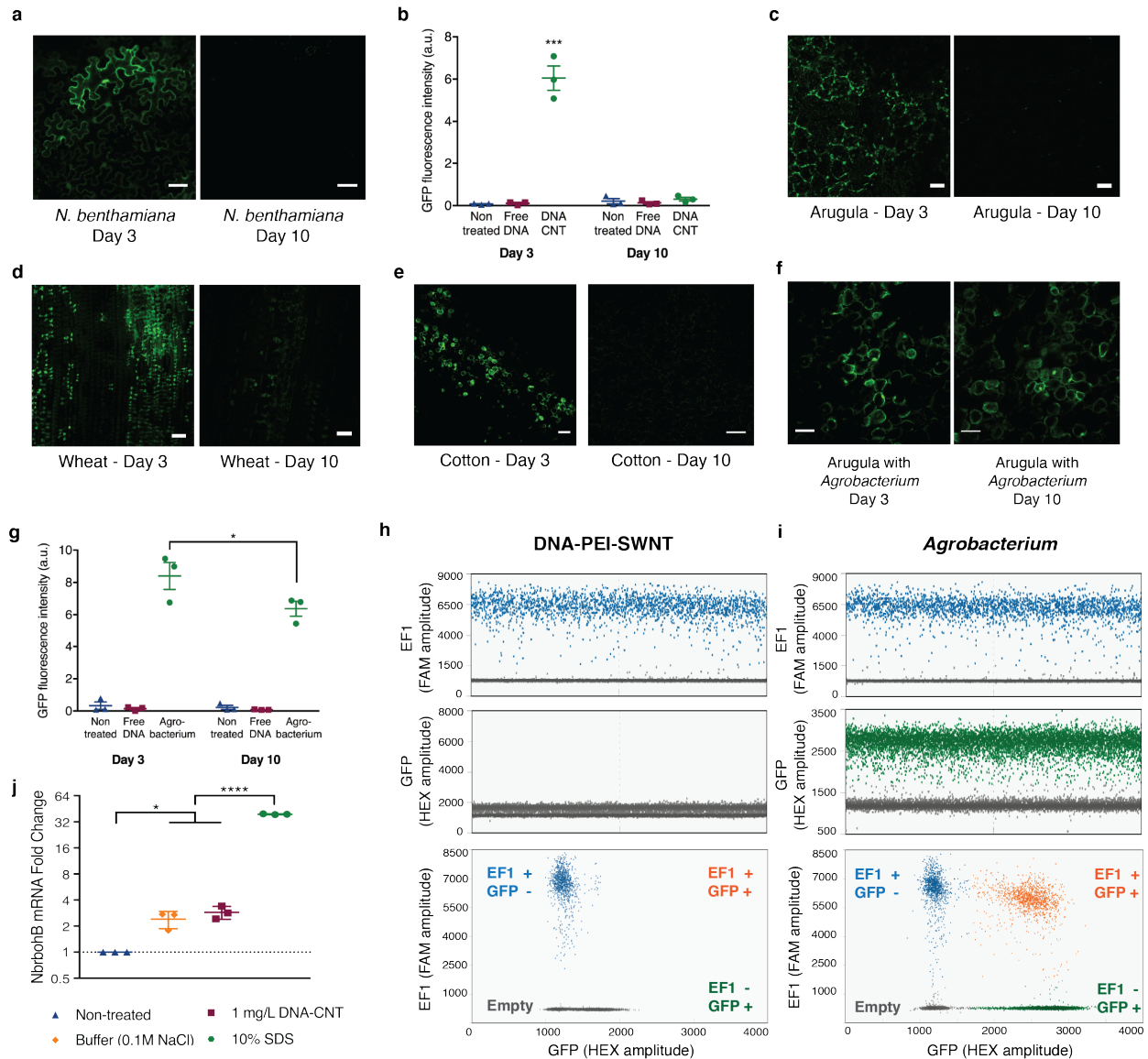
Figure 3-3. Transient SWNT-mediated GFP expression in mature plant leaves and nanoparticle toxicity assessment.

a Representative confocal microscopy images of pDNA-PEI-SWNT infiltrated mature *Nb* leaves imaged at Day 3 and 10. **b** Quantitative fluorescence intensity analysis of confocal images at 3 and 10-days post-infiltration. ***P = 0.0001 in two-way ANOVA. **c-e** Representative confocal microscopy images at Day 3 and 10 in pDNA-PEI-SWNT infiltrated mature **c** arugula, **d** wheat, and **e** cotton leaves. **f** Representative confocal microscopy images of *Agrobacterium* infiltrated mature *Nb* leaves imaged at Day 3 and 10. All scale bars, 50 μm. **g** Quantitative fluorescence intensity analysis of *Agrobacterium*-transformed leaves at 3 and 10-days post-infiltration. *P = 0.012 in two-way ANOVA. **h** Droplet digital PCR (ddPCR) results of DNA-PEI-SWNT infiltrated *Nb* leaves **i** ddPCR results of *Agrobacterium* infiltrated *Nb* leaves. **j** qPCR analysis of NbrbohB, a known stress gene in *Nb* plants, to test SWNT toxicity. *P = 0.0169 and ****P < 0.0001 in one-way ANOVA. All experiments are done with intact leaves attached to healthy plants.

Our results both at the mRNA transcript and fluorescent protein levels demonstrate that GFP expression is transient and suggest that genes delivered into plant cells via SWNT nanocarriers do not integrate into the plant nuclear genome. We tested the non-integration of plasmid DNA into the plant nuclear genome via droplet digital PCR (ddPCR). ddPCR is a recently developed method that allows high-precision and absolute quantification of nucleic acid target sequences[248–252]. Here, we used ddPCR to determine whether DNA delivered with SWNTs integrate into plant genomic DNA and compared genomic DNA integration rates of SWNT nanocarriers and *Agrobacterium*-mediated delivery methods. Our ddPCR experiments reveal that there is no transgene integration when DNA is delivered via SWNTs (**Figure 3-3h**), whereas high frequency GFP transgene integration events are shown when *Agrobacterium*-mediated delivery is performed (**Figure 3-3i**). We performed additional ddPCR control samples such as no template control (NTC), non-treated leaf, and free DNA infiltrated leaf. As expected, amplification of neither EF1 nor GFP genes is observed in the NTC (as there is no genomic DNA added), and amplification of only the EF1 gene is observed in non-treated or free DNA infiltrated leaves (**Figure 3-8**). The transient production of GFP in leaves induced by DNA-PEI-SWNT and *Agrobacterium*-mediated delivery was quantified 3-days after infiltration. We find that PEI-SWNTs versus *Agrobacterium* mediated DNA delivery produces 13.6 μg and 21.9 μg GFP per gram fresh weight of leaves, respectively.

3.4 Conclusions

Genetic engineering of plants may address the crucial challenge of cultivating sufficient food, natural product therapeutics, and bioenergy for an increasing global population living under changing climatic conditions. Despite advances in genetic engineering across many biological species, the transport of biomolecules into plant cells remains as one of the major limitations for rapid, broad-scale and high-throughput implementation of plant genetic engineering, particularly for intact plant tissues and organs. We thus present a nanomaterial-based delivery platform that permits diverse conjugation chemistries to achieve DNA delivery without transgene integration in both model and crop plants, and in both dicot and monocot plants, with high efficiency and without toxicity or tissue damage. In this study, we show the development and optimization of dialysis and electrostatic grafting methods for loading biomolecules onto high aspect ratio SWNTs. We confirm the feasibility and test the efficacy of this platform by delivering reporter GFP DNA constructs into mature *Nicotiana benthamiana*, arugula, wheat, and cotton leaves, and arugula protoplasts, and obtain strong expression of a functional transgenic protein.

The nanomaterial-based transient plant transformation approach demonstrated herein is beneficial for plant biotechnology applications where gene expression without transgene integration is desired, and is amenable to multiplexing whereby multiple gene vectors are to be delivered and tested rapidly in a combinatorial manner and in parallel[253]. This approach may aid high-throughput screening in mature plants to rapidly identify genotypes that result in desired phenotypes, mapping and optimization of plant biosynthetic pathways, and maximization of plant-mediated natural product synthesis, most of which currently rely on *Agrobacterium*-mediated transformation[254]. SWNT-mediated delivery is well-suited for such transient applications as it is easy, cost effective, non-destructive, fast, species-independent, and scalable.

Additionally, global regulatory oversight for genetically-modified organisms (GMOs) motivate the future development of non-integrative and/or DNA-free plant genetic transformation approaches in which the delivered gene expression is transient and foreign DNA is not integrated into the plant genome[183]. However, the most used tool today for plant genetic transformations – *Agrobacterium*-mediated transformation technology – is unable to perform DNA- and transgene-free editing and yields random DNA integration. Similarly, DNA delivery methods that utilize a gene gun or other external forces such as vortexing can cause cell damage, which leads to increased rates of transgene integration, possibly due to the over-activation of endogenous cellular DNA repair mechanisms commonly induced by stress and cell/DNA damage.

Notably, when combined with nuclease-based genome editing cargoes such as ZFNs, TALENs, Cpf1, and CRISPR/Cas9, SWNTs could enable transient expression of these tools for production of permanent (stable) edits. As such, SWNT-based delivery of these biomolecular cargoes could enable high-efficiency genome modification without transgene integration, thus avoiding strict GMO regulations. This latter application of the presented technology could be particularly beneficial for heterogeneous plant species such as cassava, cacao, sugarcane, etc. in which crossing cannot be used to remove transgenes. Furthermore, SWNTs are shown herein to protect DNA cargo against nuclease degradation, a feature of SWNT-based delivery that may be extended to the protection of other biological cargoes of interest.

Thus, in this study, we develop nanoparticle-based plant transformation biotechnologies that show high efficiency and species-independent delivery of plasmid DNA and transient expression of encoded proteins, which can potentially be used as a transgene-free plant genetic engineering approach, when combined with nuclease-based genome editing tools. As such, SWNT-based plant transformations are a useful addition to the plant biotechnology toolkit.

3.5 Materials and Methods

3.5.1 Plant Growth

Italian arugula *(Eruca sativa)* seeds purchased from Renee's Garden were germinated in SunGro Sunshine LC1 Grower soil mix by planting the seeds half an inch deep into the soil of a standard propagation liner tray (Nursery Supplies). The germinated plants were then moved to a Hydrofarm LED growth chamber (12h light at ~22˚C / 12h dark at 18˚C). Plants were allowed to mature to 3-4 weeks of age within the chamber before experimental use. Wild type *Nb* and transgenic mGFP5 *Nb* seeds obtained from the Staskawicz Lab, UC Berkeley, were germinated and grown in SunGro Sunshine LC1 Grower soil mix for four weeks before experimental in a growth chamber, 12-hour light at 24°C: 12-hour dark at 18°C cycle. Spring wheat (*Triticum aestivum* L., cv. Fielder) were

grown in Supersoil (Rod McClellan Co., South San Francisco, CA, USA) in a Conviron growth chamber with 60% relative humidity, 18-hour light at 24°C: 8-hour dark at 18°C cycle, and 3-4-week-old plants were used for experiments. Cotton seedlings were purchased from Cottonman.com and allowed to mature within the Hydrofarm LED growth chamber (12h light at ~22˚C / 12h dark at 18˚C). All experiments (except gene gun) were done with intact leaves attached to plants, where plants were incubated in the growth chamber until the time of data collection.

3.5.2 Cy3-DNA-SWNT Preparation

For toxicity, tissue damage and internalization assays, SWNTs were suspended in single-stranded DNA (ssDNA) polymers with $(GT)_{15}$ or Cy3-tagged $(GT)_{15}$ sequences through probe-tip sonication as previously described[255]. Briefly, ssDNA was dissolved at a concentration of 100 mg/mL in 0.1 M NaCl. 20 μL of this ssDNA solution was aliquoted into 980 μL 0.1 M NaCl and 1 mg HiPCO SWNTs was added. The mixture was bath sonicated for 10 min, followed by probe-tip sonication with a 3-mm tip at 50% amplitude (~7W) for 30 min in an ice bath. The resulting solution rested at room temperature for 30 minutes before centrifugation at 16,100g for 1 h to remove unsuspended SWNT aggregates and metal catalyst precursor. Unbound (free) ssDNA was removed via spin-filtering (Amicon, 100 K) 10-15 times and the concentration of ssDNA-SWNTs was determined by measuring the SWNT absorbance at 632 nm with an extinction coefficient of 0.036 L/g-cm.

3.5.3 Electrostatic Grafting of DNA onto SWNTs

Chemical modification of SWNTs to carry positive charge is described elsewhere[256] and applied here with some modifications. 10 mg COOH-SWNT powder was added to 10 ml water (can be scaled up or down as desired at 1mg/ml concentration). The solution was bath sonicated for 5 minutes and probe-tip sonicated with 6-mm tip at 10% amplitude for 30 min on ice. It was rested 30 minutes at room temperature and centrifuged at 16,000g for 1 h. Supernatant was taken and SWNT concentration was measured via absorbance at 632 nm with extinction coefficient of 0.036 to convert to mg/L. Prepared COOH-SWNT solution was mixed with PEI at a mass ratio of 1:10 SWNT:PEI. The solution was bath sonicated for several minutes, and subsequently heated at 84 °C with stirring for 16 h (the reaction can be scaled up or down as desired by keeping the PEI to SWNT mass ratio constant). The reaction mixture was subsequently cooled to room temperature and filtered with a 0.4 μm Whatman Nucleopore membrane to filter SWNTs. The filtered product was washed vigorously with water 10 times to remove unreacted PEI from the reaction mixture, then dried and collected. 3 mg of dried product (PEI-SWNT) was subsequently suspended in 3 mL water by probe-tip sonication with a 6-mm tip at 10% amplitude for 30 min in an ice bath. The resulting solution was rested at room temperature for 30 minutes before centrifugation at 16,100g for 1 h to remove unsuspended SWNT aggregates. The PEI-SWNT solution containing 1 μg of SWNTs was added into 1 μg of DNA dropwise, pipetted in and out 10 times, and incubated at room temperature for 30 minutes (DNA incubation can be scaled up or down by keeping the DNA to PEI-SWNT mass ratio constant).

3.5.4 AFM Characterization

3 μL of sample was deposited on a freshly cleaved mica surface and left to adsorb on the surface for 5 minutes. The mica surface was then slowly rinsed with water for three times (each time with 10 μL water) to remove the salt. Then, the mica surface was dried with a mild air stream by an ear-washing bulb and was imaged with a MultiMode 8 AFM with NanoScope V Controller (Bruker, Inc.) under tapping mode in air. All AFM images were analyzed by NanoScope Analysis v1.50.

3.5.5 Plasmid DNA Protection Assay

Total proteins (including nucleases) were extracted from wild type *Nb* leaves by grinding in liquid nitrogen to get dry frozen powders. The frozen powders were transferred to a microcentrifuge tube with pre-prepared lysis buffer containing 400 μL of 10 mM Tris/HCl (pH 7.5), 150 mM NaCl, 1 mM EDTA, 0.1% NP-40, 5% glycerol, and 1% Cocktail and vortexed briefly to mix well. After lysis at 50°C for 5 minutes, the tube was centrifuged at 10,000 rpm for 30 minutes and the supernatant containing whole proteins was collected to a new tube. Total protein extract was quantified by a Pierce 660 nm Protein Assay (Thermo, Prod# 22660). 5 μg free pDNA and 5 μg pDNA on PEI-SWNTs were each incubated with cell lysate proteins obtained from one *Nb* leaf to mimic the intracellular degradation conditions for 6, 12, 24 and 72 hours.

After incubation, all pDNA was desorbed from SWNTs at 95°C for 1 hour in the presence of 2% SDS and 1.5 M NaCl. Desorbed pDNA and cell lysate treated free pDNA were run on a 1% agarose gel with pDNA standards of known quantity to measure the intact versus degraded DNA in each sample. DNA amounts on the agarose gel were quantified by using band intensity as a proxy (ImageJ Gel Analyzer) and normalized with the lanes containing known DNA quantities (all agarose gel DNA quantifications are conducted as described here).

3.5.6 Infiltration of Leaves with SWNTs

Healthy and fully developed leaves from arugula (3-4 week old), *Nicotiana benthamiana* (4 week old), wheat (4 week old), and cotton (4 week old) plants were selected for experiments. A small puncture on the abaxial surface of the arugula and cotton leaf lamina was introduced with a pipette tip, and 100-200 μL of the plasmid DNA-CNT solution (or of any control solution) was infiltrated from the hole with a 1 mL needleless syringe by applying a gentle pressure, with caution not to damage the leaf. For *Nb* infiltration, a tiny puncture on the abaxial surface of the leaf lamina was introduced with a sharp razor, and 100-200 μL of DNA-SWNT solution (or of any control solution) was infiltrated through the puncture with a 1 mL needleless syringe by applying a gentle pressure.

3.5.7 Imaging of Infiltrated Leaves for Internalization and GFP Expression

After infiltration, plants with attached infiltrated leaves were left in the plant growth chamber to allow for internalization for 6 h and imaged with the confocal microscope to track Cy3 tagged DNA-SWNTs in leaves. For GFP expression and transience studies, infiltrated leaves were imaged after 3 and 10 days with confocal microscope. For wheat leaf infiltrations, a sharp razor blade was used to produce a small puncture on the abaxial surface of 3-4-week-old plant leaves, and 100-200 μL of the plasmid DNA-SWNT solution (or of any control solution) was infiltrated with a 1 mL needless syringe. Plants were returned to growth chamber and imaged with confocal microscope after 3 and 10 days-post-infiltration.

3.5.8 Quantitative Fluorescence Intensity Analysis of GFP Gene Expression

DNA-SWNT infiltrated plant leaves were prepared for confocal imaging 72-hours post-infiltration by cutting a small leaf section of the infiltrated leaf tissue and inserting the tissue section between a glass slide and cover slip of #1 thickness. 100 μL water was added between the glass slide and cover slip to keep the leaves hydrated during imaging. A Zeiss LSM 710 confocal microscope was used to image the plant tissue with 488 nm laser excitation and with a GFP filter cube. GFP gene expression images were obtained at 10x and 20x magnification. Confocal image data was analyzed to quantify GFP expression across samples. For each sample, 3 biological replicates (3 infiltrations

into 3 different plants) were performed, and for each biological replicate, 15 technical replicates (15 non-overlapping confocal field of views from each leaf) were collected. Each field of view was analyzed with custom ImageJ analysis to quantify the GFP fluorescence intensity value for that field of view, and all 15 field of views were then averaged to obtain a mean fluorescence intensity value for that sample. The same protocol was repeated for all 3 biological replicates per sample, and averaged again for a final fluorescence intensity value, which correlates with the GFP expression produced by that sample.

3.5.9 Single Molecule TIRF to Image DNA Protection by SWNTs

The sequence of DNA used for this assay is the same as that used in co-localization experiments, $(GT)_{15}$. While Cy3 was used for co-localization assays in planta, the Cy5 fluorophore was selected for the TIRF assay due to lower levels of background noise in the collection region. 10 µM 3' labelled Cy5 DNA was added to an equal mass of HiPCO SWNT. The suspension and clearing of unbound DNA followed the same protocol as described in SDS-SWNT, ssDNA-SWNT and Cy3-DNA-SWNT preparation. The positive control comprised of 5' labelled biotin with a Cy5 fluorophore on the 3' end.

6-channel µ-slides (ibidi, µ-Slide VI 0.5 Glass Bottom) were used for single-molecule TIRF microscopy. The slides were initially washed by pipetting 100 µL of 100 mM NaCl solutions in nuclease-free water filtered with a sterile 0.2 µm syringe filter into one reservoir and removing 60 µL the other end, leaving just enough solution to fully wet the channel. Each subsequent step involved depositing the desired solution volume into the reservoir and removing the equivalent volume from the other end of the channel. 50 µL of 0.25 mg/mL BSA-Biotin was added to coat the surface of the glass slide for 5 minutes. Next, 50 µL of 0.05 mg/mL NeutrAvidin was added, followed by 50 µL of 1.0 mg/L DNA-loaded SWNT. For the positive control, 50 µL of 100 pM biotinylated Cy5-DNA was added in place of DNA-loaded SWNT. The addition of each component comprised of a 5-minute incubation period, followed by gently flushing the channel with 50 µL of NaCl solution to remove unbound entities. Each channel was exposed to 50 µL of 2.8 U/uL S1 Nuclease for 30 minutes at room temperature. The reaction was stopped by rinsing the channel with 1 mM ATP solution to inactivate the nuclease. To minimize disturbance of bound DNA or DNA-SWNT, no imaging buffer was used; each field of view obtained was ensured to not have been imaged previously.

Following slide preparation and immobilized procedure as outlined above, we obtain a surface coverage of ~ 300-400 fluorescent molecules of DNA-loaded SWNT for each field of view, imaged with a 642 nm laser line, collected with a 655 LP filter, with a 1000 ms exposure time and an EMCCD gain of 300 under TIRF microscopy (Zeiss ELYRA PS.1).

3.5.10 Droplet Digital PCR (ddPCR) Experiments

Genomic DNA (gDNA) was extracted from leaves, 14 days after the treatment with pDNA-PEI-SWNTs and Agrobacterium, via CTAB extraction modified from a previous method8. Briefly, 200 mg leaf tissue was ground in liquid nitrogen with a mortar and pestle, and the leaf powder was transferred into 600 µl CTAB buffer (10 g CTAB, 50 mL 1 M Tris-HCl pH 8, 20 mL 0.5M EDTA pH 8, 140 mL 5 M NaCl and 5 g PVP). The mixture was vortexed well and incubated at 65˚C for 45 minutes. 600 µl chloroform: isopropanol (39:1) was added to mixture and vortexed well. The mixture was centrifuged at 18,000g for 10 minutes and the upper phase was transferred into a new

microcentrifuge tube. 600 µl isopropanol was added to the new tube, incubated 5 minutes at room temperature, and then mixed softly. The mixture was centrifuged at 18,000g for 10 minutes. The supernatant (isopropanol) was removed and 100 µl 70% ethanol was added. The mixture was centrifuged at 18,000g for 10 minutes. The supernatant (ethanol) was removed as much as possible and the tube was left to dry at 37˚C for 30 minutes. The gDNA pellet was resuspended in 200 µl autoclaved MilliQ water and the concentration and purity was measured by Nanodrop. All gDNA samples were digested overnight with HindIII-HF in CutSmart buffer. 2 µg gDNA was digested with 20U enzyme in a 50 µl reaction volume for 16 hours at 37˚C. Note that the restriction enzyme was selected so as not cut inside the reference or target gene. We have confirmed that the extracted genomic DNA does not contain any of the infiltrated plasmid DNA via several measures. First, 14-days incubation is assumed to be long enough for plasmid DNA to degrade inside the cells. Second, plasmid DNA is not present in any of the agarose gels we have run (ddPCR control gels in Supplementary Fig. 9). Last, all samples were treated the same and if there was any plasmid DNA left at the time of PCR, it would be present not only in the Agrobacterium sample, but in all samples (which is not the case, as controls and DNA-PEI-SWNT samples did not show any amplification with PCR).

ddPCR was performed via probe chemistry in a duplex assay for reference EF1 and target GFP genes. The GFP probe (5'-TGCCGTCCTCCTTGAAGTCG-3') was labeled with HEX at 5', Iowa Black Hole Quencher at the 3' end and with an internal ZEN quencher 9 nucleotides away from the 5' end. The EF1 probe (5'-AGGTCTACCAACCTTGACTGGT-3') was labeled with FAM at the 5'end, with Iowa Black Hole Quencher at the 3' end, and with internal ZEN quencher 9 nucleotides away from the 5' end. Primers used for GFP gene: 5'-GACTTCTTCAAGTCCGCCAT-3' and 5'-CGTTGTGGCTGTTGTAGTTG-3', primers used for EF1 gene: 5'-TCCAAGGCTAGGTATGATGA-3' and 5'-GGGCTCATTAATCTGGTCAA-3'. 20X probe-primer mixes (18 µM PCR primers (each), 5 µM probe) were prepared for both genes.

ddPCR reaction mixes were prepared according to the instructions in ddPCR Supermix for Probes (No dUTP) #1863024 kit. For each sample, we prepared 10 wells, each containing 100 ng digested gDNA, so that a total of 1µg DNA was screened for transgene integration for each sample. Droplets were generated with a QX200 droplet generator right after the ddPCR reaction mixes were prepared. 20 µL of each sample mastermix was transferred to the sample row and 70 µL droplet generation oil was transferred to the oil row in the droplet generation cartridge. After the droplets were generated, 40 µL of droplets were transferred to a new 96-well plate and the plate was sealed for 5 s at 180ºC in plate sealer. The PCR was run in a deep-well thermal cycler with the following PCR program: enzyme activation 95˚C 10 min, denaturation 94˚C 30 sec (40X), annealing/extension 60˚C 1 min (40X), stabilization 98˚C 10 min, and hold 4˚C. The fluorescence of the droplets was measured 4 hours after PCR (kept in the dark and at 4˚C) with a QX200 droplet reader, and the results were analyzed with the Bio-Rad Quantasoft Pro Software.

3.5.11 Quantification of GFP Protein Amount in Leaves

Month-old Nb leaves were infiltrated with either pDNA-PEI-SWNTs or Agrobacterium solutions. Three days post-infiltration, leaves were harvested, weighed, then frozen and ground in liquid nitrogen to obtain powder. The powder was placed in a liquid nitrogen-cooled tube to which 350 µL of lysis buffer containing 10 mM Tris/HCl (pH 7.5), 150 mM NaCl, 1 mM EDTA, 0.1% NP-40, 5% glycerol, and 1% Cocktail was added. The tube was immediately vortexed for 2-3 seconds

before being placed on ice while other samples were similarly harvested. All tubes were incubated in a 50˚C water bath for 3 minutes, then centrifuged at 16,000 g for 40 minutes. The supernatant containing proteins were then transferred to a fresh tube.

A GFP-Trap (ChromoTek GFP-Trap_A) was used to purify and concentrate GFP present in the supernatant. For each sample, 25 µL of GFP-Trap beads was pipetted into ice-cold dilution buffer composed of 10mM Tris/HCl (pH 7.5), 150 mM NaCl and 0.5 mM EDTA. The beads were centrifuged at 2,500 g for 2 min at 4oC and the supernatant was discarded. This was then repeated twice. The beads were added to the supernatant along with 300 µL dilution buffer, and the tube placed on a tube rotator for 1 hour at 4˚C. Samples were centrifuged at 2,500 g for 2 min at 4˚C with the supernatant discarded. Then, 500 µL ice-cold dilution buffer was added to each sample, which was again centrifuged at 2,500 g for 2 min at 4˚C with the supernatant discarded three times. The bound GFP was eluted by constant mixing with 50 µL 0.2M glycine at pH 2.5 for 30 s followed by centrifugation. The supernatant was transferred to a fresh tube and 5 µL 1M Tris Base pH 10.4 added for neutralization. The protein elution step was executed twice to obtain two tubes of approximately 55 µL each per sample.

A Qubit Protein Assay Kit (Invitrogen) was used to quantify the mass of GFP eluted. Briefly, 20 µL of eluted protein was added to 180 µL Qubit Working Solution. The samples were vortexed for 3 seconds and incubated at room temperature for 15 minutes. Standard calibrations and measurements were collected via a Qubit 4 Fluorometer.

3.6 Chapter Supporting Information

3.6.1 Supplementary Figures and Table

a

	COOH-SWCNT	PEI-SWCNT	pDNA-PEI-SWCNT
Zeta Potential (mV)	-54.7	+42.4	+30.7
AFM Height (nm)	1.37	8.3	16.43
AFM Length (nm)	820	616	590

b

plasma incubation

1. 35S:GFP pDNA
2. pDNA-PEI-SWCNT in plasma 1 h
3. pDNA-PEI-SWCNT in plasma 24 h
4. pDNA-PEI-SWCNT in plasma 48 h
5. pDNA-PEI-SWCNT in plasma 72 h
6. plasma with 0.2 mg/μl protein

c

cell lysate treatment

1. pDNA standard
2. Free pDNA 6 h
3. pDNA on PEI-SWCNT 6 h
4. Free pDNA 12 h
5. pDNA on PEI-SWCNT 12 h
6. Free pDNA 24 h
7. pDNA on PEI-SWCNT 24 h
8. Free pDNA 72 h
9. pDNA on PEI-SWCNT 72 h

Figure 3-4. Confirmation of synthesis and DNA adsorption on PEI-SWNTs with loading efficiency characterization.
a Characterization of nanoconjugates prepared with the electrostatic method of DNA loading on SWNTs: zeta potential and AFM height and length. **b** pDNA-PEI-SWNTs are incubated in plasma containing 0.2 mg/μL total protein to approximate the DNA desorption rate in intracellular conditions. Results show that even after a 72-hour incubation in plasma at 21ºC, almost half of the DNA is still adsorbed on PEI-SWNTs. **c** Agarose gel electrophoresis of free pDNA and pDNA on PEI-SWNTs incubated with plant lysate solution for 6, 12, 24, and 72 hours to determine pDNA protection against nuclease degradation on PEI-SWNTs. All DNA pieces (degraded and intact) are desorbed from the SWNT surface after cell lysate treatment and prior to running the gel.

a

Cy5-DNA-Biotin Complex

NeutrAvidin
BSA-Biotin
Cy5
Biotin

Cy5-DNA-SWCNT Complex

Microscopy Slide

Microscopy Slide

b

Before incubation
After incubation

Cy5 molecules

900
750
600
450
300
150
0

Salt
Free DNA + Salt
Free DNA + S1 Nuclease (1)
Free DNA + S1 Nuclease (2)
Free DNA + S1 Nuclease (3)

c

Before incubation
After incubation

Cy5 molecules

900
750
600
450
300
150
0

Salt
DNA SWCNT + Salt
DNA SWCNT + S1 Nuclease (1)
DNA SWCNT + S1 Nuclease (2)
DNA SWCNT + S1 Nuclease (3)

d

Before   After

Empty + Salt

Free DNA + Salt

Free DNA + S1 Nuclease

e

Before   After

Empty + Salt

DNA-SWCNT + Salt

DNA-SWCNT + S1 Nuclease

124

Figure 3-5. Single molecule TIRF (smTIRF) microscopy demonstrates DNA protection against nuclease degradation when on SWNTs.
a Schematics of microscopy slides for immobilization of Cy5-DNA-Biotin and Cy5-DNA-SWNT complexes. The microscopy slide surface is first coated with BSA-Biotin, then incubated with NeutrAvidin. Cy5-DNA-Biotin is immobilized on the surface via Biotin-NeutrAvidin attraction, and Cy5-DNA-SWNT is next immobilized on the surface via non-specific interaction of NeutrAvidin with SWNTs. **b** Raw smTIRF data for empty channel rinsed with salt solution, free DNA incubated with salt solution, and three experimental replicates of free DNA incubated with 2.8U/µL S1 nuclease, blue: before incubation and orange: after incubation. Data from 30 fields of view plotted for each sample before and after nuclease treatment. **c** Raw smTIRF data for empty channel rinsed with salt solution, DNA-SWNT incubated with salt solution, and three experimental replicates of DNA-SWNT incubated with 2.8U/µL S1 nuclease, blue: before incubation and orange: after incubation. Data from 30 fields of view plotted for each sample before and after nuclease treatment. All channels contain BSA-Biotin and NeutrAvidin. **d** Representative smTIRF microscopy images for each sample of free DNA before and after incubation with salt and 2.8U/µL S1 nuclease. Scale bars, 10 µm. **e** Representative TIRF microscopy images for each sample of DNA-SWNTs before and after incubation with salt and 2.8U/µL S1 nuclease. Scale bars, 10 µm.
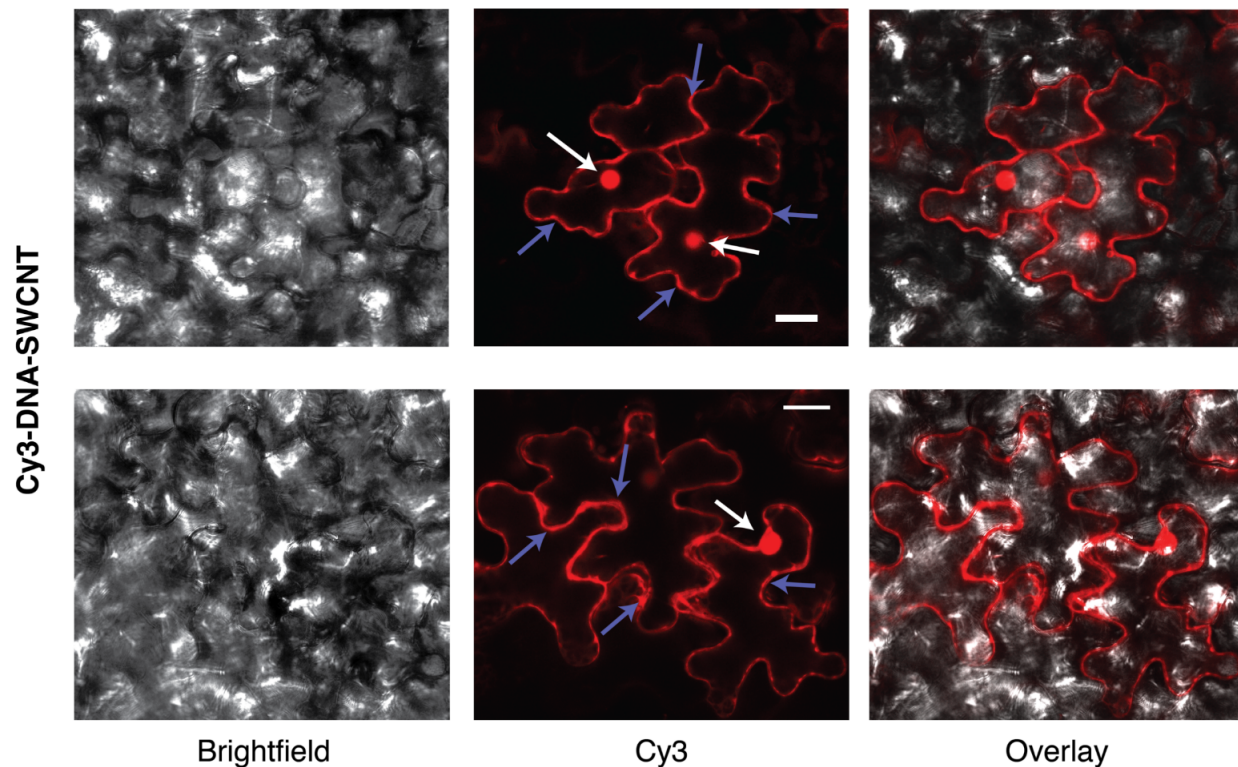
Figure 3-6. Subcellular localization of Cy3-DNA-SWNT in wild type *Nicotiana benthamiana* intact leaves.

Cy3 fluorescence is observed both in the cell cytosol and nuclei 6 hours after infiltration of Cy3-DNA-SWNT conjugates. White arrows show cell nuclei and blue arrows show cell cytoplasm containing Cy3-DNA-SWNT conjugates. Scale bars, 25 μm. All experiments are done with intact leaves attached to healthy plants.
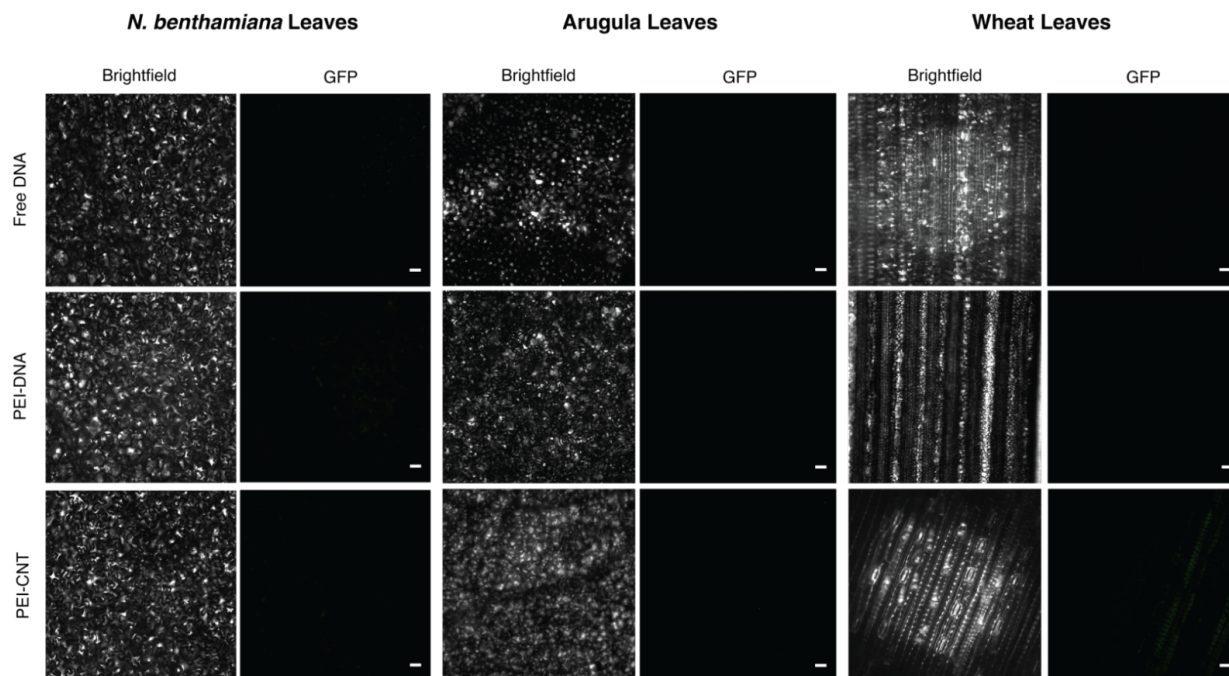
Figure 3-7. Control studies for DNA-SWNT delivery and GFP protein expression in mature *Nicotiana benthamiana*, arugula, and wheat leaves.
When free plasmid DNA, or PEI-DNA, or PEI-SWNT is delivered, no GFP expression is detected in any plant species via confocal microscopy at 72h post-infiltration, as shown by representative confocal images obtained with the same optical parameters with DNA-SWNT induced GFP expression imaging. Scale bars, 50 µm. All experiments are done with intact leaves attached to healthy plants.
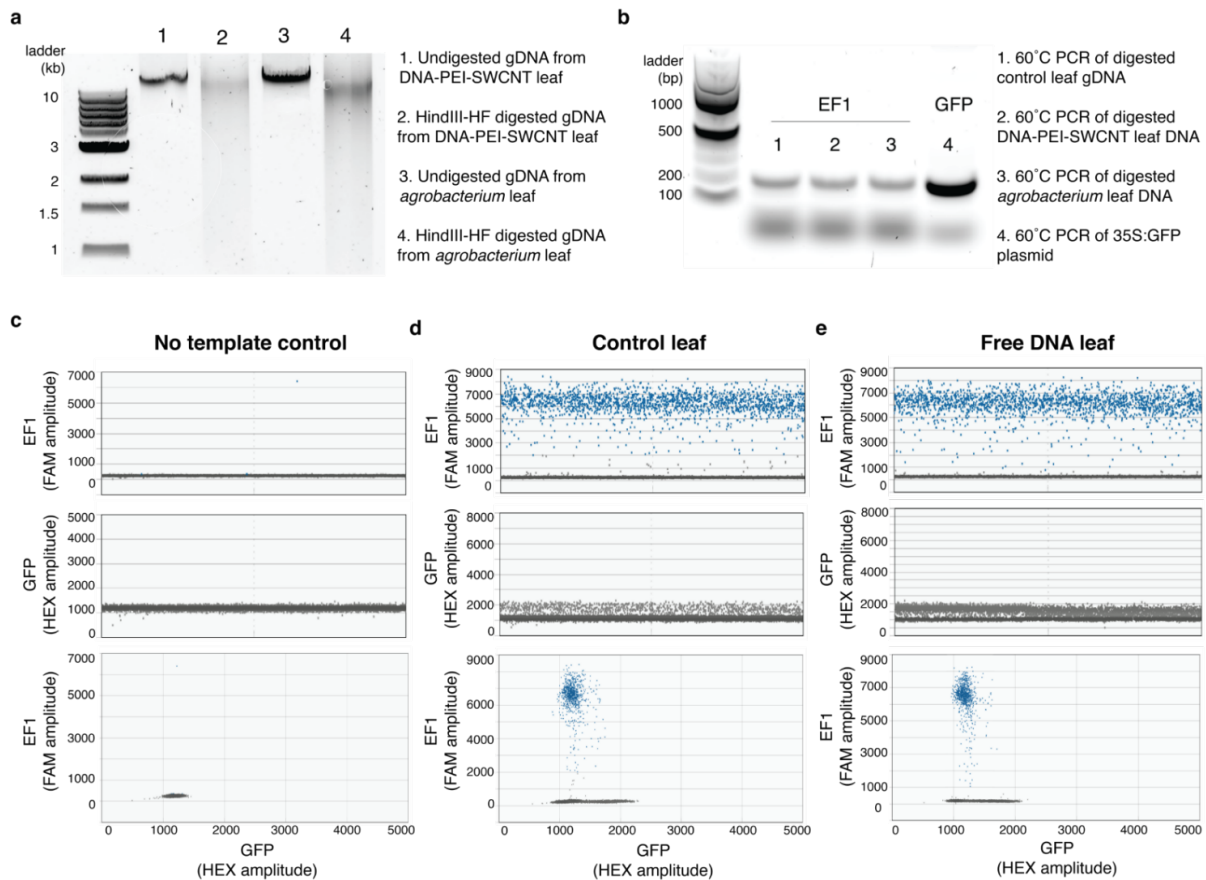
Figure 3-8. Droplet digital PCR (ddPCR) control experiments.
a Genomic DNA extraction and digestion with HindIII-HF restriction enzyme is optimized for ddPCR experiments. Agarose gel electrophoresis showing successful and pure genomic DNA extraction in wells 1 and 3. Wells 2 and 4 show successful genomic DNA digestion of DNA-PEI-SWNT and agroinfiltrated leaves. No plasmid DNA contamination was observed in any of our genomic DNA extractions. **b** Agarose gel electrophoresis shows that EF1 and GFP primers perform optimally during PCR at 60˚C with the correct amplicon at size ~200 bp both for the EF1 reference gene and also for the GFP target gene. **c** ddPCR run showing no amplification of the EF1 or GFP genes in the no template control well. **d** ddPCR run result showing significant amplification of the EF1 gene but no amplification of the GFP gene in the control (non-treated) leaf. **e** ddPCR run result showing significant amplification of the EF1 gene but no amplification of the GFP gene in the free plasmid DNA infiltrated leaf, as expected. The EF1 gene is labeled with a FAM tagged probe and the GFP gene is labeled with a HEX tagged probe. Both probes are initially quenched with a 3' Iowa Black Hole Quencher and a ZEN internal quencher manufactured by IDT. All experiments are done with intact leaves attached to healthy plants.

4 Nanoparticle-mediated protein delivery *in planta*

4.1 Chapter Abstract

Delivery of proteins into walled plant cells remains a challenge with few tractable solutions. Recent advances in biomacromolecule delivery using nanotechnology may evince methods to be exploited for protein delivery. While protein delivery remains no small feat, even in mammalian systems, the ability for nanoparticles to penetrate the cell wall and be decorated with a plethora of functional moieties makes them ideal protein vehicles in plants. Now, as advances in protein biotechnology accelerate, the need for a commensurate delivery system becomes clear. However, the road to nanoparticle-mediated protein delivery is fraught with challenges regarding cell wall penetration, intracellular delivery, endosomal escape and nanoparticle chemistry and design. The dearth of literature surrounding protein delivery in walled plant cells hints at the challenge of this problem but also indicates a wide-open space for new innovations in plant tailored nanotechnology.[††]

4.2 Introduction

For several decades, breakthroughs in nanomaterial synthesis, production, and characterization have advanced electronics, medicine, and basic research. Nanomaterials are now broadly commercially available, with functionalization approaches that are readily accessible in most laboratories, enabling ease of access and use in a diverse range of applications[257,258]. Although recent nanotechnology-based accomplishments have been made in sensing, delivery, and targeting of nanomaterials *in planta*, both fundamental and applied plant nanoscience lag behind other fields of nano-biotechnology[88,164,259,260]. In particular, the delivery of molecular biology cargoes such as DNA, RNA, and proteins to plant cells have become increasingly important goals. Of these goals, protein delivery remains the most difficult to accomplish, and as such, protein delivery strategies using nanomaterial carriers are only nascent in plants[81,141,189,261]. The development of gene editing tools motivates *in planta* delivery of proteins that could enable DNA-free gene edited plants and could accelerate the development of both engineered crops and basic plant science. Recent *in planta* protein delivery successes have leveraged protein biolistics for DNA-free gene editing. While these new protocols have enabled DNA-free genome editing applications in plants, they involve specialized instrumentation and intensive low-throughput screening of hits due to low protein delivery efficiencies[262,263]. Given these limitations, a nanoparticle-mediated protein delivery technology could simplify workflows and streamline plant genome engineering.

To emphasize how challenging protein delivery to walled plant cells can be, we consider that evolution has not generated a "passive" way to bypass the barrier of the cell wall. To our knowledge, no intact plant virus has been found to diffuse across the plant cell wall despite possessing nanoscale (~15-200 nm) dimensions. Viral infection is instead mediated by injury to the plant cell wall upon mechanical damage by weather, animals, or fungal attack[264]. Other

---

[††] Published as Goh, N.S.*, Wang, J.W.*, Cunningham, F.J.*, Boozarpour, N.N., Pham, M. and Landry, M.P., 2021. Nanoparticles for protein delivery in planta. *Current opinion in plant biology*, *60*, p.102052.

pathogens have evolved elaborate secretory systems as seen in *Agrobacterium* or anatomical structures such as fungal haustoria to deliver proteins past the cell wall[265,266]. In contrast, certain engineered nanoparticles (NPs) have been shown to internalize into walled cells, lending credence to their potential application as protein carriers in plants[127,189,267,268]. Why and how NPs, defined as constructs synthesized with at least 1 dimension below 100 nm, are seemingly able to pass the cell wall remains an unanswered question in plant nanotechnology. Hypotheses put forward include optimized charge density, high stiffness, and small (<10 nm) size of NPs.

Regardless of mechanism, recent research suggests that NPs or other chemical approaches may play a role in developing generalizable strategies for protein delivery to plant cells. Research on nanoparticle-mediated delivery of plasmid DNA[88,140,164] and RNA[168], biomolecules many-fold larger than proteins in molecular weight, serve to motivate intensified efforts for protein delivery. While recent publications have shown the delivery of pDNA to plant cells for gene expression using a variety of nanocarriers, expression has been shown to be sporadic, with efficiencies lower than with biotic delivery methods such as *Agrobacterium*[269]. Thus, nano-scientists should consider whether gene delivery offers the highest phenotypic effect and whether nanoparticles may offer a practical solution. In this opinion, we discuss the barriers of the cell wall, cellular entry and endosomal escape, and what chemical and nano-engineering strategies have been attempted or could aid in plant protein delivery.

4.3   Barriers for Plant Cellular Delivery

We outline the key barriers for biomolecule delivery in plant cells – the plant cell wall, cell membrane, and endosomal escape – in **Chapter 1.6.3**. In considering the barriers for protein delivery in plant cells, we hypothesize the requirements for designing efficient protein delivery systems. Firstly, the protein and carriers *in toto* should be near or smaller than the SEL of the cell wall, which strictly limits the choice of nanocarrier. Secondly, the protein must be imparted by its carrier with pro-internalization motifs or another mechanism of cell membrane bypass. Thankfully, many NPs such as single-walled carbon nanotubes (SWNTs) and quantum dots (QDs) appear to elicit endocytosis[270,271], or carriers can be functionalized with pro-endocytic peptide motifs, such as HIV-1 derived Tat peptide[272]. Finally, pro-endosomolytic moieties that allow endocytosed material to escape degradation and enter the cytosol should be present. A third barrier that we do not fully elaborate on exists for intact plant tissues and organs: the cuticle. In a laboratory setting, the hydrophobic cuticular barrier is often overcome via the application of the carrier/bio-molecule solution. Recent examples have employed vacuum infiltration[273], syringe infiltration[168], and foliar spray[274], with or without non-ionic surfactants such as Silwet L-77, to deliver the active solution to plant cells. Given that these solutions largely involve formulation rather than NP design, we will not further digress. Clearly, many variables in not just chemical strategies but also protocols must be considered in developing NP strategies for protein delivery. In the next section we will elaborate on biochemical and nanocarrier approaches that may aid in developing *in planta* protein delivery systems.

4.4   Chemistries for Plant Cellular Delivery

The design of an efficacious protein delivery system for plants remains challenging due to variability in protein sizes, protein structural sensitivity to chemical and mechanical perturbations, and the lack of amplified expression that could result from the delivery of DNA or RNA vectors,

with the relative impact of each of these considerations being highly dependent on the protein of interest, the carrier, and the desired functional outcome. Despite these complexities, we can consider carrier systems for protein delivery and then separately delve into how proteins might be conjugated to said carriers. Examples of non-biolistic, mechano-/electro-poration, or protoplast-based methods of protein delivery in plants are scant in literature (**Table 4-1**). The Numata group has been prolific in employing synthetic CPPs for protein delivery in plants[129,140,141,261,275]. In this study, peptides bearing a protein-binding domain and a CPP domain are complexed with the cargo protein. However, given that carrier-protein complexes measure ~200-nm in radius, their ability to bypass the cell wall intact is difficult to explain[141]. One plausible explanation could be activity of non-complexed pro-endocytotic peptides causing uptake of non-bound proteins. Such an effect has been observed in mammalian cells where co-incubation with free CPPs enhances uptake and endosomal escape[139]. Another recent development was by Santana *et al* where inorganic QDs were targeted to the chloroplast using an engineered chloroplast transduction peptide[189]. In this case, the size of the carrier *in toto* was over 24-nm in diameter, suggesting some possible polydispersity in the cell wall SEL while also demonstrating the feasibility of transiting proteinaceous materials using a hard NP. As their final design lacks an explicit mechanism for endocytosis or endosomal rupture, we cannot say what roles the nanocarrier or peptide play in their successful delivery.

Table 4-1. Selected examples of protein delivery to plants.

Carrier	Species and tissue type	Protein Cargo	Delivery Method	Method of Validation
Biolistic delivery in walled plant cells				
Au-capped MSNs (0.6 µm diameter)[154]	Onion epidermis, tobacco leaves, teosinte leaves	FITC/TRITC-BSA, GFP	Biolistic	Widefield FL microscopy
Au-capped MSNs (0.6 µm diameter)[93]	Maize embryos	Cre recombinase	Biolistic	Widefield FL microscopy, southern blot (1-20% T0 recombinants)
Au microparticles (0.6 µm diameter)[262]	Onion epidermis, tobacco leaves	GFP, dsRed, BSA-TRITC, GUS, RNAse A, trypsin	Biolistic	Widefield FL microscopy
Au microparticles (0.6 µm diameter)[276]	Maize embryos	Cas9 RNP	Biolistic	Amplicon deep sequencing (2-9% mutated T0 progeny)
Au particles + cationic lipid-polymer mixture[277]	Rice embryos	Cas9 RNPs + hygR selection plasmid	Biolistic	Sanger sequencing (63% of selected transformants carried mutations)
Au microparticles (0.6 µm diameter)[278]	Rice embryos	Cas9 and Cas12a RNPs + hygR selection plasmid	Biolistic	NGS (3% WT Cas9, 9% HiFi Cas9, 32% Cas12a)
Peptide-mediated transfection in walled plant cells				

AID peptide complexes[279]	Onion and tomato roots, onion epidermis	GFP, RFP	Incubation with protein-peptide solution	Confocal FL microscopy
Tat PTD and R9 AID peptide complexes[280]	Onion and maize roots, onion epidermis	GFP, RFP	Incubation with protein-peptide solution	Confocal FL microscopy
R9 AID peptide complexes[281]	Onion roots	GFP, RFP (covalent and noncovalent codelivery)	Incubation with protein-peptide solution	Confocal FL microscopy
TpI CPP complexes[282]	Wheat and rapeseed roots and protoplasts	GUS	Incubation with protein-peptide solution	Confocal FL microscopy, GUS fluorimetric analysis
BP100(KH)9 and BP100CH7 CPP complexes[141]	Rice callus	YFP	Vacuum infiltration	Confocal FL microscopy
2BP100-K8 CPP fusion[261]	Apple leaves	Neomycin phosphotransferase II (NPTII)	Leaf infiltration	Confocal FL microscopy
(BP100)2K8 and BP100(KH)9 CPP fusion[275]	Arabidopsis leaves	BSA-RhB, ADH-RhB, YFP	Leaf infiltration	Confocal FL microscopy
Electroporation in walled plant cells				
_[283]	Tobacco BY2 culture	ERD14 and ERD10 intrinsically disordered proteins (IDPs)	Electroporation	Confocal FL microscopy

	Arabidopsis T87 culture	Cre recombinase	Electroporation	GUS fluorometric analysis, genomic PCR
[284]	Arabidopsis T87 culture	Cre recombinase	Electroporation	GUS fluorometric analysis, genomic PCR
Protoplast transfection				
PEG[285]	Arabidopsis, tobacco, rice, lettuce protoplasts	Cas9 RNP	PEG transfection	T7E1 (44% mutation rate), RFLP (46% mutation rate)
PEG[286]	Tobacco protoplasts	GFP, I-SceI meganuclease + YFP positive selection plasmid, Host-targeting TALEN	PEG transfection	Flow cytometry (2.7% YFP expression) and 454 pyrosequencing (1.4% mutation rate)
PEG[287]	Petunia protoplasts	Cas9 RNP	PEG transfection	T7E1 (2-20% mutation rate), amplicon deep sequencing (11.5 ± 2% mutation rate)
PEG[288]	Grapevine and apple protoplasts	Cas9 RNP	PEG transfection	Amplicon deep sequencing (2-7% mutation rate)
PEG[289]	Bread wheat protoplasts	Cas9 RNP	PEG transfection	RFLP, amplicon deep sequencing (2-4% mutated T0 progeny)
PEG[290]	Potato protoplasts	Cas9 RNP	PEG transfection	Sanger sequencing (1-20% mutated T0 progeny)
PEG[291]	Wheat protoplasts	Base editor fusion protein A3A-PBE-ΔUGI	PEG transfection	Amplicon deep sequencing (1.8% C-to-T conversion)
Lipofectamine 3000[142]	Tobacco BY2 protoplasts	Cas9 RNP	Liposome transfection	Widefield FL microscopy

123

Given our described requirements for NP-mediated protein delivery, the list of eligible candidates appears short. Where delivery of efficacious quantities of proteins and delivery moieties requires a particle of considerable size to maximize loading, the SEL of the cell wall pushes design toward the smaller end of nanoscale. In this regard, we hypothesize that high-aspect ratio nanomaterials, where one dimension is much longer than other dimensions, may provide the necessary surface area for protein conjugation and chemical modification and be plausibly wall-penetrant if one dimension remains considerably smaller than the cell wall SEL. The premier 1-D nanomaterial, SWNTs, possesses a length on the order of 100-1000 nm and a non-functionalized diameter of only 1-nm. SWNTs have previously been used for nucleic acid delivery in walled plant cells[88,164] and protein delivery in mammalian systems. Results from Zubkovs and coworkers demonstrate several protein-conjugation techniques yielding protein-SWNT conjugates that limit perturbations to the cargo's structure. In this case, ssDNA is used to both solubilize the SWNT and anchor proteins to the surface using alkyne click chemistry[292]. However, SWNTs are not the only viable 1-D nanomaterial; protein delivery to mammalian cells has been demonstrated using inorganic nanowires of similar dimensions to SWNT[293]. Given the diversity of materials that can be fashioned with high-aspect ratios, the number of viable protein nanocarriers becomes much broader[294]. With a diversity of untested carriers, further complicating an NP approach is the development of chemistries to conjugate proteins and other functional motifs to the NP vehicle. In the next section we elaborate on considerations for conjugation strategies.

4.4.1 *Sticking it to the Particle*

Size variability is significant across proteins of interest for delivery, with the most common fluorescent reporter, GFP, being much smaller than the most common gene editing nuclease, spCas9 RNP (**Figure 4-1**). As proteins alone already approach the cell wall SEL, the addition of a carrier usually increases the complex size beyond the SEL. Furthermore, the role of size on intracellular delivery efficiency remains unclear. For example, Martin-Ortigosa *et al* show that BSA undergoes release from mesoporous silica nanoparticle (MSN) carriers 3.5x more effectively than GFP despite being twice as large[154]. This points to the importance of understanding and modulating both protein-nanocarrier interactions and protein-nanocarrier-host interactions.

Association of a protein with its carrier can be accomplished through covalent bioconjugation or nonspecific adsorption. While nonspecific loading has been the dominant method employed in the literature for carrier-mediated protein delivery to plants, the advantages that site-specific bioconjugation have brought to mammalian biology for decades[295] allude to their potential implementation in plants. Bioconjugation chemistry describes a class of fast, high-specificity reactions that site-specifically link biomolecules and has been widely employed for covalent and non-covalent delivery strategies. Bioconjugates can be engineered with responsive chemical mechanisms for inducible release upon reaching the intracellular target. Protein bioconjugation chemistries have found promise for enhancing drug efficacy, delivery, and specificity in mammals[136,295–297], though adaptations of these chemistries for use in plants have not been widely explored.
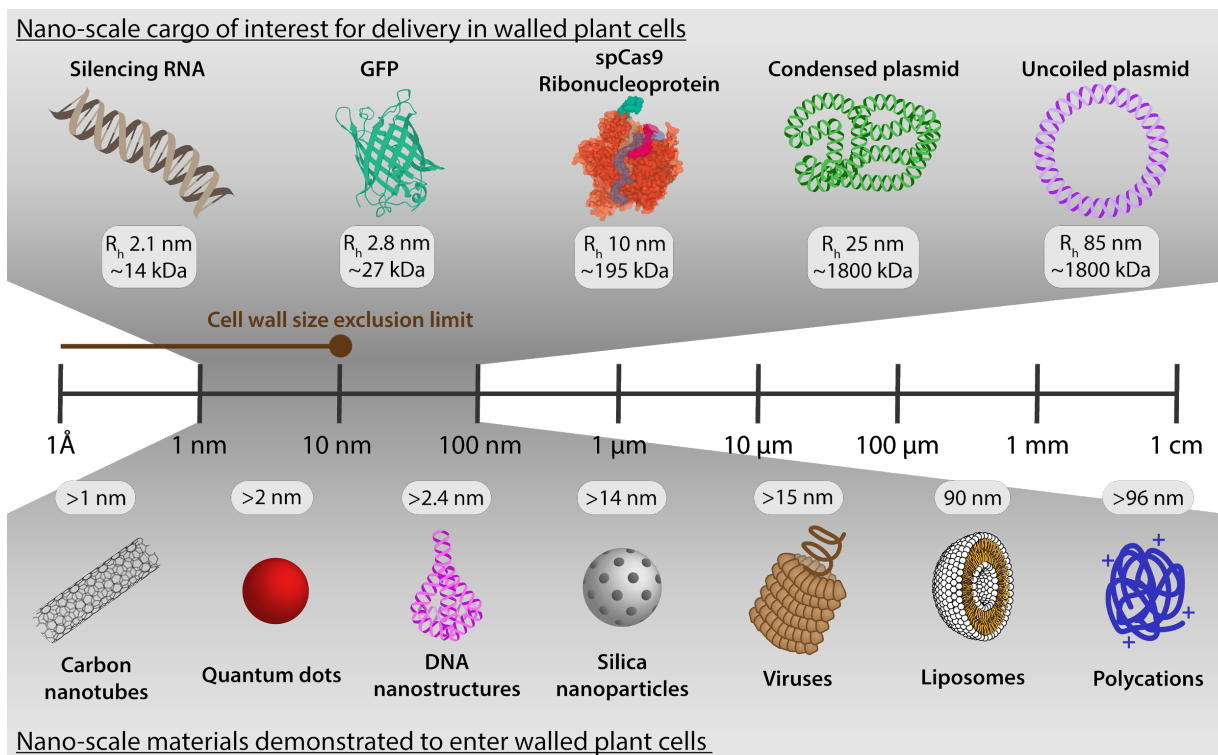
Figure 4-1. Schematic showing common cargoes and a representative but not exhaustive list of nanoscale materials for delivery to plant cells that have been demonstrated to enter walled plant cells.

As evidenced by the hydrodynamic radius of the represented biomolecules[298–301], cargoes vary widely in Stokes radius and molecular weight. The size exclusion limit of the plant cell wall lies around 10 nm, suggesting constructs below 10 nm are unlikely to diffuse through cell wall pores. Nevertheless, several nanoscale materials with smallest dimensions both below and above the SEL have been demonstrated to enter walled plant cells[88,121,140,164,166,264,267,302].

In contrast to site-specific conjugation, nonspecific loading strategies rely singularly on nonspecific association such as electrostatics (e.g. PEI-DNA) or local concentration gradients (e.g. diffusion into an MSN pore). A notable caveat is that electrostatic grafting strategies onto nanoparticles employed for nucleic acid delivery are not generalizable to proteins. Because strongly cationic environments can cause protein inactivation, targeted conjugation chemistries, encapsulation or gentler adsorptive methods, as in the case of MSNs, are preferred for protein delivery. That said, efforts have been made to temper the high charge of cationic polymers by modification with hydrophobic moieties or through fluorination[303]. Finally, the reliance on weaker interactions for nonspecific loading may not by default a disadvantage, however, as a weaker interaction with the carrier could translate to effective release of protein cargo into the cytosol.

4.4.2 Alternatives to NP Carriers

Designing nanocarrier-based protein delivery systems for plants presents a major engineering challenge that may require alternatives to those presented above. Direct covalent or non-covalent modification of proteins with cell penetrating materials could be a viable alternative. In 2020, Tai *et al* utilized a cholesterol-Coomassie dye conjugate to enable endocytosis-independent, cytosolic

136

delivery of proteins in mammalian tissue culture[304]. The result is a generalizable strategy that noncovalently links a small molecular carrier to the protein, generating small, penetrating particles. Other efforts have included covalent modification of the protein itself with larger molecules such as CPPs[141,261,275] or endosomolytic polymers[305]. Others have proposed comprehensive protein engineering strategies such as supercharging or protein resurfacing[306]. However, these approaches are neither trivial nor generalizable. As an additional question for alternative delivery systems, it has not been shown in literature whether small molecule endo-osmolytic agents such as chloroquine[228] are effective in plant cells.

Finally, several strategies exist based on enzymatic or mechanical disruption to forcibly overcome the cell wall-such is the logos for protoplast transfection and biolistic bombardment. Protoplast transfection of functional proteins has been widely demonstrated (), but the limitations of callus regeneration often overshadow the benefits of protein delivery. To date, the biolistic method has been adapted for delivery of protein across the plant cell wall and cell membrane () via dehydration of the protein onto 0.6-µm gold particles via lyophilization or air-drying[263]. While similar in practice to biolistic DNA loading, which is widely employed, the disadvantage of loading proteins by dehydration is the potential for protein functional deactivation via irreversible disruption of secondary structure - thus the amount of active loaded protein may be low. Additionally, the bombardment method itself contains inherent drawbacks, namely tissue damage. In comparison, studies of NPs in plants highlight growth benefits, enhanced immunity but also phytotoxicity and reduced biomass[307,308]. The benefit or harm of NPs in plants remains inconclusive but promising, particularly for short-term use or in applications requiring selection across generations which would reduce or eliminate NP prevalence in the final product.

4.5   Conclusions

The ability to deliver proteins into walled plant cells could enable diverse plant biotechnology applications, particularly for CRISPR Cas-9-based genome editing applications. In plants, most Cas-9 strategies rely on delivery of plasmids coding for Cas-9 and gRNA using *Agrobacterium tumefaciens* or gene gun bombardment[309]. Plasmid delivery techniques are hampered by both species-specificity and by their potential to incorporate the delivered gene into the host plant genome which may generate off-target effects or trigger regulatory oversight[183]. Conversely, delivery of CRISPR Cas-9 proteins is DNA-free and thus could enable generation of edited plants without risking transgene integration. Recent strides in DNA-free editing have been made by adapting already existing techniques for protein delivery; however, these approaches often require manual selection of hundreds of *in vitro* transformants and may not be applicable to species with less robust tissue culture protocols or where regeneration remains elusive. A promising direction is in the characterization of morphogenic transcription factors towards generating edited explants *in situ*, simplifying regeneration[310]. Such technological advancements, when co-delivered with editing nucleases, exemplifies a system with untapped potential for nanoparticle-mediated protein delivery applications.

To advance nanoparticle-mediated protein delivery to plants in such a way that moves towards generalizable platforms for the many applications in agriculture, biotechnology, and academic research, we must engineer complex systems that address a multitude of factors including protein conjugation and release, *in planta* translocation, endosomal escape, subcellular localization, and

transformant selection. We emphasize the need for more proof-of-concept studies in reduced biological representations of a whole plant - such as walled suspension cells, leaves, or regenerable tissue in model species such as *Arabidopsis* or *Nicotiana benthamiana* - that provide a simple system in which to test novel delivery strategies or reproduce results across numerous labs. Furthermore, the development of more robust microscopic methods (apart from diffraction-limited fluorescence imaging) for reproducibly assaying nanoparticle internalization and localization within plant cells is an area with great unmet need. We also point out that testing pre-existing or novel conjugation chemistries for a wide array of proteins should be pursued in parallel to testing in plant cells, especially as this work would have applications in other fields besides plant science. We hypothesize that a focus on nanomaterial conjugation of smaller proteins with less functional reliance on secondary structure (such as intrinsically disordered peptides) could improve chances of success upon translation to *in planta* studies, due to the smaller net carrier size and reduced need to maintain a precise protein fold during conjugation and delivery.

5 Understanding Biocorona Formation on Nanoparticles for Functional Design

5.1 Chapter Abstract

Climate change and population growth are straining agricultural output. To counter these changes and meet the growing demand for food and energy, monitoring and engineering of crops is becoming increasingly necessary. Nanoparticle-based sensors have emerged in recent years as new tools to advance agricultural practices. As these nanoparticle-based sensors enter and travel through the complex biofluids within plants, biomolecules including proteins, metabolites, lipids, and carbohydrates adsorb onto the nanoparticle surfaces, forming a coating known as the "biocorona". Understanding these nanoparticle-biomolecule interactions that govern nanosensor function in plants will be essential to successfully develop and translate nanoparticle-based sensors into broader agricultural practice.[‡‡]

5.2 Introduction

As changing climates and population growth increasingly place pressures on agricultural production, the monitoring and engineering of crops becomes essential to meet the rising demand for food and energy[311–313]. To maximize the efficient use of limited resources, crops can be remotely monitored using sensors to adjust plant management strategies rapidly, minimizing losses and maximizing yields[312]. In particular, innovations in nanotechnology have advanced the collection of agricultural metrics such as nutrient levels, pathogen infection, and pesticide accumulation in plants[314]. Nanoparticle-based sensors have garnered much interest in agricultural applications in recent years, as reviewed elsewhere[315,315,316]. The unique physical and chemical properties of nanoparticles have been leveraged to design sensing platforms that are highly portable, rapid, sensitive, and amenable to high-throughput measurements[317].

The application of nanosensors, and more broadly, of nanotechnologies in plants presents distinct obstacles that must be taken into consideration during the design phase, as the unique plant environment could drastically alter the intended nanoparticle function. Biological barriers like the waxy leaf cuticle challenge nanoparticle uptake[318], while the varying biochemical compositions in plant tissues alter nanoparticle functionality[319]. When nanoparticles enter and traverse complex biological milieus in plants, biomolecules including proteins, metabolites, lipids, and carbohydrates adsorb onto the nanoparticle surfaces, forming a coating known as the "biocorona"[319–321]. As such, one major bottleneck for the seamless translation of nanosensors from *in vitro* validation to *in planta* use is in the spontaneous and as-of-yet unpredictable adsorption of biomolecules on nanosensor surfaces that attenuates their intended function (**Figure 5-1**). For the practical translation of nanotechnologies to plants, it is imperative that we understand the interactions between the nanoparticles and the biomolecules they encounter during in-plant transport.
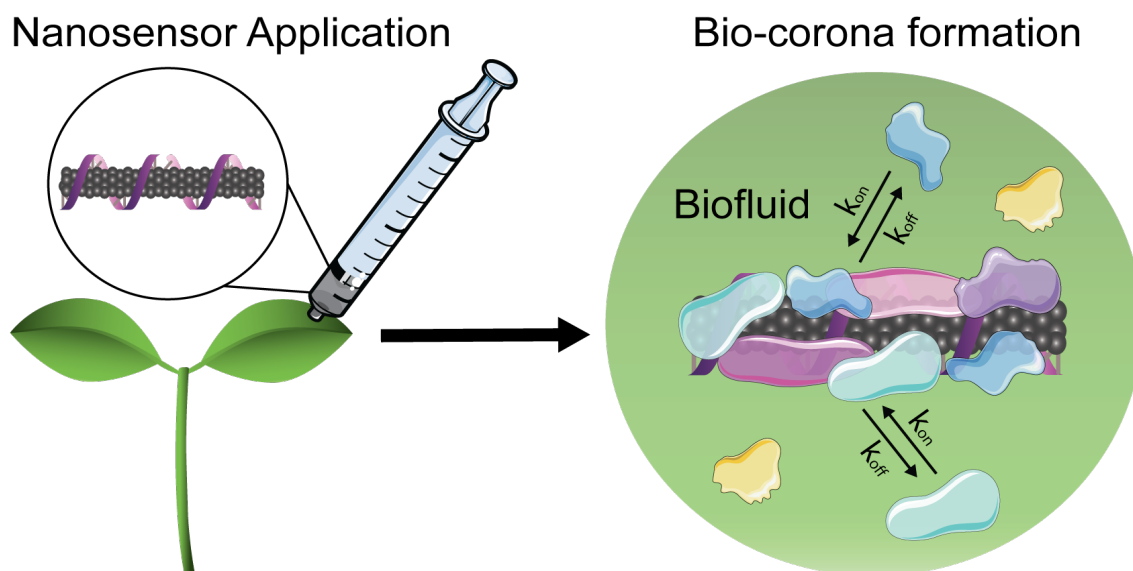
Figure 5-1. Schematic of biocorona formation on nanosensors.
Biomolecules adsorb on the surface of nanosensors as they travel through complex plant biofluids, altering the intended nanosensor function and creating a bottleneck for the translation of nanosensors from the laboratory to applications in intact plants.

The future of health and developmental monitoring in plants depends on the successful translation of nanosensors from the benchtop to practical applications in the field. As these sensors are implemented in plants for crop management, sensors will encounter challenges in less controlled environments: nanosensor biofouling is known to attenuate or abate nanosensor function, and nanosensor transport and bioaccumulation within the plant or within the environment remains unpredictable. As such, nanoparticle-biomolecule interactions in plants and agricultural settings will dictate our ability to preserve nanoparticle function *in planta* and will need to be evaluated for environmentally conscious translation of these nanotechnologies from the lab to the field. To these ends, understanding the phenomenon of biocorona formation on nanosensors will inform designs with improved sensing capabilities and biostabilities, increasing the likelihood of success when these technologies are translated into broader applications. The process of protein corona formation on nanoparticle surfaces has been described extensively for non-plant systems elsewhere[322–324], however, it remains to be elucidated for plant and agricultural systems.

5.3 Nanoparticle-Based Sensors for Agricultural Use

Sensing systems for precision agriculture have been developed to monitor water content, soil conditions, and crop health. These sensors monitor soil moisture, temperature, and nutrient levels[325–328], providing key information for crop management. Sensors for pesticides, herbicides, and insecticides in the soil or water have also been developed[329–332], and are useful for improving yields and supporting food and water safety[333]. Directly sensing plant health signals through wearable electronic devices and embedded sensors have more recently emerged as an exciting strategy to monitor crops[316,334,335]. These sensing systems vary widely in sensing mode, from electrochemical sensors that translate chemical reactions into measured voltages, to optical sensors that measure changes in fluorescence emission for analyte quantification.

Table 5-1. Nanoparticle-based sensing systems for agricultural engineering.

System	Target	Signal Transduction	Material	Limit of Detection
Rice[331, 332]	Carbosulfan (pesticide)	Electrochemical - voltammetry	Zinc oxide (ZnO) nanocuboids modified platinum (Pt) electrode	0.24 nM
Soil[329,332]	Atrazine (herbicide)	Electrochemical - voltammetry	Titanium dioxide (TiO_2) nanotubes	0.1 ppt
On plant[335]	Light and humidity	Wearable optical sensor	$ZnIn_2S_4$ (ZIS) nanosheets	~ 4 ms (light response)
Water[330,332]	Malathion (insecticide)	Optical - Surface-Enhanced Raman Spectroscopy (SERS)	Aptamer–polymeric microsphere–gold nanoparticles (AuNPs)	3.3 μg mL^{-1}
Water[336]	Nitrite	Optical - fluorescence	Silver nanoclusters	100 nM
In vitro[337]	DNA sequence of *Ganoderma boninense* gene (oil palm pathogen)	Optical - fluorescence	Quantum dots (QDs)	3.55 nM
In plant[338]	Glucose	Optical - fluorescence	Thioglycolic acid-capped QDs and boronic acid-conjugated QDs	500 μM
In plant[260]	H_2O_2	Optical - fluorescence	Single-walled carbon nanotubes (SWNTs)	10 μM
In plant[339]	NO	Optical - fluorescence	SWNTs	100 μM

The majority of these plant and crop sensors enable precise measurements but rely on tissue-destructive techniques that involve field- or lab-based protocols, limiting these measurements to distinct timepoints. We highlight a specific class of engineered nanoparticle-based sensors (< 100 nm in their smallest dimension), termed "nanosensors," that can enable continuous *in planta* environmental sensing and plant health monitoring in intact plants. As autosamplers and bio-concentrators of their surrounding environment[340], plants provide an exciting platform for sensing.

Combining nanotechnology with the natural features of plants facilitates rapid in-field detection that circumvents expensive and time-intensive laboratory techniques. Continuous gas and fluid exchange between plants and their environment enables this mode of sensing to be used in a variety of different contexts, be it probing the soil for specific analytes or monitoring chemical signals for plant health reports in agricultural settings. Thus far, nanosensors have been used for detecting ground soil contaminants and quantifying plant defense-related biomarkers and signaling molecules (**Figure 5-2**)[334,338,339]. While genetically encoded plant sensors may confer similar advantages as nanosensors, they are limited by species-specific genetic transformations that require large amounts of time and effort[312]. In contrast, engineered nanosensors are species independent and thus more easily translated across plant systems. Although plants have been genetically engineered as biochemical detectors in the past, the addition of nanoparticle-based sensors to utilize plants as detectors is just emerging as a field of study[246,341]. As such, the use of nanosensors in plants is promising for agricultural sustainability, with several recent examples of nanoparticle-based sensors for plant and crop monitoring outlined in **Table 5-1** and reviewed in more detail elsewhere[314,328,332,342,343].
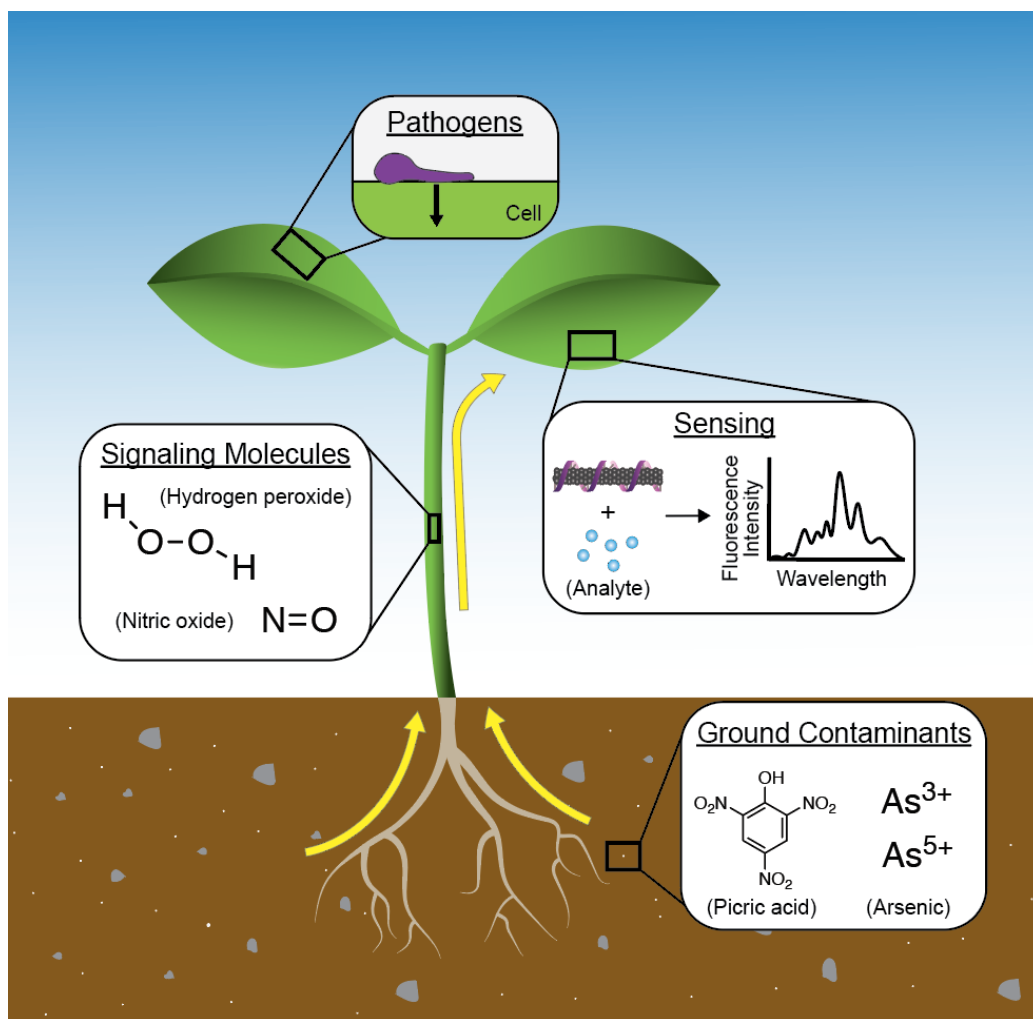
Figure 5-2. Overview of nanosensor usage in agriculture.

Nanosensors are used in plants for detecting soil contamination, signaling molecules, and pathogens. Early and rapid communication of plant stress through sensing innovations has the potential to improve agricultural management, while further development of plant biomarker sensors can be used to understand the complex signaling pathways within plants.

5.3.1 *Environmental Nanosensors for Soil Sensing and Pathogen Detection*

The monitoring of groundwater, soil contaminants, and early detection of plant pathogens are crucial activities in recognizing and addressing potential threats to human and plant health. Capitalizing on the innate properties of plants as microfluidic devices that sample their immediate surroundings, plant-based nanosensors have been designed for real-time biochemical sensing of soil contaminants, including explosive nitroaromatics and arsenic[246,340]. In the former example, peptide-coated single-walled carbon nanotubes (SWNTs) were embedded in spinach leaves to enable near-infrared (and thus plant-tissue transparent) optical detection of nitroaromatic compounds[246]. The nitroaromatic compounds are taken up by the roots and transported through plant vasculature to the leaves where the SWNT sensors reside. Similarly, leaf-embedded SWNT-based sensors have been used to detect arsenic in the soil through root uptake in *Spinacia oleracea* (spinach), *Oryza sativa* (rice), and *Pteris cretica* (ferns)[340]. Of note, these SWNT-based plant nanosensors provide both a rapid response in the presence of target analytes and a stable performance over a period of months[260,312].

In addition to sampling toxic ground contaminants, nanosensors can prevent disease spread among crops by non-destructively detecting the presence of plant pathogens prior to symptom onset. Current disease diagnostics for plants are morphology-based analyses, which occur after the disease has progressed, or sample-destructive and pathogen-specific assays such as enzyme-linked immunosorbent assay (ELISA) and polymerase chain reaction (PCR). Although robotic imaging platforms are improving detection sensitivity, such technologies often fail to detect disease before symptom onset[344]. Conversely, nanoparticle-based sensors for pathogen detection have been demonstrated to function successfully *in planta*[315,345], though such nanoparticle-based sensors are more widely used *ex vivo* in rapid detection kits. A common class of nanoparticle-based sensing technologies are lateral flow immunoassays, whereby pathogens are detected with an antibody, aptamer, or DNA probe conjugated to a gold, magnetic, or fluorescent nanoparticle[346]. These assays have been used to detect a variety of plant viruses such as *Citrus tristeza virus* from citrus leaves and fruits, *Potato virus x,* and the bacterial pathogen of Stewart's wilt in sweet corn[346–349]. These *ex vivo* sensing strategies enable convenient plant pathogen detection, yet remain limited to sampling at distinct timepoints. Like the *ex vivo* assay, a combination of antibodies, aptamers, or DNA probes and nanoparticles could be used to detect the pathogen in plant tissue. A major barrier towards translating these nanosensors *in planta* applications is in preserving nanosensor function in the biologically complex milieu of living plants, which would allow continuous and rapid detection during the early stages of pathogenesis. Moving forward, advancing early-stage disease and pathogen detection necessitates continuous and real-time sensing capabilities with the use of *in planta* compatible nanosensors.

5.3.2 Biomarker Nanosensors for Monitoring Plant Health

Sensing biomarkers that are indicative of plant stress and energy production provide essential insight into plant signaling and health[338,339]. Abiotic stresses such as droughts and heat as well as biotic stressors like plant pathogens elicit a defense response[350]. Unlike animal systems, plants have a passive immune system, and plant cells rely heavily on cell-to-cell signaling to communicate environmental threats through immunogenic signals that activate plant defenses[334,351–353]. Nanosensors can be used to translate these plant chemical stress signals to electronic signals for real-time sensing, which would serve to report crop health and thus, diagnosis of plant environmental stressors with appropriate intervention[312,354]. Examples of such plant stress biomarkers include reactive oxygen species (ROS) and glucose. Fluorescent SWNT sensors have been developed to recognize ROS such as hydrogen peroxide (H_2O_2), a biomarker for plant defense produced in response to stress, and nitric oxide (NO), another key signaling molecule in plants[339]. Specifically, Wu et al. developed a H_2O_2 sensor based on SWNTs functionalized with a DNA aptamer that binds to hemin (HeAptDNA-SWNT). Mechanistically, this sensor takes advantage of hemin that undergoes a reaction with H_2O_2, producing hydroxyl radicals, resulting in SWNT fluorescence quenching. By measuring changes in SWNT fluorescence emission with a near-infrared camera, these H_2O_2 nanosensors enable continuous, real-time monitoring of plant health in response to UV-B light, high light, and pathogens, but not plant wounding in *Arabidopsis thaliana* which likely has H_2O_2 levels below the limit of detection (**Figure 5-3**)[260,339]. More recently, a different single-stranded DNA-functionalized SWNT H_2O_2 nanosensor was developed and can sense the plant response to wounding in several common plant species including *Lactuca sativa* (lettuce), *Eruca sativa* (arugula), and *Spinacia oleracea* (spinach)[334]. SWNT sensors have also been used for the detection of NO[339]. Similarly, a quantum dot-based nanosensor has been used to radiometrically detect glucose[338]. As indicators of environmental stressors, these nanosensors for analytes like glucose and ROS have the potential to improve crop management through rapid, continuous, and non-destructive sensing.
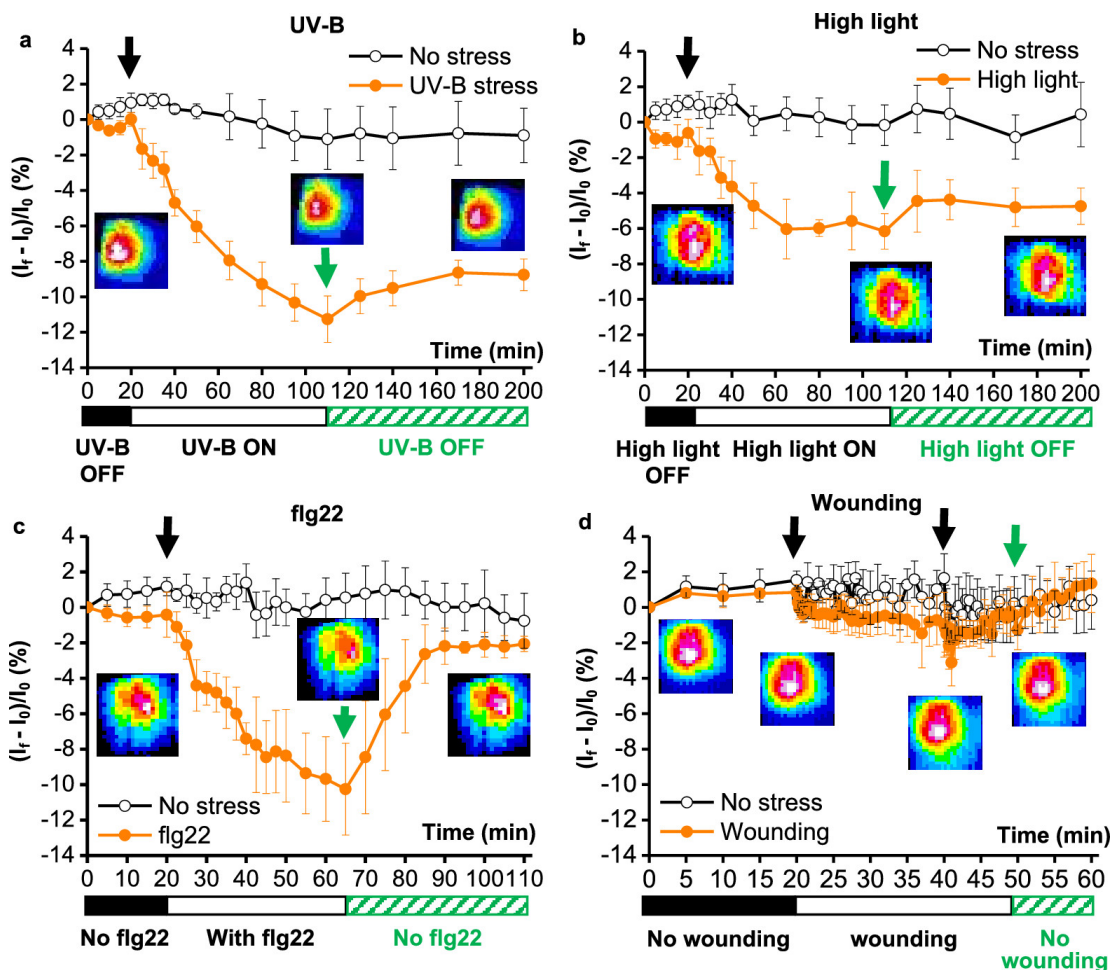
Figure 5-3. *In planta* **monitoring of plant health signaling molecules in response to common plant stresses via a SWNT H$_2$O$_2$ nanosensor.**
Near-infrared fluorescence intensity changes of the nanosensor embedded in leaves indicate signs of stress. The nanosensor's near-infrared fluorescence emission decreases in the presence of **a** UV-B light, **b** high light, and **c** a pathogen-associated peptide (flg22). **d** Mechanical leaf wounding did not result in a change in the nanosensor's near-infrared fluorescence emission, likely due to the relatively lower levels of H$_2$O$_2$ production. Reprinted from Wu, H.; Nißler, R.; Morris, V.; Herrmann, N.; Hu, P.; Jeon, S.-J.; Kruss, S.; Giraldo, J. P. Monitoring Plant Health with Near-Infrared Fluorescent H$_2$O$_2$ Nanosensors. *Nano Lett.* 2020, *20* (4), 2432–2442. Copyright (2020) American Chemical Society.

5.3.3 Understanding Biocorona Formation to Increase the Translational Value of Plant Nanosensors

Although nanosensors have the potential to revolutionize agriculture, the parameters governing nanosensor performance *in planta* have been understudied in plant systems. The successful translation of these nanosensor technologies requires a more thorough understanding of the interactions between the nanosensor and its local plant environment. Despite the prevalence of protein corona characterization in nanomedicine towards human health applications, biocorona

formation in plant systems has only received limited acknowledgment and research[171]. Plant-based nanosensors are developed and implemented without taking into account the inevitable changes in physicochemical properties as the nanosensor is progressed from *in vitro* development to *in vivo* use. We propose that more informed plant nanosensor designs can be developed and predictably translated into practical applications, guided by fundamental studies of plant nanoparticle biocoronas.

The field of nanomedicine has largely motivated the study of nanoparticle-protein interactions to improve nanoparticle function in applications including drug delivery, disease diagnostics, treatment, and prevention[355–359]. Nanoparticle-based sensors have been used to detect metal ions, small molecules, and proteins including biomarkers for early cancer and kidney disease[360–362]. As nanotechnologies become more widely used in biological settings, it is increasingly important to understand and predict nanoparticle function and fate *in vivo*; despite the successes of some, many nanomaterials produce unsatisfactory results or off-target effects during clinical trials[363–367]. This translation of nanomedicines from laboratory development to clinical practice is limited by our lack of control of interactions between the nanoparticle and its surrounding bio-environment[324,366,368–370]. Although the intrinsic physicochemical characteristics of the nanoparticle determine *in vitro* functionality, the environment around the nanoparticle in the applied setting, such as blood plasma for intravenous delivery, will play a dominant role in determining the ultimate nanoparticle fate and function.

Likewise, to develop a fundamental understanding of biocorona formation on nanoparticles in plants, the governing parameters must be considered. Biocorona formation is determined by the interplay of intrinsic properties of nanoparticles, including electrostatic charge, hydrophobicity, and surface structure, and characteristics of the environment surrounding the nanoparticle, such as biomolecule composition and solution conditions[371]. As nanoparticles are introduced to a bio-environment, an inner layer of more tightly bound, higher affinity biomolecules forms, referred to as the "hard corona," and a rapidly exchanging outer layer of biomolecules, the "soft corona," more loosely associates[372–374]. This coating of biomolecules alters the lab-engineered properties of the nanoparticle since in many cases it is this biocorona that ultimately interacts with the biological environment[320,375,376]. Accordingly, these biomolecular interactions can lead to loss of nanoparticle targeting ability[368], impact nanoparticle uptake *in vivo* by influencing membrane adhesion and internalization pathways[369,376,377], and even eliminate nanoparticle efficacy[371,378]. More specifically, nanoparticle-protein interactions often lead to protein denaturation on the nanoparticle surface and colloidal aggregation of the complexes[371,379,380]. By preemptively considering this phenomenon, we can reduce biofouling and preserve nanoparticle functionality *in planta*.

5.4 Current Studies Probing Biocorona Formation on Nanoparticles in Plants

Proteomic and metabolomic studies detailing biocorona composition are necessary to understand the biological identity that nanoparticles acquire in plants. In turn, knowledge of biocorona constituents will inform improved sensor design strategies to reduce biofouling and even tune biocorona formation to enhance nanosensor localization and function. These studies are crucial, but, in contrast to animal systems, the literature on biocorona formation and the corresponding impact on nanoparticle behavior in plant systems is limited.

5.4.1 Proteomic and Metabolomic Analyses of Biocorona Formation in Plant Biofluids

Based on available literature, plant-based biocorona formation has been investigated with three types of nanoparticles: titanium dioxide nanoparticles (TiO_2), magnetic nanoparticles, and gold nanoparticles. These studies have focused on individual assessments of either the protein or metabolite corona in plant biofluids.

In vitro combinations of nanoparticles and specific plant proteins demonstrate the significance of protein identity in resulting biocorona formation, as anticipated from analogous studies in animal systems[372]. Bing et al. studied the effects of incubating common plant proteins including glutenin, gliadin, zein, and soy protein with TiO_2 nanoparticles and found that the corona formed in the presence of each protein produced varied effects on TiO_2 surface potential and morphology, with 4-60 nm thickness of the adsorbed protein layers[381]. Separately, a recent study probed the evolution of the protein corona on 16 nm gold nanoparticles in crude protein extracts and nuclear fractions of *Brassica juncea* and observed differences in protein corona components between the two biofluids, with more than a quarter of the hard corona proteins in the crude protein fraction involved in energy generation pathways[382]. Given that gold nanoparticles have been shown to induce a change in *B. juncea* overall growth and seed yield[44], Prakash and Deswal suggest that the protein corona could be implicated in system-level effects observed from nanomaterial-plant interactions.

Although corona formation has system-wide implications, the phenomenon of biocorona formation can instead be harnessed for molecularly specific applications. The Smalle group has pioneered an approach coined "nano-harvesting" in which nanoparticles preferentially bind and extract catechol-containing flavonoids from plants. Within this body of work, Kurepa et al. conducted multiple studies centered around the metabolite corona formed on TiO_2 nanoparticles in *Arabidopsis thaliana*, *Ocimum sanctum*, and *Rubia tinctorum*[383–385]. TiO_2 nanoparticles were incubated with mature leaves, and after subsequent metabolomic analysis, the nanoparticle surface was found to be enriched in lipids and in particular flavonoids, which are polyphenolic small molecules involved in secondary metabolism[384]. These results also revealed that lipids and flavonoids compete for nanoparticle surface sites during biocorona formation. In a separate study, Qing and coworkers used human serum albumin-functionalized magnetic nanoparticles to extract bioactive molecules from *Dioscorea panthaica* via preferential corona binding, greatly expediting the isolation of four saponin compounds[386]. In combination with Kurepa's work, these findings show that biocorona formation can be leveraged to achieve desirable molecule enrichment. The tuning of nanoparticle surface properties to control biocorona formation while retaining targeting and delivery functions has been achieved in nanomedicine[387,388], and provides a roadmap in harnessing knowledge of the biocorona to design nanosensors that maintain their utility *in planta*.

5.4.2 Challenges Associated with Nanoparticle-Based Proteomic and Metabolomic Studies in Plants

Technological advances have led to more rigorous characterization of the biocorona formed on nanoparticles, yet several challenges persist before the process of studying plant-based protein and metabolite coronae is rapid, comprehensive, and efficient. These obstacles are briefly summarized here and detailed more comprehensively in other reviews[389–392].

The main challenge in advancing biocorona studies in plants is the lack of sufficient proteomic and metabolomic information on the plants alone, in contrast to the extensive -omics characterization of human and many model animal systems. Obtaining this data for plants requires a meticulously designed experimental process and in-depth data analytics, which are both time and energy intensive. Additional experimental considerations apply in data collection because plant physiology and biochemistry vary across different strata: (i) spatial resolution, accounting for plant organs, subcellular and extracellular spaces, and (ii) temporal distribution, spanning growth stages, photoperiodism and seasonal variations[389]. These distinctive protein abundance patterns in plant tissues[393] and biochemical changes over time that represent challenges to proteomic and metabolomics studies will further influence biocorona formation. Thus, it is essential to address the gap in proteomic and metabolomic plant literature to accurately characterize these nanoparticle-biomolecule interactions.

The plant metabolome poses significant difficulties in compound identification and quantification: between 100,000 - 1,000,000 metabolites are estimated to belong to the plant kingdom[394], while the number of detected and quantified human metabolites is only 18,609[395]. The metabolomic compositional complexity also differs vastly across plant species[389], and the dynamic range of abundances (up to twelve orders of magnitude) and identity of sampled metabolites are heavily dependent on biotic and abiotic factors during plant growth[392,396]. Proteomic analysis encounters similar challenges, requiring careful and unbiased sample preparation[397]. Protein identification and quantification must also consider the high dynamic range and harness genomes, which for plants like barley (5000 Mbp genome) are larger than the human genome ($\sim$ 3300 Mbp)[398], and expressed sequence tag (EST) data[399,400], presenting a challenge in itself since there is no central curated database[401].

Advances in proteomic and metabolomic data acquisition and analysis remain key to furthering the study of the biocorona in plants (**Figure 5-4**). Such advances will subsequently enable correlation of proteins and metabolites in the nanoparticle biocorona with biological effects of nanoparticles on plants. The prospect of these advances motivates the synthesis of genomics, proteomics, and metabolomics information to uncover biochemical pathways. Excitingly, the rise of integrative approaches to -omics[402], decreasing cost of high-throughput sequencing and mass spectrometry, as well as developments in bioinformatics promise to accelerate the development of plant -omics[403–405]. Through these innovations, knowledge of plant -omics is quickly expanding[393], enabling biocorona characterization on nanoparticles in plant tissues with distinct biochemical compositions. As these technologies, tools, and databases become more widely developed and utilized, compositional knowledge of the biocorona can be employed to better inform plant-based nanosensor design strategies.
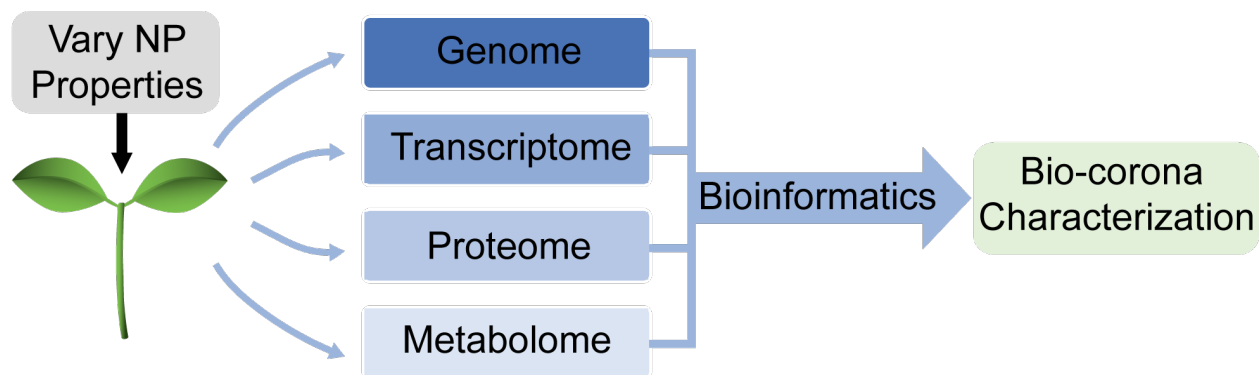
Figure 5-4. Overview of how -omics techniques can be used in biocorona characterization. Innovations in -omics research will enable improved nanoparticle (NP)-based sensor design through biocorona characterization with the high-throughput combination of genomics, transcriptomics, proteomics, and metabolomics with bioinformatics. Previous biocorona studies have broadly shown preferential enrichment of biomolecules but fail to consider the multiple unique bio-environments that a nanosensor encounters within the plant. We must carefully consider the physiological and biochemical compositions in which nanoparticles travel through and/or localize at to understand the full picture of nanoparticle-biomolecule interactions. For instance, to study the efficiency of a nanosensor that traverses through plant vasculature would require nanoparticle incubation within phloem or xylem sap. Conversely, investigating nanosensor biofouling for a nanosensor embedded within a leaf might necessitate considering the different localization end points such as the cytosol or cell wall. In future research, contextualizing studies of biocorona formation may provide more realistic insight into nanoparticle fate.

5.5 Physiological Characteristics of Plants Relevant to Biocorona Formation

The broad concepts and underlying physical phenomena driving biocorona formation can be readily translated to nanoparticles in plant bio-environments. Yet, we emphasize that additional factors must be considered in terms of the distinct biological characteristics and obstacles that nanoparticles encounter while moving through plants in comparison to those more widely studied in animal systems. Such plant-specific aspects include: (i) the modes of nanoparticle transport, (ii) unique biological barriers, such as the presence of a multi-layered cellulosic cell wall, and (iii) markedly different biofluid conditions and constituents.

5.5.1 Transport Phenomena of Nanoparticles in Plants

Modes of nanoparticle transport through plants predominantly consist of nanoparticle uptake, translocation, internalization, and accumulation, as reviewed elsewhere[184,318,406,407]. In addition to more traditionally considered nanoparticle characteristics like size and charge, biocorona formation on nanoparticles is expected to influence and be influenced by each of these modes of movement. Yet, the effect of nanoparticle corona formation has not been studied in relation to nanoparticle transport. As such, this molecular phenomenon of corona formation will propagate effects through the macro- and micro-scales of nanosensor outcomes in plant bio-environments. Macro-scale transport through plant vasculature occurs can be classified into the movement of water and ions via the xylem with pore diameters ranging from 40-340 nm and the movement of photosynthetic products via the phloem with pore diameters ranging from 200-1500 nm[318].

Conversely, micro-scale transport through the plant cell wall and membrane is reserved for smaller nanosensors developed for intracellular measurements that must be below the size exclusion limit of approximately 5-20 nm[408].

Nanoparticle transport through plant vasculature begins with uptake, as governed by the method of delivery, generally including foliar application (onto leaves), root application, or direct injection into other plant tissues. While the latter method is considered the most efficient for nanoparticle delivery[318], foliar and root application are ideal for certain nanosensing applications, whereby numerous studies have demonstrated that leaves are the main sinks of airborne contaminants and roots serve to uptake organic compounds in the soil[246]. For example, the nitroaromatic, arsenic, and hydrogen peroxide nanosensors, as discussed in earlier sections, involve embedding nanosensors directly in the spongy leaf mesophyll[246,334,340]. In this case, nanoparticle transport needs end upon uptake, as the analytes localize to the leaf-residing nanosensors. However, even this seemingly straightforward journey requires interaction with the leaf cuticle, stomata, and parenchyma of leaf lamina, all of which may result in dynamic biocorona formation that impacts nanosensor function.

Beyond direct foliar embedding, nanosensors requiring longer distance transport will translocate through the plant vascular system. Typically, nanosensors are directly embedded in the target tissue and do not translocate through the vasculature, but as these technologies are scaled from the laboratory to the field, feeding nanoparticles directly to crops is emerging as a delivery method[8]. Considering how nanoparticle transport through vascular tissue will impact biocorona formation is necessary for developing these technologies. Colloidal interactions of nanoparticles with vascular walls are expected to play a role in ease of translocation. It has been demonstrated with classic colloids modeling using a DLVO framework[318], with experimental validation[409,410], that approximately neutral (+5 mV) and positively charged (+35 mV) nanoparticles that lack steric stabilization will resist transport by depositing on negatively charged vascular walls. In contrast, negatively charged (-35 mV) nanoparticles can more freely translocate through plant vessels. As the adsorption of biomolecules onto nanoparticles from the surrounding plant medium will modulate nanoparticle size, effective surface charge, steric character, and other nanoparticle surface properties, biocorona formation becomes imperative to understand in optimizing efficient nanoparticle transport phenomena in plants.

5.5.2 *Biological Barriers that Nanoparticles Encounter in Plants*

Distinct biological barriers obstruct nanoparticle transport into and through plants. Additionally, an adsorbed biocorona can either hinder nanoparticle passage or be influenced by the different biological conditions that the nanoparticles are exposed to during passage, as studied in animal systems[411]. Nanoparticles encounter barriers in plants during (i) initial uptake through roots and leaves and (ii) eventual entry into the plant cell, across the cell wall, cell membrane, and potentially organelle membranes (**Figure 5-5**). Even if nanoparticles are expected to pass through these structures based on characterization of the pristine nanoparticle hydrodynamic size, unintended biocorona formation and nanoparticle aggregation may prevent nanoparticle transport through such barriers. For context, the protein corona can add approximately 10-30 nm to the nanoparticle diameter in animal circulation environments[322], increasing the hydrodynamic size by 50% in the case of 60 nm diameter gold nanoparticles in blood serum[412].

150
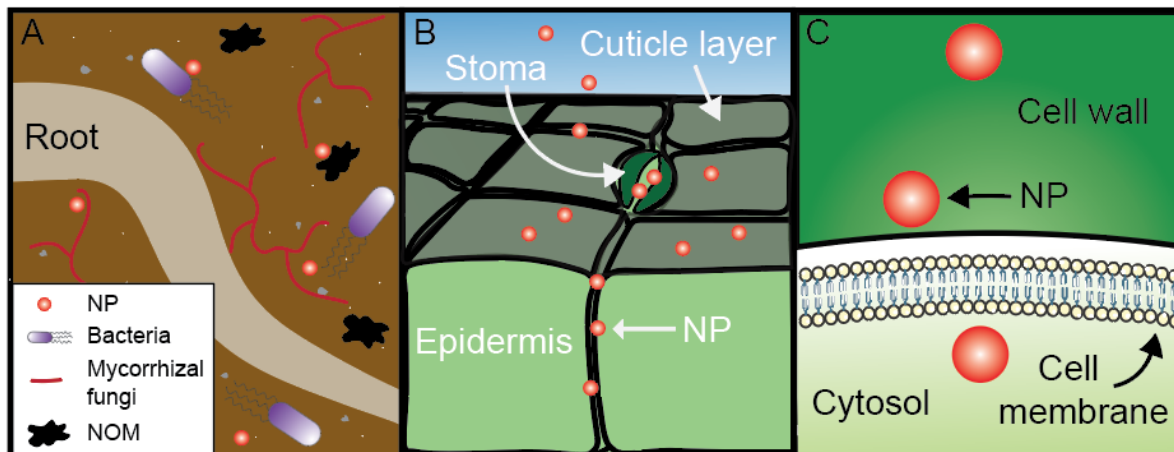
Figure 5-5. Nanoparticles encounter barriers and interact with a variety of biomolecules in plant bio-environments.
a During uptake through roots, nanoparticles interact with microorganisms, such as bacteria and mycorrhizal fungi, and natural organic matter (NOM). **b** In foliar application, NPs encounter the waxy cuticle coating leaf surfaces, and stomatal pores for gas exchange. **c** As NPs are internalized by the cell, they must cross the cell wall, with a size exclusion limit of 5-20 nm, and the cell membrane.

Nanoparticle uptake by roots is often reported to have low efficiencies, presumably occurring through passage cells of intact roots or at sites of new or damaged roots, bypassing the root cuticle[318,413]. An added complexity expected to influence root uptake of nanoparticles is that of the rhizosphere. The rhizosphere presents a rich environment of root exudates and mucilage originating from plants, in addition to the surrounding population of soil-based microorganisms including bacteria and mycorrhizal fungi. Nanoparticle interaction with these secreted substances and organisms of the rhizosphere is a key, yet underexplored, consideration anticipated to affect the biocorona formed on nanoparticles, and thus nanoparticle surface properties, stability, and bioavailability[407,413,414]. Accordingly, this rhizosphere-imparted corona on nanoparticles may at least partly explain the frequent observation of little-to-no nanoparticle uptake by root application[413]. As an illustrative example, flavonoid signaling in the rhizosphere has been well established, and nanoparticles have previously been shown to form a biocorona rich with flavonoid compounds[384]. These results suggest that the rhizosphere will impact nanoparticle corona composition and subsequent plant uptake, and that nanoparticles can interfere with native signaling functions necessary for healthy organism maintenance[384,413,415].

After the rhizosphere has been navigated and nanoparticles engage directly with the roots, multiple studies have found that positively charged nanoparticles are more readily adsorbed onto and in through root surfaces[267,407,409,416]. However, once inside the plant, the opposite trend occurs, whereby negatively charged nanoparticles promote higher translocation efficiency. This presents an opportunity to harness an engineered biocorona, promoting either shedding or adsorption of an outer layer to enable charge reversal upon internalization, such as the adsorption of negatively charged root mucilage upon root traversal. Similar scenarios exist in animal systems, such as with the mucosal and intestinal barriers that nanoparticles encounter during oral delivery, and designer corona approaches have displayed success in allowing a changing surface charge to mediate effective biological barrier passage[417].

For foliar application, nanoparticles first encounter the leaf cuticle and stomata openings. The cuticle is a waxy coating designed to protect the plant from water loss and nonselective molecular entry and consists of lipids and hydrocarbons that cover most of the leaf exterior. The cuticular pathway comprises modes of access for lipophilic molecules via diffusion and permeation or for polar and ionic solutes via pores, with pore diameters < 5 nm[413]. Although nanoparticle passage through the cuticle is typically not observed unless surfactants are employed[318,406], Avellan et al. found that PVP-coated gold nanoparticles at least partly enter leaves via disruption and/or diffusion through the leaf cuticle[171]. This cuticular uptake route or mere interaction with the surface could bestow nanoparticles with a hydrophobic surface coating that fundamentally modifies subsequent nanoparticle interactions with the internal biofluid. However, nanoparticle entry through leaves is generally found to occur through stomata, despite this uptake mechanism remaining unclear[308,318]. Stomata are the leaf pores for gas exchange, displaying pore openings of tens of microns (although the actual size exclusion limit is found to be a few orders of magnitude smaller[413]) that also facilitate nanoparticle entry and access to the phloem for transport through plants[318,406]. Akin to the rhizosphere for roots and similarly understudied in the context of nanoparticles, leaves support a phyllosphere of microorganisms that secrete extracellular polymeric substances that are expected to modulate nanoparticle surface properties through introduction of a biocorona[413].

The plant cell wall, otherwise absent in animal systems, presents a barrier that hinders nanoparticle movement and targeted localization. Even for nanosensors that do not explicitly require cell internalization, nanoparticles must cross cell walls simply to reach the vasculature for translocation to other plant organs. As such, the unique parameters facilitating cell wall traversal must be considered. Cell walls exhibit a small size exclusion limit of approximately 5-20 nm[408]. Additionally, stiffer nanoparticle constructs have exhibited higher plant cell internalization[166]. Biocorona formation is expected to play a role in prohibiting cell uptake due to the increase in hydrodynamic nanoparticle size and the reduction of inherent nanoparticle stiffness, with the adsorption of a soft biomolecular shell. More broadly, analogous cellular internalization studies in animal systems demonstrate that this process is both governed by the extracellular corona and further imparts an intracellular corona on nanoparticles, potentially disrupting nanotechnology function[418–420]. However, fundamental understanding of the interaction of nanoparticles with cell walls and how the corona would impact internalization is lacking due to the difficulties of both measuring and modeling such systems, where more focus has been placed on corona-coated nanoparticle interactions with cell membranes[421,422]. For cell membrane passage, the biocorona is expected to govern uptake mechanisms, as seen in mammalian systems[423]. Intracellular nanosensors may also traverse the lipid bilayers of organelle membranes, such as for carbon nanotube-based sensors used in chloroplasts[188,334]. Toward this latter point, a model termed Lipid Exchange Envelope Penetration (LEEP) has been developed to describe nanoparticle internalization into chloroplasts as a function of effective nanoparticle surface charge (zeta potential) and smallest dimension[241]. Interestingly, this study reveals that the magnitude, not the sign, of the zeta potential governs spontaneous nanoparticle uptake and trapping in chloroplasts. Biocorona formation is expected to modulate both nanoparticle parameters, such as adsorbed ligands reducing electrostatic stabilization to potentially prohibit effective chloroplast localization.

5.5.3 Biological Conditions that Nanoparticles Encounter in Plants

Beyond the modes of nanoparticle transport and barriers to such movement, the molecular entities and conditions uniquely present in plants at each of these points must be considered in the context of biocorona composition. Broadly, such constituents include biomolecules (proteins, sugars, lipids, etc.), inorganic ions, and natural organic matter (NOM) in the surrounding environment, and conditions such as ionic strength, pH, and sap flow rates. Plant organs each express similar proteins at different abundance levels, with a dynamic range of over six orders of magnitude for the case of *Arabidopsis thaliana*[393], and plant saps exhibit distinct constituents dependent on function, such as xylem versus phloem sap[318,424].

Soil-administered nanoparticles are expected to possess an adsorbed biocorona prior to contact with plant roots, likely entailing NOM. Nanoparticle-bound organic macromolecules including humic acid, fulvic acid, citric acid, and soluble extracellular polymeric substances have been demonstrated to enhance nanoparticle stability against high ionic strength-induced nanoparticle aggregation[425,426], particularly as driven by divalent cations (Ca^{2+} and Mg^{2+})[427]. Increased stability is presumably by means of both electrostatic and steric stabilization, yet polymer bridging effects could also bring about nanoparticle flocculation. NOM adsorption has the potential to displace pre-existing surface moieties and form highly heterogeneous surface coatings[428], potentially rendering the nanosensor construct nonfunctional.

In the vasculature, nanoparticles can interact with the distinct sap constituents of the xylem versus the phloem. Studies delving into the interactions of sap components with nanoparticles, and the subsequent impact on nanoparticle fate in plants, remain rare in the literature[318]. Both the xylem and phloem vascular bundles transport water, nutrients, and metabolites, and the phloem additionally plays a role in transporting signaling molecules including proteins and small signaling molecules such as hormones and mRNAs[424]. To briefly summarize the differing compositions, the phloem consists of appreciable amounts of potassium, calcium, magnesium, sodium, chlorine, phosphorous, nitrogen, sulfur, sugars, amino acids, organic acids, and proteins, while the xylem consists of similar inorganic ions and proteins at lower concentrations (approximately an order of magnitude for the former) and no sugars or organic acids[318]. As such, nanoparticles entering by roots and traveling by xylem may be challenged with adsorption of far fewer biomolecules, in contrast to nanoparticles entering by leaves and traveling by phloem.

Plant biofluids can be further distinguished on the microscale in terms of the apoplastic and symplastic fluids as well as organelles. The apoplast is the space outside of plant cell membranes, encompassing the cell wall matrix and intercellular spaces. As the apoplastic fluid acts as the interface between the xylem and phloem, the composition correspondingly reflects exchange between the vascular bundles, while specifically leaf apoplastic fluid consists mainly of proteins for metabolic processes[424]. The symplast comprises the intracellular region, facilitating cell-to-cell transport of biomacromolecules that is rarely observed for nanoparticles[413]. Although the apoplastic space has been posited as a nanoparticle translocation pathway, there is no general agreement in literature as to whether or not nanoparticles primarily move through the apoplast or symplast pathway[184]. Within organelles, prior work has taken advantage of the large pool of flavonoids inside vacuoles[384], yet such highly abundant metabolites may interfere with intended nanosensor outcomes and must be taken into account *a priori*. For example, the highly abundant protein RuBisCO that composes nearly half of the stroma protein content of chloroplasts may be

relevant for the biocorona expected on nanosensors localizing to the chloroplasts, important for sensing tasks such as monitoring photosynthesis[429]. It is important to also note that morphological and physiological characteristics of plant biofluids and tissues vary as functions of plant species, growth stage, and external conditions including weather, time of day, and nutrients[318,413]. All such factors lead to variability in experiments that must be evaluated on a case-by-case basis.

5.6 Conclusions

The translation of nanoparticle-based sensors for widespread agricultural applications could greatly advance plant monitoring through continuous, non-destructive sensing techniques. Although nanoparticle interactions and transformations in the context of these plant bio-environments have been reported, our understanding of biocorona formation in plant systems and its impact on nanoparticle function remain fairly limited. To further develop our knowledge of biocorona formation on nanosensors, studies in animal systems provide a template to guide our inquiry into plant systems, with key challenges for working in plants that include proteomic and metabolomic considerations, plant transport, biological barriers, and biofluid constituents. By addressing these biological differences in plant systems and considering the intrinsic nanosensor properties, we can tune and improve nanosensor design for the seamless translation of these nanotechnologies in agricultural practice.

6   Concluding Remarks and Suggested Future Directions

Nanoparticles have immense potential for use in agricultural applications due to their highly tunable chemical and physical properties. In order to more rapidly advance their use in agriculture, it is essential we develop our understanding of nanomaterial interactions with plants on multiple scales: molecular, cellular, and macroscale. Within the context of nanoparticle-mediated biomolecule delivery, I have developed a workflow that enables us to study siRNA delivery of gold nanoparticles to mature plant leaves on both a molecular and cellular level. I have shown that nanoparticle morphology can impact both nanomaterial transport within a leaf and delivery efficacy to induce gene silencing, making this a key attribute for the design of efficient delivery vehicles. This workflow can be used to study how other nanoparticle attributes impact transport and delivery efficacy. In this work, I also focus on developing a SWNT formulation capable of delivering functional pDNA to a variety of plant species to achieve gene expression without transgene integration. This is a promising addition to the limited toolbox of DNA delivery to plants. These studies represent a step towards enhancing our understanding of nanoparticles in agricultural applications and pave the way for rational nanoparticle design.

To briefly summarize topics as covered throughout the chapters:

(1) Technological advancements are key to address urgent challenges with our food and agricultural systems. Nanomaterials can be a valuable addition to this toolbox by leveraging their unique properties for use as biomolecule delivery vehicles, growth stimulators, and sensors.

(2) The delivery of biomolecules into plant cells is a key challenge in the context of biomolecule-enabled genetic engineering. On a cellular level, biological barriers responsible for making efficient delivery difficult include the cell wall and cell membrane.

(3) Given that the size exclusion limit of the plant cell wall falls around 20 nm, it logically follows that engineered nanoparticle systems below this size limit are more likely to bypass the cell wall barrier and thus deliver biomolecular cargo more efficiently. However, our results suggest that nanoparticles do not need to cross the cell wall or internalize into the plant cell to achieve siRNA delivery.

(4) Nanoparticle size and shape impact nanoparticle transport and delivery ability within mature plant leaves. SWNTs possess unique properties that make them effective delivery agents for pDNA transport into the nucleus. Interestingly, the DNA delivered is available for transcription and subsequently translation, though it is not integrated into the plant genome. This is unlike *Agrobacterium*, which similarly delivers DNA into plants but inevitably results in transgene integration.

(5) Protein delivery presents more complications than RNA and DNA delivery. Incremental progress in this field is key, whereby testing of smaller proteins in reduced plant systems would be a good first step.

(6) Testing of nanoparticles as delivery vehicles has primarily occurred within the lab. Translation from the bench scale to the greenhouse or field scales may necessitate changes in nanoparticle design or formulation due to new complexities that were previously unaccounted for within the controlled laboratory space. Biocorona formation occurs upon nanoparticle introduction into a biofluid and could enhance or impede nanoparticle function. We can harness an understanding of how nanoparticle properties impact biocorona formation to move towards rational nanoparticle design.

This chapter concludes by suggesting future directions that might resolve some outstanding questions:

(1) How might we design a high-throughput workflow for testing the performance of different nanomaterial formulations? Can we identify easily quantifiable metrics that enable rapid performance testing?

It remains difficult to identify the best-performing formulation within the field of nanoparticle-mediated biomolecule delivery. Experiments have differed across plant species, tissue treated, treatment approach, cargo quantity, and experimental validation, preventing equivalent comparisons from being made. In this work, molecular validation for whether nanoparticles have achieved successful delivery involves RT-PCR or Western Blots, which are extremely time-consuming. Testing the performance of a variety of nanoparticle formulations in the same way would take excessive amounts of time. A high-throughput approach to test formulation performance is necessary to speed up developments in the field. A step towards streamlining this workflow might include targeting transgenic luciferase-expressing plants for siRNA delivery and quantifying the change in luciferase expression upon treatment.

The importance of testing each nanoparticle formulation using the same treatment and metrics is further underscored by the recent finding that transgenes more readily undergo post-transcriptional gene silencing than endogenous genes[430]. As such, we need to temper our expectations of nanoparticle formulations whose effectiveness at RNA delivery has been demonstrated solely by targeting transgenes. Certainly, the use of transgenes such as GFP or luciferase expression enables more accessible preliminary screens using microscopy or kit-based plate assays, but these results may be overly optimistic. Moving forward, we should aim to test formulations by also targeting endogenous genes in order to obtain a more realistic gauge of formulation effectiveness in field applications. Identifying an endogenous gene whose silencing results in an easily detectable genotype or phenotype would further facilitate a high-throughput workflow.

(2) How might we gain a better mechanistic understanding of nanoparticle internalization into plants?

Nanoparticle interaction and internalization into plant cells remains difficult to study to date. This is due to three key reasons, (i) depending on material, nanoparticles can be very difficult to track, (ii) the innate structure of plant cells (large central vacuole pushing the cytoplasm to line the cell wall) limits the capability of microscopy to accurately track cellular internalization and subcellular localization, and (iii) subcellular organelles in walled plant cells cannot be reliably stained.

Because of this, nanoparticle interactions with, uptake into, and fate within a plant cell continues to be a black box. Nanoparticle delivery into plants can be comprised of several steps: bypassing macromolecular structures such as the cuticle, intercalating with the plant cell, entry through the cell membrane, endosomal disruption, entry through an organelle membrane, desorption of cargo, and cell utilization of cargo. Assays of nanoparticle interaction and successful internalization for delivery rely on testing for whether there is

modulation in gene expression. While this approach allows us to directly sample whether the cargo delivered has resulted in gene silencing or expression, we lack the capability to troubleshoot the process. In other words, we cannot associate the reason for an unsuccessful formulation with any of the steps because we lack the tools to probe these steps in the process. Building tools and reporter systems that allow us to probe these steps individually can prove valuable in understanding nanoparticle behavior and building more effective delivery systems. As discussed in **Chapter 2** and **4**, confocal microscopy is an insufficient tool to ascertain nanoparticle internalization into cells due to the diffraction limit. Thus, there remains a need in this space to create an improved fluorescence-based system that leverages a turn-on response only when the nanoparticle has successfully internalized into the plant cell. Additionally, the development of organelle staining dyes for mature plant tissue will prove valuable to localization studies.

(3) How can we use harness mechanistic knowledge towards rational design of nanoparticles for a range of biological delivery applications? How can we extensively explore the nanoparticle design space for passive delivery in plants?

Rational nanoparticle design within this space requires further discovery and definition on *how* nanoparticles interact with plants across multiple length (molecular, cellular, macromolecular) and time scales, *how* this might impact delivery outcomes, and *what* key nanoparticle design characteristics govern these interactions. To study molecular interactions, a multi-omics method as explained in **Chapter 4** would be highly useful. This data can then be used as a training set in a machine learning model[431], allowing us to predict interactions with different nanoparticles or biological environments without having to manually explore those design spaces. My work in **Chapter 2** represents a step towards advancing these understandings primarily on a cellular scale. On the macromolecular scale, there have been many studies conducted probing the tissue-specific fate of nanoparticles upon application to plants, but work done in the context of nanoparticle delivery (particles engineered specifically to bypass biological barriers and potentially internalize into cells) has been minimal. Our deepened understanding on the molecular and cellular interactions acquired from multi-omics and high-throughput testing can be integrated with macromolecular nanoparticle fate studies. Ultimately, drawing connections between disparate length and time scales will be integral towards rational tuning of nanoparticles properties.

7 References

(1)   Rockström, J.; Edenhofer, O.; Gaertner, J.; DeClerck, F. Planet-Proofing the Global Food System. *Nat Food* **2020**, *1* (1), 3–5. https://doi.org/10.1038/s43016-019-0010-4.

(2)   Lin, B. B. Resilience in Agriculture through Crop Diversification: Adaptive Management for Environmental Change. *BioScience* **2011**, *61* (3), 183–193. https://doi.org/10.1525/bio.2011.61.3.4.

(3)   Elliott Joshua; Deryng Delphine; Müller Christoph; Frieler Katja; Konzmann Markus; Gerten Dieter; Glotter Michael; Flörke Martina; Wada Yoshihide; Best Neil; Eisner Stephanie; Fekete Balázs M.; Folberth Christian; Foster Ian; Gosling Simon N.; Haddeland Ingjerd; Khabarov Nikolay; Ludwig Fulco; Masaki Yoshimitsu; Olin Stefan; Rosenzweig Cynthia; Ruane Alex C.; Satoh Yusuke; Schmid Erwin; Stacke Tobias; Tang Qiuhong; Wisser Dominik. Constraints and Potentials of Future Irrigation Water Availability on Agricultural Production under Climate Change. *Proceedings of the National Academy of Sciences* **2014**, *111* (9), 3239–3244. https://doi.org/10.1073/pnas.1222474110.

(4)   Doungmanee, P. The Nexus of Agricultural Water Use and Economic Development Level. *Kasetsart Journal of Social Sciences* **2016**, *37* (1), 38–45. https://doi.org/10.1016/j.kjss.2016.01.008.

(5)   Mbow, C.; Rosenzweig, C.; Barioni, L. G.; Benton, T. G.; Herrero, M.; Krishnapillai, M.; Liwenga, E.; Pradhan, P.; Rivera-Ferre, M.-G.; Sapkota, T. Food Security. In *Climate Change and Land*; 2019; pp 437–550.

(6)   Alengebawy, A.; Abdelkhalek, S. T.; Qureshi, S. R.; Wang, M.-Q. Heavy Metals and Pesticides Toxicity in Agricultural Soil and Plants: Ecological Risks and Human Health Implications. *Toxics* **2021**, *9* (3), 42. https://doi.org/10.3390/toxics9030042.

(7)   Tang, F. H. M.; Lenzen, M.; McBratney, A.; Maggi, F. Risk of Pesticide Pollution at the Global Scale. *Nat. Geosci.* **2021**, *14* (4), 206–210. https://doi.org/10.1038/s41561-021-00712-5.

(8)   Fan, M.; Shen, J.; Yuan, L.; Jiang, R.; Chen, X.; Davies, W. J.; Zhang, F. Improving Crop Productivity and Resource Use Efficiency to Ensure Food Security and Environmental Quality in China. *Journal of Experimental Botany* **2012**, *63* (1), 13–24. https://doi.org/10.1093/jxb/err248.

(9)   Hebinck, A.; Selomane, O.; Veen, E.; de Vrieze, A.; Hasnain, S.; Sellberg, M.; Sovová, L.; Thompson, K.; Vervoort, J.; Wood, A. Exploring the Transformative Potential of Urban Food. *npj Urban Sustain* **2021**, *1* (1), 1–9. https://doi.org/10.1038/s42949-021-00041-x.

(10)   Pimentel, D.; Pimentel, M. Sustainability of Meat-Based and Plant-Based Diets and the Environment. *The American Journal of Clinical Nutrition* **2003**, *78* (3), 660S-663S. https://doi.org/10.1093/ajcn/78.3.660S.

(11)   Record $5 billion invested in alt proteins in 2021 https://gfi.org/press/record-5-billion-invested-in-alt-proteins-in-2021/ (accessed 2022 -04 -08).

(12)   Witte, B.; Obloj, P.; Koktenturk, S.; Morach, B.; Brigl, M.; Rogg, J.; Schulze, U.; Walker, D.; Von Koeller, E.; Dehnert, N.; Grosse-Holz, F. *Food for Thought: The Protein Transformation*; BCG, 2021.

(13)   Kim, Y. G.; Cha, J.; Chandrasegaran, S. Hybrid Restriction Enzymes: Zinc Finger Fusions to Fok I Cleavage Domain. *Proceedings of the National Academy of Sciences of the United States of America* **1996**, *93* (3), 1156–1160.

(14)   Jinek, M.; Chylinski, K.; Fonfara, I.; Hauer, M.; Doudna, J. A.; Charpentier, E. A Programmable Dual-RNA-Guided DNA Endonuclease in Adaptive Bacterial Immunity. *Science (New York, N.Y.)* **2012**, *337* (6096), 816–821. https://doi.org/10.1126/science.1225829.

(15)   Cong, L.; Ran, F. A.; Cox, D.; Lin, S.; Barretto, R.; Habib, N.; Hsu, P. D.; Wu, X.; Jiang, W.; Marraffini, L. A.; Zhang, F. Multiplex Genome Engineering Using CRISPR/Cas Systems. *Science (New York, N.Y.)* **2013**, *339* (6121), 819–823. https://doi.org/10.1126/science.1231143.

(16)   Boch, J.; Scholze, H.; Schornack, S.; Landgraf, A.; Hahn, S.; Kay, S.; Lahaye, T.; Nickstadt, A.; Bonas, U. Breaking the Code of DNA Binding Specificity of TAL-Type III Effectors. *Science* **2009**, *326* (5959), 1509–1512. https://doi.org/10.1126/science.1178811.

(17)   Moscou, M. J.; Bogdanove, A. J. A Simple Cipher Governs DNA Recognition by TAL Effectors. *Science* **2009**, *326* (5959), 1501–1501. https://doi.org/10.1126/science.1178817.

(18)   ISAAA. Global Status of Commercialized Biotech/GM Crops: 2016. *ISAAA Briefs* **2016**, *52*.

(19)   Camacho, A.; Van Deynze, A.; Chi-Ham, C.; Bennett, A. B. Genetically Engineered Crops That Fly under the US Regulatory Radar. *Nature Biotechnology* **2014**, *32* (11), 1087–1091. https://doi.org/10.1038/nbt.3057.

(20)   Jones, H. D. Regulatory Uncertainty over Genome Editing. *Nature Plants* **2015**, *1* (1), 14011. https://doi.org/10.1038/nplants.2014.11.

(21)   Parliament, E. U. *Directive 2001/18/EC of the European Parliament and of the Council of 12 March 2001 on the Deliberate Release into the Environment of Genetically Modified Organisms and Repealing Council Directive*; Off. J. Eur. Comm. L, 2001; pp 1–38.

(22)   Bobek, M. Opinion of Advocate General Bobek in Case C-528/16. *Court of Justice of the European Union* **2018**.

(23)   Ishii, T.; Araki, M. A Future Scenario of the Global Regulatory Landscape Regarding Genome-Edited Crops. *GM crops & food* **2017**, *8* (1), 44–56. https://doi.org/10.1080/21645698.2016.1261787.

(24)   Gao, W.; Xu, W.-T.; Huang, K.-L.; Guo, M.; Luo, Y.-B. Risk Analysis for Genome Editing-Derived Food Safety in China. *Food Control* **2018**, *84*, 128–137. https://doi.org/10.1016/j.foodcont.2017.07.032.

(25)   McCarthy, M. Genetic Modification Laws Set for Shake-up, with Health and Agriculture Research Industries to Benefit (Interview with Raj Bhula). *ABC Australia* **2018**.

(26)   Schuttelaar & Partners. The Regulatory Status of New Breeding Techniques in Countries Outside the European Union. **2015**.

(27)   Waltz, E. With a Free Pass, CRISPR-Edited Plants Reach Market in Record Time. *Nature Biotechnology* **2018**, *36* (1), 6–7. https://doi.org/10.1038/nbt0118-6b.

(28)   Bevan, M. Binary Agrobacterium Vectors for Plant Transformation. *Nucleic Acids Research* **1984**, *12* (22).

(29)   Klein, T. M.; Wolf, E. D.; Wu, R.; Sanford, J. C. High-Velocity Microprojectiles for Delivering Nucleic Acids into Living Cells. *Nature* **1987**, *327* (6117), 70–73. https://doi.org/10.1038/327070a0.

(30)   Nyaboga, E.; Tripathi, J. N.; Manoharan, R.; Tripathi, L. Agrobacterium-Mediated Genetic Transformation of Yam (Dioscorea Rotundata): An Important Tool for Functional Study of Genes and Crop Improvement. *Frontiers in plant science* **2014**, *5*, 463. https://doi.org/10.3389/fpls.2014.00463.

(31)   Gelvin, S. B. Integration of *Agrobacterium* T-DNA into the Plant Genome. *Annual Review of Genetics* **2017**, *51* (1), 195–217. https://doi.org/10.1146/annurev-genet-120215-035320.

(32)   Gleba, Y.; Klimyuk, V.; Marillonnet, S. Magnifection—a New Platform for Expressing Recombinant Vaccines in Plants. *Vaccine* **2005**, *23* (17), 2042–2048. https://doi.org/10.1016/j.vaccine.2005.01.006.

(33)   Stoddard, T.; Baltes, N. J.; Luo, S. Agrobacterium-Mediated Genome Modification without t-Dna Integration. Google Patents August 2016.

(34)   Lowe, K.; Wu, E.; Wang, N.; Hoerster, G.; Hastings, C.; Cho, M.-J.; Scelonge, C.; Lenderts, B.; Chamberlin, M.; Cushatt, J.; Wang, L.; Ryan, L.; Khan, T.; Chow-Yiu, J.; Hua, W.; Yu, M.; Banh, J.; Bao, Z.; Brink, K.; Igo, E.; Rudrappa, B.; Shamseer, P.; Bruce, W.; Newman, L.; Shen, B.; Zheng, P.; Bidney, D.; Falco, C.; Register, J.; Zhao, Z.-Y.; Xu, D.; Jones, T.; Gordon-Kamm, W. Morphogenic Regulators Baby Boom and Wuschel Improve Monocot Transformation. *The Plant Cell* **2016**, *28* (9), 1998–2015. https://doi.org/10.1105/tpc.16.00124.

(35)   Subcommittee, N. The National Nanotechnology Initiative. *Nanotechnology* **2007**, No. L. https://doi.org/10.4135/9781412972093.n338.

(36)   Johlin, E.; Al-Obeidi, A.; Nogay, G.; Stuckelberger, M.; Buonassisi, T.; Grossman, J. C. Nanohole Structuring for Improved Performance of Hydrogenated Amorphous Silicon Photovoltaics. *ACS Applied Materials & Interfaces* **2016**, *8* (24), 15169–15176. https://doi.org/10.1021/acsami.6b00033.

(37)   Lee, Y. M.; Lee, D.; Kim, J.; Park, H.; Kim, W. J. RPM Peptide Conjugated Bioreducible Polyethylenimine Targeting Invasive Colon Cancer. *Journal of Controlled Release* **2015**, *205*, 172–180. https://doi.org/10.1016/J.JCONREL.2015.01.020.

(38)   LaVan, D. A.; McGuire, T.; Langer, R. Small-Scale Systems for in Vivo Drug Delivery. *Nature Biotechnology* **2003**, *21*, 1184.

(39)   Cavalcanti, A.; Shirinzadeh, B.; Freitas Jr, R. A.; Hogg, T. Nanorobot Architecture for Medical Target Identification. *Nanotechnology* **2007**, *19* (1), 15103.

(40)   Zadegan, R. M.; Norton, M. L. Structural DNA Nanotechnology: From Design to Applications. *International Journal of Molecular Sciences* . 2012. https://doi.org/10.3390/ijms13067149.

(41)   Ghormade, V.; Deshpande, M. V.; Paknikar, K. M. Perspectives for Nano-Biotechnology Enabled Protection and Nutrition of Plants. *Biotechnology Advances* **2011**, *29* (6), 792–803. https://doi.org/10.1016/j.biotechadv.2011.06.007.

(42)   Thangavelu, R. M.; Gunasekaran, D.; Jesse, M. I.; S.U, M. R.; Sundarajan, D.; Krishnan, K. Nanobiotechnology Approach Using Plant Rooting Hormone Synthesized Silver Nanoparticle as "Nanobullets" for the Dynamic Applications in Horticulture – An in Vitro and Ex Vitro Study. *Arabian Journal of Chemistry* **2018**, *11* (1), 48–61. https://doi.org/10.1016/j.arabjc.2016.09.022.

(43) Barrena, R.; Casals, E.; Colón, J.; Font, X.; Sánchez, A.; Puntes, V. Evaluation of the Ecotoxicity of Model Nanoparticles. *Chemosphere* **2009**, *75* (7), 850–857. https://doi.org/10.1016/j.chemosphere.2009.01.078.

(44) Arora, S.; Sharma, P.; Kumar, S.; Nayan, R.; Khanna, P. K.; Zaidi, M. G. H. Gold-Nanoparticle Induced Enhancement in Growth and Seed Yield of Brassica Juncea . *Plant Growth Regulation* **2012**, *66* (3), 303–310. https://doi.org/10.1007/s10725-011-9649-z.

(45) Salama, H. M. H. Effects of Silver Nanoparticles in Some Crop Plants, Common Bean (Phaseolus Vulgaris L.) and Corn (Zea Mays L.). *Int Res J Biotechnol* **2012**, *3* (10), 190–197.

(46) Zhao, H.; Lin, Z. Y.; Yildirimer, L.; Dhinakar, A.; Zhao, X.; Wu, J. Polymer-Based Nanoparticles for Protein Delivery: Design, Strategies and Applications. *J. Mater. Chem. B* **2016**, *4060* (4), 4060–4071. https://doi.org/10.1039/c6tb00308g.

(47) Wang, L.; Li, F.; Dang, L.; Liang, C.; Wang, C.; He, B.; Liu, J.; Li, D.; Wu, X.; Xu, X.; Lu, A.; Zhang, G. In Vivo Delivery Systems for Therapeutic Genome Editing. *International journal of molecular sciences* **2016**, *17* (5). https://doi.org/10.3390/ijms17050626.

(48) Kim, I.-Y.; Joachim, E.; Choi, H.; Kim, K. Toxicity of Silica Nanoparticles Depends on Size, Dose, and Cell Type. *Nanomedicine: Nanotechnology, Biology, and Medicine* **2015**, *11*, 1407–1416. https://doi.org/10.1016/j.nano.2015.03.004.

(49) Shang, L.; Nienhaus, K.; Nienhaus, G. U. Engineered Nanoparticles Interacting with Cells: Size Matters. *Journal of Nanobiotechnology*. 2014. https://doi.org/10.1186/1477-3155-12-5.

(50) Petersen, M. A.; Hillmyer, M. A.; Kokkoli, E. Bioresorbable Polymersomes for Targeted Delivery of Cisplatin. *Bioconjugate Chemistry* **2013**, *24* (4), 533–543. https://doi.org/10.1021/bc3003259.

(51) Tekedereli, I.; Alpay, S. N.; Akar, U.; Yuca, E.; Ayugo-Rodriguez, C.; Han, H.-D.; Sood, A. K.; Lopez-Berestein, G.; Ozpolat, B. Therapeutic Silencing of Bcl-2 by Systemically Administered SiRNA Nanotherapeutics Inhibits Tumor Growth by Autophagy and Apoptosis and Enhances the Efficacy of Chemotherapy in Orthotopic Xenograft Models of ER (-) and ER (+) Breast Cancer. *Molecular therapy. Nucleic acids* **2013**, *2* (9), e121. https://doi.org/10.1038/mtna.2013.45.

(52) Yin, P. T.; Shah, B. P.; Lee, K.-B. Combined Magnetic Nanoparticle-Based MicroRNA and Hyperthermia Therapy to Enhance Apoptosis in Brain Cancer Cells HHS Public Access. *Small. October* **2014**, *29* (1020), 4106–4112. https://doi.org/10.1002/smll.201400963.

(53) Zhang, K.; Hao, L.; Hurst, S. J.; Mirkin, C. A. Antibody-Linked Spherical Nucleic Acids for Cellular Targeting. *Journal of the American Chemical Society* **2012**, *134* (40), 16488–16491. https://doi.org/10.1021/ja306854d.

(54) Smith, B. R.; Ghosn, E. E. B.; Rallapalli, H.; Prescher, J. A.; Larson, T.; Herzenberg, L. A.; Gambhir, S. S. Selective Uptake of Single-Walled Carbon Nanotubes by Circulating Monocytes for Enhanced Tumour Delivery. *Nature Nanotechnology* **2014**, *9* (6), 481–487. https://doi.org/10.1038/nnano.2014.62.

(55) Chen, P.-C.; Liu, X.; Hedrick, J. L.; Xie, Z.; Wang, S.; Lin, Q.-Y.; Hersam, M. C.; Dravid, V. P.; Mirkin, C. A. Polyelemental Nanoparticle Libraries. *Science (New York, N.Y.)* **2016**, *352* (6293), 1565–1569. https://doi.org/10.1126/science.aaf8402.

(56) Lu, J.; Low, K.-B.; Lei, Y.; Libera, J. A.; Nicholls, A.; Stair, P. C.; Elam, J. W. Toward Atomically-Precise Synthesis of Supported Bimetallic Nanoparticles Using Atomic Layer Deposition. *Nature Communications* **2014**, *5*, 3264. https://doi.org/10.1038/ncomms4264.

(57) Hu, X.; Hu, J.; Tian, J.; Ge, Z.; Zhang, G.; Luo, K.; Liu, S. Polyprodrug Amphiphiles: Hierarchical Assemblies for Shape-Regulated Cellular Internalization, Trafficking, and Drug Delivery. *Journal of the American Chemical Society* **2013**, *135* (46), 17617–17629. https://doi.org/10.1021/ja409686x.

(58) Chhipa, H. Nanofertilizers and Nanopesticides for Agriculture. *Environ Chem Lett* **2017**, *15* (1), 15–22. https://doi.org/10.1007/s10311-016-0600-4.

(59) Lahiani, M. H.; Dervishi, E.; Chen, J.; Nima, Z.; Gaume, A.; Biris, A. S.; Khodakovskaya, M. V. Impact of Carbon Nanotube Exposure to Seeds of Valuable Crops. *ACS Appl. Mater. Interfaces* **2013**, *5* (16), 7965–7973. https://doi.org/10.1021/am402052x.

(60) Siddiqui, M. H.; Al-Whaibi, M. H. Role of Nano-SiO2 in Germination of Tomato (Lycopersicum Esculentum Seeds Mill.). *Saudi J Biol Sci* **2014**, *21* (1), 13–17. https://doi.org/10.1016/j.sjbs.2013.04.005.

(61) Shah, T.; Latif, S.; Saeed, F.; Ali, I.; Ullah, S.; Abdullah Alsahli, A.; Jan, S.; Ahmad, P. Seed Priming with Titanium Dioxide Nanoparticles Enhances Seed Vigor, Leaf Water Status, and Antioxidant Enzyme Activities in Maize (Zea Mays L.) under Salinity Stress. *Journal of King Saud University - Science* **2021**, *33* (1), 101207. https://doi.org/10.1016/j.jksus.2020.10.004.

(62) Gao, J.; Wang, Y.; Folta, K. M.; Krishna, V.; Bai, W.; Indeglia, P.; Georgieva, A.; Nakamura, H.; Koopman, B.; Moudgil, B. Polyhydroxy Fullerenes (Fullerols or Fullerenols): Beneficial Effects on Growth and Lifespan in Diverse Biological Models. *PLOS ONE* **2011**, *6* (5), e19976. https://doi.org/10.1371/journal.pone.0019976.

(63) Pallavi; Mehta, C. M.; Srivastava, R.; Arora, S.; Sharma, A. K. Impact Assessment of Silver Nanoparticles on Plant Growth and Soil Bacterial Diversity. *3 Biotech* **2016**, *6* (2), 254. https://doi.org/10.1007/s13205-016-0567-7.

(64) Shang, Y.; Hasan, Md. K.; Ahammed, G. J.; Li, M.; Yin, H.; Zhou, J. Applications of Nanotechnology in Plant Growth and Crop Protection: A Review. *Molecules* **2019**, *24* (14), 2558. https://doi.org/10.3390/molecules24142558.

(65) Zeng, X.; Morgenstern, R.; Nyström, A. M. Nanoparticle-Directed Sub-Cellular Localization of Doxorubicin and the Sensitization Breast Cancer Cells by Circumventing GST-Mediated Drug Resistance. *Biomaterials* **2014**, *35* (4), 1227–1239. https://doi.org/10.1016/J.BIOMATERIALS.2013.10.042.

(66) Dekiwadia, C. D.; Lawrie, A. C.; Fecondo, J. V. Peptide-Mediated Cell Penetration and Targeted Delivery of Gold Nanoparticles into Lysosomes. *Journal of Peptide Science* **2012**, *18* (8), 527–534. https://doi.org/10.1002/psc.2430.

(67) Mout, R.; Ray, M.; Yesilbag Tonga, G.; Lee, Y.-W.; Tay, T.; Sasaki, K.; Rotello, V. M. Direct Cytosolic Delivery of CRISPR/Cas9-Ribonucleoprotein for Efficient Gene Editing. *ACS Nano* **2017**, *11* (3), 2452–2458. https://doi.org/10.1021/acsnano.6b07600.

(68) Zhong, J.; Li, L.; Zhu, X.; Guan, S.; Yang, Q.; Zhou, Z.; Zhang, Z.; Huang, Y. A Smart Polymeric Platform for Multistage Nucleus-Targeted Anticancer Drug Delivery. *Biomaterials* **2015**, *65*, 43–55. https://doi.org/10.1016/J.BIOMATERIALS.2015.06.042.

(69) Mao, H.-Q.; Roy, K.; Troung-Le, V. L.; Janes, K. A.; Lin, K. Y.; Wang, Y.; August, J. T.; Leong, K. W. Chitosan-DNA Nanoparticles as Gene Carriers: Synthesis, Characterization and Transfection Efficiency. *Journal of Controlled Release* **2001**, *70* (3), 399–421. https://doi.org/10.1016/S0168-3659(00)00361-8.

(70) Davis, M. E.; Zuckerman, J. E.; Choi, C. H. J.; Seligson, D.; Tolcher, A.; Alabi, C. A.; Yen, Y.; Heidel, J. D.; Ribas, A. Evidence of RNAi in Humans from Systemically Administered SiRNA via Targeted Nanoparticles. *Nature* **2010**, *464* (7291), 1067–1070. https://doi.org/10.1038/nature08956.

(71) Yan, M.; Du, J.; Gu, Z.; Liang, M.; Hu, Y.; Zhang, W.; Priceman, S.; Wu, L.; Zhou, Z. H.; Liu, Z.; Segura, T.; Tang, Y.; Lu, Y. A Novel Intracellular Protein Delivery Platform Based on Single-Protein Nanocapsules. *Nature Nanotechnology* **2010**, *5* (1), 48–53. https://doi.org/10.1038/nnano.2009.341.

(72) Sengupta, S.; Eavarone, D.; Capila, I.; Zhao, G.; Watson, N.; Kiziltepe, T.; Sasisekharan, R. Temporal Targeting of Tumour Cells and Neovasculature with a Nanoscale Delivery System. *Nature* **2005**, *436* (7050), 568–572. https://doi.org/10.1038/nature03794.

(73) Swyer, T.; Strom, J.; Larson, D. Nanoparticle Oxygen Delivery to the Ischemic Heart. *Perfusion* **2014**, *29* (6), 539–543. https://doi.org/10.1177/0267659114534290.

(74) Haham, M.; Ish-Shalom, S.; Nodelman, M.; Duek, I.; Segal, E.; Kustanovich, M.; Livney, Y. D. Stability and Bioavailability of Vitamin D Nanoencapsulated in Casein Micelles. *Food & Function* **2012**, *3* (7), 737. https://doi.org/10.1039/c2fo10249h.

(75) Karimi, M.; Ghasemi, A.; Sahandi Zangabad, P.; Rahighi, R.; Moosavi Basri, S. M.; Mirshekari, H.; Amiri, M.; Shafaei Pishabad, Z.; Aslani, A.; Bozorgomid, M.; Ghosh, D.; Beyzavi, A.; Vaseghi, A.; Aref, A. R.; Haghani, L.; Bahrami, S.; Hamblin, M. R. Smart Micro/Nanoparticles in Stimulus-Responsive Drug/Gene Delivery Systems. *Chem. Soc. Rev.* **2016**, *45* (5), 1457–1501. https://doi.org/10.1039/C5CS00798D.

(76) Ta, T.; Bartolak-Suki, E.; Park, E.-J.; Karrobi, K.; Mcdannold, N. J.; Porter, T. M. Localized Delivery of Doxorubicin in Vivo from Polymer-Modified Thermosensitive Liposomes with MR-Guided Focused Ultrasound-Mediated Heating. **2014**. https://doi.org/10.1016/j.jconrel.2014.08.013.

(77) Mu, Q.; Jeon, M.; Hsiao, M.-H.; Patton, V. K.; Wang, K.; Press, O. W.; Zhang, M. Stable and Efficient Paclitaxel Nanoparticles for Targeted Glioblastoma Therapy. *Advanced healthcare materials* **2015**, *4* (8), 1236–1245. https://doi.org/10.1002/adhm.201500034.

(78) Svenson, S.; Case, R. I.; Cole, R. O.; Hwang, J.; Kabir, S. R.; Lazarus, D.; Lim Soo, P.; Ng, P.-S.; Peters, C.; Shum, P.; Sweryda-Krawiec, B.; Tripathi, S.; van der Poll, D.; Eliasof, S. Tumor Selective Silencing Using an RNAi-Conjugated Polymeric Nanopharmaceutical. *Molecular Pharmaceutics* **2016**, *13* (3), 737–747. https://doi.org/10.1021/acs.molpharmaceut.5b00608.

(79) Hou, X.-F.; Chen, Y.; Liu, Y. Enzyme-Responsive Protein/Polysaccharide Supramolecular Nanoparticles. *Soft Matter* **2015**, *11* (12), 2488–2493. https://doi.org/10.1039/C4SM02896A.

(80) Wang, M.; Zuris, J. A.; Meng, F.; Rees, H.; Sun, S.; Deng, P.; Han, Y.; Gao, X.; Pouli, D.; Wu, Q.; Georgakoudi, I.; Liu, D. R.; Xu, Q. Efficient Delivery of Genome-Editing Proteins Using Bioreducible Lipid Nanoparticles. *Proceedings of the National Academy of Sciences of the United States of America* **2016**, *113* (11), 2868–2873. https://doi.org/10.1073/pnas.1520244113.

(81)   Hoshino, A.; Fujioka, K.; Oku, T.; Nakamura, S.; Suga, M.; Yamaguchi, Y.; Suzuki, K.; Yasuhara, M.; Yamamoto, K. Quantum Dots Targeted to the Assigned Organelle in Living Cells. *Microbiology and immunology* **2004**, *48* (12), 985–994.

(82)   Lai, C. Y.; Trewyn, B. G.; Jeftinija, D. M.; Jeftinija, K.; Xu, S.; Jeftinija, S.; Lin, V. S.-Y. A Mesoporous Silica Nanosphere-Based Carrier System with Chemically Removable CdS Nanoparticle Caps for Stimuli-Responsive Controlled Release of Neurotransmitters and Drug Molecules. *Journal of the American Chemical Society* **2003**, *125* (15), 4451–4459. https://doi.org/10.1021/ja028650l.

(83)   Naqvi, S.; Maitra, A. N.; Abdin, M. Z.; Akmal, Md.; Arora, I.; Samim, Md. Calcium Phosphate Nanoparticle Mediated Genetic Transformation in Plants. *Journal of Materials Chemistry* **2012**, *22* (8), 3500. https://doi.org/10.1039/c2jm11739h.

(84)   Antonelli, N. M.; Stadler, J. Genomic DNA Can Be Used with Cationic Methods for Highly Efficient Transformation of Maize Protoplasts. *Theor Appl Genet* **1990**, *80*, 395–401.

(85)   Ragelle, H.; Riva, R.; Vandermeulen, G.; Naeye, B.; Pourcelle, V.; Le Duff, C. S.; D'Haese, C.; Nysten, B.; Braeckmans, K.; De Smedt, S. C.; Jérôme, C.; Préat, V. Chitosan Nanoparticles for SiRNA Delivery: Optimizing Formulation to Increase Stability and Efficiency. *Journal of Controlled Release* **2014**, *176*, 54–63. https://doi.org/10.1016/J.JCONREL.2013.12.026.

(86)   Zuris, J. A.; Thompson, D. B.; Shu, Y.; Guilinger, J. P.; Bessen, J. L.; Hu, J. H.; Maeder, M. L.; Joung, J. K.; Chen, Z.-Y.; Liu, D. R. Cationic Lipid-Mediated Delivery of Proteins Enables Efficient Protein-Based Genome Editing in Vitro and in Vivo. *Nature Biotechnology* **2015**, *33* (1), 73–80. https://doi.org/10.1038/nbt.3081.

(87)   Pantarotto, D.; Singh, R.; McCarthy, D.; Erhardt, M.; Briand, J.-P.; Prato, M.; Kostarelos, K.; Bianco, A. Functionalized Carbon Nanotubes for Plasmid DNA Gene Delivery. *Angewandte Chemie International Edition* **2004**, *43* (39), 5242–5246. https://doi.org/10.1002/anie.200460437.

(88)   Demirer, G. S.; Zhang, H.; Matos, J. L.; Goh, N. S.; Cunningham, F. J.; Sung, Y.; Chang, R.; Aditham, A. J.; Chio, L.; Cho, M.-J.; Staskawicz, B.; Landry, M. P. High Aspect Ratio Nanomaterials Enable Delivery of Functional Genetic Material without DNA Integration in Mature Plants. *Nat. Nanotechnol.* **2019**, *14* (5), 456–464. https://doi.org/10.1038/s41565-019-0382-5.

(89)   Nadine Wong Shi Kam; Zhuang Liu, and; Dai*, H. Functionalization of Carbon Nanotubes via Cleavable Disulfide Bonds for Efficient Intracellular Delivery of SiRNA and Potent Gene Silencing. **2005**. https://doi.org/10.1021/JA053962K.

(90)   Kneuer, C.; Sameti, M.; Bakowsky, U.; Schiestel, T.; Schirra, H.; Schmidt, H.; Lehr, C. M. A Nonviral DNA Delivery System Based on Surface Modified Silica-Nanoparticles Can Efficiently Transfect Cells in Vitro. *Bioconjugate Chemistry* **2000**, *11* (6), 926–932. https://doi.org/10.1021/bc0000637.

(91)   Torney, F.; Trewyn, B. G.; Lin, V. S. Y.; Wang, K. Mesoporous Silica Nanoparticles Deliver DNA and Chemicals into Plants. *Nature Nanotechnology* **2007**, *2* (5), 295–300. https://doi.org/10.1038/nnano.2007.108.

(92)   Chen, A. M.; Zhang, M.; Wei, D.; Stueber, D.; Taratula, O.; Minko, T.; He, H. Co-Delivery of Doxorubicin and Bcl-2 SiRNA by Mesoporous Silica Nanoparticles Enhances the Efficacy of Chemotherapy in Multidrug-Resistant Cancer Cells. *Small* **2009**, *5* (23), 2673–2677. https://doi.org/10.1002/smll.200900621.

(93)   Martin-Ortigosa, S.; Peterson, D. J.; Valenstein, J. S.; Lin, V. S. Y.; Trewyn, B. G.; Alexander Lyznik, L.; Wang, K. Mesoporous Silica Nanoparticle-Mediated Intracellular Cre Protein Delivery for Maize Genome Editing via LoxP Site Excision. *Plant Physiology* **2014**, *164* (2), 537–547. https://doi.org/10.1104/pp.113.233650.

(94)   Boussif, O.; Lezoualc 'ht, F.; Antonietra Zanta, M.; Mergnyt, D.; Schermant, D.; Demeneixt, B.; Behr, J.-P. A Versatile Vector for Gene and Oligonucleotide Transfer into Cells in Culture and in Vivo: Polyethylenimine. *Biochemistry* **1995**, *92*, 7297–7301.

(95)   Negrutiu, I.; Shillito, R.; Potrykus, I.; Biasini, G.; Sala, F. Hybrid Genes in the Analysis of Transformation Conditions. *Plant Molecular Biology* **1987**, *8*, 363–373.

(96)   Aigner, A.; Fischer, D.; Merdan, T.; Brus, C.; Kissel, T.; Czubayko, F. Delivery of Unmodified Bioactive Ribozymes by an RNA-Stabilizing Polyethylenimine (LMW-PEI) Efficiently down-Regulates Gene Expression. *Gene Therapy* **2002**, *9* (24), 1700–1707. https://doi.org/10.1038/sj.gt.3301839.

(97)   Silva, A. T.; Nguyen, A.; Ye, C.; Verchot, J.; Moon, J. H. Conjugated Polymer Nanoparticles for Effective SiRNA Delivery to Tobacco BY-2 Protoplasts. *BMC Plant Biology* **2010**, *10* (1), 291. https://doi.org/10.1186/1471-2229-10-291.

(98)   Sgolastra, F.; Backlund, C. M.; Ilker Ozay, E.; Deronde, B. M.; Minter, L. M.; Tew, G. N. Sequence Segregation Improves Non-Covalent Protein Delivery HHS Public Access Increased Hydrophobic/Hydrophilic Segregation in a Class of Polymeric Mimics of Protein Transduction Domains Generates More Efficient Vehicles for Non-Covalent Protein Delivery. *J Control Release* **2017**, *254*, 131–136. https://doi.org/10.1016/j.jconrel.2017.03.387.

(99)   Mizutani, O.; Masaki, K.; Gomi, K.; Iefuji, H. Modified Cre-LoxP Recombination in Aspergillus Oryzae by Direct Introduction of Cre Recombinase for Marker Gene Rescue. *Applied and environmental microbiology* **2012**, *78* (12), 4126–4133. https://doi.org/10.1128/AEM.00080-12.

(100) Sun, W.; Ji, W.; Hall, J. M.; Hu, Q.; Wang, C.; Beisel, C. L.; Gu, Z. Self-Assembled DNA Nanoclews for the Efficient Delivery of CRISPR-Cas9 for Genome Editing. *Angewandte Chemie (International ed. in English)* **2015**, *54* (41), 12029–12033. https://doi.org/10.1002/anie.201506030.

(101) Woo, J. W.; Kim, J.-S. J.; Kwon, S. Il; Corvalán, C.; Cho, S. W.; Kim, H.; Kim, S.-T. S.-G.; Kim, S.-T. S.-G.; Choe, S.; Kim, J.-S. J. DNA-Free Genome Editing in Plants with Preassembled CRISPR-Cas9 Ribonucleoproteins. *Nature Biotechnology* **2015**, *33* (11), 1162–1164. https://doi.org/10.1038/nbt.3389.

(102) Sandhu, K. K.; McIntosh, C. M.; Simard, J. M.; Smith, S. W.; Rotello, V. M. Gold Nanoparticle-Mediated Transfection of Mammalian Cells. *Bioconjugate Chemistry* **2002**, *13* (1), 3–6. https://doi.org/10.1021/bc015545c.

(103) Zhao, X.; Meng, Z.; Wang, Y.; Chen, W.; Sun, C.; Cui, B.; Cui, J.; Yu, M.; Zeng, Z.; Guo, S.; Luo, D.; Cheng, J. Q.; Zhang, R.; Cui, H. Pollen Magnetofection for Genetic Modification with Magnetic Nanoparticles as Gene Carriers. *Nature Plants* **2017**, *3* (12), 956–964. https://doi.org/10.1038/s41477-017-0063-z.

(104) Lee, J.-H.; Lee, K.; Moon, S. H.; Lee, Y.; Park, T. G.; Cheon, J. All-in-One Target-Cell-Specific Magnetic Nanoparticles for Simultaneous Molecular Imaging and SiRNA Delivery. *Angewandte Chemie International Edition* **2009**, *48* (23), 4174–4179. https://doi.org/10.1002/anie.200805998.

(105)   Mout, R.; Ray, M.; Tay, T.; Sasaki, K.; Yesilbag Tonga, G.; Rotello, V. M. General Strategy for Direct Cytosolic Protein Delivery via Protein-Nanoparticle Co-Engineering. *ACS Nano* **2017**, *11* (6), 6416–6421. https://doi.org/10.1021/acsnano.7b02884.

(106)   Lee, K.; Conboy, M.; Park, H. M.; Jiang, F.; Kim, H. J.; Dewitt, M. A.; Mackley, V. A.; Chang, K.; Rao, A.; Skinner, C.; Shobha, T.; Mehdipour, M.; Liu, H.; Huang, W.; Lan, F.; Bray, N. L.; Li, S.; Corn, J. E.; Kataoka, K.; Doudna, J. A.; Conboy, I.; Murthy, N. Nanoparticle Delivery of Cas9 Ribonucleoprotein and Donor DNA in Vivo Induces Homology-Directed DNA Repair. *Nature Biomedical Engineering* **2017**, *1* (11), 889–901. https://doi.org/10.1038/s41551-017-0137-2.

(107)   Schwab, F.; Zhai, G.; Kern, M.; Turner, A.; Schnoor, J. L.; Wiesner, M. R. Barriers, Pathways and Processes for Uptake, Translocation and Accumulation of Nanomaterials in Plants – Critical Review. *Nanotoxicology* **2015**, *10* (3), 1–22. https://doi.org/10.3109/17435390.2015.1048326.

(108)   Wang, P.; Lombi, E.; Zhao, F.-J.; Kopittke, P. M. Nanotechnology: A New Opportunity in Plant Sciences. *Trends in Plant Science* **2016**, *21* (8), 699–712. https://doi.org/10.1016/j.tplants.2016.04.005.

(109)   Cosgrove, D. J. Assembly and Enlargement of the Primary Cell Wall in Plants. *Annual Review of Cell and Developmental Biology* **1997**, *13* (1), 171–201. https://doi.org/10.1146/annurev.cellbio.13.1.171.

(110)   Eichert, T.; Goldbach, H. E. Equivalent Pore Radii of Hydrophilic Foliar Uptake Routes in Stomatous and Astomatous Leaf Surfaces – Further Evidence for a Stomatal Pathway. *Physiologia Plantarum* **2008**, *132* (4), 491–502. https://doi.org/10.1111/j.1399-3054.2007.01023.x.

(111)   Eichert, T.; Kurtz, A.; Steiner, U.; Goldbach, H. E. Size Exclusion Limits and Lateral Heterogeneity of the Stomatal Foliar Uptake Pathway for Aqueous Solutes and Water-Suspended Nanoparticles. *Physiologia Plantarum* **2008**, *134* (1), 151–160. https://doi.org/10.1111/j.1399-3054.2008.01135.x.

(112)   Ma, X.; Geiser-Lee, J.; Deng, Y.; Kolmakov, A. Interactions between Engineered Nanoparticles (ENPs) and Plants: Phytotoxicity, Uptake and Accumulation. *Science of The Total Environment* **2010**, *408* (16), 3053–3061. https://doi.org/10.1016/J.SCITOTENV.2010.03.031.

(113)   Larue, C.; Castillo-Michel, H.; Sobanska, S.; Cécillon, L.; Bureau, S.; Barthès, V.; Ouerdane, L.; Carrière, M.; Sarret, G. Foliar Exposure of the Crop Lactuca Sativa to Silver Nanoparticles: Evidence for Internalization and Changes in Ag Speciation. *Journal of Hazardous Materials* **2014**, *264*, 98–106. https://doi.org/10.1016/j.jhazmat.2013.10.053.

(114)   Tripathi, D. K.; Shweta; Singh, S.; Singh, S.; Pandey, R.; Singh, V. P.; Sharma, N. C.; Prasad, S. M.; Dubey, N. K.; Chauhan, D. K. An Overview on Manufactured Nanoparticles in Plants: Uptake, Translocation, Accumulation and Phytotoxicity. *Plant Physiology and Biochemistry* **2017**, *110*, 2–12. https://doi.org/10.1016/j.plaphy.2016.07.030.

(115)   Chesson, A.; Gardner, P. T.; Wood, T. J. Cell Wall Porosity and Available Surface Area of Wheat Straw and Wheat Grain Fractions. *Journal of the Science of Food and Agriculture* **1997**, *75* (3), 289–295. https://doi.org/10.1002/(SICI)1097-0010(199711)75:3<289::AID-JSFA879>3.0.CO;2-R.

(116) McCann, M.C.; Wells, B.; Roberts, K. Direct Visualization of Cross-Links in the Primary Plant Cell Wall. *Journal of Cell Science* **1990**, *96*, 323–334.

(117) Jiang, Y.; Lawrence, M.; Ansell, M. P.; Hussain, A. Cell Wall Microstructure, Pore Size Distribution and Absolute Density of Hemp Shiv. *R. Soc. open sci.* **2018**, *5* (4), 171945. https://doi.org/10.1098/rsos.171945.

(118) MCCANN, M. C.; WELLS, B.; ROBERTS, K. Direct Visualization of Cross-Links in the Primary Plant Cell Wall. *Journal of Cell Science* **1990**, *96* (2), 323–334. https://doi.org/10.1242/jcs.96.2.323.

(119) Jiang, Y.; Lawrence, M.; Ansell, M. P.; Hussain, A. Cell Wall Microstructure, Pore Size Distribution and Absolute Density of Hemp Shiv. *Royal Society Open Science 5* (4), 171945. https://doi.org/10.1098/rsos.171945.

(120) Raliya, R.; Franke, C.; Chavalmane, S.; Nair, R.; Reed, N.; Biswas, P. Quantitative Understanding of Nanoparticle Uptake in Watermelon Plants. *Frontiers in plant science* **2016**, *7*, 1288. https://doi.org/10.3389/fpls.2016.01288.

(121) Karny, A.; Zinger, A.; Kajal, A.; Shainsky-Roitman, J.; Schroeder, A. Therapeutic Nanoparticles Penetrate Leaves and Deliver Nutrients to Agricultural Crops. *Scientific Reports* **2018**, *8* (1), 1–10. https://doi.org/10.1038/s41598-018-25197-y.

(122) Katagiri, F.; Thilmony, R.; He, S. Y. The Arabidopsis Thaliana-Pseudomonas Syringae Interaction. *Arabidopsis Book* **2002**, *1*. https://doi.org/10.1199/tab.0039.

(123) Mad' Atari, M. F. bin; Folta, K. M. Transformation Improvement with the Standardized Pressure Agrobacterium Infiltration Device (SPAID). *BMC Res Notes* **2019**, *12* (1), 144. https://doi.org/10.1186/s13104-019-4117-3.

(124) Carpita, N.; Sabularse, D.; Montezinos, D.; Delmer, D. P. Determination of the Pore Size of Cell Walls of Living Plant Cells. *Science* **1979**, *205* (4411), 1144–1147. https://doi.org/10.1126/science.205.4411.1144.

(125) Medeiros, A. H.; Franco, F. P.; Matos, J. L.; de Castro, P. A.; Santos-Silva, L. K.; Henrique-Silva, F.; Goldman, G. H.; Moura, D. S.; Silva-Filho, M. C. Sugarwin: A Sugarcane Insect-Induced Gene with Antipathogenic Activity. *MPMI* **2012**, *25* (5), 613–624. https://doi.org/10.1094/MPMI-09-11-0254.

(126) Milewska-Hendel, A.; Zubko, M.; Karcz, J.; Stróż, D.; Kurczyńska, E. Fate of Neutral-Charged Gold Nanoparticles in the Roots of the Hordeum Vulgare L. Cultivar Karat. *Sci Rep* **2017**, *7* (1), 1–13. https://doi.org/10.1038/s41598-017-02965-w.

(127) Etxeberria, E.; Gonzalez, P.; Baroja-Fernandez, E.; Romero, J. P. Fluid Phase Endocytic Uptake of Artificial Nano-Spheres and Fluorescent Quantum Dots by Sycamore Cultured Cells: Evidence for the Distribution of Solutes to Different Intracellular Compartments. *Plant signaling & behavior* **2006**, *1* (4), 196–200.

(128) Zhai, G.; Walters, K. S.; Peate, D. W.; Alvarez, P. J. J.; Schnoor, J. L. Transport of Gold Nanoparticles through Plasmodesmata and Precipitation of Gold Ions in Woody Poplar. *Environ. Sci. Technol. Lett.* **2014**, *1* (2), 146–151. https://doi.org/10.1021/ez400202b.

(129) Midorikawa, K.; Kodama, Y.; Numata, K. Vacuum/Compression Infiltration-Mediated Permeation Pathway of a Peptide-PDNA Complex as a Non-Viral Carrier for Gene Delivery in Planta. *Scientific Reports* **2019**, *9* (1), 271. https://doi.org/10.1038/s41598-018-36466-1.

(130) Bayer, E.; Thomas, C. L.; Maule, A. J. Plasmodesmata in Arabidopsis Thaliana Suspension Cells. *Protoplasma* **2004**, *223* (2), 93–102. https://doi.org/10.1007/s00709-004-0044-8.

(131) Surpin, M.; Raikhel, N. Traffic Jams Affect Plant Development and Signal Transduction. *Nature Reviews Molecular Cell Biology* **2004**, *5* (2), 100–109. https://doi.org/10.1038/nrm1311.

(132) Fouad, M.; Kaji, N.; Jabasini, M.; Tokeshi, M.; Baba, Y. NANOTECHNOLOGY MEETS PLANT BIOTECHNOLOGY: CARBON NANOTUBES DELIVER DNA AND INCORPORATE INTO THE PLANT CELL STRUCTURE. *San Diego* **2008**, 3.

(133) Cheuk, A.; Houde, M. A Rapid and Efficient Method for Uniform Gene Expression Using the Barley Stripe Mosaic Virus. *Plant Methods* **2017**, *13* (1), 24. https://doi.org/10.1186/s13007-017-0175-5.

(134) Contento, A. L.; Bassham, D. C. Structure and Function of Endosomes in Plant Cells. *Journal of Cell Science* **2012**, *125* (15), 3511–3518. https://doi.org/10.1242/jcs.093559.

(135) Al-Dosari, M. S.; Gao, X. Nonviral Gene Delivery: Principle, Limitations, and Recent Progress. *The AAPS journal* **2009**, *11* (4), 671–681. https://doi.org/10.1208/s12248-009-9143-y.

(136) Fu, A.; Tang, R.; Hardie, J.; Farkas, M. E.; Rotello, V. M. Promises and Pitfalls of Intracellular Delivery of Proteins. *Bioconjugate Chem.* **2014**, *25* (9), 1602–1608. https://doi.org/10.1021/bc500320j.

(137) Zhang, Y.; Røise, J. J.; Lee, K.; Li, J.; Murthy, N. Recent Developments in Intracellular Protein Delivery. *Current Opinion in Biotechnology* **2018**, *52*, 25–31. https://doi.org/10.1016/j.copbio.2018.02.009.

(138) Won, Y.-Y.; Sharma, R.; Konieczny, S. F. Missing Pieces in Understanding the Intracellular Trafficking of Polycation/DNA Complexes. *J Control Release* **2009**, *139* (2), 88–93. https://doi.org/10.1016/j.jconrel.2009.06.031.

(139) Pei, D.; Buyanova, M. Overcoming Endosomal Entrapment in Drug Delivery. *Bioconjug Chem* **2019**, *30* (2), 273–283. https://doi.org/10.1021/acs.bioconjchem.8b00778.

(140) Lakshmanan, M.; Kodama, Y.; Yoshizumi, T.; Sudesh, K.; Numata, K. Rapid and Efficient Gene Delivery into Plant Cells Using Designed Peptide Carriers. *Biomacromolecules* **2013**, *14* (1), 10–16. https://doi.org/10.1021/bm301275g.

(141) Guo, B.; Itami, J.; Oikawa, K.; Motoda, Y.; Kigawa, T.; Numata, K. Native Protein Delivery into Rice Callus Using Ionic Complexes of Protein and Cell-Penetrating Peptides. *PLOS ONE* **2019**, *14* (7), e0214033. https://doi.org/10.1371/journal.pone.0214033.

(142) Liu, W.; Rudis, M. R.; Cheplick, M. H.; Millwood, R. J.; Yang, J.-P.; Ondzighi-Assoume, C. A.; Montgomery, G. A.; Burris, K. P.; Mazarei, M.; Chesnut, J. D.; Stewart, C. N. Lipofection-Mediated Genome Editing Using DNA-Free Delivery of the Cas9/GRNA Ribonucleoprotein into Plant Cells. *Plant Cell Rep* **2020**, *39* (2), 245–257. https://doi.org/10.1007/s00299-019-02488-w.

(143) Vijayaraghavan, K.; Ashokkumar, T. Plant-Mediated Biosynthesis of Metallic Nanoparticles: A Review of Literature, Factors Affecting Synthesis, Characterization Techniques and Applications. *Journal of Environmental Chemical Engineering* **2017**, *5* (5), 4866–4883. https://doi.org/10.1016/j.jece.2017.09.026.

(144) Baker, S.; Volova, T.; Prudnikova, S. V.; Satish, S.; Prasad M.N., N. Nanoagroparticles Emerging Trends and Future Prospect in Modern Agriculture System. *Environmental Toxicology and Pharmacology*. July 2017, pp 10–17. https://doi.org/10.1016/j.etap.2017.04.012.

(145)   Zuverza-Mena, N.; Martínez-Fernández, D.; Du, W.; Hernandez-Viezcas, J. A.; Bonilla-Bird, N.; López-Moreno, M. L.; Komárek, M.; Peralta-Videa, J. R.; Gardea-Torresdey, J. L. Exposure of Engineered Nanomaterials to Plants: Insights into the Physiological and Biochemical Responses-A Review. *Plant Physiology and Biochemistry*. Elsevier Masson January 1, 2017, pp 236–264. https://doi.org/10.1016/j.plaphy.2016.05.037.

(146)   Hussain, H. I.; Yi, Z.; Rookes, J. E.; Kong, L. X.; Cahill, D. M. Mesoporous Silica Nanoparticles as a Biomolecule Delivery Vehicle in Plants. *Journal of Nanoparticle Research* **2013**, *15* (6), 1676–1676. https://doi.org/10.1007/s11051-013-1676-4.

(147)   Liu, Q.; Chen, B.; Wang, Q.; Shi, X.; Xiao, Z.; Lin, J.; Fang, X. Carbon Nanotubes as Molecular Transporters for Walled Plant Cells. *Nano Letters* **2009**, *9* (3), 1007–1010. https://doi.org/10.1021/nl803083u.

(148)   Koo, Y.; Wang, J.; Zhang, Q.; Zhu, H.; Chehab, E. W.; Colvin, V. L.; Alvarez, P. J. J.; Braam, J. Fluorescence Reports Intact Quantum Dot Uptake into Roots and Translocation to Leaves of *Arabidopsis Thaliana* and Subsequent Ingestion by Insect Herbivores. *Environmental Science & Technology* **2015**, *49* (1), 626–632. https://doi.org/10.1021/es5050562.

(149)   Kurepa, J.; Paunesku, T.; Vogt, S.; Arora, H.; Rabatic, B. M.; Lu, J.; Wanzer, M. B.; Woloschak, G. E.; Smalle, J. A. Uptake and Distribution of Ultrasmall Anatase TiO_2 Alizarin Red S Nanoconjugates in *Arabidopsis Thaliana*. *Nano Letters* **2010**, *10* (7), 2296–2302. https://doi.org/10.1021/nl903518f.

(150)   González-Melendi, P.; Fernández-Pacheco, R.; Coronado, M. J.; Corredor, E.; Testillano, P. S.; Risueño, M. C.; Marquina, C.; Ibarra, M. R.; Rubiales, D.; Pérez-de-Luque, A. Nanoparticles as Smart Treatment-Delivery Systems in Plants: Assessment of Different Techniques of Microscopy for Their Visualization in Plant Tissues. *Annals of Botany* **2008**, *101* (1), 187–195. https://doi.org/10.1093/aob/mcm283.

(151)   Larue, C.; Laurette, J.; Herlin-Boime, N.; Khodja, H.; Fayard, B.; Flank, A.-M.; Brisset, F.; Carriere, M. Accumulation, Translocation and Impact of TiO2 Nanoparticles in Wheat (Triticum Aestivum Spp.): Influence of Diameter and Crystal Phase. *Science of The Total Environment* **2012**, *431*, 197–208. https://doi.org/10.1016/j.scitotenv.2012.04.073.

(152)   Birnbaum, K. D.; Sánchez Alvarado, A. Slicing across Kingdoms: Regeneration in Plants and Animals. *Cell* **2008**, *132* (4), 697–710. https://doi.org/10.1016/j.cell.2008.01.040.

(153)   Zhu, Z.-J.; Wang, H.; Yan, B.; Zheng, H.; Jiang, Y.; Miranda, O. R.; Rotello, V. M.; Xing, B.; Vachet, R. W. Effect of Surface Charge on the Uptake and Distribution of Gold Nanoparticles in Four Plant Species. *Environmental Science & Technology* **2012**, *46* (22), 12391–12398. https://doi.org/10.1021/es301977w.

(154)   Martin-Ortigosa, S.; Valenstein, J. S.; Lin, V. S.-Y.; Trewyn, B. G.; Wang, K. Gold Functionalized Mesoporous Silica Nanoparticle Mediated Protein and DNA Codelivery to Plant Cells Via the Biolistic Method. *Advanced Functional Materials* **2012**, *22* (17), 3576–3582. https://doi.org/10.1002/adfm.201200359.

(155)   Liu, J.; Wang, F. H.; Wang, L. L.; Xiao, S. Y.; Tong, C. Y.; Tang, D. Y.; Liu, X. M. Preparation of Fluorescence Starch-Nanoparticle and Its Application as Plant Transgenic Vehicle. *Journal of Central South University of Technology (English Edition)* **2008**, *15* (6), 768–773. https://doi.org/10.1007/s11771-008-0142-4.

(156) Hao, Y.; Yang, X.; Shi, Y.; Song, S.; Xing, J.; Marowitch, J.; Chen, J. J. Magnetic Gold Nanoparticles as a Vehicle for Fluorescein Isothiocyanate and DNA Delivery into Plant Cells. *Botany* **2013**, *91* (7), 457–466. https://doi.org/10.1139/cjb-2012-0281.

(157) Finiuk, N.; Buziashvili, A.; Burlaka, O.; Zaichenko, A.; Mitina, N.; Miagkota, O.; Lobachevska, O.; Stoika, R.; Blume, Y.; Yemets, A. Investigation of Novel Oligoelectrolyte Polymer Carriers for Their Capacity of DNA Delivery into Plant Cells. *Plant Cell, Tissue and Organ Culture* **2017**, *131* (1), 27–39. https://doi.org/10.1007/s11240-017-1259-7.

(158) Pasupathy, K.; Lin, S.; Hu, Q.; Luo, H.; Ke, P. C. Direct Plant Gene Delivery with a Poly(Amidoamine) Dendrimer. *Biotechnology Journal* **2008**, *3* (8), 1078–1082. https://doi.org/10.1002/biot.200800021.

(159) Burlaka, O. M.; Pirko, Ya. V.; Yemets, A. I.; Blume, Ya. B. Plant Genetic Transformation Using Carbon Nanotubes for DNA Delivery. *Cytology and Genetics* **2015**, *49* (6), 349–357. https://doi.org/10.3103/S009545271506002X.

(160) Jiang, L.; Ding, L.; He, B.; Shen, J.; Xu, Z.; Yin, M.; Zhang, X. Systemic Gene Silencing in Plants Triggered by Fluorescent Nanoparticle-Delivered Double-Stranded RNA. *Nanoscale* **2014**, *6* (17), 9965. https://doi.org/10.1039/C4NR03481C.

(161) Chang, F.-P.; Kuang, L.-Y.; Huang, C.-A.; Jane, W.-N.; Hung, Y.; Hsing, Y. C.; Mou, C.-Y. A Simple Plant Gene Delivery System Using Mesoporous Silica Nanoparticles as Carriers. *Journal of Materials Chemistry B* **2013**, *1* (39), 5279. https://doi.org/10.1039/c3tb20529k.

(162) Li, T.; Liu, B.; Spalding, M. H.; Weeks, D. P.; Yang, B. High-Efficiency TALEN-Based Gene Editing Produces Disease-Resistant Rice. *Nature Biotechnology* **2012**, *30* (5), 390–392. https://doi.org/10.1038/nbt.2199.

(163) Liu, Y. Y.; Wu, H.; Chen, H.; Liu, Y. Y.; He, J.; Kang, H.; Sun, Z.; Pan, G.; Wang, Q.; Hu, J.; Zhou, F.; Zhou, K.; Zheng, X.; Ren, Y.; Chen, L.; Wang, Y.; Zhao, Z.; Lin, Q.; Wu, F.; Zhang, X.; Guo, X.; Cheng, X.; Jiang, L.; Wu, C.; Wang, H.; Wan, J. A Gene Cluster Encoding Lectin Receptor Kinases Confers Broad-Spectrum and Durable Insect Resistance in Rice. *Nature Biotechnology* **2015**, *33* (3), 301–305. https://doi.org/10.1038/nbt.3069.

(164) Kwak, S.-Y.; Lew, T. T. S.; Sweeney, C. J.; Koman, V. B.; Wong, M. H.; Bohmert-Tatarev, K.; Snell, K. D.; Seo, J. S.; Chua, N.-H.; Strano, M. S. Chloroplast-Selective Gene Delivery and Expression in Planta Using Chitosan-Complexed Single-Walled Carbon Nanotube Carriers. *Nature Nanotechnology* **2019**, *14* (5), 447–455. https://doi.org/10.1038/s41565-019-0375-4.

(165) Mitter, N.; Worrall, E. A.; Robinson, K. E.; Li, P.; Jain, R. G.; Taochy, C.; Fletcher, S. J.; Carroll, B. J.; Lu, G. Q.; Xu, Z. P. Clay Nanosheets for Topical Delivery of RNAi for Sustained Protection against Plant Viruses. *Nature Plants* **2017**, *3* (2). https://doi.org/10.1038/nplants.2016.207.

(166) Zhang, H.; Demirer, G. S.; Zhang, H.; Ye, T.; Goh, N. S.; Aditham, A. J.; Cunningham, F. J.; Fan, C.; Landry, M. P. DNA Nanostructures Coordinate Gene Silencing in Mature Plants. *Proc Natl Acad Sci USA* **2019**, *116* (15), 7543–7548. https://doi.org/10.1073/pnas.1818290116.

(167) Lei, W.-X.; An, Z.-S.; Zhang, B.-H.; Wu, Q.; Gong, W.-J.; Li, J.-M.; Chen, W.-L. Construction of Gold-SiRNANPR1 Nanoparticles for Effective and Quick Silencing of

NPR1 in Arabidopsis Thaliana. *RSC Adv.* **2020**, *10* (33), 19300–19308. https://doi.org/10.1039/D0RA02156C.

(168) Demirer, G. S.; Zhang, H.; Goh, N. S.; Pinals, R. L.; Chang, R.; Landry, M. P. Carbon Nanocarriers Deliver SiRNA to Intact Plant Cells for Efficient Gene Knockdown. *Science Advances* **2020**, *6* (26), 495–495. https://doi.org/10.1126/sciadv.aaz0495.

(169) Zhang, H.; Cao, Y.; Xu, D.; Goh, N. S.; Demirer, G. S.; Cestellos-Blanco, S.; Chen, Y.; Landry, M. P.; Yang, P. Gold-Nanocluster-Mediated Delivery of SiRNA to Intact Plant Cells for Efficient Gene Knockdown. *Nano Lett.* **2021**, *21* (13), 5859–5866. https://doi.org/10.1021/acs.nanolett.1c01792.

(170) Bao, W.; Wang, J.; Wang, Q.; O'Hare, D.; Wan, Y. Layered Double Hydroxide Nanotransporter for Molecule Delivery to Intact Plant Cells. *Scientific Reports* **2016**, *6* (1), 1–9. https://doi.org/10.1038/srep26738.

(171) Avellan, A.; Yun, J.; Zhang, Y.; Spielman-Sun, E.; Unrine, J. M.; Thieme, J.; Li, J.; Lombi, E.; Bland, G.; Lowry, G. V. Nanoparticle Size and Coating Chemistry Control Foliar Uptake Pathways, Translocation, and Leaf-to-Rhizosphere Transport in Wheat. *ACS Nano* **2019**, *13* (5), 5291–5305. https://doi.org/10.1021/acsnano.8b09781.

(172) Spielman-Sun, E.; Avellan, A.; D. Bland, G.; T. Clement, E.; V. Tappero, R.; S. Acerbo, A.; V. Lowry, G. Protein Coating Composition Targets Nanoparticles to Leaf Stomata and Trichomes. *Nanoscale* **2020**, *12* (6), 3630–3636. https://doi.org/10.1039/C9NR08100C.

(173) Chithrani, B. D.; Ghazani, A. A.; Chan, W. C. W. Determining the Size and Shape Dependence of Gold Nanoparticle Uptake into Mammalian Cells. *Nano Letters* **2006**, *6* (4), 662–668. https://doi.org/10.1021/nl052396o.

(174) Herd, H.; Daum, N.; Jones, A. T.; Huwer, H.; Ghandehari, H.; Lehr, C.-M. Nanoparticle Geometry and Surface Orientation Influence Mode of Cellular Uptake. *ACS Nano* **2013**, *7* (3), 1961–1973. https://doi.org/10.1021/nn304439f.

(175) Zhang, S.; Gao, H.; Bao, G. Physical Principles of Nanoparticle Cellular Endocytosis. *ACS nano* **2015**, *9* (9), 8655–8671. https://doi.org/10.1021/acsnano.5b03184.

(176) Xie, X.; Liao, J.; Shao, X.; Li, Q.; Lin, Y. The Effect of Shape on Cellular Uptake of Gold Nanoparticles in the Forms of Stars, Rods, and Triangles. *Scientific Reports* **2017**, *7* (1), 1–9. https://doi.org/10.1038/s41598-017-04229-z.

(177) Shi, X.; von dem Bussche, A.; Hurt, R. H.; Kane, A. B.; Gao, H. Cell Entry of One-Dimensional Nanomaterials Occurs by Tip Recognition and Rotation. *Nature Nanotechnology* **2011**, *6* (11), 714–719. https://doi.org/10.1038/nnano.2011.151.

(178) Vácha, R.; Martinez-Veracoechea, F. J.; Frenkel, D. Receptor-Mediated Endocytosis of Nanoparticles of Various Shapes. *Nano Letters* **2011**, *11* (12), 5391–5395. https://doi.org/10.1021/nl2030213.

(179) Huang, C.; Zhang, Y.; Yuan, H.; Gao, H.; Zhang, S. Role of Nanoparticle Geometry in Endocytosis: Laying down to Stand Up. *Nano Letters* **2013**, *13* (9), 4546–4550. https://doi.org/10.1021/nl402628n.

(180) Yi, X.; Shi, X.; Gao, H. A Universal Law for Cell Uptake of One-Dimensional Nanomaterials. *Nano Letters* **2014**, *14* (2), 1049–1055. https://doi.org/10.1021/nl404727m.

(181) Hui, Y.; Yi, X.; Hou, F.; Wibowo, D.; Zhang, F.; Zhao, D.; Gao, H.; Zhao, C.-X. Role of Nanoparticle Mechanical Properties in Cancer Drug Delivery. *ACS Nano* **2019**, *13* (7), 7410–7424. https://doi.org/10.1021/acsnano.9b03924.

(182) Houston, K.; Tucker, M. R.; Chowdhury, J.; Shirley, N.; Little, A. The Plant Cell Wall: A Complex and Dynamic Structure as Revealed by the Responses of Genes under Stress Conditions. *Frontiers in Plant Science* **2016**, *7* (AUG2016), 984–984. https://doi.org/10.3389/fpls.2016.00984.

(183) Cunningham, F. J.; Goh, N. S.; Demirer, G. S.; Matos, J. L.; Landry, M. P. Nanoparticle-Mediated Delivery towards Advancing Plant Genetic Engineering. *Trends in Biotechnology* **2018**, *36* (9), 882–897. https://doi.org/10.1016/j.tibtech.2018.03.009.

(184) Hubbard, J. D.; Lui, A.; Landry, M. P. Multiscale and Multidisciplinary Approach to Understanding Nanoparticle Transport in Plants: Multiscale and Multidisciplinary Approach to Understanding Nanoparticle Transport in Plants. *Current Opinion in Chemical Engineering* **2020**, *30*, 135–143. https://doi.org/10.1016/j.coche.2020.100659.

(185) Corredor, E.; Testillano, P. S.; Coronado, M.-J.; González-Melendi, P.; Fernández-Pacheco, R.; Marquina, C.; Ibarra, M. R.; de la Fuente, J. M.; Rubiales, D.; Pérez-de-Luque, A.; Risueño, M.-C. Nanoparticle Penetration and Transport in Living Pumpkin Plants: In Situsubcellular Identification. *BMC Plant Biology* **2009**, *9* (1), 45–45. https://doi.org/10.1186/1471-2229-9-45.

(186) Bao, D.; Oh, Z. G.; Chen, Z. Characterization of Silver Nanoparticles Internalized by Arabidopsis Plants Using Single Particle ICP-MS Analysis. *Frontiers in Plant Science* **2016**, *7*, 32–32.

(187) Zhang, P.; Xie, C.; Ma, Y.; He, X.; Zhang, Z.; Ding, Y.; Zheng, L.; Zhang, J. Shape-Dependent Transformation and Translocation of Ceria Nanoparticles in Cucumber Plants. **2017**. https://doi.org/10.1021/acs.estlett.7b00359.

(188) Giraldo, J. P.; Landry, M. P.; Faltermeier, S. M.; McNicholas, T. P.; Iverson, N. M.; Boghossian, A. A.; Reuel, N. F.; Hilmer, A. J.; Sen, F.; Brew, J. A. Plant Nanobionics Approach to Augment Photosynthesis and Biochemical Sensing. *Nature materials* **2014**, *13* (4), 400–400.

(189) Santana, I.; Wu, H.; Hu, P.; Giraldo, J. P. Targeted Delivery of Nanomaterials with Chemical Cargoes in Plants Enabled by a Biorecognition Motif. *Nat Commun* **2020**, *11* (1), 2045. https://doi.org/10.1038/s41467-020-15731-w.

(190) Zhang, X.; Servos, M. R.; Liu, J. Instantaneous and Quantitative Functionalization of Gold Nanoparticles with Thiolated DNA Using a PH-Assisted and Surfactant-Free Route. *Journal of the American Chemical Society* **2012**, *134* (17), 7266–7269. https://doi.org/10.1021/ja3014055.

(191) Yang, G.; Liu, Y.; Hui, Y.; Tengjisi; Chen, D.; Weitz, D. A.; Zhao, C.-X. Implications of Quenching-to-Dequenching Switch in Quantitative Cell Uptake and Biodistribution of Dye-Labeled Nanoparticles. *Angewandte Chemie* **2021**, *133* (28), 15554–15563. https://doi.org/10.1002/ange.202101730.

(192) Sattelmacher, B. The Apoplast and Its Significance for Plant Mineral Nutrition. *New Phytologist* **2001**, *149* (2), 167–192. https://doi.org/10.1046/j.1469-8137.2001.00034.x.

(193) Yu, M.; Wang, J.; Yang, Y.; Zhu, C.; Su, Q.; Guo, S.; Sun, J.; Gan, Y.; Shi, X.; Gao, H. Rotation-Facilitated Rapid Transport of Nanorods in Mucosal Tissues. **2016**. https://doi.org/10.1021/acs.nanolett.6b03515.

(194) Matsuoka, K.; Bassham, D. C.; Raikhel, N. V.; Nakamura, K. Different Sensitivity to Wortmannin of Two Vacuolar Sorting Signals Indicates the Presence of Distinct Sorting Machineries in Tobacco Cells. *Journal of Cell Biology* **1995**, *130* (6), 1307–1318. https://doi.org/10.1083/jcb.130.6.1307.

(195)   Elkin, S. R.; Oswald, N. W.; Reed, D. K.; Mettlen, M.; MacMillan, J. B.; Schmid, S. L. Ikarugamycin: A Natural Product Inhibitor of Clathrin-Mediated Endocytosis. *Traffic* **2016**, *17* (10), 1139–1149. https://doi.org/10.1111/tra.12425.

(196)   Aniento, F.; Robinson, D. G. Testing for Endocytosis in Plants. *Protoplasma* **2005**, *226* (1–2), 3–11. https://doi.org/10.1007/s00709-005-0101-y.

(197)   Reynolds, G. D.; Wang, C.; Pan, J.; Bednarek, S. Y. Inroads into Internalization: Five Years of Endocytic Exploration1[OPEN]. *Plant Physiol* **2018**, *176* (1), 208–218. https://doi.org/10.1104/pp.17.01117.

(198)   Meister, G.; Tuschl, T. Mechanisms of Gene Silencing by Double-Stranded RNA. *Nature* **2004**, *431* (7006), 343–349. https://doi.org/10.1038/nature02873.

(199)   Tiwari, M.; Sharma, D.; Trivedi, P. K. Artificial MicroRNA Mediated Gene Silencing in Plants: Progress and Perspectives. *Plant Molecular Biology* **2014**, *86* (1–2). https://doi.org/10.1007/s11103-014-0224-7.

(200)   Bennett, M.; Deikman, J.; Hendrix, B.; Iandolino, A. Barriers to Efficient Foliar Uptake of DsRNA and Molecular Barriers to DsRNA Activity in Plant Cells. *Frontiers in Plant Science* **2020**, *11*.

(201)   Pinals, R. L.; Yang, D.; Lui, A.; Cao, W.; Landry, M. P. Corona Exchange Dynamics on Carbon Nanotubes by Multiplexed Fluorescence Monitoring. *J. Am. Chem. Soc.* **2020**, *142* (3), 1254.

(202)   Geilfus, C.-M. The PH of the Apoplast: Dynamic Factor with Functional Impact Under Stress. *Molecular Plant* **2017**, *10* (11), 1371–1386. https://doi.org/10.1016/j.molp.2017.09.018.

(203)   Mori, I. C.; Schroeder, J. I. Reactive Oxygen Species Activation of Plant Ca2+ Channels. A Signaling Mechanism in Polar Growth, Hormone Transduction, Stress Signaling, and Hypothetically Mechanotransduction. *Plant Physiology* **2004**, *135* (2), 702–708. https://doi.org/10.1104/pp.104.042069.

(204)   Chehab, E. W.; Eich, E.; Braam, J. Thigmomorphogenesis: A Complex Plant Response to Mechano-Stimulation. *Journal of Experimental Botany* **2009**, *60* (1), 43–56. https://doi.org/10.1093/jxb/ern315.

(205)   Baldock, B. L.; Hutchison, J. E. UV–Visible Spectroscopy-Based Quantification of Unlabeled DNA Bound to Gold Nanoparticles. *Anal. Chem.* **2016**, *88* (24), 12072–12080. https://doi.org/10.1021/acs.analchem.6b02640.

(206)   Marcus, M. A.; MacDowell, A. A.; Celestre, R.; Manceau, A.; Miller, T.; Padmore, H. A.; Sublett, R. E. Beamline 10.3.2 at ALS: A Hard X-Ray Microprobe for Environmental and Materials Sciences. *J Synchrotron Rad* **2004**, *11* (3), 239–247. https://doi.org/10.1107/S0909049504005837.

(207)   Mitov, M. I.; Greaser, M. L.; Campbell, K. S. GelBandFitter – A Computer Program for Analysis of Closely Spaced Electrophoretic and Immunoblotted Bands. *Electrophoresis* **2009**, *30* (5), 848–851. https://doi.org/10.1002/elps.200800583.

(208)   Toni, L. S.; Garcia, A. M.; Jeffrey, D. A.; Jiang, X.; Stauffer, B. L.; Miyamoto, S. D.; Sucharov, C. C. Optimization of Phenol-Chloroform RNA Extraction. *MethodsX* **2018**, *5*, 599–608. https://doi.org/10.1016/j.mex.2018.05.011.

(209)   O'Leary, B. M.; Rico, A.; McCraw, S.; Fones, H. N.; Preston, G. M. The Infiltration-Centrifugation Technique for Extraction of Apoplastic Fluid from Plant Leaves Using Phaseolus Vulgaris as an Example. *JoVE* **2014**, No. 94, e52113–e52113. https://doi.org/10.3791/52113.

(210) Nicot, N.; Hausman, J.-F.; Hoffmann, L.; Evers, D. Housekeeping Gene Selection for Real-Time RT-PCR Normalization in Potato during Biotic and Abiotic Stress. *Journal of Experimental Botany* **2005**, *56* (421), 2907–2914. https://doi.org/10.1093/jxb/eri285.

(211) Selvakesavan, R. K.; Franklin, G. Nanoparticles Affect the Expression Stability of Housekeeping Genes in Plant Cells. *Nanotechnology, Science and Applications* **2020**, *13*, 77–88. https://doi.org/10.2147/NSA.S265641.

(212) Schmittgen, T. D.; Livak, K. J. Analyzing Real-Time PCR Data by the Comparative CT Method. *Nature Protocols* **2008**, *3* (6), 1101–1108. https://doi.org/10.1038/nprot.2008.73.

(213) Borniego, M. L.; Molina, M. C.; Guiamét, J. J.; Martinez, D. E. Physiological and Proteomic Changes in the Apoplast Accompany Leaf Senescence in Arabidopsis. *Frontiers in Plant Science* **2020**, *10*.

(214) Tsai, D.-H.; Shelton, M. P.; DelRio, F. W.; Elzey, S.; Guha, S.; Zachariah, M. R.; Hackley, V. A. Quantifying Dithiothreitol Displacement of Functional Ligands from Gold Nanoparticles. *Anal Bioanal Chem* **2012**, *404* (10), 3015–3023. https://doi.org/10.1007/s00216-012-6418-4.

(215) Liang, P.; Canoura, J.; Yu, H.; Alkhamis, O.; Xiao, Y. Dithiothreitol-Regulated Coverage of Oligonucleotide-Modified Gold Nanoparticles To Achieve Optimized Biosensor Performance. *ACS Appl. Mater. Interfaces* **2018**, *10* (4), 4233–4242. https://doi.org/10.1021/acsami.7b16914.

(216) Yoshioka, H.; Numata, N.; Nakajima, K.; Katou, S.; Kawakita, K.; Rowland, O.; Jones, J. D. G.; Doke, N. Nicotiana Benthamiana Gp91phox Homologs Nbrboha and Nbrbohb Participate in H2O2 Accumulation and Resistance to Phytophthora Infestans. *Plant Cell* **2003**, *15* (3), 706–718. https://doi.org/10.1105/tpc.008680.

(217) Pombo, M. A.; Ramos, R. N.; Zheng, Y.; Fei, Z.; Martin, G. B.; Rosli, H. G. Transcriptome-Based Identification and Validation of Reference Genes for Plant-Bacteria Interaction Studies Using Nicotiana Benthamiana. *Sci Rep* **2019**, *9* (1), 1632. https://doi.org/10.1038/s41598-018-38247-2.

(218) Shen, D.; Chai, C.; Ma, L.; Zhang, M.; Dou, D. Comparative RNA-Seq Analysis of Nicotiana Benthamiana in Response to Phytophthora Parasitica Infection. *Plant Growth Regul* **2016**, *80* (1), 59–67. https://doi.org/10.1007/s10725-016-0163-1.

(219) Safavi-Rizi, V.; Herde, M.; Stöhr, C. Identification of Nitric Oxide (NO)-Responsive Genes under Hypoxia in Tomato (Solanum Lycopersicum L.) Root. *Sci Rep* **2020**, *10* (1), 16509. https://doi.org/10.1038/s41598-020-73613-z.

(220) Deng, X.-G.; Zhu, T.; Zhang, D.-W.; Lin, H.-H. The Alternative Respiratory Pathway Is Involved in Brassinosteroid-Induced Environmental Stress Tolerance in Nicotiana Benthamiana. *Journal of Experimental Botany* **2015**, *66* (20), 6219–6232. https://doi.org/10.1093/jxb/erv328.

(221) Zhang, H.-X.; Zhu, W.-C.; Feng, X.-H.; Jin, J.-H.; Wei, A.-M.; Gong, Z.-H. Transcription Factor CaSBP12 Negatively Regulates Salt Stress Tolerance in Pepper (Capsicum Annuum L.). *International Journal of Molecular Sciences* **2020**, *21* (2), 444. https://doi.org/10.3390/ijms21020444.

(222) Qin, C.; Ahanger, M. A.; Lin, B.; Huang, Z.; Zhou, J.; Ahmed, N.; Ai, S.; Mustafa, N. S. A.; Ashraf, M.; Zhang, L. Comparative Transcriptome Analysis Reveals the Regulatory Effects of Acetylcholine on Salt Tolerance of Nicotiana Benthamiana. *Phytochemistry* **2021**, *181*, 112582. https://doi.org/10.1016/j.phytochem.2020.112582.

(223) Kuang, C.; Li, S.; Liu, W.; Hao, X.; Gu, Z.; Wang, Y.; Ge, J.; Li, H.; Liu, X. Breaking the Diffraction Barrier Using Fluorescence Emission Difference Microscopy. *Sci Rep* **2013**, *3* (1), 1441. https://doi.org/10.1038/srep01441.

(224) González-Grandío, E.; Demirer, G. S.; Jackson, C. T.; Yang, D.; Ebert, S.; Molawi, K.; Keller, H.; Landry, M. P. Carbon Nanotube Biocompatibility in Plants Is Determined by Their Surface Chemistry. *Journal of Nanobiotechnology* **2021**, *19* (1), 431. https://doi.org/10.1186/s12951-021-01178-8.

(225) Yang, H.; Chen, Z.; Zhang, L.; Yung, W.-Y.; Leung, K. C.-F.; Chan, H. Y. E.; Choi, C. H. J. Mechanism for the Cellular Uptake of Targeted Gold Nanorods of Defined Aspect Ratios. *Small* **2016**, *12* (37), 5178–5189. https://doi.org/10.1002/smll.201601483.

(226) Oliveira, S.; van Rooy, I.; Kranenburg, O.; Storm, G.; Schiffelers, R. M. Fusogenic Peptides Enhance Endosomal Escape Improving SiRNA-Induced Silencing of Oncogenes. *International Journal of Pharmaceutics* **2007**, *331* (2), 211–214. https://doi.org/10.1016/j.ijpharm.2006.11.050.

(227) Whitehead, K. A.; Langer, R.; Anderson, D. G. Knocking down Barriers: Advances in SiRNA Delivery. *Nat Rev Drug Discov* **2009**, *8* (2), 129–138. https://doi.org/10.1038/nrd2742.

(228) Du Rietz, H.; Hedlund, H.; Wilhelmson, S.; Nordenfelt, P.; Wittrup, A. Imaging Small Molecule-Induced Endosomal Escape of SiRNA. *Nat Commun* **2020**, *11* (1), 1809. https://doi.org/10.1038/s41467-020-15300-1.

(229) Altpeter, F.; Springer, N. M.; Bartley, L. E.; Blechl, A. E.; Brutnell, T. P.; Citovsky, V.; Conrad, L. J.; Gelvin, S. B.; Jackson, D. P.; Kausch, A. P.; Lemaux, P. G.; Medford, J. I.; Orozco-Cárdenas, M. L.; Tricoli, D. M.; Van Eck, J.; Voytas, D. F.; Walbot, V.; Wang, K.; Zhang, Z. J.; Stewart, C. N., Jr. Advancing Crop Transformation in the Era of Genome Editing. *The Plant Cell* **2016**, *28* (7), 1510–1520. https://doi.org/10.1105/tpc.16.00196.

(230) Herrera-Estrella, L.; Depicker, A.; Van Montagu, M.; Schell, J. Expression of Chimaeric Genes Transferred into Plant Cells Using a Ti-Plasmid-Derived Vector. *Nature* **1983**, *303* (5914), 209–213. https://doi.org/10.1038/303209a0.

(231) Baltes, N. J.; Gil-Humanes, J.; Voytas, D. F. Genome Engineering and Agriculture: Opportunities and Challenges. *Progress in Molecular Biology and Translational Science* **2017**, *149*, 1–26. https://doi.org/10.1016/bs.pmbts.2017.03.011.

(232) Ibrahim, A.; Odon, V.; Kormelink, R. Plant Viruses in Plant Molecular Pharming: Toward the Use of Enveloped Viruses. *Front Plant Sci* **2019**, *10*, 803. https://doi.org/10.3389/fpls.2019.00803.

(233) Gleba, Y.; Klimyuk, V.; Marillonnet, S. Viral Vectors for the Expression of Proteins in Plants. *Current Opinion in Biotechnology* **2007**, *18* (2), 134–141. https://doi.org/10.1016/j.copbio.2007.03.002.

(234) Song, S.; Hao, Y.; Yang, X.; Patra, P.; Chen, J. Using Gold Nanoparticles as Delivery Vehicles for Targeted Delivery of Chemotherapy Drug Fludarabine Phosphate to Treat Hematological Cancers. *Journal of Nanoscience and Nanotechnology* **2016**, *16* (3), 2582–2586. https://doi.org/10.1166/jnn.2016.12349.

(235) Mizrachi, A.; Shamay, Y.; Shah, J.; Brook, S.; Soong, J.; Rajasekhar, V. K.; Humm, J. L.; Healey, J. H.; Powell, S. N.; Baselga, J.; Heller, D. A.; Haimovitz-Friedman, A.; Scaltriti, M. Tumour-Specific PI3K Inhibition via Nanoparticle-Targeted Delivery in

Head and Neck Squamous Cell Carcinoma. *Nat Commun* **2017**, *8* (1), 14292. https://doi.org/10.1038/ncomms14292.

(236) Demirer, G. S.; Landry, M. P. Delivering Genes to Plants. *Chemical Engineering Progress* **2017**, *113* (4).

(237) Martin-Ortigosa, S.; Valenstein, J. S.; Sun, W.; Moeller, L.; Fang, N.; Trewyn, B. G.; Lin, V. S.-Y.; Wang, K. Parameters Affecting the Efficient Delivery of Mesoporous Silica Nanoparticle Materials and Gold Nanorods into Plant Tissues by the Biolistic Method. *Small* **2012**, *8* (3), 413–422. https://doi.org/10.1002/smll.201101294.

(238) Liu, J.; Wang, F. H.; Wang, L. L.; Xiao, S. Y.; Tong, C. Y.; Tang, D. Y.; Liu, X. M. Preparation of Fluorescence Starch-Nanoparticle and Its Application as Plant Transgenic Vehicle. *Journal of Central South University of Technology (English Edition)* **2008**, *15* (6), 768–773. https://doi.org/10.1007/s11771-008-0142-4.

(239) Chang, F.-P.; Kuang, L.-Y.; Huang, C.-A.; Jane, W.-N.; Hung, Y.; Hsing, Y. C.; Mou, C.-Y. A Simple Plant Gene Delivery System Using Mesoporous Silica Nanoparticles as Carriers. *Journal of Materials Chemistry B* **2013**, *1* (39), 5279–5279. https://doi.org/10.1039/c3tb20529k.

(240) Bao, W.; Wan, Y.; Baluška, F. Nanosheets for Delivery of Biomolecules into Plant Cells. *Trends in Plant Science* **2017**, *22* (6), 445–447. https://doi.org/10.1016/j.tplants.2017.03.014.

(241) Wong, M. H.; Misra, R. P.; Giraldo, J. P.; Kwak, S.-Y.; Son, Y.; Landry, M. P.; Swan, J. W.; Blankschtein, D.; Strano, M. S. Lipid Exchange Envelope Penetration (LEEP) of Nanoparticles for Plant Engineering: A Universal Localization Mechanism. *Nano Lett* **2016**, *16*, 43–43. https://doi.org/10.1021/acs.nanolett.5b04467.

(242) Wu, Y.; Phillips, J. A.; Liu, H.; Yang, R.; Tan, W. Carbon Nanotubes Protect DNA Strands during Cellular Delivery. *ACS Nano* **2008**, *2* (10), 2023–2028. https://doi.org/10.1021/nn800325a.

(243) Zheng, M.; Jagota, A.; Semke, E. D.; Diner, B. A.; Mclean, R. S.; Lustig, S. R.; Richardson, R. E.; Tassi, N. G. DNA-Assisted Dispersion and Separation of Carbon Nanotubes. *Nature Mater* **2003**, *2* (5), 338–342. https://doi.org/10.1038/nmat877.

(244) Wang, H.; Koleilat, G. I.; Liu, P.; Jiménez-Osés, G.; Lai, Y.-C.; Vosgueritchian, M.; Fang, Y.; Park, S.; Houk, K. N.; Bao, Z. High-Yield Sorting of Small-Diameter Carbon Nanotubes for Solar Cells and Transistors. *ACS Nano* **2014**, *8* (3), 2609–2617. https://doi.org/10.1021/nn406256y.

(245) Serag, M. F.; Kaji, N.; Gaillard, C.; Okamoto, Y.; Terasaka, K.; Jabasini, M.; Tokeshi, M.; Mizukami, H.; Bianco, A.; Baba, Y. Trafficking and Subcellular Localization of Multiwalled Carbon Nanotubes in Plant Cells. *ACS Nano* **2011**, *5* (1), 493–499. https://doi.org/10.1021/nn102344t.

(246) Wong, M. H.; Giraldo, J. P.; Kwak, S.-Y.; Koman, V. B.; Sinclair, R.; Lew, T. T. S.; Bisker, G.; Liu, P.; Strano, M. S. Nitroaromatic Detection and Infrared Communication from Wild-Type Plants Using Plant Nanobionics. *Nature Materials* **2017**, *16* (2), 264–272. https://doi.org/10.1038/nmat4771.

(247) Tinland, B. The Integration of T-DNA into Plant Genomes. *Trends in Plant Science* **1996**, *1* (6), 178–184. https://doi.org/10.1016/1360-1385(96)10020-0.

(248) McDermott, G. P.; Do, D.; Litterst, C. M.; Maar, D.; Hindson, C. M.; Steenblock, E. R.; Legler, T. C.; Jouvenot, Y.; Marrs, S. H.; Bemis, A.; Shah, P.; Wong, J.; Wang, S.; Sally, D.; Javier, L.; Dinio, T.; Han, C.; Brackbill, T. P.; Hodges, S. P.; Ling, Y.; Klitgord, N.;

Carman, G. J.; Berman, J. R.; Koehler, R. T.; Hiddessen, A. L.; Walse, P.; Bousse, L.; Tzonev, S.; Hefner, E.; Hindson, B. J.; Cauly, T. H.; Hamby, K.; Patel, V. P.; Regan, J. F.; Wyatt, P. W.; Karlin-Neumann, G. A.; Stumbo, D. P.; Lowe, A. J. Multiplexed Target Detection Using DNA-Binding Dye Chemistry in Droplet Digital PCR. *Anal. Chem.* **2013**, *85* (23), 11619–11627. https://doi.org/10.1021/ac403061n.

(249) Głowacka, K.; Kromdijk, J.; Leonelli, L.; Niyogi, K. K.; Clemente, T. E.; Long, S. P. An Evaluation of New and Established Methods to Determine T-DNA Copy Number and Homozygosity in Transgenic Plants. *Plant, Cell & Environment* **2016**, *39* (4), 908–917. https://doi.org/10.1111/pce.12693.

(250) Dobnik, D.; Štebih, D.; Blejec, A.; Morisset, D.; Žel, J. Multiplex Quantification of Four DNA Targets in One Reaction with Bio-Rad Droplet Digital PCR System for GMO Detection. *Sci Rep* **2016**, *6* (1), 35451. https://doi.org/10.1038/srep35451.

(251) Collier, R.; Dasgupta, K.; Xing, Y.-P.; Hernandez, B. T.; Shao, M.; Rohozinski, D.; Kovak, E.; Lin, J.; de Oliveira, M. L. P.; Stover, E.; McCue, K. F.; Harmon, F. G.; Blechl, A.; Thomson, J. G.; Thilmony, R. Accurate Measurement of Transgene Copy Number in Crop Plants Using Droplet Digital PCR. *The Plant Journal* **2017**, *90* (5), 1014–1025. https://doi.org/10.1111/tpj.13517.

(252) Miyaoka, Y.; Mayerl, S. J.; Chan, A. H.; Conklin, B. R. Detection and Quantification of HDR and NHEJ Induced by Genome Editing at Endogenous Gene Loci Using Droplet Digital PCR. In *Digital PCR: Methods and Protocols*; Karlin-Neumann, G., Bizouarn, F., Eds.; Methods in Molecular Biology; Springer: New York, NY, 2018; pp 349–362. https://doi.org/10.1007/978-1-4939-7778-9_20.

(253) Sullivan, A. M.; Arsovski, A. A.; Lempe, J.; Bubb, K. L.; Weirauch, M. T.; Sabo, P. J.; Sandstrom, R.; Thurman, R. E.; Neph, S.; Reynolds, A. P.; Stergachis, A. B.; Vernot, B.; Johnson, A. K.; Haugen, E.; Sullivan, S. T.; Thompson, A.; Neri, F. V.; Weaver, M.; Diegel, M.; Mnaimneh, S.; Yang, A.; Hughes, T. R.; Nemhauser, J. L.; Queitsch, C.; Stamatoyannopoulos, J. A. Mapping and Dynamics of Regulatory DNA and Transcription Factor Networks in A. Thaliana. *Cell Reports* **2014**, *8* (6), 2015–2030. https://doi.org/10.1016/j.celrep.2014.08.019.

(254) Lau, W.; Sattely, E. S. Six Enzymes from Mayapple That Complete the Biosynthetic Pathway to the Etoposide Aglycone. *Science* **2015**, *349* (6253), 1224–1228. https://doi.org/10.1126/science.aac7202.

(255) Beyene, A. G.; Demirer, G. S.; Landry, M. P. Nanoparticle-Templated Molecular Recognition Platforms for Detection of Biological Analytes. *Current Protocols in Chemical Biology* **2016**, *8* (3), 197–223. https://doi.org/10.1002/cpch.10.

(256) Ma, L.; Zhuang, H. L.; Wei, S.; Hendrickson, K. E.; Kim, M. S.; Cohn, G.; Hennig, R. G.; Archer, L. A. Enhanced Li–S Batteries Using Amine-Functionalized Carbon Nanotubes in the Cathode. *ACS Nano* **2016**, *10* (1), 1050–1059. https://doi.org/10.1021/acsnano.5b06373.

(257) Khan, I.; Saeed, K.; Khan, I. Nanoparticles: Properties, Applications and Toxicities. *Arabian Journal of Chemistry* **2017**. https://doi.org/10.1016/J.ARABJC.2017.05.011.

(258) Sanità, G.; Carrese, B.; Lamberti, A. Nanoparticle Surface Functionalization: How to Improve Biocompatibility and Cellular Internalization. *Front. Mol. Biosci.* **2020**, *7*. https://doi.org/10.3389/fmolb.2020.587012.

(259) Wu, H.; Tito, N.; Giraldo, J. P. Anionic Cerium Oxide Nanoparticles Protect Plant Photosynthesis from Abiotic Stress by Scavenging Reactive Oxygen Species. *ACS Nano* **2017**, *11* (11), 11283–11297. https://doi.org/10.1021/acsnano.7b05723.

(260) Wu, H.; Nißler, R.; Morris, V.; Herrmann, N.; Hu, P.; Jeon, S.-J.; Kruss, S.; Giraldo, J. P. Monitoring Plant Health with Near-Infrared Fluorescent H2O2 Nanosensors. *Nano Lett.* **2020**. https://doi.org/10.1021/acs.nanolett.9b05159.

(261) Numata, K.; Horii, Y.; Motoda, Y.; Hirai, N.; Nishitani, C.; Watanabe, S.; Kigawa, T.; Kodama, Y. Direct Introduction of Neomycin Phosphotransferase II Protein into Apple Leaves to Confer Kanamycin Resistance. *Plant Biotechnol (Tokyo)* **2016**, *33* (5), 403–407. https://doi.org/10.5511/plantbiotechnology.16.0929a.

(262) Martin-Ortigosa, S.; Wang, K. Proteolistics: A Biolistic Method for Intracellular Delivery of Proteins. *Transgenic Research* **2014**, *23* (5), 743–756. https://doi.org/10.1007/s11248-014-9807-y.

(263) Martin-Ortigosa, S.; Wang, K. Proteolistics: A Protein Delivery Method. In *Biolistic DNA Delivery in Plants: Methods and Protocols*; Rustgi, S., Luo, H., Eds.; Methods in Molecular Biology; Springer US: New York, NY, 2020; pp 295–307. https://doi.org/10.1007/978-1-0716-0356-7_16.

(264) Plant Virology - 5th Edition https://www.elsevier.com/books/plant-virology/hull/978-0-12-384871-0 (accessed 2020 -10 -09).

(265) Christie, P. J. Type IV Secretion: The Agrobacterium VirB/D4 and Related Conjugation Systems. *Biochimica et Biophysica Acta (BBA) - Molecular Cell Research* **2004**, *1694* (1), 219–234. https://doi.org/10.1016/j.bbamcr.2004.02.013.

(266) Selin, C.; de Kievit, T. R.; Belmonte, M. F.; Fernando, W. G. D. Elucidating the Role of Effectors in Plant-Fungal Interactions: Progress and Challenges. *Frontiers in Microbiology* **2016**, *7*.

(267) Hu, P.; An, J.; Faulkner, M. M.; Wu, H.; Li, Z.; Tian, X.; Giraldo, J. P. Nanoparticle Charge and Size Control Foliar Delivery Efficiency to Plant Cells and Organelles. *ACS Nano* **2020**, *14* (7), 7970–7986. https://doi.org/10.1021/acsnano.9b09178.

(268) Sun, X.-D.; Yuan, X.-Z.; Jia, Y.; Feng, L.-J.; Zhu, F.-P.; Dong, S.-S.; Liu, J.; Kong, X.; Tian, H.; Duan, J.-L.; Ding, Z.; Wang, S.-G.; Xing, B. Differentially Charged Nanoplastics Demonstrate Distinct Accumulation in Arabidopsis Thaliana. *Nat. Nanotechnol.* **2020**, *15* (9), 755–760. https://doi.org/10.1038/s41565-020-0707-4.

(269) Mann, A.; Thakur, G.; Shukla, V.; Singh, A. K.; Khanduri, R.; Naik, R.; Jiang, Y.; Kalra, N.; Dwarakanath, B. S.; Langel, U.; Ganguli, M. Differences in DNA Condensation and Release by Lysine and Arginine Homopeptides Govern Their DNA Delivery Efficiencies. *Mol. Pharmaceutics* **2011**, *8* (5), 1729–1741. https://doi.org/10.1021/mp2000814.

(270) Yaron, P. N.; Holt, B. D.; Short, P. A.; Lösche, M.; Islam, M. F.; Dahl, K. N. Single Wall Carbon Nanotubes Enter Cells by Endocytosis and Not Membrane Penetration. *Journal of Nanobiotechnology* **2011**, *9* (1), 45. https://doi.org/10.1186/1477-3155-9-45.

(271) Oh, N.; Park, J.-H. Endocytosis and Exocytosis of Nanoparticles in Mammalian Cells. *Int J Nanomedicine* **2014**, *9* (Suppl 1), 51–63. https://doi.org/10.2147/IJN.S26592.

(272) Madani, F.; Lindberg, S.; Langel, Ü.; Futaki, S.; Gräslund, A. Mechanisms of Cellular Uptake of Cell-Penetrating Peptides. *Journal of Biophysics* **2011**, *2011*, e414729. https://doi.org/10.1155/2011/414729.

(273)   Wu, H.; Santana, I.; Dansie, J.; Giraldo, J. P. In Vivo Delivery of Nanoparticles into Plant Leaves. In *Current Protocols in Chemical Biology*; John Wiley & Sons, Inc.: Hoboken, NJ, USA, 2017; Vol. 9, pp 269–284. https://doi.org/10.1002/cpch.29.

(274)   Schwartz, S. H.; Hendrix, B.; Hoffer, P.; Sanders, R. A.; Zheng, W. Carbon Dots for Efficient Small Interfering RNA Delivery and Gene Silencing in Plants. *Plant Physiology* **2020**, *184* (2), 647–657. https://doi.org/10.1104/pp.20.00733.

(275)   Ng, K. K.; Motoda, Y.; Watanabe, S.; Othman, A. S.; Kigawa, T.; Kodama, Y.; Numata, K. Intracellular Delivery of Proteins via Fusion Peptides in Intact Plants. *PLOS ONE* **2016**, *11* (4), e0154081. https://doi.org/10.1371/journal.pone.0154081.

(276)   Svitashev, S.; Schwartz, C.; Lenderts, B.; Young, J. K.; Mark Cigan, A. Genome Editing in Maize Directed by CRISPR–Cas9 Ribonucleoprotein Complexes. *Nature Communications* **2016**, *7*, 13274–13274. https://doi.org/10.1038/ncomms13274.

(277)   Banakar, R.; Eggenberger, A. L.; Lee, K.; Wright, D. A.; Murugan, K.; Zarecor, S.; Lawrence-Dill, C. J.; Sashital, D. G.; Wang, K. High-Frequency Random DNA Insertions upon Co-Delivery of CRISPR-Cas9 Ribonucleoprotein and Selectable Marker Plasmid in Rice. *Scientific Reports* **2019**, *9* (1), 19902. https://doi.org/10.1038/s41598-019-55681-y.

(278)   Banakar, R.; Schubert, M.; Collingwood, M.; Vakulskas, C.; Eggenberger, A. L.; Wang, K. Comparison of CRISPR-Cas9/Cas12a Ribonucleoprotein Complexes for Genome Editing Efficiency in the Rice Phytoene Desaturase (OsPDS) Gene. *Rice* **2020**, *13* (1), 4. https://doi.org/10.1186/s12284-019-0365-z.

(279)   Chang, M.; Chou, J.-C.; Lee, H.-J. Cellular Internalization of Fluorescent Proteins via Arginine-Rich Intracellular Delivery Peptide in Plant Cells. *Plant Cell Physiol* **2005**, *46* (3), 482–488. https://doi.org/10.1093/pcp/pci046.

(280)   Chang, M.; Chou, J.-C.; Chen, C.-P.; Liu, B. R.; Lee, H.-J. Noncovalent Protein Transduction in Plant Cells by Macropinocytosis. *New Phytologist* **2007**, *174* (1), 46–56. https://doi.org/10.1111/j.1469-8137.2007.01977.x.

(281)   Lu, S.-W.; Hu, J.-W.; Liu, B. R.; Lee, C.-Y.; Li, J.-F.; Chou, J.-C.; Lee, H.-J. Arginine-Rich Intracellular Delivery Peptides Synchronously Deliver Covalently and Noncovalently Linked Proteins into Plant Cells. *J. Agric. Food Chem.* **2010**, *58* (4), 2288–2294. https://doi.org/10.1021/jf903039j.

(282)   Jain, A.; Yadav, B. K.; Chugh, A. Marine Antimicrobial Peptide Tachyplesin as an Efficient Nanocarrier for Macromolecule Delivery in Plant and Mammalian Cells. *The FEBS Journal* **2015**, *282* (4), 732–745. https://doi.org/10.1111/febs.13178.

(283)   Cedeño, C.; Pauwels, K.; Tompa, P. Protein Delivery into Plant Cells: Toward In Vivo Structural Biology. *Front. Plant Sci.* **2017**, *8*. https://doi.org/10.3389/fpls.2017.00519.

(284)   Furuhata, Y.; Sakai, A.; Murakami, T.; Morikawa, M.; Nakamura, C.; Yoshizumi, T.; Fujikura, U.; Nishida, K.; Kato, Y. A Method Using Electroporation for the Protein Delivery of Cre Recombinase into Cultured Arabidopsis Cells with an Intact Cell Wall. *Scientific Reports* **2019**, *9* (1), 2163. https://doi.org/10.1038/s41598-018-38119-9.

(285)   Woo, J. W.; Kim, J.; Kwon, S. I.; Corvalán, C.; Cho, S. W.; Kim, H.; Kim, S.-G.; Kim, S.-T.; Choe, S.; Kim, J.-S. DNA-Free Genome Editing in Plants with Preassembled CRISPR-Cas9 Ribonucleoproteins. *Nature Biotechnology* **2015**, *33* (11), 1162–1164. https://doi.org/10.1038/nbt.3389.

(286)   Luo, S.; Li, J.; Stoddard, T. J.; Baltes, N. J.; Demorest, Z. L.; Clasen, B. M.; Coffman, A.; Retterath, A.; Mathis, L.; Voytas, D. F.; Zhang, F. Non-Transgenic Plant Genome

Editing Using Purified Sequence-Specific Nucleases. *Molecular Plant* **2015**, *8* (9), 1425–1427. https://doi.org/10.1016/j.molp.2015.05.012.

(287)   Subburaj, S.; Chung, S. J.; Lee, C.; Ryu, S.-M.; Kim, D. H.; Kim, J.-S.; Bae, S.; Lee, G.-J. Site-Directed Mutagenesis in Petunia × Hybrida Protoplast System Using Direct Delivery of Purified Recombinant Cas9 Ribonucleoproteins. *Plant Cell Rep* **2016**, *35* (7), 1535–1544. https://doi.org/10.1007/s00299-016-1937-7.

(288)   Malnoy, M.; Viola, R.; Jung, M.-H.; Koo, O.-J.; Kim, S.; Kim, J.-S.; Velasco, R.; Nagamangala Kanchiswamy, C. DNA-Free Genetically Edited Grapevine and Apple Protoplast Using CRISPR/Cas9 Ribonucleoproteins. *Front. Plant Sci.* **2016**, *7*. https://doi.org/10.3389/fpls.2016.01904.

(289)   Liang, Z.; Chen, K.; Li, T.; Zhang, Y.; Wang, Y.; Zhao, Q.; Liu, J.; Zhang, H.; Liu, C.; Ran, Y.; Gao, C. Efficient DNA-Free Genome Editing of Bread Wheat Using CRISPR/Cas9 Ribonucleoprotein Complexes. *Nature Communications* **2017**, *8* (1), 14261. https://doi.org/10.1038/ncomms14261.

(290)   Andersson, M.; Turesson, H.; Olsson, N.; Fält, A.-S.; Ohlsson, P.; Gonzalez, M. N.; Samuelsson, M.; Hofvander, P. Genome Editing in Potato via CRISPR-Cas9 Ribonucleoprotein Delivery. *Physiologia Plantarum* **2018**, *164* (4), 378–384. https://doi.org/10.1111/ppl.12731.

(291)   Zong, Y.; Song, Q.; Li, C.; Jin, S.; Zhang, D.; Wang, Y.; Qiu, J.-L.; Gao, C. Efficient C-to-T Base Editing in Plants Using a Fusion of NCas9 and Human APOBEC3A. *Nature Biotechnology* **2018**, *36* (10), 950–953. https://doi.org/10.1038/nbt.4261.

(292)   Zubkovs, V.; Wu, S.-J.; Rahnamaee, S. Y.; Schuergers, N.; Boghossian, A. A. Site-Specific Protein Conjugation onto Fluorescent Single-Walled Carbon Nanotubes. *Chem. Mater.* **2020**, acs.chemmater.0c02051. https://doi.org/10.1021/acs.chemmater.0c02051.

(293)   Das, P.; Jana, N. R. Length-Controlled Synthesis of Calcium Phosphate Nanorod and Nanowire and Application in Intracellular Protein Delivery. *ACS Appl. Mater. Interfaces* **2016**, *8* (13), 8710–8720. https://doi.org/10.1021/acsami.6b01667.

(294)   Garnett, E.; Mai, L.; Yang, P. Introduction: 1D Nanomaterials/Nanowires. *Chem. Rev.* **2019**, *119* (15), 8955–8957. https://doi.org/10.1021/acs.chemrev.9b00423.

(295)   Stephanopoulos, N.; Francis, M. B. Choosing an Effective Protein Bioconjugation Strategy. *Nature Chemical Biology* **2011**, *7* (12), 876–884. https://doi.org/10.1038/nchembio.720.

(296)   Sunasee, R.; Narain, R. Covalent and Noncovalent Bioconjugation Strategies. In *Chemistry of Bioconjugates*; John Wiley & Sons, Ltd, 2014; pp 1–75. https://doi.org/10.1002/9781118775882.ch1.

(297)   B. Gunnoo, S.; Madder, A. Bioconjugation – Using Selective Chemistry to Enhance the Properties of Proteins and Peptides as Therapeutics and Carriers. *Organic & Biomolecular Chemistry* **2016**, *14* (34), 8002–8013. https://doi.org/10.1039/C6OB00808A.

(298)   He, S.; Arscott, P. G.; Bloomfield, V. A. Condensation of DNA by Multivalent Cations: Experimental Studies of Condensation Kinetics. *Biopolymers* **2000**, *53* (4), 329–341. https://doi.org/10.1002/(SICI)1097-0282(20000405)53:4<329::AID-BIP5>3.0.CO;2-6.

(299)   Yan, M.; Liang, M.; Wen, J.; Liu, Y.; Lu, Y.; Chen, I. S. Y. Single SiRNA Nanocapsules for Enhanced RNAi Delivery. *J Am Chem Soc* **2012**, *134* (33), 13542–13545. https://doi.org/10.1021/ja304649a.

(300) Baum, M.; Erdel, F.; Wachsmuth, M.; Rippe, K. Retrieving the Intracellular Topology from Multi-Scale Protein Mobility Mapping in Living Cells. *Nature Communications* **2014**, *5* (1), 4494. https://doi.org/10.1038/ncomms5494.

(301) Mout, R.; Ray, M.; Lee, Y.-W.; Scaletti, F.; Rotello, V. M. In Vivo Delivery of CRISPR/Cas9 for Therapeutic Gene Editing: Progress and Challenges. *Bioconjugate Chem.* **2017**, *28* (4), 880–884. https://doi.org/10.1021/acs.bioconjchem.7b00057.

(302) Slomberg, D. L.; Schoenfisch, M. H. Silica Nanoparticle Phytotoxicity to Arabidopsis Thaliana. *Environ. Sci. Technol.* **2012**, 120827122017009. https://doi.org/10.1021/es300949f.

(303) Zhang, Z.; Shen, W.; Ling, J.; Yan, Y.; Hu, J.; Cheng, Y. The Fluorination Effect of Fluoroamphiphiles in Cytosolic Protein Delivery. *Nat Commun* **2018**, *9* (1), 1377. https://doi.org/10.1038/s41467-018-03779-8.

(304) Tai, W.; Zhao, P.; Gao, X. Cytosolic Delivery of Proteins by Cholesterol Tagging. *Science Advances 6* (25), eabb0310. https://doi.org/10.1126/sciadv.abb0310.

(305) Duvall, C. L.; Convertine, A. J.; Benoit, D. S. W.; Hoffman, A. S.; Stayton, P. S. Intracellular Delivery of a Proapoptotic Peptide via Conjugation to a RAFT Synthesized Endosomolytic Polymer. *Mol. Pharmaceutics* **2010**, *7* (2), 468–476. https://doi.org/10.1021/mp9002267.

(306) Bruce, V. J.; McNaughton, B. R. Inside Job: Methods for Delivering Proteins to the Interior of Mammalian Cells. *Cell Chemical Biology* **2017**, *24* (8), 924–934. https://doi.org/10.1016/j.chembiol.2017.06.014.

(307) Miralles, P.; Church, T. L.; Harris, A. T. Toxicity, Uptake, and Translocation of Engineered Nanomaterials in Vascular Plants. *Environmental Science & Technology* **2012**, *46* (17), 9224–9239. https://doi.org/10.1021/es202995d.

(308) El-Shetehy, M.; Moradi, A.; Maceroni, M.; Reinhardt, D.; Petri-Fink, A.; Rothen-Rutishauser, B.; Mauch, F.; Schwab, F. Silica Nanoparticles Enhance Disease Resistance in Arabidopsis Plants. *Nature Nanotechnology* **2020**, 1–10. https://doi.org/10.1038/s41565-020-00812-0.

(309) Sedeek, K. E. M.; Mahas, A.; Mahfouz, M. Plant Genome Engineering for Targeted Improvement of Crop Traits. *Frontiers in Plant Science* **2019**, *10*.

(310) Maher, M. F.; Nasti, R. A.; Vollbrecht, M.; Starker, C. G.; Clark, M. D.; Voytas, D. F. Plant Gene Editing through de Novo Induction of Meristems. *Nat Biotechnol* **2020**, *38* (1), 84–89. https://doi.org/10.1038/s41587-019-0337-2.

(311) Tilman, D.; Balzer, C.; Hill, J.; Befort, B. L. Global Food Demand and the Sustainable Intensification of Agriculture. *Proceedings of the National Academy of Sciences* **2011**, *108* (50), 20260–20264. https://doi.org/10.1073/pnas.1116437108.

(312) Giraldo, J. P.; Wu, H.; Newkirk, G. M.; Kruss, S. Nanobiotechnology Approaches for Engineering Smart Plant Sensors. *Nature Nanotechnology* **2019**, *14* (6), 541–553. https://doi.org/10.1038/s41565-019-0470-6.

(313) Reid, W. V.; Ali, M. K.; Field, C. B. The Future of Bioenergy. *Global Change Biology* **2020**, *26* (1), 274–286. https://doi.org/10.1111/gcb.14883.

(314) Antonacci, A.; Arduini, F.; Moscone, D.; Palleschi, G.; Scognamiglio, V. Nanostructured (Bio)Sensors for Smart Agriculture. *TrAC Trends in Analytical Chemistry* **2018**, *98*, 95–103. https://doi.org/10.1016/j.trac.2017.10.022.

(315) Kwak, S.-Y.; Wong, M. H.; Lew, T. T. S.; Bisker, G.; Lee, M. A.; Kaplan, A.; Dong, J.; Liu, A. T.; Koman, V. B.; Sinclair, R.; Hamann, C.; Strano, M. S. Nanosensor

Technology Applied to Living Plant Systems. *Annual Review of Analytical Chemistry* **2017**, *10* (1), 113–140. https://doi.org/10.1146/annurev-anchem-061516-045310.

(316)   Roper, J. M.; Garcia, J. F.; Tsutsui, H. Emerging Technologies for Monitoring Plant Health in Vivo. *ACS Omega* **2021**, *6* (8), 5101–5107. https://doi.org/10.1021/acsomega.0c05850.

(317)   Arduini, F.; Cinti, S.; Scognamiglio, V.; Moscone, D.; Palleschi, G. How Cutting-Edge Technologies Impact the Design of Electrochemical (Bio)Sensors for Environmental Analysis. A Review. *Analytica Chimica Acta* **2017**, *959*, 15–42. https://doi.org/10.1016/j.aca.2016.12.035.

(318)   Su, Y.; Ashworth, V.; Kim, C.; Adeleye, A. S.; Rolshausen, P.; Roper, C.; White, J.; Jassby, D. Delivery, Uptake, Fate, and Transport of Engineered Nanoparticles in Plants: A Critical Review and Data Analysis. *Environ. Sci.: Nano* **2019**, *6* (8), 2311–2331. https://doi.org/10.1039/C9EN00461K.

(319)   Nel, A. E.; Mädler, L.; Velegol, D.; Xia, T.; Hoek, E. M. V.; Somasundaran, P.; Klaessig, F.; Castranova, V.; Thompson, M. Understanding Biophysicochemical Interactions at the Nano–Bio Interface. *Nature Materials* **2009**, *8* (7), 543–557. https://doi.org/10.1038/nmat2442.

(320)   Monopoli, M. P.; Åberg, C.; Salvati, A.; Dawson, K. A. Biomolecular Coronas Provide the Biological Identity of Nanosized Materials. *Nature Nanotechnology* **2012**, *7* (12), 779–786. https://doi.org/10.1038/nnano.2012.207.

(321)   Chetwynd, A. J.; Lynch, I. The Rise of the Nanomaterial Metabolite Corona, and Emergence of the Complete Corona. *Environ. Sci.: Nano* **2020**, *7* (4), 1041–1060. https://doi.org/10.1039/C9EN00938H.

(322)   Monopoli, M. P.; Walczyk, D.; Campbell, A.; Elia, G.; Lynch, I.; Baldelli Bombelli, F.; Dawson, K. A. Physical−Chemical Aspects of Protein Corona: Relevance to in Vitro and in Vivo Biological Impacts of Nanoparticles. *J. Am. Chem. Soc.* **2011**, *133* (8), 2525–2534. https://doi.org/10.1021/ja107583h.

(323)   Lundqvist, M.; Stigler, J.; Cedervall, T.; Berggård, T.; Flanagan, M. B.; Lynch, I.; Elia, G.; Dawson, K. The Evolution of the Protein Corona around Nanoparticles: A Test Study. *ACS Nano* **2011**, *5* (9), 7503–7509. https://doi.org/10.1021/nn202458g.

(324)   Pinals, R. L.; Yang, D.; Rosenberg, D. J.; Chaudhary, T.; Crothers, A. R.; Iavarone, A. T.; Hammel, M.; Landry, M. P. Quantitative Protein Corona Composition and Dynamics on Carbon Nanotubes in Biological Environments. *Angew. Chem., Int. Ed. Engl.* **2020**, *59* (52), 23668.

(325)   McGee, T. D. *Principles and Methods of Temperature Measurement*; John Wiley & Sons, 1988.

(326)   AndradeSánchez, P.; Upadhyaya, S. D.; AgüeraVega, J.; Jenkins, B. Evaluation of a Capacitance-Based Soil Moisture Sensor for Real-Time Applications. *Transactions of the ASAE* **2004**, *47*, 1281–1287. https://doi.org/10.13031/2013.16562.

(327)   Ali, Md. A.; Wang, X.; Chen, Y.; Jiao, Y.; Mahal, N. K.; Moru, S.; Castellano, M. J.; Schnable, J. C.; Schnable, P. S.; Dong, L. Continuous Monitoring of Soil Nitrate Using a Miniature Sensor with Poly(3-Octyl-Thiophene) and Molybdenum Disulfide Nanocomposite. *ACS Appl. Mater. Interfaces* **2019**, *11* (32), 29195–29206. https://doi.org/10.1021/acsami.9b07120.

(328) Yin, H.; Cao, Y.; Marelli, B.; Zeng, X.; Mason, A. J.; Cao, C. Soil Sensors and Plant Wearables for Smart and Precision Agriculture. *Advanced Materials* **2021**, *33* (20), 2007764. https://doi.org/10.1002/adma.202007764.

(329) Yu, Z.; Zhao, G.; Liu, M.; Lei, Y.; Li, M. Fabrication of a Novel Atrazine Biosensor and Its Subpart-per-Trillion Levels Sensitive Performance. *Environ. Sci. Technol.* **2010**, *44* (20), 7878–7883. https://doi.org/10.1021/es101573s.

(330) Barahona, F.; Bardliving, C. L.; Phifer, A.; Bruno, J. G.; Batt, C. A. An Aptasensor Based on Polymer-Gold Nanoparticle Composite Microspheres for the Detection of Malathion Using Surface-Enhanced Raman Spectroscopy. *Industrial Biotechnology* **2013**, *9* (1), 42–50. https://doi.org/10.1089/ind.2012.0029.

(331) Nesakumar, N.; Sethuraman, S.; Krishnan, U. M.; Rayappan, J. B. B. Electrochemical Acetylcholinesterase Biosensor Based on ZnO Nanocuboids Modified Platinum Electrode for the Detection of Carbosulfan in Rice. *Biosensors and Bioelectronics* **2016**, *77*, 1070–1077. https://doi.org/10.1016/j.bios.2015.11.010.

(332) Srivastava, A. K.; Dev, A.; Karmakar, S. Nanosensors and Nanobiosensors in Food and Agriculture. *Environ Chem Lett* **2018**, *16* (1), 161–182. https://doi.org/10.1007/s10311-017-0674-7.

(333) Yang, T.; Duncan, T. V. Challenges and Potential Solutions for Nanosensors Intended for Use with Foods. *Nat. Nanotechnol.* **2021**, *16* (3), 251–265. https://doi.org/10.1038/s41565-021-00867-7.

(334) Lew, T. T. S.; Koman, V. B.; Silmore, K. S.; Seo, J. S.; Gordiichuk, P.; Kwak, S.-Y.; Park, M.; Ang, M. C.-Y.; Khong, D. T.; Lee, M. A.; Chan-Park, M. B.; Chua, N.-H.; Strano, M. S. Real-Time Detection of Wound-Induced H 2 O 2 Signalling Waves in Plants with Optical Nanosensors. *Nature Plants* **2020**, *6* (4), 404–415. https://doi.org/10.1038/s41477-020-0632-4.

(335) Lu, Y.; Xu, K.; Zhang, L.; Deguchi, M.; Shishido, H.; Arie, T.; Pan, R.; Hayashi, A.; Shen, L.; Akita, S.; Takei, K. Multimodal Plant Healthcare Flexible Sensor System. *ACS Nano* **2020**, *14* (9), 10966–10975. https://doi.org/10.1021/acsnano.0c03757.

(336) Chen, C.; Yuan, Z.; Chang, H.-T.; Lu, F.; Li, Z.; Lu, C. Silver Nanoclusters as Fluorescent Nanosensors for Selective and Sensitive Nitrite Detection. *Analytical Methods* **2016**, *8* (12), 2628–2633. https://doi.org/10.1039/C6AY00214E.

(337) Bakhori, N. M.; Yusof, N. A.; Abdullah, A. H.; Hussein, M. Z. Development of a Fluorescence Resonance Energy Transfer (FRET)-Based DNA Biosensor for Detection of Synthetic Oligonucleotide of Ganoderma Boninense. *Biosensors* **2013**, *3* (4), 419–428. https://doi.org/10.3390/bios3040419.

(338) Li, J.; Wu, H.; Santana, I.; Fahlgren, M.; Giraldo, J. P. Standoff Optical Glucose Sensing in Photosynthetic Organisms by a Quantum Dot Fluorescent Probe. *ACS Appl. Mater. Interfaces* **2018**, *10* (34), 28279–28289. https://doi.org/10.1021/acsami.8b07179.

(339) Giraldo, J. P.; Landry, M. P.; Kwak, S.-Y.; Jain, R. M.; Wong, M. H.; Iverson, N. M.; Ben-Naim, M.; Strano, M. S. A Ratiometric Sensor Using Single Chirality Near-Infrared Fluorescent Carbon Nanotubes: Application to In Vivo Monitoring. *Small* **2015**, *11* (32), 3973–3984. https://doi.org/10.1002/smll.201403276.

(340) Lew, T. T. S.; Park, M.; Cui, J.; Strano, M. S. Plant Nanobionic Sensors for Arsenic Detection. *Advanced Materials* **2021**, *33* (1), 2005683. https://doi.org/10.1002/adma.202005683.

(341)   Nagata, T.; Nakamura, A.; Akizawa, T.; Pan-Hou, H. Genetic Engineering of Transgenic Tobacco for Enhanced Uptake and Bioaccumulation of Mercury. *Biological and Pharmaceutical Bulletin* **2009**, *32* (9), 1491–1495. https://doi.org/10.1248/bpb.32.1491.

(342)   Kundu, M.; Krishnan, P.; Kotnala, R. K.; Sumana, G. Recent Developments in Biosensors to Combat Agricultural Challenges and Their Future Prospects. *Trends in Food Science & Technology* **2019**, *88*, 157–178. https://doi.org/10.1016/j.tifs.2019.03.024.

(343)   Tomer, A.; Sigh, R.; Dwivedi, S. *Biobased Nanotechnology for Green Applications*; 2020. https://doi.org/10.1007/978-3-030-61985-5_8.

(344)   Mishra, P.; Polder, G.; Vilfan, N. Close Range Spectral Imaging for Disease Detection in Plants Using Autonomous Platforms: A Review on Recent Studies. *Curr Robot Rep* **2020**, *1* (2), 43–48. https://doi.org/10.1007/s43154-020-00004-7.

(345)   Yao, K. S.; Li, S. J.; Tzeng, K. C.; Cheng, T. C.; Chang, C. Y.; Chiu, C. Y.; Liao, C. Y.; Hsu, J. J.; Lin, Z. P. Fluorescence Silica Nanoprobe as a Biomarker for Rapid Detection of Plant Pathogens. *Advanced Materials Research* **2009**, *79–82*, 513–516. https://doi.org/10.4028/www.scientific.net/AMR.79-82.513.

(346)   Khater, M.; de la Escosura-Muñiz, A.; Merkoçi, A. Biosensors for Plant Pathogen Detection. *Biosensors and Bioelectronics* **2017**, *93*, 72–86. https://doi.org/10.1016/j.bios.2016.09.091.

(347)   Salomone, A.; Mongelli, M.; Roggero, P.; Boscia, D. Reliability of Detection of Citrus Tristeza Visua by an Immunochromatographic Lateral Flow Assay in Comparison with ELISA. *Journal of Plant Pathology* **2004**, *86* (1), 43–48.

(348)   Drygin, Y. F.; Blintsov, A. N.; Grigorenko, V. G.; Andreeva, I. P.; Osipov, A. P.; Varitzev, Y. A.; Uskov, A. I.; Kravchenko, D. V.; Atabekov, J. G. Highly Sensitive Field Test Lateral Flow Immunodiagnostics of PVX Infection. *Appl Microbiol Biotechnol* **2012**, *93* (1), 179–189. https://doi.org/10.1007/s00253-011-3522-x.

(349)   Zhang, F.; Zou, M.; Chen, Y.; Li, J.; Wang, Y.; Qi, X.; Xue, Q. Lanthanide-Labeled Immunochromatographic Strips for the Rapid Detection of Pantoea Stewartii Subsp. Stewartii. *Biosensors and Bioelectronics* **2014**, *51*, 29–35. https://doi.org/10.1016/j.bios.2013.06.065.

(350)   Pandey, P.; Irulappan, V.; Bagavathiannan, M. V.; Senthil-Kumar, M. Impact of Combined Abiotic and Biotic Stresses on Plant Growth and Avenues for Crop Improvement by Exploiting Physio-Morphological Traits. *Frontiers in Plant Science* **2017**, *8*.

(351)   Savatin, D. V.; Gramegna, G.; Modesti, V.; Cervone, F. Wounding in the Plant Tissue: The Defense of a Dangerous Passage. *Frontiers in Plant Science* **2014**, *5*.

(352)   Hedrich, R.; Salvador-Recatalà, V.; Dreyer, I. Electrical Wiring and Long-Distance Plant Communication. *Trends in Plant Science* **2016**, *21* (5), 376–387. https://doi.org/10.1016/j.tplants.2016.01.016.

(353)   Zhou, J.-M.; Zhang, Y. Plant Immunity: Danger Perception and Signaling. *Cell* **2020**, *181* (5), 978–989. https://doi.org/10.1016/j.cell.2020.04.028.

(354)   Lew, T. T. S.; Koman, V. B.; Gordiichuk, P.; Park, M.; Strano, M. S. The Emergence of Plant Nanobionics and Living Plants as Technology. *Advanced Materials Technologies* **2020**, *5* (3), 1900657. https://doi.org/10.1002/admt.201900657.

(355) Cherukuri, P.; Glazer, E. S.; Curley, S. A. Targeted Hyperthermia Using Metal Nanoparticles. *Advanced Drug Delivery Reviews* **2010**, *62* (3), 339–345. https://doi.org/10.1016/j.addr.2009.11.006.

(356) Baetke, S. C.; Lammers, T.; Kiessling, F. Applications of Nanoparticles for Diagnosis and Therapy of Cancer. *BJR* **2015**, *88* (1054), 20150207. https://doi.org/10.1259/bjr.20150207.

(357) Han, X.; Xu, K.; Taratula, O.; Farsad, K. Applications of Nanoparticles in Biomedical Imaging. *Nanoscale* **2019**, *11* (3), 799–819. https://doi.org/10.1039/C8NR07769J.

(358) Fasoli, E. Protein Corona: Dr. Jekyll and Mr. Hyde of Nanomedicine. *Biotechnology and Applied Biochemistry* **2021**, *68* (6), 1139–1152. https://doi.org/10.1002/bab.2035.

(359) Martínez-Negro, M.; González-Rubio, G.; Aicart, E.; Landfester, K.; Guerrero-Martínez, A.; Junquera, E. Insights into Colloidal Nanoparticle-Protein Corona Interactions for Nanomedicine Applications. *Advances in Colloid and Interface Science* **2021**, *289*, 102366. https://doi.org/10.1016/j.cis.2021.102366.

(360) Chinen, A. B.; Guan, C. M.; Ferrer, J. R.; Barnaby, S. N.; Merkel, T. J.; Mirkin, C. A. Nanoparticle Probes for the Detection of Cancer Biomarkers, Cells, and Tissues by Fluorescence. *Chemical Reviews* **2015**, *115* (19), 10530–10574. https://doi.org/10.1021/acs.chemrev.5b00321.

(361) Du, B.; Yu, M.; Zheng, J. Transport and Interactions of Nanoparticles in the Kidneys. *Nat Rev Mater* **2018**, *3* (10), 358–374. https://doi.org/10.1038/s41578-018-0038-3.

(362) Singh, S.; Gill, A. A. S.; Nlooto, M.; Karpoormath, R. Prostate Cancer Biomarkers Detection Using Nanoparticles Based Electrochemical Biosensors. *Biosensors and Bioelectronics* **2019**, *137*, 213–221. https://doi.org/10.1016/j.bios.2019.03.065.

(363) Getts, D. R.; Shea, L. D.; Miller, S. D.; King, N. J. C. Harnessing Nanoparticles for Immune Modulation. *Trends in Immunology* **2015**, *36* (7), 419–427. https://doi.org/10.1016/j.it.2015.05.007.

(364) Ledford, H. Bankruptcy Filing Worries Developers of Nanoparticle Cancer Drugs. *Nature* **2016**, *533* (7603), 304–305.

(365) Tang, J.; Pérez-Medina, C.; Zhao, Y.; Sadique, A.; Mulder, W. J. M.; Reiner, T. A Comprehensive Procedure to Evaluate the In Vivo Performance of Cancer Nanomedicines. *JoVE (Journal of Visualized Experiments)* **2017**, No. 121, e55271. https://doi.org/10.3791/55271.

(366) He, H.; Liu, L.; Morin, E. E.; Liu, M.; Schwendeman, A. Survey of Clinical Translation of Cancer Nanomedicines—Lessons Learned from Successes and Failures. *Acc. Chem. Res.* **2019**, *52* (9), 2445–2461. https://doi.org/10.1021/acs.accounts.9b00228.

(367) Lima, T.; Bernfur, K.; Vilanova, M.; Cedervall, T. Understanding the Lipid and Protein Corona Formation on Different Sized Polymeric Nanoparticles. *Sci Rep* **2020**, *10* (1), 1129. https://doi.org/10.1038/s41598-020-57943-6.

(368) Salvati, A.; Pitek, A. S.; Monopoli, M. P.; Prapainop, K.; Bombelli, F. B.; Hristov, D. R.; Kelly, P. M.; Åberg, C.; Mahon, E.; Dawson, K. A. Transferrin-Functionalized Nanoparticles Lose Their Targeting Capabilities When a Biomolecule Corona Adsorbs on the Surface. *Nature Nanotech* **2013**, *8* (2), 137–143. https://doi.org/10.1038/nnano.2012.237.

(369) Tenzer, S.; Docter, D.; Kuharev, J.; Musyanovych, A.; Fetz, V.; Hecht, R.; Schlenk, F.; Fischer, D.; Kiouptsi, K.; Reinhardt, C.; Landfester, K.; Schild, H.; Maskos, M.; Knauer, S. K.; Stauber, R. H. Rapid Formation of Plasma Protein Corona Critically Affects

Nanoparticle Pathophysiology. *Nature Nanotech* **2013**, *8* (10), 772–781.
https://doi.org/10.1038/nnano.2013.181.

(370) Mahmoudi, M. Debugging Nano–Bio Interfaces: Systematic Strategies to Accelerate
Clinical Translation of Nanotechnologies. *Trends in Biotechnology* **2018**, *36* (8), 755–
769. https://doi.org/10.1016/j.tibtech.2018.02.014.

(371) Pinals, R. L.; Chio, L.; Ledesma, F.; Landry, M. P. Engineering at the Nano-Bio
Interface: Harnessing the Protein Corona towards Nanoparticle Design and Function.
Analyst **2020**, *145* (15), 5090.

(372) Lundqvist, M.; Stigler, J.; Elia, G.; Lynch, I.; Cedervall, T.; Dawson, K. A. Nanoparticle
Size and Surface Properties Determine the Protein Corona with Possible Implications for
Biological Impacts. *Proceedings of the National Academy of Sciences* **2008**, *105* (38),
14265–14270. https://doi.org/10.1073/pnas.0805135105.

(373) Docter, D.; Westmeier, D.; Markiewicz, M.; Stolte, S.; K. Knauer, S.; H. Stauber, R. The
Nanoparticle Biomolecule Corona: Lessons Learned – Challenge Accepted? *Chemical
Society Reviews* **2015**, *44* (17), 6094–6121. https://doi.org/10.1039/C5CS00217F.

(374) Weiss, A. C. G.; Kempe, K.; Förster, S.; Caruso, F. Microfluidic Examination of the
"Hard" Biomolecular Corona Formed on Engineered Particles in Different Biological
Milieu. *Biomacromolecules* **2018**, *19* (7), 2580–2594.
https://doi.org/10.1021/acs.biomac.8b00196.

(375) Walkey, C. D.; Chan, W. C. W. Understanding and Controlling the Interaction of
Nanomaterials with Proteins in a Physiological Environment. *Chem. Soc. Rev.* **2012**, *41*
(7), 2780–2799. https://doi.org/10.1039/C1CS15233E.

(376) García, K. P.; Zarschler, K.; Barbaro, L.; Barreto, J. A.; O'Malley, W.; Spiccia, L.;
Stephan, H.; Graham, B. Zwitterionic-Coated "Stealth" Nanoparticles for Biomedical
Applications: Recent Advances in Countering Biomolecular Corona Formation and
Uptake by the Mononuclear Phagocyte System. *Small* **2014**, *10* (13), 2516–2529.
https://doi.org/10.1002/smll.201303540.

(377) Lesniak, A.; Fenaroli, F.; Monopoli, M. P.; Åberg, C.; Dawson, K. A.; Salvati, A. Effects
of the Presence or Absence of a Protein Corona on Silica Nanoparticle Uptake and
Impact on Cells. *ACS Nano* **2012**, *6* (7), 5845–5857. https://doi.org/10.1021/nn300223w.

(378) Naidu, P. S. R.; Gavriel, N.; Gray, C. G. G.; Bartlett, C. A.; Toomey, L. M.; Kretzmann,
J. A.; Patalwala, D.; McGonigle, T.; Denham, E.; Hee, C.; Ho, D.; Taylor, N. L.; Norret,
M.; Smith, N. M.; Dunlop, S. A.; Iyer, K. S.; Fitzgerald, M. Elucidating the Inability of
Functionalized Nanoparticles to Cross the Blood–Brain Barrier and Target Specific Cells
in Vivo. *ACS Appl. Mater. Interfaces* **2019**, *11* (25), 22085–22095.
https://doi.org/10.1021/acsami.9b01356.

(379) Raoufi, M.; Javad Hajipour, M.; Shahri, S. M. K.; Schoen, I.; Linn, U.; Mahmoudi, M.
Probing Fibronectin Conformation on a Protein Corona Layer around Nanoparticles.
Nanoscale **2018**, *10* (3), 1228–1233. https://doi.org/10.1039/C7NR06970G.

(380) Warning, L. A.; Zhang, Q.; Baiyasi, R.; Landes, C. F.; Link, S. Nanoscale Surface-
Induced Unfolding of Single Fibronectin Is Restricted by Serum Albumin Crowding. *J.
Phys. Chem. Lett.* **2020**, *11* (3), 1170–1177. https://doi.org/10.1021/acs.jpclett.9b03446.

(381) Bing, J.; Xiao, X.; McClements, D. J.; Biao, Y.; Chongjiang, C. Protein Corona
Formation around Inorganic Nanoparticles: Food Plant Proteins-TiO2 Nanoparticle
Interactions. *Food Hydrocolloids* **2021**, *115*, 106594.
https://doi.org/10.1016/j.foodhyd.2021.106594.

(382) Prakash, S.; Deswal, R. Analysis of Temporally Evolved Nanoparticle-Protein Corona Highlighted the Potential Ability of Gold Nanoparticles to Stably Interact with Proteins and Influence the Major Biochemical Pathways in Brassica Juncea. *Plant Physiology and Biochemistry* **2020**, *146*, 143–156. https://doi.org/10.1016/j.plaphy.2019.10.036.

(383) Kurepa, J.; Nakabayashi, R.; Paunesku, T.; Suzuki, M.; Saito, K.; Woloschak, G. E.; Smalle, J. A. Direct Isolation of Flavonoids from Plants Using Ultra-Small Anatase TiO2 Nanoparticles. *The Plant Journal* **2014**, *77* (3), 443–453. https://doi.org/10.1111/tpj.12361.

(384) Kurepa, J.; Shull, T. E.; Smalle, J. A. Metabolomic Analyses of the Bio-Corona Formed on TiO2 Nanoparticles Incubated with Plant Leaf Tissues. *Journal of Nanobiotechnology* **2020**, *18* (1), 28. https://doi.org/10.1186/s12951-020-00592-8.

(385) Kurepa, J.; Smalle, J. A. Composition of the Metabolomic Bio-Coronas Isolated from Ocimum Sanctum and Rubia Tinctorum. *BMC Res Notes* **2021**, *14*. https://doi.org/10.1186/s13104-020-05420-8.

(386) Qing, L.-S.; Shan, X.-Q.; Xu, X.-M.; Xue, Y.; Deng, W.-L.; Li, B.-G.; Wang, X.-L.; Liao, X. Rapid probe and isolation of bioactive compounds from Dioscorea panthaica using human serum albumin functionalized magnetic nano-particles (HSA-MNPs)-based ligand fishing coupled with electrospray ionization mass spectrometry. *Rapid Communications in Mass Spectrometry* **2010**, *24* (22), 3335–3339. https://doi.org/10.1002/rcm.4777.

(387) Oh, J. Y.; Kim, H. S.; Palanikumar, L.; Go, E. M.; Jana, B.; Park, S. A.; Kim, H. Y.; Kim, K.; Seo, J. K.; Kwak, S. K.; Kim, C.; Kang, S.; Ryu, J.-H. Cloaking Nanoparticles with Protein Corona Shield for Targeted Drug Delivery. *Nature Communications* **2018**, *9* (1), 4548. https://doi.org/10.1038/s41467-018-06979-4.

(388) Wang, C.; Feng, N.; Chang, F.; Wang, J.; Yuan, B.; Cheng, Y.; Liu, H.; Yu, J.; Zou, J.; Ding, J.; Chen, X. Injectable Cholesterol-Enhanced Stereocomplex Polylactide Thermogel Loading Chondrocytes for Optimized Cartilage Regeneration. *Advanced Healthcare Materials* **2019**, *8*, 1900312. https://doi.org/10.1002/adhm.201900312.

(389) Hegeman, A. D. Plant Metabolomics—Meeting the Analytical Challenges of Comprehensive Metabolite Analysis. *Briefings in Functional Genomics* **2010**, *9* (2), 139–148. https://doi.org/10.1093/bfgp/elp053.

(390) Shannahan, J. The Biocorona: A Challenge for the Biomedical Application of Nanoparticles. *Nanotechnology Reviews* **2017**, *6* (4), 345–353. https://doi.org/10.1515/ntrev-2016-0098.

(391) Heazlewood, J. L.; Millar, A. H. Plant Proteomics: Challenges and Resources. In *Annual Plant Reviews online*; American Cancer Society, 2018; pp 1–31. https://doi.org/10.1002/9781119312994.apr0287.

(392) Peters, K.; Worrich, A.; Weinhold, A.; Alka, O.; Balcke, G.; Birkemeyer, C.; Bruelheide, H.; Calf, O. W.; Dietz, S.; Dührkop, K.; Gaquerel, E.; Heinig, U.; Kücklich, M.; Macel, M.; Müller, C.; Poeschl, Y.; Pohnert, G.; Ristok, C.; Rodríguez, V. M.; Ruttkies, C.; Schuman, M.; Schweiger, R.; Shahaf, N.; Steinbeck, C.; Tortosa, M.; Treutler, H.; Ueberschaar, N.; Velasco, P.; Weiß, B. M.; Widdig, A.; Neumann, S.; Dam, N. M. van. Current Challenges in Plant Eco-Metabolomics. *Int J Mol Sci* **2018**, *19* (5). https://doi.org/10.3390/ijms19051385.

(393) Mergner, J.; Frejno, M.; List, M.; Papacek, M.; Chen, X.; Chaudhary, A.; Samaras, P.; Richter, S.; Shikata, H.; Messerer, M.; Lang, D.; Altmann, S.; Cyprys, P.; Zolg, D. P.;

Mathieson, T.; Bantscheff, M.; Hazarika, R. R.; Schmidt, T.; Dawid, C.; Dunkel, A.; Hofmann, T.; Sprunck, S.; Falter-Braun, P.; Johannes, F.; Mayer, K. F. X.; Jürgens, G.; Wilhelm, M.; Baumbach, J.; Grill, E.; Schneitz, K.; Schwechheimer, C.; Kuster, B. Mass-Spectrometry-Based Draft of the Arabidopsis Proteome. *Nature* **2020**, *579* (7799), 409–414. https://doi.org/10.1038/s41586-020-2094-2.

(394) Fang, C.; Fernie, A. R.; Luo, J. Exploring the Diversity of Plant Metabolism. *Trends in Plant Science* **2019**, *24* (1), 83–98. https://doi.org/10.1016/j.tplants.2018.09.006.

(395) Adav, S. S.; Wang, Y. Metabolomics Signatures of Aging: Recent Advances. *Aging Dis* **2021**, *12* (2), 646–661. https://doi.org/10.14336/AD.2020.0909.

(396) Jorge, T. F.; Mata, A. T.; António, C. Mass Spectrometry as a Quantitative Tool in Plant Metabolomics. *Philosophical Transactions of the Royal Society A: Mathematical, Physical and Engineering Sciences* **2016**, *374* (2079), 20150370. https://doi.org/10.1098/rsta.2015.0370.

(397) Liu, Y.; Lu, S.; Liu, K.; Wang, S.; Huang, L.; Guo, L. Proteomics: A Powerful Tool to Study Plant Responses to Biotic Stress. *Plant Methods* **2019**, *15* (1), 135. https://doi.org/10.1186/s13007-019-0515-8.

(398) Bindschedler, L. V.; Cramer, R. Quantitative Plant Proteomics. *PROTEOMICS* **2011**, *11* (4), 756–775. https://doi.org/10.1002/pmic.201000426.

(399) Wijk, K. J. van. Challenges and Prospects of Plant Proteomics. *Plant Physiology* **2001**, *126* (2), 501–508. https://doi.org/10.1104/pp.126.2.501.

(400) Chandramouli, K.; Qian, P.-Y. Proteomics: Challenges, Techniques and Possibilities to Overcome Biological Sample Complexity. *Hum Genomics Proteomics* **2009**, *2009*, 239204. https://doi.org/10.4061/2009/239204.

(401) Subba, P.; Narayana Kotimoole, C.; Prasad, T. S. K. Plant Proteome Databases and Bioinformatic Tools: An Expert Review and Comparative Insights. *OMICS: A Journal of Integrative Biology* **2019**, *23* (4), 190–206. https://doi.org/10.1089/omi.2019.0024.

(402) Karczewski, K. J.; Snyder, M. P. Integrative Omics for Health and Disease. *Nat Rev Genet* **2018**, *19* (5), 299–310. https://doi.org/10.1038/nrg.2018.4.

(403) Pérez-Alonso, M.-M.; Carrasco-Loba, V.; Pollmann, S. Advances in Plant Metabolomics. In *Annual Plant Reviews online*; John Wiley & Sons, Ltd, 2018; pp 557–588. https://doi.org/10.1002/9781119312994.apr0660.

(404) Tsugawa, H. Advances in Computational Metabolomics and Databases Deepen the Understanding of Metabolisms. *Current Opinion in Biotechnology* **2018**, *54*, 10–17. https://doi.org/10.1016/j.copbio.2018.01.008.

(405) Timp, W.; Timp, G. Beyond Mass Spectrometry, the next Step in Proteomics. *Science Advances 6* (2), eaax8978. https://doi.org/10.1126/sciadv.aax8978.

(406) Schwab, F.; Zhai, G.; Kern, M.; Turner, A.; Schnoor, J. L.; Wiesner, M. R. Barriers, Pathways and Processes for Uptake, Translocation and Accumulation of Nanomaterials in Plants - Critical Review. *Nanotoxicology* **2016**, *10* (3), 257–278. https://doi.org/10.3109/17435390.2015.1048326.

(407) Ma, C.; White, J. C.; Zhao, J.; Zhao, Q.; Xing, B. Uptake of Engineered Nanoparticles by Food Crops: Characterization, Mechanisms, and Implications. *Annual Review of Food Science and Technology* **2018**, *9* (1), 129–153. https://doi.org/10.1146/annurev-food-030117-012657.

(408) Navarro, E.; Baun, A.; Behra, R.; Hartmann, N. B.; Filser, J.; Miao, A.-J.; Quigg, A.; Santschi, P. H.; Sigg, L. Environmental Behavior and Ecotoxicity of Engineered

Nanoparticles to Algae, Plants, and Fungi. *Ecotoxicology* **2008**, *17* (5), 372–386. https://doi.org/10.1007/s10646-008-0214-0.

(409) Zhu, Z.-J.; Wang, H.; Yan, B.; Zheng, H.; Jiang, Y.; Miranda, O. R.; Rotello, V. M.; Xing, B.; Vachet, R. W. Effect of Surface Charge on the Uptake and Distribution of Gold Nanoparticles in Four Plant Species. *Environ. Sci. Technol.* **2012**, *46* (22), 12391–12398. https://doi.org/10.1021/es301977w.

(410) Spielman-Sun, E.; Avellan, A.; D. Bland, G.; V. Tappero, R.; S. Acerbo, A.; M. Unrine, J.; Pablo Giraldo, J.; V. Lowry, G. Nanoparticle Surface Charge Influences Translocation and Leaf Distribution in Vascular Plants with Contrasting Anatomy. *Environmental Science: Nano* **2019**, *6* (8), 2508–2519. https://doi.org/10.1039/C9EN00626E.

(411) Cox, A.; Andreozzi, P.; Dal Magro, R.; Fiordaliso, F.; Corbelli, A.; Talamini, L.; Chinello, C.; Raimondo, F.; Magni, F.; Tringali, M.; Krol, S.; Jacob Silva, P.; Stellacci, F.; Masserini, M.; Re, F. Evolution of Nanoparticle Protein Corona across the Blood–Brain Barrier. *ACS Nano* **2018**, *12* (7), 7292–7300. https://doi.org/10.1021/acsnano.8b03500.

(412) Zhang, Y.; Wu, J. L. Y.; Lazarovits, J.; Chan, W. C. W. An Analysis of the Binding Function and Structural Organization of the Protein Corona. *J. Am. Chem. Soc.* **2020**, *142* (19), 8827–8836. https://doi.org/10.1021/jacs.0c01853.

(413) Lv, J.; Christie, P.; Zhang, S. Uptake, Translocation, and Transformation of Metal-Based Nanoparticles in Plants: Recent Advances and Methodological Challenges. *Environmental Science: Nano* **2019**, *6* (1), 41–59. https://doi.org/10.1039/C8EN00645H.

(414) Avellan, A.; Schwab, F.; Masion, A.; Chaurand, P.; Borschneck, D.; Vidal, V.; Rose, J.; Santaella, C.; Levard, C. Nanoparticle Uptake in Plants: Gold Nanomaterial Localized in Roots of Arabidopsis Thaliana by X-Ray Computed Nanotomography and Hyperspectral Imaging. *Environ. Sci. Technol.* **2017**, *51* (15), 8682–8691. https://doi.org/10.1021/acs.est.7b01133.

(415) Dai, Y.; Chen, F.; Yue, L.; Li, T.; Jiang, Z.; Xu, Z.; Wang, Z.; Xing, B. Uptake, Transport, and Transformation of CeO2 Nanoparticles by Strawberry and Their Impact on the Rhizosphere Bacterial Community. *ACS Sustainable Chem. Eng.* **2020**, *8* (12), 4792–4800. https://doi.org/10.1021/acssuschemeng.9b07422.

(416) Li, J.; V. Tappero, R.; S. Acerbo, A.; Yan, H.; Chu, Y.; V. Lowry, G.; M. Unrine, J. Effect of CeO 2 Nanomaterial Surface Functional Groups on Tissue and Subcellular Distribution of Ce in Tomato (Solanum Lycopersicum). *Environmental Science: Nano* **2019**, *6* (1), 273–285. https://doi.org/10.1039/C8EN01287C.

(417) Wang, A.; Yang, T.; Fan, W.; Yang, Y.; Zhu, Q.; Guo, S.; Zhu, C.; Yuan, Y.; Zhang, T.; Gan, Y. Protein Corona Liposomes Achieve Efficient Oral Insulin Delivery by Overcoming Mucus and Epithelial Barriers. *Advanced Healthcare Materials* **2019**, *8* (12), 1801123. https://doi.org/10.1002/adhm.201801123.

(418) Bertoli, F.; Garry, D.; Monopoli, M. P.; Salvati, A.; Dawson, K. A. The Intracellular Destiny of the Protein Corona: A Study on Its Cellular Internalization and Evolution. *ACS Nano* **2016**, *10* (11), 10471–10479. https://doi.org/10.1021/acsnano.6b06411.

(419) Gravely, M.; Safaee, M. M.; Roxbury, D. Biomolecular Functionalization of a Nanomaterial To Control Stability and Retention within Live Cells. *Nano Lett.* **2019**, *19* (9), 6203–6212. https://doi.org/10.1021/acs.nanolett.9b02267.

(420) Wang, C.; Chen, B.; He, M.; Hu, B. Composition of Intracellular Protein Corona around Nanoparticles during Internalization. *ACS Nano* **2021**, *15* (2), 3108–3122. https://doi.org/10.1021/acsnano.0c09649.

(421) Forest, V.; Pourchez, J. Preferential Binding of Positive Nanoparticles on Cell Membranes Is Due to Electrostatic Interactions: A Too Simplistic Explanation That Does Not Take into Account the Nanoparticle Protein Corona. *Materials Science and Engineering: C* **2017**, *70*, 889–896. https://doi.org/10.1016/j.msec.2016.09.016.

(422) Shadmani, P.; Mehrafrooz, B.; Montazeri, A.; Naghdabadi, R. Protein Corona Impact on Nanoparticle-Cell Interactions: Toward an Energy-Based Model of Endocytosis. *J. Phys.: Condens. Matter* **2019**, *32* (11), 115101. https://doi.org/10.1088/1361-648X/ab5a14.

(423) Digiacomo, L.; Cardarelli, F.; Pozzi, D.; Palchetti, S.; A. Digman, M.; Gratton, E.; L. Capriotti, A.; Mahmoudi, M.; Caracciolo, G. An Apolipoprotein-Enriched Biomolecular Corona Switches the Cellular Uptake Mechanism and Trafficking Pathway of Lipid Nanoparticles. *Nanoscale* **2017**, *9* (44), 17254–17262. https://doi.org/10.1039/C7NR06437C.

(424) Rodríguez-Celma, J.; Ceballos-Laita, L.; Grusak, M. A.; Abadía, J.; López-Millán, A.-F. Plant Fluid Proteomics: Delving into the Xylem Sap, Phloem Sap and Apoplastic Fluid Proteomes. *Biochimica et Biophysica Acta (BBA) - Proteins and Proteomics* **2016**, *1864* (8), 991–1002. https://doi.org/10.1016/j.bbapap.2016.03.014.

(425) Adeleye, A. S.; Keller, A. A. Interactions between Algal Extracellular Polymeric Substances and Commercial TiO2 Nanoparticles in Aqueous Media. *Environ. Sci. Technol.* **2016**, *50* (22), 12258–12265. https://doi.org/10.1021/acs.est.6b03684.

(426) Yang, X.; Wang, Q.; Qu, X.; Jiang, W. Bound and Unbound Humic Acids Perform Different Roles in the Aggregation and Deposition of Multi-Walled Carbon Nanotubes. *Science of The Total Environment* **2017**, *586*, 738–745. https://doi.org/10.1016/j.scitotenv.2017.02.050.

(427) Barbero, F.; Mayall, C.; Drobne, D.; Saiz-Poseu, J.; Bastús, N. G.; Puntes, V. Formation and Evolution of the Nanoparticle Environmental Corona: The Case of Au and Humic Acid. *Science of The Total Environment* **2021**, 144792. https://doi.org/10.1016/j.scitotenv.2020.144792.

(428) Lead, J. R.; Batley, G. E.; Alvarez, P. J. J.; Croteau, M.-N.; Handy, R. D.; McLaughlin, M. J.; Judy, J. D.; Schirmer, K. Nanomaterials in the Environment: Behavior, Fate, Bioavailability, and Effects—An Updated Review. *Environmental Toxicology and Chemistry* **2018**, *37* (8), 2029–2063. https://doi.org/10.1002/etc.4147.

(429) Ferro, M.; Brugière, S.; Salvi, D.; Seigneurin-Berny, D.; Court, M.; Moyet, L.; Ramus, C.; Miras, S.; Mellal, M.; Gall, S. L.; Kieffer-Jaquinod, S.; Bruley, C.; Garin, J.; Joyard, J.; Masselon, C.; Rolland, N. AT_CHLORO, a Comprehensive Chloroplast Proteome Database with Subplastidial Localization and Curated Information on Envelope Proteins *. *Molecular & Cellular Proteomics* **2010**, *9* (6), 1063–1084. https://doi.org/10.1074/mcp.M900325-MCP200.

(430) Butel, N.; Yu, A.; Le Masson, I.; Borges, F.; Elmayan, T.; Taochy, C.; Gursanscky, N. R.; Cao, J.; Bi, S.; Sawyer, A.; Carroll, B. J.; Vaucheret, H. Contrasting Epigenetic Control of Transgenes and Endogenous Genes Promotes Post-Transcriptional Transgene Silencing in Arabidopsis. *Nat Commun* **2021**, *12* (1), 2787. https://doi.org/10.1038/s41467-021-22995-3.

(431)   Ouassil, N.; Pinals, R. L.; Del Bonis-O'Donnell, J. T.; Wang, J. W.; Landry, M. P. Supervised Learning Model Predicts Protein Adsorption to Carbon Nanotubes. *Science Advances 8* (1), eabm0898. https://doi.org/10.1126/sciadv.abm0898.